Holographic toy models for de Sitter spacetime

Von der Fakultät für Mathematik und Physik
der Gottfried Wilhelm Leibniz Universität Hannover

zur Erlangung des akademischen Grades
Doktorin der Naturwissenschaften
Dr. rer. nat.

genehmigte Dissertation von

M. Sc. Laura Charlotte Niermann

2024

Referent	Prof. Dr. Tobias J. Osborne
Korreferent	Prof. Dr. Domenico Giulini
Korreferent	Prof. Dr. Časlav Brukner

Tag der Disputation: 05.06.2024

"Remember to look up at the stars and not down at your feet. Try to make sense of what you see and wonder about what makes the universe exist. Be curious."

Stephen Hawking

Abstract

Quantum information tools have yielded crucial insights into quantum gravity, particularly within the framework of anti-de Sitter spacetime, where the AdS/CFT correspondence is well-established. The assumption has intensified that this connection can be extended to a broader context of quantum gravity. Bridging the knowledge gap from anti-de Sitter to de Sitter spacetime has been a significant pursuit in recent decades. This thesis takes a step in advancing our comprehension of quantum gravity in the context of low-dimensional de Sitter spacetime using holography.

To achieve this, we develop a holographic toy model to describe the dS/CFT correspondence. This model is defined as a tensor network associated with the tessellation of de Sitter spacetime, which is interpreted as a propagator from de Sitter's past to its future boundary. Notably, the symmetry action on the boundaries of this holographic model is fully characterized using Thompson's group T; with this, we provide a dynamical toy model for the dS/CFT correspondence. By extending the holographic models to various curvatures of de Sitter, we establish a correlation between the curvature of spacetime and the quantum capacity of the channel defined by the tensor network, which is reminiscent of the Λ-N correspondence. Another key property of the holographic model is that it captures an isometric time evolution in expanding spacetime, which is in contrast to a unitary time evolution established in standard quantum mechanics.

To relate the holographic model to the language of quantum mechanics, we define Hilbert spaces at the holographic boundaries and physical quantum states living in these Hilbert spaces. It is crucial to emphasize that the properties of tensors within the holographic model significantly influence the characteristics of permissible states and with that the model's physical significance. Unlike in the anti-de Sitter case, using quantum error correction here only yields a trivial theory.

To further motivate more concrete properties of the tensors, we investigate how a local observer experiences the expansion of de Sitter spacetime. For this, we suggest a de Sitter vacuum state with quantum fluctuations as a globally defined initial state of de Sitter spacetime. We derive how its evolution is perceived by a local observer who experiences proper acceleration due to the spacetimes expansion. We refer to this as an Unruh channel in de Sitter spacetime. The obtained channel exhibits properties of an optimal cloning channel, which establishes another connection between aspects of quantum information theory and the expansion of spacetime.

One central principle that sets quantum physics apart from classical physics is quantum superposition. At the end of this thesis, we extend our studies of the Unruh effect to allow for the detector to be in a quantum superposition of trajectories. For this, we consider trajectories in a de Sitter static patch with a constant distance from one another and analyze the resulting state of the detector. We find that the state of the detector is not only a mixture of thermal states known from a well-defined trajectory, but we find interference terms between different trajectories in the excited state of the detector. These coherences can be associated with the properties of the particles absorbed by the detector.

Keywords: dS/CFT, holography, Thompson's group, Unruh effect, optimal cloning, superposition

Kurzzusammenfassung

Methoden aus der Quanteninformationstheorie haben entscheidende Einblicke in die Quantengravitation geliefert, insbesondere im Rahmen der Anti-de Sitter (AdS) Raumzeit, wo sie dazu beigetragen haben die AdS/CFT-Korrespondenz zu verstehen. Es wird vermutet, dass Quanteninformationstheorie auch außerhalb von Anti-de Sitter Raumzeiten zu einem besseren Verständnis von Quantengravitation beitragen kann. In den letzten Jahren war es ein zentrales Ziel, die Wissenslücke von der Anti-de Sitter zur de Sitter (dS) Raumzeit zu überbrücken.

Dazu entwickeln wir ein vereinfachtes holographisches Modell zur Beschreibung der dS/CFT-Korrespondenz. Dieses ist als Tensornetzwerk definiert, das mit der Kachelung der de Sitter-Raumzeit assoziiert und als Propagator zwischen den zeitlichen Grenzen der de Sitter-Raumzeit interpretiert wird. Die Wirkung der Symmetrie an den Grenzen dieses holographischen Modells wird vollständig durch die Thompson-Gruppe T charakterisiert. Indem wir die holographischen Modelle auf de Sitter Raumzeiten mit verschiedene Krümmungen verallgemeinern, stellen wir eine Korrelation zwischen der Raumzeitkrümmung und der Quantenkapazität des Modells her. Eine weitere zentrale Eigenschaft des holographischen Modells besteht darin, dass es eine isometrische Zeitentwicklung in der expandierenden Raumzeit beschreibt, welche im Gegensatz zu der in der Standard-Quantenmechanik etablierten unitären Zeitentwicklung steht.

Um das holographische Modell mit der Sprache der Quantenmechanik zu verbinden, definieren wir Hilbert-Räume an den Grenzen des Modells und die zugehöriogen physikalischen Quantenzustände. Es ist wichtig zu betonen, dass die Eigenschaften der Tensoren innerhalb des holographischen Modells die Eigenschaften der zulässigen Zustände und die physikalische Bedeutung des Modells wesentlich beeinflussen. Die Verwendung der Quantenfehlerkorrektur, die im AdS-Fall sehr erfolgreich war, führt hier nur zu einer trivialen Theorie.

Um weitere konkrete Eigenschaften der Tensoren zu motivieren, untersuchen wir, wie ein lokaler Beobachter die Expansion der de Sitter-Raumzeit erlebt. Dazu betrachten wir einen globalen Anfangszustand der de Sitter-Raumzeit als Vakuumszustand mit Quantenfluktuationen. Wir leiten ab, wie seine Entwicklung von einem lokalen Beobachter wahrgenommen wird. Aufgrund der Expansion der Raumzeit erfährt der lokale Beobachter eine Eigenbeschleunigung, weshalb wir von einem Unruh Effekt in der de-Sitter-Raumzeit sprechen. Der erhaltene Kanal weist Eigenschaften eines optimalen Klonkanals auf, was eine weitere Verbindung zwischen Aspekten der Quanteninformationstheorie und der Expansion der Raumzeit herstellt.

Ein zentrales Prinzip, das die Quantenphysik von der klassischen Physik unterscheidet, ist die Quantenüberlagerung verschiedener Zustände. Am Ende dieser Arbeit erweitern wir unsere Untersuchungen des Unruh-Effekts so, dass sich der lokale Detektor in einer Quantenüberlagerung von Trajektorien befindet. Dazu betrachten wir Trajektorien in der de Sitter Raumzeit mit konstantem Abstand zueinander und analysieren den resultierenden Zustand des Detektors, der sich in einer Überlagerung dieser Trajektorien befindet.

Schlagwörter: dS/CFT, Holografie, Thompson's Gruppe, Unruh Effekt, optimales Klonen, Superposition

Acknowledgements

I want to take this opportunity to thank all the people who have supported me over the last few years and thus contributed to the development of this work.

Special thanks go to my supervisor, Tobias Osborne, for guiding me through the past years and enabling me to dive into the fascinating field connecting quantum information and gravity. This endeavor was only possible with the countless valuable discussions, all the shared knowledge, and the overall guidance in various areas of academic work. I am extremely grateful to Domenico Giulini and Časlav Brukner for the feedback and advice I received from them, their interest in this project, and the commitment to agreeing to be a referee and, with that, participate in my doctoral procedure. Many thanks also go to all the members (current and past) of the quantum information group in Hannover for creating such a welcoming and positive working environment, which made coming to the institute every day a pleasure. In particular, I would like to thank you for the nice company and interesting conversations, which made lunch breaks at Mensa as enjoyable as they were – here a special thanks goes to Bence Temesi for treating us with baked goods on a regular basis, which always increased motivation in the afternoon. Thank you very much to all of you for the great time in the group!

I also had the pleasure of collaborating with Jordan Cotler, whom I thank for the valuable and inspiring discussions and invaluable exchange of ideas. Special thanks also go to the members of the Institute for Quantum Optics and Quantum Information of the University in Vienna, in particular, Luis Barbado, for the interesting and valuable collaboration that developed after my visit. I want to thank all the people who supported me in the teaching activities I was involved in during the past years and all the students who actively participated and shared their positive feedback at the end of the term! I also thank all the Master's and Bachelor's students I supervised for their interest, investment, and enjoyable meetings in the past years. Thanks should also go to Shawn Skelton, Ugne Liaubaite, Viktoria-Sophie Schmiesing, and Luis Barbado for their assistance in proofreading and helping me get the thesis to its final form.

All of this would not have been possible without my family and great friends! Many thanks go to everyone who contributed to keeping me sane and happy in the past years. Thank you to everyone who contributed to amazing bouldering and climbing sessions, which exhibited a great combination of spending quality time with amazing people and bringing some much-needed movement into everyday life. The same goes for many enjoyable acrobatics sessions, which started as a course at the university and evolved to great sessions at CircO and outside in the summer. I would also like to thank my friends for spending many great evenings with good food and comforting conversations whenever needed.

I want to express my deepest gratitude to my parents, Ute and Stefan, for their never-ending support and love and to my brother, Lennart, for always being there for me if I need him. Most importantly, I would like to thank Steffen Katz for his unconditional love, support, and patience! You have always been there for me and supported me in any way possible, and I appreciate this more than I can put into words. Thank you so much!

Table of Contents

Chapter 1

Introduction

Quantum gravity is an important field in theoretical physics with the goal of unifying general relativity and quantum mechanics. *General relativity* is the theory that provides a thorough understanding of gravity, characterizing it as a geometric property of spacetime, and quantum mechanics is a fundamental theory in physics that describes physical principles at a microscopic scale. To this day, the unification of these two theories and, with that, a general understanding of quantum gravity is vastly out of reach. As a first step in gaining a deeper understanding of quantum gravity in general, the focus lies on understanding the fundamental properties of quantum gravity for comparatively simple solutions of Einstain's field equation in general relativity. Two examples that stand out due to their constant curvature and with that hyperbolic structure are *de Sitter* (dS) and *anti-de Sitter* (AdS) spacetime introduced by de Sitter in 1917 [dS17a, dS17b]. In the past, there has been great progress in understanding the relationship between quantum gravity theories in the semiclassical limit and strongly interacting conformal field theories (CFTs) for anti-de Sitter spacetimes. This duality is formulated as the *AdS/CFT correspondence* in [Mal98, Mal99]. This original work was followed by a multitude of studies exploring this holographic correspondence in a variety of settings in the field of high energy physics, starting with early works from Susskind in [Sus95], Gubser, Klebanov, and Polyakov in [GKP98] and Witten in [Wit98]. This correspondence has provided many insights into the fundamental structure of quantum gravity. In this context, quantum information tools have provided valuable insights for a better understanding of quantum gravity. There are profound reasons to believe there is a deep connection between quantum gravity and quantum information theory beyond the AdS/CFT correspondence [Bou02b].

In the past decades, there has been an active interest in exploring the connection between quantum gravity and quantum information further, where the use of *holographic principles* took a central role. In particular, holographic properties manifested in the relation between quantum entanglement of a boundary region and the corresponding minimal surface area of the bulk characterized by Ryu and Takayanagi in [RT06], which was further discussed in [RT17]. The use of quantum entanglement in this context has developed from there: Van Raamsdonk suggested in [Raa10] that classically connected spacetimes, in general, are directly related to the quantum entanglement on the boundary. Maldacena and Susskind have proposed in [MS13] that two distant black holes connected via a wormhole (which is a solution to the field equations in general relativity) can be interpreted as a maximally entangled state of two black holes. This work was the starting point for relating quantum entanglement and Hamiltonian complexity theory to the quantum physics of black holes [Har16, BRS$^+$16, HNQ$^+$16].

One highly relevant tool from quantum information theory (also well-known in many-body physics) to implement holographic principles is tensor networks. In particular, tensor networks have provided a valuable tool to define holographic toy models in the context of anti-de Sitter spacetime. Two important examples of toy models capturing the AdS/CFT correspondence are the one pro-

posed by Swingle in [Swi12a] and another one from Pastawski, Yoshida, Harlow, and Preskill suggested in [PYHP15], which both model a discretized spatial slice of anti-de Sitter. In [Swi12a], this correspondence was established by linking the Multi-Scale Entanglement Renormalization Ansatz (MERA) to anti-de Sitter spacetime. This work was an important motivation for the toy model presented in [PYHP15] describing the holographic duality and giving a discretized description of the AdS/CFT correspondence. This duality is often referred to as the *holographic code*, which is built from special tensors coming from *quantum error correction* (QEC) known as *perfect tensors*. This toy model was the starting point to further investigate and generalize holographic codes in the context of the AdS/CFT correspondence [HNQ$^+$16, BCC$^+$15, YHQ16, BGHL16, May17] and perfect tensors [GAL$^+$15, EWŻ16, RGRA18, LHGZ17, PR17, DMMW17]. In holographic tensor network models, the relation between QEC and bulk locality in the AdS/CFT correspondence initially pointed out by Almheiri, Dong, and Harlow in [ADH15] has taken a central role in understanding the bulk-boundary correspondence in anti-de Sitter. The upgrade to a full dynamical toy model of the AdS/CFT correspondence was possible using powerful results of Jones [Jon14, Jon17] stating that *Thompson's group T* [CFP96, Bel04] is a unitary representation of a discretization of the conformal group. Tensor networks have proven to be a valuable tool in capturing the holographic correspondence, which goes beyond the geometry of the spacetime but greatly helped in characterizing the bulk boundary correspondence in particular in anti-de Sitter spacetime.

For the past decades, many observations such as [RFC$^+$98, SSP$^+$98, PAG$^+$99, Car01, PKV$^+$03] have strongly supported the idea that we live in a universe that is asymptotically de Sitter. Arguably, de Sitter is the spacetime with more physical relevance to us than anti-de Sitter. There has been progress in the past years in developing a dS/CFT correspondence with key works including [Ban01, Bou99a, Bou99b, Bou00, Wit01, BHM01, HMS01, Mal03, HS11]. One remarkable result, which has attracted lots of attention and has been quite counter-intuitive for years, is that global de Sitter spacetime only exhibits a *finite* number of degrees of freedom depending on the curvature of spacetime. This conjecture is referred to as the Λ-N correspondence and was first argued by Banks and Bousso [Ban01, Bou99a, Bou99b, Bou00] and further refined in the coming years by Witten [Wit01]. Despite this significant progress in understanding the properties of the dS/CFT correspondence, to this day, the insights gained in de Sitter do not match those in anti-de Sitter spacetime. The main objective of this thesis is to learn more about quantum gravity in the context of de Sitter spacetime. The goal is to develop a holographic toy model capturing properties of the dS/CFT correspondence by transferring knowledge about quantum gravity in anti-de Sitter spacetime to de Sitter and adapting properties of holographic models describing the AdS/CFT correspondence. In the upcoming work, we develop a holographic model for de Sitter and relate its quantum information properties to the Λ-N correspondence.

Many obstacles arise in directly transferring results from anti-de Sitter to de Sitter spacetimes, as they have *fundamentally different* physical properties. One difference that needs to be highlighted is that de Sitter spacetime has two spatially disconnected temporal boundaries, which lie in the far past and future, respectively. In contrast, anti-de Sitter spacetime has one spatial boundary. The drastic difference in the boundaries highly affects the holographic model where the boundary of spacetime characterizes the properties in the bulk. Another striking difference is the fundamental difference in time: in AdS, time is periodic; this is not the case in dS. Also, a local observer in de Sitter can only have access to part of the spacetime, which makes it difficult to define one correct set of observables in de Sitter spacetime rigorously. These profound differences have far-reaching consequences and impose challenges in transferring formulations of quantum gravity models of the AdS/CFT correspondence to the de Sitter case.

In spite of these difficulties, Strominger has introduced ideas to study the *holographic duality*

captured by the dS/CFT correspondence in [Str01a, Str01b] and many other papers built on these ideas and generalized the models such as [BdBM02, AHS16]. Tensor networks are the primary tool in implementing holographic models. The work from Kunkolienkar and Banerjee in [KB17] was an attempt to use a tensor network to describe the dS/CFT correspondence with a generalization of *MERA*, which had already been successful in the AdS/CFT case. Different from the anti-de Sitter case, which models one spatial slice, this tensor network captures the entirety of de Sitter spacetime, where time is defined along the direction between the two boundaries, and each constant time slice contains information about the entanglement structure at the boundary. MERA exhibits the useful property that it is possible to define a notion of causality on the tensor network as shown in [Bén13]. This model is a holographic model where observables of de Sitter live on timelike infinity. This model captures the kinematical properties of the dS/CFT correspondence but cannot describe dynamics. To this day, a complete quantum gravity in $(3+1)$-dimensional de Sitter spacetime is still beyond reach, but there has been considerable progress in the low dimensional case. Jackiw and Teitelboim provided a formulation of low dimensional gravity often referred to as *JT gravity* in [Jac85, Jac92, Tei83], which provided the foundation for understanding the structure of the Hilbert space and the quantum theory of gravity in $(1+1)$-dimensional de Sitter spacetime as discussed in [CJM20, CS23]. These low-dimensional theories of gravity have no propagating degrees of freedom. They still share the property that all observables live on the temporal boundaries.

The centerpiece of this thesis is the development of a *holographic model* that captures properties of de Sitter spacetime, which was published in [NO22]. For constructing this holographic model, we employ techniques known for the construction of holographic codes from [PYHP15]. This holographic model is largely motivated by the underlying tree-tensor structure in the MERA tensor network discussed in [KB17], which is why the resulting fundamental structure of our tensor network is reminiscent of MERA in terms of its boundaries and causality relations. This structure is a natural consequence of expanding spacetimes with $\Lambda > 0$. Similar discussions in the context of the spacetimes geometry and its relation to holography can also be found in [Swi12b, CLMS15, CLMS16, Qi13, BCCCD17, MV18a]. Our holographic model is set apart from previous models in two main aspects: With the holographic model developed in this thesis, we can describe de Sitter spacetimes with different curvatures and with a full characterization of the discretized isometry group, also describe dynamics. This model provides a powerful tool to analyze the properties of quantum gravity in de Sitter spacetime in a low-dimensional setting.

In contrast to the anti-de Sitter case, this holographic model can be interpreted as a *propagator* from the past to the future infinity, more precisely as a *partial isometry*. As such, it exhibits some crucial properties that capture previous conjectures of the dS/CFT correspondence in a novel way: the partial isometry effectively acts on a finite-dimensional physical Hilbert space whose dimension depends on the curvature of dS. The dimension of the physical subspace and, with that, the curvature of spacetime is associated with the channel capacity of the holographic model, which is directly related to the Λ-N *correspondence*. Another property of the holographic model is that the time evolution of de Sitter spacetime is captured by the tensor network and is encoded in isometries. Different from many typical fields of research in quantum mechanics, time evolution in de Sitter spacetime accordingly is always isometric and not necessarily unitary. This non-unitarity of time evolution was further investigated in a broader context not directly related to the tensor network in [CS22, CJ23]. The isometric time evolution is directly related to the expansion of spacetime, where more degrees of freedom are added as time evolves.

To describe the dynamical properties of the holographic model, we need a discretized isometry group of the de Sitter boundaries. For this, we employ results of Jones [Jon14, Jon17] on representations of *Thompson's group* T, which have been helpful in characterizing the discretized isometry

group in the anti-de Sitter case. Elements from Thompson's group T are discretized versions of diffeomorphisms on the temporal boundaries. A subgroup of Thompson's group T, which can be identified with the modular group $\mathrm{PSL}(2,\mathbb{Z})$, is precisely the group to describe isometry transformations on the boundary. This description is reminiscent of the approach for constructing p-adic numbers in the anti-de Sitter case due to the tree structure in [GKP$^+$17, Gub17] or the symmetry proposal of a model for eternal inflation from [HSSS12], but the underlying symmetry groups differ.

We formulate a concrete relation from the holographic model to objects known in quantum physics: *physical quantum states* and *local operators*. The holographic model is interpreted as a propagator between two boundary Hilbert spaces, which both contain quantum states. These states have treelike structures, and we refer to them as physical states. The vacuum state is invariant under all isometry transformations, and the other physical states can be generated from the vacuum state by applying allowed transformations. For the allowed transformations, we can apply operators at the future de Sitter boundary. These operations propagate through the tensor network and can be interpreted at finite times. This way, we can generate local transformations in the bulk by only accessing the boundary. The way the transformations manifest at finite times is highly dependent on the properties of the tensors. In the AdS/CFT case, quantum error-correcting codes have been the best candidates for the tensor networks, as presented in [PYHP15]. This is why we try choosing random unitaries to capture the encoding of the quantum error correcting codes (QECC) for the tensor network modeling de Sitter spacetime. With that, we want to transfer the knowledge we already gained in the anti-de Sitter case. We find that – different to the anti-de Sitter case — QECC are *not* compatible with local operators in de Sitter spacetime in the sense that it is impossible to simulate different physical states in the bulk.

De Sitter spacetime is characterized by its expansion and freely falling particle detectors in expanding spacetimes register particles, even if the global state is a vacuum state. This phenomenon is known as *cosmological particle creation*, which Parker initially discussed in [Par67, Par68, Par69] and Sexl and Urbantke in [SU69]. By now, this part of the standard literature such as [BD82]. Mottola first studied cosmological particle creation with de Sitter as a cosmological background [Mot85]. Cosmological particle creation in de Sitter spacetime bears close similarities to the Unruh effect in flat spacetime, as a local observer in de Sitter spacetime experiences proper acceleration due to the spacetimes expansion. The Unruh effect is characterized by the key statement that an accelerated observer perceives the vacuum state as a thermal bath and was first studied in Minkowski spacetime [Hig87, Ful73, DFU76]. With that, it characterizes the relation between quantum reference frames and the measured particles in quantum field theories. Different from the accelerated observer in the Unruh effect, the acceleration of a local observer in de Sitter is a fundamental property of the spacetime. Even though these two effects are physically very different, the underlying mathematical properties have fundamentally the same structure and are unified by the acceleration the local observer experiences. Over the years, there has been significant research on the thermal properties of de Sitter as an expanding spacetime, using the Unruh effect as a framework. The thermal nature of de Sitter spacetime, which is directly related to its expansion, has been widely studied in the literature: Gibbons and Hawking were the first to associate a temperature to the cosmological horizon in [GH77b]. Numerous works have continued in assigning thermal properties to de Sitter spacetime such as [BDD$^+$19, CCO$^+$11, GP04, JTJ15, DL99, DL97, SUFK21, Kim16, Jac98, Jen05, Lap78, KKVV22, DZ01, ACT$^+$11, AFR23, Mar18, Yu11].

In the context of the Unruh effect in flat spacetime, the Unruh channel was studied in a slightly different setting in [BHP09, BHTW10, BHP12]. In this paper series, they considered an encoded logical qubit instead of the vacuum as an initial state of the Unruh effect. The result was that they found properties of cloning channels in the structure of the resulting Unruh channel. In this thesis, we consider a similar setup in de Sitter spacetime, which follows the work in [NO24].

We study a channel in de Sitter spacetime, where we consider an initial state, which is a de Sitter vacuum state with quantum perturbations realized as some excited particles. With this, as an initial state of de Sitter spacetime, we derive how a local observer perceives the global expansion of spacetime. The Unruh channel in the framework of de Sitter spacetime has similar mathematical properties to the one in flat spacetime and, in particular, also has properties of a cloning channel. In the context of de Sitter spacetime, this arguably is even more intriguing, as the cloning property can be directly associated with the expansion of spacetime. On a physical level, this provides a new understanding of how the initial state of the universe is perceived by a local observer associated with a static patch. With this channel, we also get a description of how quantum information is transmitted through the holographic model as spacetime expands and how this expansion affects the evolution and entanglement properties of the initial state. This description of how a local observer perceives the global expansion of spacetime can not only give more insights into quantum gravity in the context of de Sitter spacetime but also can characterize the properties of the tensor network further. The cloning properties of the channel characterize the expansion of de Sitter and shed light on the possibility that the tensor network is comprised of optimal cloners. The relationship between thermal properties and holography has been explored in several papers, such as [CG17], where it was postulated that field theory observables acquire thermal properties from the bulk.

In formulating a theory of quantum gravity, quantum superposition plays a crucial role in describing the possible states of gravitational fields and spacetime geometry. One fundamental difference between classical and quantum physics is that quantum mechanics allows for the concept of superposition, where particles can exist in multiple states simultaneously. As a formulation of quantum gravity is expected to contain characterizations of (semiclassical) spacetime geometry in quantum superposition, we can improve our understanding of quantum gravity by improving our understanding of how quantum superposition manifests in the context of gravity. One can consider different semiclassical quantum superposition scenarios involving gravity, such as the superposition of observer trajectories or the superposition of spacetime geometries. The first experimental proposals that study the gravitationally-induced entangling of two particles in a spatial superposition state were suggested in [BMM$^+$17, MV17, CR19]. Examples where the superposition of observer trajectories was considered are [FOZ20], where the interaction of the detector with a massless scalar field is characterized. The scenario where the observer follows a quantum superposition of trajectories with different proper acceleration instead of a well-defined classical trajectory is studied in the paper [BCRAvB20] in the context of the Unruh effect and the work [PB23] in measuring Hawking radiation. The superposition of conformally equivalent spacetimes was discussed in [KdlHCRB22], and other aspects of quantum superpositions of spacetime have recently been studied in [FAZM23, FZ23, FMZ23].

Recent studies [FMZ20] have considered semiclassical spacetime geometries in quantum superpositions in the context of de Sitter spacetime. This work considered an Unruh-de Witt detector as introduced in [DeW80], which follows quantum superpositions of trajectories in different scenarios. The response function of the detector is evaluated, and it is found that the superposition of trajectories from spacetimes with different curvatures is not equivalent to the superposition of spatially translated trajectories within one spacetime geometry. In the final part of the thesis, we want to generalize this approach where we follow the work [NB24]. We focus on the setting where the detector follows a quantum superposition of trajectories in one de Sitter static patch. Local observers associated with these trajectories individually would all experience different proper accelerations as we consider the superposition of uniquely distinguishable trajectories following the Killing field. As a generalization, we use a multi-level particle detector instead of the original Unruh-de Witt detector with two energy levels. We derive the final state of the detector after the interaction with the background field. The generalization to consider a multi-level particle

detector allows for a more detailed discussion of the final state of the detector. In the excited state of the detector, we find interference terms from the different trajectories. The state of the detector accordingly entails more than a mixture of thermal states corresponding to the individual trajectories. Studying a detector in superposition in the context of the Unruh effect [BCRAvB20] or in measuring Hawking radiation [PB23], similar terms of coherent interference were found.

In this thesis, we developed a holographic toy model for the dS/CFT correspondence. Key properties of this model are the Λ-N correspondence in de Sitter and its isometric time evolution. Different from preexisting models, we have fully characterized the discretized isometry group and, with that, captured the dynamic properties of this model. We require the tensors in the holographic model to be perfect tensors, but further properties of the tensors, which would enable us to determine the allowed set of physical states fully, remain to be characterized rigorously. To gain further insights into that, we have taken a look at the properties of quantum gravity in the context of de Sitter spacetime from a different angle. The derivation of the Unruh channel, which characterizes how a local observer experiences the global expansion of spacetime, has properties of a cloning channel. This might indicate that this is also true for tensors in the holographic model. The quantum superposition of trajectories considered in the final part of the thesis is also directly related to the holographic toy model, as the holographic model we developed in this thesis can be interpreted as a quantum superposition of all possible world lines. Insights found in this context may also help in further characterizing properties of the tensors in the holographic model in the future.

Outline

This thesis is organized into three parts: As it covers an interdisciplinary field, part I covers fundamental material relevant to the rest of the project. These chapters can be skipped based on the prior knowledge of the reader. In chapter 2, we review classical properties of de Sitter spacetime, including the parametrization in different coordinate systems, some fundamental properties of classical gravity with a focus on low dimensions, and the discussion of Killing fields and geodesics in de Sitter spacetime. Chapter 3 reviews the Unruh effect, which is an effect from quantum field theory relevant to the rest of this thesis and puts light on different quantizations of de Sitter spacetime and the corresponding vacuum states in the context of quantum field theory in curved spacetime. Some fundamental properties from quantum information theory, including a short introduction to quantum error correction and optimal cloning, are discussed in chapter 4. In this chapter, we also review the toy model characterizing the AdS/CFT correspondence, which served as a motivation for the holographic model from this thesis.

The holographic toy model capturing properties of the dS/CFT correspondence is featured in part II is the heart of this thesis. In chapter 5, we characterize the discretized symmetry properties in de Sitter spacetime. The construction of the holographic model is described in chapter 6. In chapter 7, we discuss the relation between properties of the tensors in the holographic model and allowed physical states; in particular, we consider QECC for characterizing the tensor network.

Part III of the thesis comprises two different approaches to consider the Unruh effect in de Sitter spacetime. In chapter 8, the Unruh channel for an initial de Sitter global vacuum state with quantum perturbations is calculated, which shines a light on how the expansion of spacetime is experienced inside a static patch. In chapter 9, we consider the Unruh effect in de Sitter spacetime, where the detector follows a quantum superposition of trajectories instead of one well-defined classical one. Finally, chapter 10 concludes our results, and we discuss potential further directions for future directions. Detailed supplementary calculations can be found in the appendix.

Part I.

Preliminaries

Chapter 2

de Sitter spacetime as a classical gravitational background

De Sitter spacetime (dS) is a maximally symmetric solution of Einstein's field equations with a constant positive curvature. It was reported as a solution to Einstein's field equations in 1917 alongside anti-de Sitter spacetime (AdS), which has constant negative curvature by Willem de Sitter [dS17b, dS17a]. For many years, de Sitter spacetime has gotten special attention because many calculations are greatly simplified compared to other cases due to the same degree of symmetry as Minkowski spacetime and the constant curvature of the spacetime. Due to observations (such as [SSP+98]), it has been hypothesized that the cosmological constant Λ of our universe is small and positive. This makes de Sitter spacetime even more interesting to study since we can draw a comparison to the universe we live in. It has been suggested in [Sun02] that de Sitter is the natural limiting spacetime for our universe. This highly motivates us to try to understand more about quantum gravity in the setting of de Sitter spacetime.

Since de Sitter spacetime is a fundamental building block of this entire thesis, we will spend some time reviewing some of its basic properties in this chapter. In this chapter, we focus on the classical description of the spacetime. In section 2.1, we review some basic properties in general relativity, including a short discussion of low dimensions. We introduce different coordinate systems relevant to this work in section 2.2. This is followed by a detailed discussion of the Killing fields in de Sitter spacetime in 2.3 where the main result is that there is no globally timelike Killing field in de Sitter spacetime. The chapter is concluded by the investigation of different trajectories and geodesics with their respective properties in section 2.4. In this chapter, the description of de Sitter spacetime is largely based on [HE75], and concepts of general relativity follow [Wal84].

For the rest of this paper, we focus on the $(1+1)$-dimensional case if not stated differently. For many aspects, it is straightforward to generalize this to higher dimensions. Even if the two-dimensional case does not allow for some physical behavior (such as propagation of gravitational waves), this low-dimensional approach captures many of the properties we want to analyze. The two-dimensional de Sitter spacetime, the spacetime we focus on throughout this thesis, is depicted in figure 1 as a single-sheeted hyperboloid in Minkowski spacetime. Readers familiar with the basic properties of de Sitter may safely skip this chapter.

2.1. Introduction to general relativity

General relativity relates the geometry of spacetime to its gravitational properties, whose principles follow the basic idea: spacetime tells matter how to move, and matter tells spacetime how to

curve. We will review some basic properties of general relativity which are relevant to the rest of the thesis. This review largely follows [Wal84], which also contains more details on the theoretical background of general relativity. One important building block in general relativity is Einstein's field equations, which take the role of equations of motion. The field equations take the general form.

$$G_{ab} + \Lambda g_{ab} = R_{ab} - \frac{1}{2} R g_{ab} + \Lambda g_{ab} = 8\pi T_{ab}.$$

Here G_{ab} is the Einstein tensor defined by the curvature of the spacetime characterized by the Ricci tensor R_{ab} and Ricci curvature R, the cosmological constant Λ, and T_{ab} is the energy-momentum tensor. The metric tensor g_{ab} is the solution to Einstein's field equations. It defines spacetime as a manifold and is related to the distribution of matter in the field equations.

The solution that we focus on in this thesis is de Sitter spacetime, which is a solution to the field equations characterized by a constant positive curvature, which also manifests in a positive cosmological constant Λ. We largely focus on de Sitter spacetime as a classical background for investigating quantum gravity, which is why, for the most part, we consider its vacuum field equations where the energy-momentum tensor T_{ab} vanishes identically.

One crucial aspect is the curvature of spacetime. The curvature of spacetime can be visualized by parallel transporting a vector along a closed curve. Different from parallel transport in flat spacetime, the direction of the vector before and after being transported along a closed curve can change and is dependent on the curve. This relation between curvature and parallel transport along a curve is characterized through *affine connections*. The parallel transport of a vector along a curve is defined with the *covariant derivative* where the Christoffel symbols are chosen as affine connections. To parallel transport a vector v^a along a curve γ with tangent t^a, the following condition with the covariant derivative ∇_a has to be fulfilled: $t^a \nabla_a v^b = 0$. The covariant derivative is a derivative operator directly associated with the metric tensor g_{ab} and, therefore, to the intrinsic structure of spacetime. For a tensor V^ν_μ a covariant derivative is defined as follows:

$$\nabla_\lambda V^\nu_\mu = \partial_\lambda V^\nu_\mu + \Gamma^\nu{}_{\lambda\kappa} V^\kappa_\mu - \Gamma^\kappa{}_{\lambda\mu} V^\nu_\kappa$$

Christoffel symbols are chosen as the affine connections in the covariant derivative because the covariant derivative of the metric vanishes in this case. In coordinate form, *Christoffel symbols*

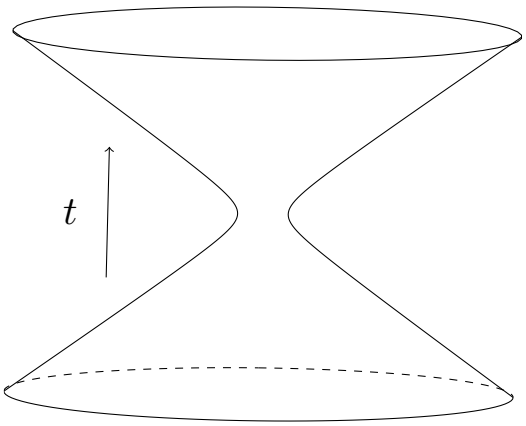

Figure 1.: Schematic depiction of two dimensional de Sitter spacetime embedded as a hyperbolic sheet in Minkowski spacetime

can be expressed as

$$\Gamma^{\sigma}{}_{\mu\nu} = \frac{1}{2}g^{\sigma\kappa}\left(\frac{\partial g_{\nu\kappa}}{\partial x^{\mu}} + \frac{\partial g_{\mu\kappa}}{\partial x^{\nu}} - \frac{\partial g_{\mu\nu}}{\partial x^{\kappa}}\right) = \frac{1}{2}g^{\sigma\kappa}(\partial_{\mu}g_{\nu\kappa} + \partial_{\nu}g_{\mu\kappa} - \partial_{\kappa}g_{\mu\nu})$$

The *Riemann curvature tensor* $R_{abc}{}^{d}$ (often referred to as Riemann tensor) fully characterizes the curvature of spacetime. Its definition is directly related to the difference between vectors before and after they are parallel transported around a small closed loop. The Riemann tensor acting on a vector field w^c is defined as

$$R_{abc}{}^{d}w^{c} = (\nabla_a\nabla_b - \nabla_b\nabla_a)w^{d}$$

In coordinate expression, the components of the Riemann tensor are expanded as follows:

$$R_{\mu\nu\rho}{}^{\sigma} = \partial_{\nu}\Gamma^{\sigma}{}_{\mu\rho} - \partial_{\mu}\Gamma^{\sigma}{}_{\nu\rho} + \Gamma^{\alpha}{}_{\mu\rho}\Gamma^{\sigma}{}_{\alpha\nu} - \Gamma^{\alpha}{}_{\nu\rho}\Gamma^{\sigma}{}_{\alpha\mu}$$

The Riemann tensor can be decomposed into its trace and trace-free part with the *Ricci tensor* R_{ab}. The Ricci tensor is defined as the trace over the second and fourth index[1] of the Riemann tensor which is also referred to as the contraction with the metric

$$R_{ab} = R_{acb}{}^{c} = g^{cd}R_{acbd} = R_{ba}$$

The *Ricci scalar* is the scalar curvature, which is defined as the trace of the Ricci tensor

$$R = g^{ab}R_{ab} = R_{a}{}^{a}$$

For the case of constant curvature, Ricci scalar R is constant, and all information of the Riemann tensor is contained in the Ricci tensor.

This curvature intrinsic to the spacetime needs to be contrasted with its extrinsic curvature, which is defined as the change of the normal vector:

$$K = \nabla_a n^a$$

For calculations in general relativity, we will use *abstract index notation* (we follow the convention introduced in [Wal84, p. 24]), which is coordinate-independent and uses Latin letters. The use of Greek letters indicates the introduction of an explicit coordinate basis.

In low dimensional spacetime, in particular, $1+1$ dimensional spacetime, this reduces to an almost trivial theory. The restriction to two dimensions directly affects the physical effects in spacetime. The Einstein tensor $G_{\mu\nu}$ vanishes identically, and there are no propagating degrees of freedom (sometimes referred to as gravitons) in two-dimensional spacetime. Notably, this also excludes the existence of gravitational waves. One way this shows is that all $1+1$ dimensional spacetimes are conformally equivalent to the Minkowski spacetime as their metric tensor can always be transformed in the form $g_{\mu\nu}(x) = \Omega(x)^2\eta_{\mu\nu}$ as described in [BD82, 3.7]. Even though the gravitational theory in two dimensions in many aspects is almost trivial, this simplified setting is very helpful in understanding fundamental properties.

A natural generalization of two-dimensional gravity which avoids these difficulties is furnished by the *Jackiw-Teitelboim* (JT) model [Jac85, Jac92, Tei83]. The properties of gravity in the two-dimensional setting are described with a scalar field ϕ, often referred to as the dilaton field.

[1] equivalently the first and third index, the trace over the first and second as well as the third and fourth index vanish

This framework allows for more possibilities and has nearly-dS solutions. In the context of de Sitter spacetime, the constant curvature condition is required:

$$R - 2\Lambda = 0 \tag{2.1}$$

The corresponding action in the bulk of $1+1$ dimensional de Sitter spacetime was also analysed in [CJM20] and is given by (see appendix A.1 for more details)

$$S = \frac{1}{16\pi G}\int \mathrm{d}^2x\sqrt{-g}\left(R - \frac{2}{\ell^2}\right)\phi(x)$$

where G is the gravitational constant and the de Sitter radius ℓ is directly related to the cosmological constant. The field equations can be derived requiring that the variation of the action with respect to the metric vanishes, which was derived initially in [GH77a]. They read

$$(\nabla_\mu\nabla_\nu + g_{\mu\nu})\phi(x) = 0$$

Although JT gravity does not have bulk gravitons, it does have boundary gravitons arising from fluctuations in the asymptotic boundaries. These manifest in the following way: In this framework, the gravitational path integral reduces to a boundary path integral, which is easier to study. This is often referred to as *Schwarzian theory* [CJM20] in the literature often studied in the context of AdS spacetime [EMV16, Jen16, MSY16]. It needs to be noted that the contributions of the fluctuating spacetime boundaries as described in [CJM20] need to be included when carefully formulating JT gravity in a de Sitter background. Later in the thesis, we will describe boundary actions derived from this different approach.

2.2. Coordinates de Sitter

There are numerous ways to parametrize *de Sitter spacetime* using different coordinate systems, all of which have advantages and disadvantages in different cases. Different ways to parametrize de Sitter spacetime with various coordinate systems have been discussed at length in the literature (see for example [BD82, HE75, Rip13, SSV03]). Here, we will introduce the de Sitter coordinates primarily used in the rest of the thesis. The most intuitive way to parametrize d-dimensional de Sitter spacetime dS_d, which has one temporal and $d-1$ spatial dimensions, is by describing it as a hypersurface embedded in $(d+1)$-dimensional Minkowski spacetime: de Sitter is then represented by a single-sheeted hyperboloid in Minkowski spacetime. The points of d-dimensional de Sitter spacetime fulfill the hyperboloid condition:

$$-x_0^2 + x_1^2 + \cdots + x_d^2 = \ell^2. \tag{2.2}$$

where the parameter ℓ is the *de Sitter radius*. The de Sitter radius characterizes the size of the bottleneck area of the spacetime and is directly related to its curvature. We parametrize the temporal coordinate x_0 so that the size of the spacetime is smallest at $x_0 = 0$. If not otherwise specified, we assume the de Sitter radius is given by $\ell = 1$. The metric of d-dimensional de Sitter spacetime is given by

$$\mathrm{d}s^2 = -\mathrm{d}x_0^2 + \mathrm{d}x_1^2 + \cdots + \mathrm{d}x_d^2.$$

For the different coordinate systems, we are interested in the *induced metric* of de Sitter metric from the embedding Minkowski metric, which is defined as

$$g_{\alpha\beta} = \frac{\partial x^\mu}{\partial y^\alpha}\frac{\partial x^\nu}{\partial y^\beta}\eta_{\mu\nu}$$

where x^μ are the coordinates embedding de Sitter in Minkowski space and y^α are the new de Sitter coordinates.

The only coordinate system to cover the entire de Sitter spacetime in one coordinate chart is called *global coordinates*. They globally describe the entire spacetime without any singularities.

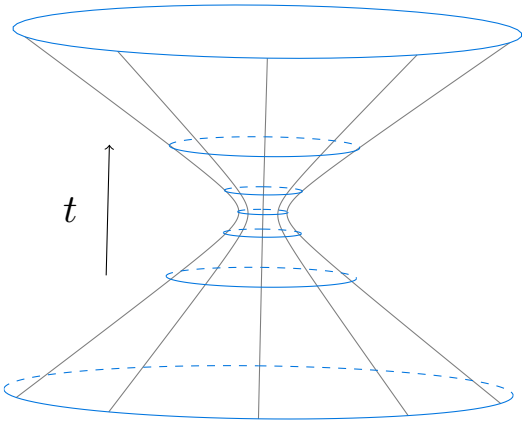

Figure 2.: Depiction of constant time slices (blue) and lines of constant angle (gray) in global coordinates

Definition 2.1 (Global coordinates in d-dimensional de Sitter spacetime)
In d-dimensional de Sitter spacetime global coordinates are defined as

$$\begin{aligned} x_0 &= \ell \sinh(\tau/\ell) \\ x_j &= \ell \omega_j \cosh(\tau/\ell), \quad j = 1, 2, \ldots, d, \end{aligned}$$

where $\tau \in \mathbb{R}$ is the temporal variable and the angular variables ω_i are defined according to

$$\begin{aligned} \omega_1 &= \cos(\theta_1), \\ \omega_2 &= \sin(\theta_1)\cos(\theta_2), \\ &\vdots \\ \omega_{d-1} &= \sin(\theta_1)\cdots\sin(\theta_{d-2})\cos(\theta_{d-1}), \\ \omega_d &= \sin(\theta_1)\cdots\sin(\theta_{d-2})\sin(\theta_{d-1}), \end{aligned}$$

where $0 \leq \theta_j < \pi$ for $1 \leq j < d-1$ and $0 \leq \theta_{d-1} < 2\pi$.

In the two-dimensional case, which will be important for the majority of this thesis, this simplifies to a description with one temporal coordinate τ and one spatial coordinate θ:

$$\vec{x}_G(\tau, \theta) = \begin{pmatrix} \ell \sinh(\tau/\ell) \\ \ell \cos(\theta) \cosh(\tau/\ell) \\ \ell \sin(\theta) \cosh(\tau/\ell) \end{pmatrix}$$

The constant time slices and lines of constant angle embedded in $2+1$ dimensional Minkowski spacetime are depicted in figure 2. The (induced) metric of dS_2 in global coordinates is

$$ds^2 = -d\tau^2 + \ell^2 \cosh^2(\tau/\ell) d\theta^2 \qquad g_{\mu\nu} = \begin{pmatrix} -1 & 0 \\ 0 & \ell^2 \cosh^2(\tau/\ell) \end{pmatrix} \tag{2.3}$$

Conformal coordinates directly follow from global coordinates by rescaling the temporal coordinate. The corresponding metric is conformally equivalent to the Minkowski metric. Two conformally equivalent metrics $g_{\mu\nu}$ and $h_{\mu\nu}$ have to satisfy the relation

$$h_{\mu\nu} = \Omega^2 g_{\mu\nu}$$

where Ω is a real-valued smooth function often referred to as the conformal factor. Conformal transformations are angle-preserving but can highly distort distances, which is why conformal coordinates are often very practical to work with but counterintuitive when it comes to length scales.

The intuition for visualizing conformal coordinates is that we take global coordinates, rescale the time to a finite interval, and cut the spacetime open along one angle as depicted in figure 3. This way, we can describe the entire spacetime in a coordinate frame of finite size, which we can mold into a rectangular shape. It is important to remember that this depiction is highly distorted, which affects the interpretation of distances and is less intuitive than the global coordinate setting. Since we can work in this rectangular frame and without further restrictions due to the hyperboloid condition, these coordinates are often easier to work with than global coordinates.

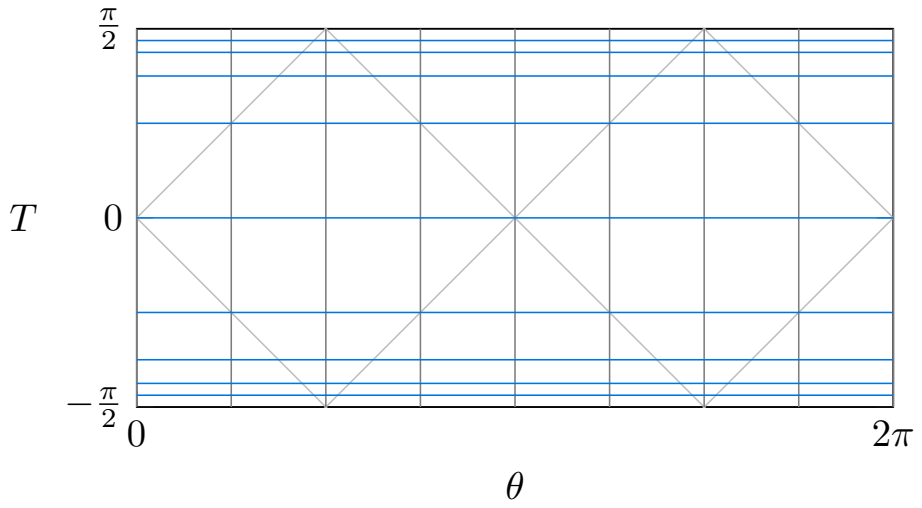

Figure 3.: Depiction of constant time slices (blue) and lines of constant angle (gray) in conformal coordinates

Definition 2.2 (Conformal coordinates)
Conformal coordinates have the same spatial coordinate(s) as the global coordinates defined in 2.1. The temporal coordinate T in conformal coordinates is rescaled with respect to the temporal coordinate τ from global coordinates such that it is defined on a finite interval $-\frac{\pi}{2} \leq T \leq \frac{T}{2}$ as follows:

$$\cosh(\tau/\ell) = \frac{1}{\cos T}$$

The metric takes the following form in conformal coordinates:

$$ds^2 = \frac{\ell^2}{\cos^2 T}(-dT^2 + d\theta^2) \qquad g_{\mu\nu} = \frac{\ell^2}{\cos^2 T}\begin{pmatrix} -1 & 0 \\ 0 & 1 \end{pmatrix} \tag{2.4}$$

We can directly see that this is conformally equivalent to the Minkowski metric with a conformal factor $\Omega = \frac{\ell}{\cos T}$.

The third coordinate system we will introduce is *static coordinates*. We are interested in this coordinate frame because the physics accessible to a local observer can be best described in static coordinates, as recently argued in [Wit23]. The physics of a local observer in a static patch follows similar rules we are familiar with from flat spacetime. The time evolution of a local observer in de

Sitter is (locally) captured by static coordinates. The reason a static patch captures the physics of a local observer best is that there is no globally timelike Killing field in de Sitter but a timelike Killing field in one static patch. Killing fields are the infinitesimal generators of isometries, in this case, time translation. We will go into further detail on that in section 2.3.

Definition 2.3 (static coordinates)
In $(1+1)$-dimensional de Sitter spacetime, static coordinates are defined as follows:

$$\vec{x}_S(r,t) = \begin{pmatrix} \sqrt{\ell^2 - r^2}\sinh(t/\ell) \\ \pm\sqrt{\ell^2 - r^2}\cosh(t/\ell) \\ r \end{pmatrix} \tag{2.5}$$

Static coordinates have a singularity at $r^2 = \ell^2$, which divides the spacetime into four different regions, as seen in figure 4. This coordinate singularity corresponds to the event horizon of an observer located at $r = 0$ whose trajectory follows a Killing vector field and is identified with the boundary of the corresponding static patch. The boundaries of the static patches at $r^2 = \ell^2$ are horizons that are a natural product of the expansion of de Sitter. A *static patch* is the part covered by static coordinates that describes the region causally accessible to a local observer in de Sitter and, later in this thesis, is also referred to as a causal diamond. The static coordinates for $r^2 < \ell^2$ describe the static patches, and the sign in $\vec{x}_S(r,t)$ determines the choice of the static patch. The expansion of spacetime also leads to two remaining regions outside the static patches, which we refer to as future ($t > 0$) and past ($t < 0$). To describe the entire spacetime, the static coordinates for different regions in de Sitter must be patched across the coordinate singularities. This can be found in the literature (e.g., [BMS01]) and will be further investigated in section 3.7. In the conformal coordinate setting, we can describe de Sitter without an embedding space. The direct relation between these settings for static coordinates is derived in appendix A.2:

$$T = \pm\,\mathrm{arcsec}\left(\pm\sqrt{r^2 - (-1+r^2)\sec^2\tilde{T}}\right)$$

$$\theta = \pm\arccos\left(\pm\frac{\sec(\tilde{T})}{\sqrt{\sec^2(\tilde{T}) - \frac{r^2}{r^2-1}}}\right)$$

This can be inverted to

$$r = \pm\sec T\sin\theta$$

$$\tilde{T} = \pm\,\mathrm{arcsec}\left(\pm\frac{\cos\theta}{\sqrt{\cos^2 T - \sin^2\theta}}\right)$$

The metric of static coordinates (for both static patches) is

$$ds^2 = \left(-1 + \frac{r^2}{\ell^2}\right)dt^2 + \frac{\ell^2}{\ell^2 - r^2}dr^2 \qquad g_{\mu\nu} = \begin{pmatrix} -1 + \frac{r^2}{\ell^2} & 0 \\ 0 & \frac{\ell^2}{\ell^2 - r^2} \end{pmatrix} \tag{2.6}$$

It needs to be noted that the choice of the static patches is not unique due to the rotational symmetry. The two static patches are always located at opposing sides of the spacetime, but both can shifted to a different location. If a local observer is considered, they are usually chosen in a fashion that the observer is located at $r = 0$ in one static patch.

Any static spacetime has a global timelike Killing field and *Cauchy surfaces* Σ, which define constant time slices, which are hypersurfaces of the spacetime. The domain of dependence of the Cauchy surface has to be the entire spacetime manifold:

$$D(\Sigma) = \{p \in M : \text{every inextendible causal curve through } p \text{ intersects } \Sigma\} = M$$

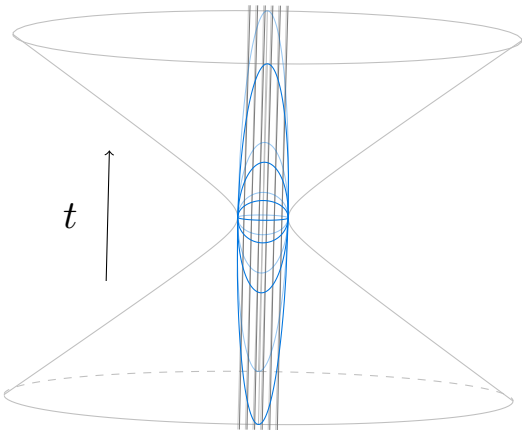

(a)

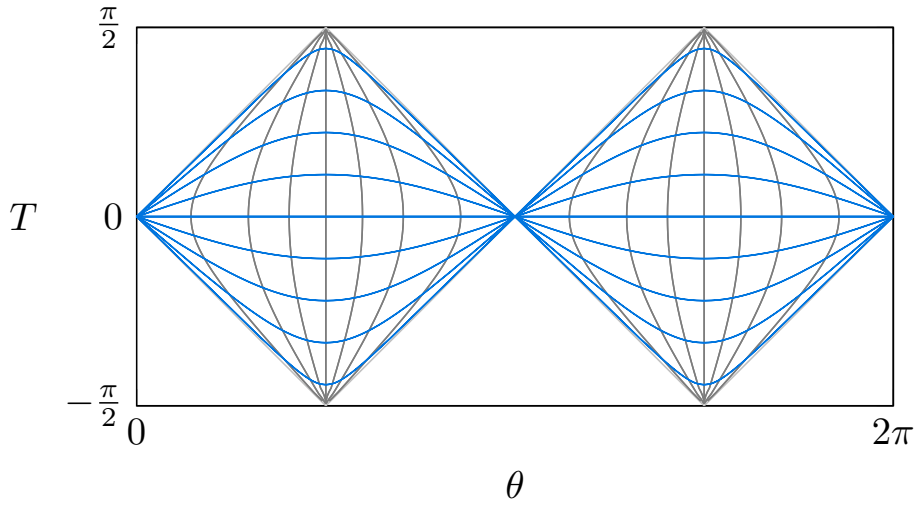

(b)

Figure 4.: Depiction of static coordinates inside the static patches in the setting of (a) global and (b) conformal coordinates: constant time slices (blue) and lines with constant r (gray).

We can obtain the metric intrinsic to the Cauchy surface by a restriction of the metric of the spacetime. The induced metric of the hypersurface is a scalar function in the $1+1$ dimensional case. For static coordinates, it follows the *induced metric* is (more details can be found in appendix A.3)

$$h_{rr} = g_{rr} = \frac{\ell^2}{\ell^2 - r^2} \tag{2.7}$$

The last coordinates we introduce are flat spacetime coordinates.

Definition 2.4 (flat spacetime coordinates)
In the $3+1$ dimensional case (which is the case usually covered in the literature), *flat spacetime coordinates* are defined as

$$\begin{aligned} x^0_F &= \ell \sinh(t/\ell) + \frac{1}{2\ell} \exp(t/\ell)(x^2 + y^2 + z^2) \\ x^1_F &= \exp(t/\ell) x \end{aligned}$$

$$\begin{aligned} x_F^2 =& \exp(t/\ell) y \\ x_F^3 =& \exp(t/\ell) z \\ x_F^4 =& \ell \cosh(t/\ell) - \frac{1}{2\ell} \exp(t/\ell)(x^2 + y^2 + z^2) \end{aligned}$$

These coordinates only cover half of the de Sitter hyperboloid. Moreover, they satisfy the hyperboloid condition. The metric induced in the de Sitter hyperboloid is known as the spatially flat Friedman-Lemaitre-Robertsen-Walker (FLRW) metric

$$\mathrm{d}s^2 = -\mathrm{d}t^2 + (e^{t/\ell})^2 \big(\mathrm{d}x^2 + \mathrm{d}y^2 + \mathrm{d}z^2\big) \tag{2.8}$$

This FLRW metric has scale factor $a(t) = \exp(Ht)$ with the Hubble constant $H = \dot{a}/a = 1/\ell$. We can introduce the conformal time $\eta = -\ell \exp\big(-\frac{t}{\ell}\big)$ to obtain a metric that is conformally equivalent to the Minkowski metric with a conformal factor $\Omega = \frac{\ell}{\eta}$:

$$\mathrm{d}s^2 = \frac{\ell^2}{\eta^2} \big(-\mathrm{d}\eta^2 + \mathrm{d}x^2 + \mathrm{d}y^2 + \mathrm{d}z^2\big)$$

The coordinate time η runs from $-\infty$ to 0 with a coordinate singularity at $\eta = 0$. In these coordinates, a trajectory with constant spatial coordinates (x, y, z) is a geodesic.

The Christoffel symbols, as well as the Ricci tensor and Ricci scalar for the coordinate systems introduced in this section, are calculated in appendix A.4. In all cases, the Ricci curvature takes the constant positive value of $R = \frac{2}{\ell^2}$, which is necessary for de Sitter spacetime.

2.3. Killing fields in two-dimensional de Sitter spacetime

A *Killing vector field* ξ^a is an infinitesimal generator of a one-parameter group of isometries. An *isometry* on a spacetime is a distance preserving diffeomorphism that leaves the metric of the spacetime invariant [Wal84, p. 438]. As a generator of isometries, Killing fields also generate time translations and thus define the notion of time. For Minkowski spacetime, we consider the "time direction" for some global family of inertial observers to correspond to the Killing field $\xi^a = \partial_t^a$. The *Killing time* is defined by the Killing field and defines the notion of time for a local observer. Accordingly, the notion of time can differ for different Killing fields.

A solution of Einstein's equations is invariant under translations along the Killing field if and only if the Killing equation is true. This is particularly interesting because de Sitter spacetime (unlike Minkowski) does not have a globally timelike Killing field. To find the Killing fields, we need to solve the Killing equation

$$\nabla_a \xi_b + \nabla_b \xi_a = 0 \tag{2.9}$$

which takes the following coordinate form (the equivalence is shown in appendix A.5.1):

$$g_{\alpha\beta,\mu}\xi^\mu + g_{\delta\beta}\xi^\delta{}_{,\alpha} + g_{\alpha\delta}\xi^\delta{}_{,\beta} = 0. \tag{2.10}$$

In a maximally symmetric d dimensional spacetime, there exist $\frac{d}{2}(d+1)$ Killing fields, which is the case for both Minkowski and de Sitter spacetime. In $3+1$ dimensional Minkowski spacetime, the 10 Killing fields are one temporal and three spatial translations, three spatial rotations, and three Lorentz boosts. For the $1+1$ dimensional case, this reduces to a total of three Killing fields, which are a temporal and spatial translation as well as a boost, which is depicted in figure 5.
The major difference between de Sitter to Minkowski spacetime is that there is no globally timelike Killing field in de Sitter spacetime. The striking consequence is that there is no global positive

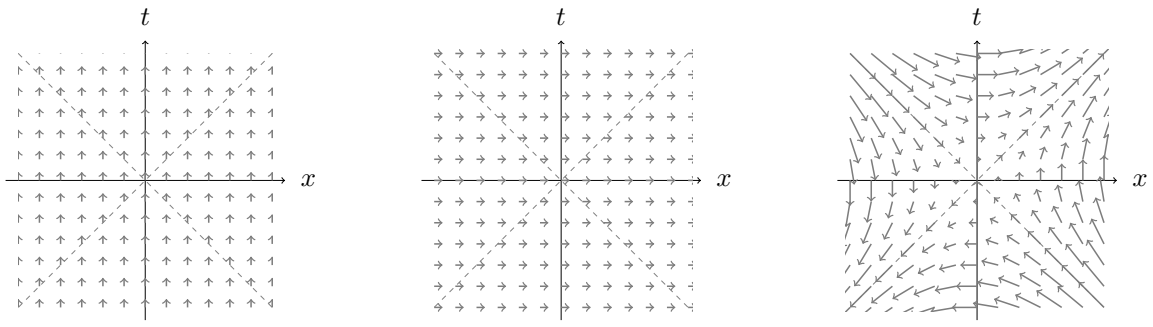

(a) (b) (c)

Figure 5.: Killing fields in $1+1$ dimensional Minkowski spacetime
(a) time translation, (b) space translation, and (c) boost

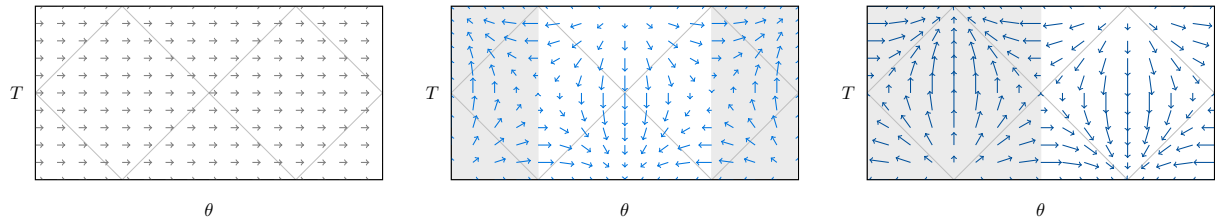

(a) (b) (c)

Figure 6.: Killing fields in 1+1 dimensional de Sitter spacetime

conserved energy quantity and no corresponding global Hamilton operator as discussed in [Wit01].

In the following, we calculate the Killing fields in $1+1$ dimensional de Sitter spacetime. For the de Sitter metric in conformal coordinates , we get the three Killing equations

$$\nabla_T \xi_T + \nabla_T \xi_T = 0 \tag{2.11}$$
$$\nabla_T \xi_\theta + \nabla_\theta \xi_T = 0 \tag{2.12}$$
$$\nabla_\theta \xi_\theta + \nabla_\theta \xi_\theta = 0 \tag{2.13}$$

These are solved by the following linear combination of Killing fields (as shown in appendix A.5.2):

$$\begin{aligned} \xi(T,\theta) &= \xi^T \partial_T + \xi^\theta \partial_\theta \\ \xi^T &= (a\cos\theta + b\sin\theta)\cos T \\ \xi^\theta &= (-a\sin\theta + b\cos\theta)\sin T + c \end{aligned}$$

This corresponds to the linear combination of the three Killing fields depicted in figure 6. The Killing field generating a translation in the angle (resulting in a rotation of the hyperboloid) is similar to the Killing field of Minkowski generating a rotation (or spatial translation, depending on the point of view). In de Sitter, we do not have a globally timelike Killing field, which is a striking difference from the flat spacetime case. We can see that things evolving with the Killing time are pushed forward in one part of the spacetime and pushed back in the antipodal region. It is important to note that de Sitter is not a static spacetime as the metric has an explicit time dependence [Wal84]. The only part of de Sitter spacetime that is static is the static patches. Accordingly, the notion of time generated by Killing vector fields differs on opposing parts of the

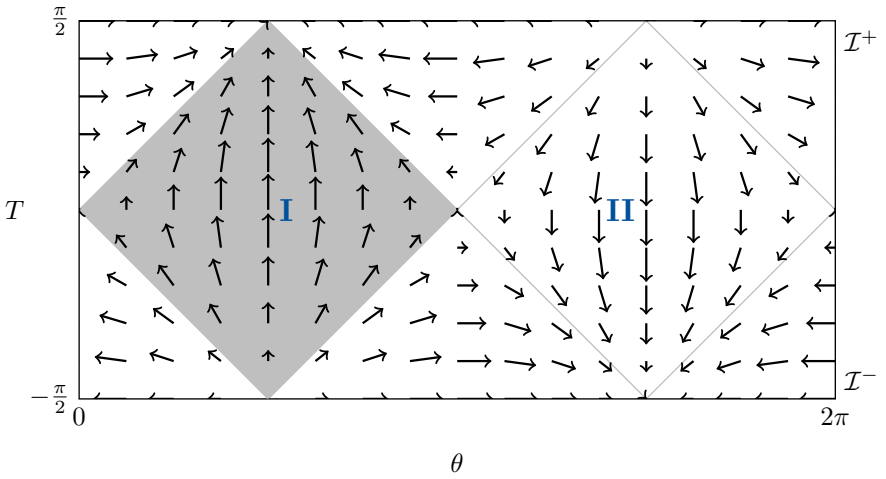

Figure 7.: Killing field de Sitter: the different notion of time in the two static patches

spacetime and, therefore, in static patch I and II. While the time runs forward in one patch, it runs backward in the other, as described in [Wit23]. This leads to the phenomenon that the notion of time in de Sitter depends on the position in spacetime. Time running in different directions in different parts of spacetime does not cause conflict for a local observer because both static patches are causally disconnected.

Since the static patches take this special role, we will look at the timelike Killing fields in one static patch in static coordinates. The Killing fields in static coordinates are

$$\begin{aligned}\xi^t(t,r) =& c - \frac{\ell^2 r}{\sqrt{r^2-\ell^2}}\left(ae^{t/\ell} + be^{-t/\ell}\right)\\ \xi^r(t,r) =& \sqrt{r^2-\ell^2}\left(ae^{t/\ell} + be^{-t/\ell}\right)\end{aligned}$$

which is derived in appendix A.5.3. The Killing field for $a = b = 0$ is only pointing in the time direction and does not change the spatial coordinate r:

$$\xi(t,r) = \xi^t\partial_t + \xi^r\partial_r = c\partial_t$$

Accordingly, trajectories with constant r are Killing trajectories.

2.4. Three spacetime trajectories and their geodesic properties

It is interesting to look at different trajectories of observers in different situations. Here, we will emphasize three different choices of trajectories. The first is the null geodesics, and the remaining two originate from global and static coordinates by fixing the spatial coordinate, respectively. We will describe the different properties and check which of these trajectories is a geodesic.
A free particle that does not experience any proper acceleration moves on a geodesic, which satisfies the geodesic equation of motion [Wal84, eq. (4.3.1)]

$$u^a\nabla_a u^b = 0$$

Geodesics can be interpreted as the straightest possible lines in spacetime and are, therefore, an important tool to describe and analyze its structure. The geodesic equation can be expressed in

a coordinate basis [Wal84, eq. (3.3.5)] as follows

$$\frac{d^2x^\mu}{dt^2} + \sum_{\sigma,\nu} \Gamma^\mu{}_{\sigma\nu} \frac{dx^\sigma}{dt}\frac{dx^\nu}{dt} = 0$$

2.4.1. Null geodesics

Null geodesics describe the propagation of light rays, which is a limiting factor for the propagation of information. The main reason we are interested in *null geodesics* is that they are an important tool for understanding causal properties of spacetime.

The null geodesics in d dimensional de Sitter spacetime may be constructed from null geodesics in $(d+1)$-dimensional Minkowski spacetime by imposing the hyperboloid constraint from eq. (2.2). In Minkowski spacetime, null geodesics are straight lines. In $1+1$ dimensional de Sitter spacetime with de Sitter radius $\ell = 1$, the null geodesics embedded in Minkowski spacetime can be parametrized as follows:

$$x(s) = \begin{pmatrix} x_0 \\ x_1 \\ x_2 \end{pmatrix} = \begin{pmatrix} s \\ u \pm vs \\ v \mp us \end{pmatrix}, \quad s \in \mathbb{R},\, u^2 + v^2 = 1.$$

The explicit relation between the embedding coordinates and the parameters u and v is derived in appendix A.6.1. The condition $u^2 + v^2 = 1$ is obtained from applying the hyperboloid condition, which can be done in matrix form:

$$x^T \eta x = 1, \quad \text{with } \eta = \mathrm{diag}(-1, 1, \cdots, 1). \tag{2.14}$$

We now see that the constraint $u^2 + v^2 = 1$ on the parameters of the null geodesic $x(s)$ arises as follows:

$$\begin{aligned} x^T(s)\eta x(s) &= -s^2 + (u \pm vs)^2 + (v \mp us)^2 \\ &= -s^2 + (u^2 + v^2) + s^2(u^2 + v^2) = 1. \end{aligned}$$

Since we obtained the null geodesics from a restriction from the Minkowski spacetime, we know that the null geodesics in de Sitter are also straight lines. In each point in two-dimensional de Sitter spacetime, there are two possible null geodesics: the left-moving and the right-moving null geodesic. Therefore, each null geodesic is specified by its intersection point with the time slice $x_0 = 0$ and a sign. The sign distinguishes between the two different classes of null geodesics, which we call *anticlockwise*- and *clockwise*-pointing null geodesics, respectively (sometimes also referred to as left- and right-moving null geodesics). This is depicted in Fig. 8, where one observes the direction of propagation around the spatial coordinate of the null geodesic on the hyperboloid either clockwise or anticlockwise. These null geodesics rule the two-dimensional de Sitter hypersurface. Because the parameters for the clockwise and anticlockwise pointing null geodesics only differ by a sign, in the sequel, we usually only consider the anticlockwise case as a representative of null geodesics in general. The calculations are very similar for clockwise-pointing null geodesics and yield identical results. It is also possible to derive the geodesics directly in the different parametrizations of the de Sitter metric.

2.4.2. Zero momentum geodesics

We consider a family of trajectories with a fixed angle in global coordinates:

$$\begin{pmatrix} \tau(s) \\ \theta(s) \end{pmatrix} = \begin{pmatrix} \tau(s) \\ \theta_j \end{pmatrix} \tag{2.15}$$

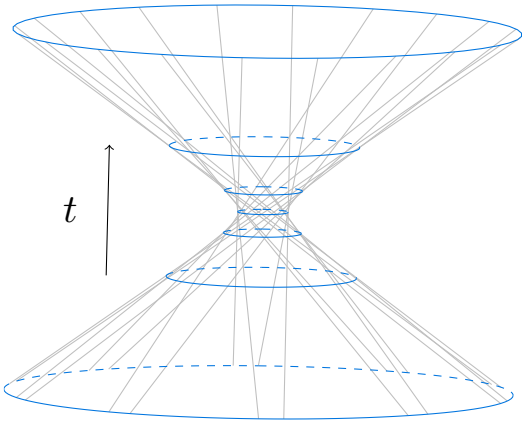

Figure 8.: dS_2 embedded in Minkowski spacetime where gray lines are null geodesics and blue circles are constant time slices

The gray lines in figure 2 are some representatives of this family of trajectories. It is shown in appendix A.6.2 that these trajectories satisfy the geodesic equation. These trajectories are the *zero momentum geodesics*.

In this parametrization of global coordinates, the coordinate time already equals the proper time, which can be directly seen with the tangent vector of the trajectory $T^\mu = (1, 0)$ and the time component of the metric $g_{\tau\tau} = -1$. When looking at the proper distance of trajectories with different constant angles, we need to calculate the respective proper distance for an (arbitrary) equal time slice where the tangent vector pointing along this equal time slice is $S^\mu = (0, 1)$:

$$l = \int_{\theta_A}^{\theta_B} \sqrt{g_{ab} S^a S^b} \mathrm{d}\theta = \int_{\theta_A}^{\theta_B} \sqrt{g_{\theta\theta}} \mathrm{d}\theta = \int_{\theta_A}^{\theta_B} \ell \cosh(\tau/\ell) \mathrm{d}\theta = \ell \cosh(\tau/\ell)(\theta_B - \theta_A)$$

Even for small displacements in the angle, we can see that the proper distance between the trajectories diverges for $\tau \to \infty$, which is an effect of the expansion of spacetime. Despite the fact that the proper distance increases with time, the proper acceleration vanishes. As a result, these trajectories are zero-momentum geodesics.

2.4.3. Killing trajectories

The timelike Killing trajectories in one static patch (derived in appendix A.5.3) are trajectories in static coordinates with constant spatial coordinate r:

$$\begin{pmatrix} t(s) \\ r(s) \end{pmatrix} = \begin{pmatrix} t(s) \\ r_j \end{pmatrix} \qquad 0 < s < \pi \tag{2.16}$$

These trajectories are only geodesics for $r_j = 0$ (as elaborated in appendix A.6.3). This is a fundamental difference from the flat spacetime scenario, where the Killing field generating time translations also follows geodesics. With its proper time τ, this family of geodesics can be expressed as

$$x_r(\tau) = \begin{pmatrix} \tau/\sqrt{1 - r_j^2/\ell^2} \\ r_j \end{pmatrix}$$

This trajectory has a proper acceleration

$$a_\mu a^\mu = \frac{\ell^2}{\ell^2 - r_j^2} \frac{r_j^2}{\ell^4}$$

We can interpret this as a family of trajectories which all have a constant r coordinate, which we will call r_j. This family of trajectories is important to look at because these trajectories follow the Killing field, which generates the time evolution in this static patch. We can directly see that the proper acceleration vanishes only for $r_j = 0$, which is also the only member of this family of trajectories that is a geodesic. In general, the proper acceleration of a particle in a static patch on a trajectory of this family is non-vanishing. The closer the trajectory is to the boundary of the static patch, the larger the acceleration becomes. In the limit of $r_j \to \pm\ell$, the acceleration diverges.

We can evaluate the proper distance between two members of this family of geodesics at the same (but arbitrary) time. For this, we need the vector, which is tangent to the constant time slice, which is $S^\mu = (0, 1)$. The proper distance is

$$\begin{aligned} l =& \int \sqrt{g_{ab} S_r^a S_r^b} dr = \int_{r_A}^{r_B} \sqrt{g_{rr} S_r^r S_r^r} dr = \int_{r_A}^{r_B} \sqrt{\frac{\ell^2}{\ell^2 - r^2}} dr \\ =& \ell \left[\arctan\left(\frac{r_B}{\sqrt{\ell^2 - r_B^2}} \right) - \arctan\left(\frac{r_A}{\sqrt{\ell^2 - r_A^2}} \right) \right] \end{aligned}$$

We can see that this distance (even though the expression is somewhat lengthy) remains constant at all times. This is one of the reasons why we refer to these as static trajectories, where the proper acceleration of a local observer on the trajectory compensates for the effect of the expansion of spacetime. Some of these Killing trajectories are depicted as gray lines in figure 4. Due to the exponential growth of de Sitter spacetime, the local observer sees a cosmological horizon.

With this fundamental knowledge of classical gravitational properties in de Sitter spacetime, chapter 3 puts focus on different quantizations of a quantum scalar field on a de Sitter background. For this, we use the coordinates introduced in this chapter for the quantizations of the field.

Chapter 3

Quantum scalar fields and vacuum states of de Sitter spacetime

In this chapter, we will focus on the quantization of the scalar field in de Sitter spacetime. A pivotal distinction in the quantization of scalar fields between curved spacetime and the flat spacetime scenario is the absence of a universally preferred method for defining a vacuum state in curved spacetime [Ful73]. Consequently, the appropriate vacuum state can vary for different settings. Bogoliubov transformations serve as a mechanism to connect and relate these diverse quantizations. In this chapter, we will introduce different vacuum states that correspond to different quantizations of spacetime.

In Minkowski spacetime, and more broadly in static spacetimes, a natural set of modes exists that gives rise to a preferred vacuum state. This preference stems from the spacetime's symmetry properties, which have the following effect: For any inertial observer, we can unambiguously divide the mode functions into their positive and negative frequency parts and, with this, define a vacuum state as a state of lowest energy of the positive frequency solutions. The notion of positive and negative frequency is, as a result of this, defined with respect to the Killing time t as described in more detail in [Wal94]. The resulting state is regarded as the preferred vacuum state, with the annihilation operators for all frequencies annihilating in this state. Moreover, this vacuum state exhibits invariance under the Poincaré group. The concept of a particle is directly associated with the corresponding creation operators. In curved spacetime, the choice of coordinate changes the distribution into positive and negative modes and, therefore, also the chosen vacuum state and the interpretation of particles. This is a striking difference from the theory of general relativity, where the principles are formulated in a coordinate-independent way.

In curved spacetime, symmetries typically do not completely determine the vacuum state. While the group of isometry transformations in de Sitter spacetime aids in identifying a suitable state vector, as detailed in [PT09], a two-parameter ambiguity characterizes the determination of the vacuum state in de Sitter space. This ambiguity corresponds to a family of distinct de Sitter invariant vacua, as initially demonstrated in [Mot85, All85]. De Sitter spacetime is the maximally symmetric solution to the vacuum Einstein field equations with a positive cosmological constant. The symmetries in de Sitter spacetime are generated by the Killing fields derived in chapter 2.3. The resulting symmetry group comprised of rotations and Lorentz transformations is often referred to as the de Sitter symmetry group. For two-dimensional de Sitter spacetime, this is the symmetry group $\mathrm{SO}(1,2)$. The de Sitter symmetry group's role in defining a preferred vacuum state can be compared to the role the Poincaré group takes in the Minkowski setting.

In the following sections, we will derive the quantum scalar field of two-dimensional de Sitter spacetime in various coordinate settings and relate this to corresponding vacuum states. The

different Fock representations are related by Bogoliubov transformations which we will also review in this chapter.

3.1. Quantization of scalar fields and Bogoliubov transformations

The quantization of scalar fields in curved spacetime is described in the standard literature numerous times and is performed in close analogy to the Minkowski case (see, for example, [Wal94, MW07, PT09]). In this section, we will only cover the basic material that is relevant for the following chapters and largely follow [BD82]; for further information, the interested reader is referred to the literature. A quantum scalar field is expanded as

$$\hat{\phi}(x) = \int_{-\infty}^{\infty} \mathrm{d}\omega \Big(\hat{a}_\omega \phi_\omega(x) + \hat{a}_\omega^\dagger \phi_\omega^*(x) \Big) \tag{3.1}$$

where the mode functions $\phi_\omega(x)$ are solutions of the Klein-Gordon equation. The Klein-Gordon equation can be directly derived similar to the Lagrangian in flat spacetime. We consider the following generalized version of the Lagrangian

$$\mathcal{L} = \frac{1}{2}\sqrt{-g}\big(g^{\mu\nu}\partial_\mu\phi\partial_\nu\phi + m^2\phi^2 + \xi R\phi^2\big)$$

with $g = \det(g)$. The additional term ξR is added for renormalization as suggested in numerous references such as [CT68, Tug69, CCJ70, Par73]. Another reason for considering this additional term is that we obtain conformal invariance in the massless case $m = 0$ of an n dimensional spacetime for $\xi = \frac{n-2}{4(n-1)}$. In four dimensions, we get $\xi = \frac{1}{6}$, and in the two-dimensional case, we get $\xi = 0$. Since big parts of this thesis focus on the two-dimensional case, we will often neglect the additional term ξR. Another way to get a Klein-Gordon equation similar to the flat case is to introduce an effective mass $m_{\text{eff}} = \sqrt{m^2 + \xi R}$, which absorbs the additional term. We derive the Klein-Gordon equation with the variational principle

$$\delta S = 0 \qquad \text{with} \qquad S = \int \mathrm{d}^n x \mathcal{L}(\phi, \nabla\phi, g_{\mu\nu})$$

which for arbitrary m and ξ leads to the following equation of motion[1] which is derived in appendix B.1

$$\big(\Box - m^2 - \xi R\big)\hat{\phi} = 0 \tag{3.2}$$

where $\Box$ is the d'Alembert operator defined with covariant derivatives

$$\Box = g^{\mu\nu}\nabla_\mu\nabla_\nu = \frac{1}{\sqrt{-g}}\partial_\mu\big(\sqrt{-g}\partial^\mu\big) \tag{3.3}$$

The equivalence of the two expressions in eq. (3.3) is demonstrated in appendix B.2. To determine solutions to the field equations, we must address the equation of motion (3.2). The initial step involves selecting a coordinate system. The chosen coordinates should facilitate the separation of the field equation using a product ansatz, enabling the solution for the field modes $\phi_\omega(x)$. These mode functions need to be normalized with respect to the *Klein-Gordon inner product*, as defined, for instance, in [BD82, PT09]

$$(\phi, \psi)_g = \mathrm{i}\int_\Sigma \mathrm{d}\Sigma\sqrt{h}(\phi^*(x)\nabla_a\psi(x) - \psi(x)\nabla_a\phi^*(x))n^a \tag{3.4}$$

[1] The sign arises from the metric's signature, with the convention of a negative time signature commonly used in General Relativity. This choice differs from the majority of Quantum Field Theory references.

where we integrate over a spacelike hypersurface Σ with n^a being a future directed unit vector orthogonal to Σ and $\mathrm{d}\Sigma$ being the volume element of the hypersurface. In a globally hyperbolic spacetime, we use a Cauchy surface as the hypersurface Σ. The value of the inner product eq. (3.4) is independent of the explicit choice of Σ, which was shown in [HE75] using the Gauss divergence theorem. To be a complete set of normalized solutions, the mode functions ϕ_ω have to satisfy

$$(\phi_\omega, \phi_{\tilde{\omega}})_g = \delta_{\omega,\tilde{\omega}}. \tag{3.5}$$

The corresponding creation and annihilation operators are time-independent and have to satisfy the usual commutation relations

$$\left[\hat{a}_\omega, \hat{a}^\dagger_{\tilde{\omega}}\right] = \delta_{\omega,\tilde{\omega}}, \qquad [\hat{a}_\omega, \hat{a}_{\tilde{\omega}}] = 0, \qquad \left[\hat{a}^\dagger_\omega, \hat{a}^\dagger_{\tilde{\omega}}\right] = 0. \tag{3.6}$$

With the conditions from eq. (3.5) and eq. (3.6), we ensure that the quantum scalar field follows the equal time commutation relations

$$\left[\hat{\phi}(t,\vec{x}), \hat{\pi}(t,\vec{y})\right] = \mathrm{i}\delta(\vec{x}-\vec{y}), \quad \left[\hat{\phi}(t,\vec{x}), \hat{\phi}(t,\vec{y})\right] = 0 \quad \text{and} \quad [\hat{\pi}(t,\vec{x}), \hat{\pi}(t,\vec{y})] = 0$$

where $\hat{\pi}(x)$ is the conjugate momentum field defined as $\hat{\pi}(x) = \partial_\tau \hat{\phi}(x)$. From this, we can directly define the corresponding vacuum state, which is the state annihilated by all positive frequency modes

$$\hat{a}_\omega |\Omega\rangle = 0 \qquad \forall\omega.$$

There is no unique or preferred way to quantize a scalar field: different choices of coordinates lead to different quantization and different creation and annihilation operators. This then results in different representations in Fock space as well as physically different vacuum states. The transformation between the different Fock representations of a scalar field is performed with a *Bogoliubov transformation*, which is described in the standard literature such as [BD82]. Consider the scenario where the field from eq. (3.1) has an alternative valid quantization:

$$\hat{\phi} = \int_{-\infty}^{\infty} \mathrm{d}\omega \Big(\hat{a}_\omega \phi_\omega(x) + \hat{a}^\dagger_\omega \phi^*_\omega(x)\Big) = \int_{-\infty}^{\infty} \mathrm{d}\omega \Big(\hat{b}_\omega \psi_\omega(x) + \hat{b}^\dagger_\omega \psi^*_\omega(x)\Big)$$

The relationship between the creation and annihilation operators $\hat{a}_\omega$ and $\hat{b}_\omega$ as well as the mode functions ϕ_ω and ψ_ω is described through the Bogoliubov transformation as follows:

$$\begin{aligned} \hat{a}_\omega &= \int d\sigma \Big(\alpha_{\sigma\omega}\hat{b}_\sigma + \beta^*_{\sigma\omega}\hat{b}^\dagger_\sigma\Big) & \hat{b}_\omega &= \int d\sigma \Big(\alpha^*_{\omega\sigma}\hat{a}_\sigma - \beta^*_{\omega\sigma}\hat{a}^\dagger_\sigma\Big) \\ \phi_\omega &= \int d\sigma (\alpha^*_{\sigma\omega}\psi_\sigma - \beta_{\sigma\omega}\psi^*_\sigma) & \psi_\omega &= \int d\sigma (\alpha_{\omega\sigma}\phi_\sigma + \beta_{\omega\sigma}\phi^*_\sigma). \end{aligned} \tag{3.7}$$

The *Bogoliubov coefficients* α and β are defined by

$$\begin{aligned} \alpha_{\sigma\omega} &= (\psi_\sigma, \phi_\omega) \\ \beta_{\sigma\omega} &= -(\psi_\sigma, \phi^*_\omega). \end{aligned}$$

These coefficients possess the following properties

$$\begin{aligned} \int \mathrm{d}\sigma (\alpha_{\mu\sigma}\alpha^*_{\nu\sigma} - \beta_{\mu\sigma}\beta^*_{\nu\sigma}) &= \delta_{\mu\nu} \\ \int \mathrm{d}\sigma (\alpha_{\mu\sigma}\beta_{\nu\sigma} - \beta_{\mu\sigma}\alpha^*_{\nu\sigma}) &= 0. \end{aligned}$$

The different creation and annihilation operators define (in general) different vacuum states for the different representations of the quantum scalar field, which we label with the corresponding index

$$\hat{a}_\omega \left|0_a\right\rangle = 0$$
$$\hat{b}_\omega \left|0_b\right\rangle = 0.$$

This not only results in physically distinct vacuum states but also gives rise to a different conceptualization of particles, which is intricately linked to the creation and annihilation operators. By definition, there are no "a-particles" in the vacuum state $|0_a\rangle$. However, this vacuum state encompasses "b-particles." The quantification of the number of "b-particles" in the ω-mode of the "a-vacuum" can be determined through the following procedure:

$$\left\langle 0_a\right| \hat{b}^\dagger_\omega \hat{b}_\omega \left|0_a\right\rangle = \int \mathrm{d}\nu \left|\beta_{\nu,\omega}\right|^2.$$

In the quantization of scalar quantum fields, the Killing time serves as a fundamental tool for constructing quantum scalar fields within a stationary spacetime. The Hilbert space is intentionally selected as a subspace comprising solutions, which exhibit positive frequency when Fourier analyzed along the orbits of the timelike Killing field ξ^a, aligning with the Killing time t. The classification of mode functions into positive and negative frequency modes is accomplished with respect to a chosen timelike Killing field ξ responsible for generating the time evolution. Positive frequency mode functions ϕ_ω satisfy the following relation with respect to the Lie derivative:

$$\mathcal{L}_\xi \phi_\omega = -\mathrm{i}\omega\phi_\omega, \qquad \omega > 0.$$

The *Lie derivative* evaluates the change of ϕ_ω along the Killing field ξ. The positive frequency mode functions ϕ_ω annihilate the corresponding vacuum state $\hat{a}_\omega \left|0_a\right\rangle$. For the sets of positive frequency solutions ψ_ω to also annihilate the same vacuum state, they must be linear combinations of the mode functions ϕ_ω (excluding their conjugates). Consequently, different sets of mode functions share a common vacuum state only if they are linear combinations of one another. From eq. (3.7), it is evident that the modes are linearly independent only when $\beta_{\omega\sigma} \neq 0$. In such cases, it is also feasible to express the annihilation operators as linear combinations of one another.

Distinct notions of vacuum states also exist in flat spacetime, with a key distinction being the consensus on a preferred vacuum state, known as the Minkowski vacuum. All inertial observers universally measure this preferred vacuum state. The agreement on the Minkowski vacuum is possible because both the set of all inertial observers and the Minkowski vacuum state remain invariant under the Poincaré group. In curved spacetime, one is forced to accept the absence of a preferred vacuum state in the general setting. The acknowledgment of this absence necessitates an acceptance that there is no unique definition of particles, given that the definition of a particle is inherently linked to the vacuum state. Depending on the specific context, exploring different vacuum states can prove useful. It is crucial to bear in mind that the vacuum states discussed in the following chapters represent deliberate *choices* arising from the process of quantization.

3.2. Unruh effect in flat spacetime: Accelerated observer

In this section, we will consider the fundamental properties of the *Unruh effect* originally published in [Unr76]. Due to its close relation to publications by Davies [DFU76] and Fulling [Ful73], it is sometimes also referred to as the Fulling–Davies–Unruh effect. The central result is that a uniformly accelerated observer in quantum field theory perceives a vacuum state as a thermal bath of particles with a temperature depending on the acceleration. This result can be explained

through different Fock representations related to the Bogoliubov transformation of an inertial and accelerated observer, which leads to different notions of particles.

The Unruh effect describes how an accelerated observer perceives a state that has been prepared in an inertial frame in Minkowski spacetime. This effect has been widely studied in the literature and we will give a review in this section. Results on the Unruh effect were first published in [Unr76] and presented in a mathematically rigorous way in [Wal94]. A more intuitive approach can be found in [BD82, CHM08]. Here, we will find a middle ground between these approaches.

The acceleration of the observer has two major consequences: The Killing field, which describes the trajectory of the accelerated observer and thus characterizes its time evolution, is no longer globally timelike, and the Rindler horizon restricts the events the observer can see. The most famous Unruh effect result is that the accelerated observer perceives the Minkowski vacuum as a thermal state. In the following, we will sketch the fundamental properties of the Unruh effect and go over concepts that are important for the following work. For calculating the Unruh effect, we basically need two steps: the Bogoliubov transformation, which changes the Fock representation from the inertial Minkowski spacetime to the accelerated frame, and then the partial trace, which implements the restriction to the area causally accessible to the accelerated observer. Preliminary material of quantum scalar fields and Bogoliubov transformations are covered in chapter 3.2 as well as in the standard literature.

We start out in Minkowski spacetime with the metric $\eta_{\mu\nu} = -dt^2 + dx^2$ with the corresponding d'Alembert operator

$$\Box = -\partial_t^2 + \partial_x^2.$$

The quantum scalar field in Minkowski spacetime is expanded as follows in the $1+1$ dimensional case[2]:

$$\hat{\phi} = \int_{-\infty}^{\infty} dk \Big(\hat{a}_k \phi_k(t,x) + \hat{a}_k^\dagger \phi_k^*(t,s) \Big) \tag{3.8}$$

with the mode functions

$$\phi_k = \frac{1}{\sqrt{4\pi\omega_k}} e^{\mathrm{i}kx - \mathrm{i}\omega t} = \frac{1}{\sqrt{4\pi\omega_k}} e^{\mathrm{i}kx - \mathrm{i}|k|t}.$$

This field can be separated into the left- and right-moving parts of the field, which do not interact with one another: $\phi_-(u)$ which is only dependent on $u = t + x$ and $\phi_+(v)$ which is only dependent on $v = t - x$.

$$\begin{aligned}
\hat{\phi} =& \int_0^\infty \frac{dk}{\sqrt{4\pi|k|}} \Big(\hat{a}_{-k} e^{-\mathrm{i}|k|t - \mathrm{i}kx} + (\hat{a}_{-k})^\dagger e^{\mathrm{i}|k|t + \mathrm{i}kx} + \hat{a}_k e^{-\mathrm{i}|k|t + \mathrm{i}kx} + (\hat{a}_k)^\dagger e^{\mathrm{i}|k|t - \mathrm{i}kx} \Big) \\
=& \int_0^\infty \frac{dk}{\sqrt{4\pi|k|}} \phi_k^-(u) + \int_0^\infty \frac{dk}{\sqrt{4\pi|k|}} \phi_k^+(v) \\
=& \hat{\phi}_-(u) + \hat{\phi_+}(v)
\end{aligned}$$

This way, we can separate the scalar field into its left- and right-moving parts, which can be discussed separately. We will proceed to discuss the Unruh effect only for $\phi_k^+(v)$, which is the left-moving part of the field. This discussion can easily be generalized to the right-moving part, which behaves identically. The field is divided into the positive and negative frequency part,

[2] The typical signature of the metric used in the standard literature differs in the context of general relativity and quantum field theory. Throughout the thesis, we remain consistent with the signature of the metric, which is why we deviate slightly from the convention in QFT.

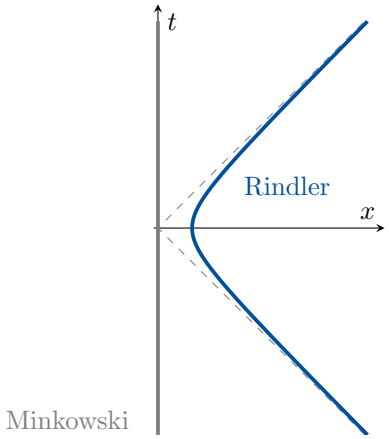

Figure 9.: Trajectory of Minkowski and Rindler observer in Minkowski spacetime

which is characterized with respect to the Killing time. The mode functions ϕ_k are of positive frequency with respect to the timelike Killing field ∂_t. These are the frequencies to annihilate a Minkowski vacuum state:

$$\hat{a}_p \left|\Omega_M\right\rangle = 0 \quad \forall p \tag{3.9}$$

We consider an inertial observer in Minkowski spacetime preparing the Minkowski vacuum state. A second observer with uniform acceleration is often referred to as the *Rindler observer*. The Rindler observer often plays the role of the detector and is depicted in figure 9. We introduce co-moving coordinates η and ξ to describe the Rindler observer with acceleration a:

$$\begin{aligned} t =& \frac{e^{a\xi}}{a}\sinh(a\eta) \\ x =& \frac{e^{a\xi}}{a}\cosh(a\eta) \\ ds^2 =& -dt^2 + dx^2 = e^{2a\xi}\left(-d\eta^2 + d\xi^2\right). \end{aligned}$$

Accordingly, the metric corresponding to the co-moving coordinates of the Rindler observer is conformally equivalent to the Minkowski metric, and the field equation is solved by the following mode function:

$$\chi_k = \frac{1}{\sqrt{4\pi\omega_k}} e^{\mathrm{i}k\xi \pm \mathrm{i}\omega\eta} \qquad \omega = |k| > 0, \quad -\infty < k < \infty \tag{3.10}$$

where the "+"-case corresponds to the left and the "−"-case to the right Rindler wedge. Similar to the Minkowski case, this can be separated into the left- and right-moving parts.
The Killing fields generating time in the Minkowski and Rindler setting are depicted in figure 10. The Killing field generating time evolution in the Rindler setting is a Lorentz boost

$$b^a = \alpha[X(\partial/\partial T)^a + T(\partial/\partial X)^a].$$

A stationary observer in this setting follows the orbits of b^a corresponding to the accelerated Minkowski observer, where the acceleration varies from orbit to orbit. This Killing field is timelike in a globally hyperbolic region[3] with $|t| < x$ which is often referred to as the *Rindler wedge* as depicted in figure 11. The Rindler wedge is the area causally accessible to the Rindler observer. The left and right Rindler wedges are considered separately; we can construct a quantum scalar

[3] A globally hyperbolic region is defined by having a Cauchy surface as characterized for example in [Wal84, p. 201] or [Wal94, p. 56].

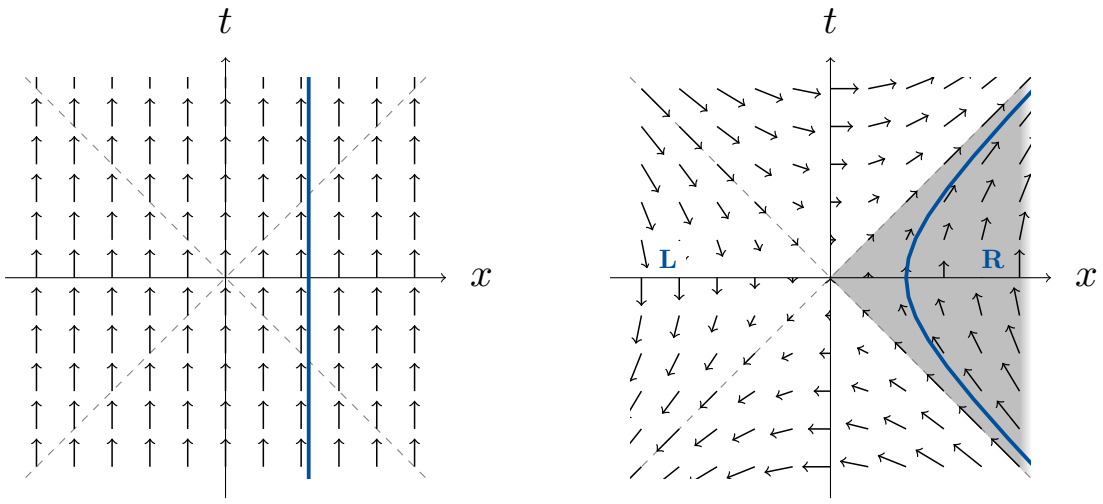

(a) (b)

Figure 10.: Killing field generating time evolution
(a) as time translation in Minkowski spacetime and
(b) as a Lorentz boost in Rindler spacetime

field with the time imposed by the Killing field in the Rindler wedges as they each have a (negative) globally timelike Killing field. The Hilbert spaces corresponding to the left and right wedge are considered separately, and their respective Fock spaces are constructed.

This different notion of time manifests in the Rindler modes χ_k in eq. (3.10) and the sign change in the time coordinate. The Rindler modes are of positive frequency with respect to the co-moving coordinate time η. We can define these mode functions in the left and right Rindler wedge:

$$\chi_k^R = \begin{cases} \frac{1}{\sqrt{4\pi\omega_k}} e^{ik\xi - i\omega\eta} & \text{in Rindler wedge } R \\ 0 & \text{in Rindler wedge } L \end{cases}$$

$$\chi_k^L = \begin{cases} 0 & \text{in Rindler wedge } R \\ \frac{1}{\sqrt{4\pi\omega_k}} e^{ik\xi + i\omega\eta} & \text{in Rindler wedge } L \end{cases}$$

These sets of mode functions are complete in the left and right Rindler wedge, respectively, but not in the entire Minkowski spacetime. However, they can be analytically continued to be extended to the other wedge. This way, they also describe the future and past where a then becomes imaginary. The mode functions can be used to expand the Rindler quantum scalar field as

$$\hat{\phi} = \int_{-\infty}^{\infty} dk \left(\hat{b}_k^L \chi_k^L + (\hat{b}_k^L)^\dagger (\chi_k^L)^* + \hat{b}_k^R \chi_k^R + (\hat{b}_k^R)^\dagger (\chi_k^R)^* \right) \tag{3.11}$$

The field expansions in eq. (3.8) and eq. (3.11) are quantizations for the same field. However, the different Fock expansion yields a Rindler vacuum state, which is different from the Minkowski vacuum state defined in eq. (3.9):

$$\hat{b}_k^L |\Omega_R\rangle = \hat{b}_k^R |\Omega_R\rangle = 0 \qquad \forall k.$$

These vacuum states are different because the Rindler modes also contain negative frequency Minkowski modes, and the mixing of positive and negative frequency modes changes the vacuum

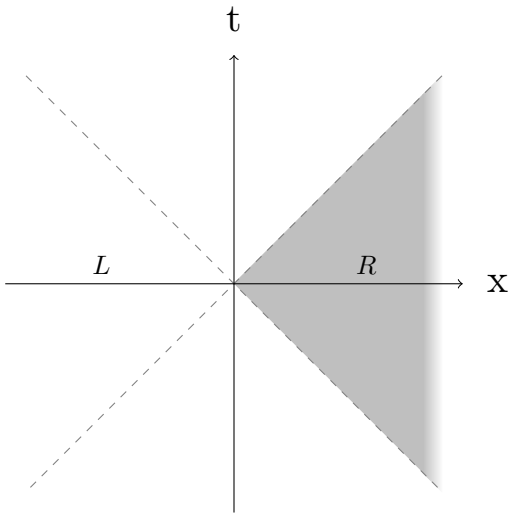

Figure 11.: Schematic representation of left and right Rindler wedge

state. Following [Unr76], we can write down the linear combinations of Rindler mode functions from eq. (3.10) to obtain mode functions that are analytic and bounded in Minkowski spacetime:

$$\begin{aligned}\tilde{\phi}_k^{(1)} =& \chi_k^R + e^{-\pi\omega/a}(\chi_{-k}^L)^* \\ \tilde{\phi}_k^{(2)} =& (\chi_{-k}^R)^* + e^{\pi\omega/a}\chi_k^L\end{aligned} \tag{3.12}$$

which can be inverted to

$$\begin{aligned}\chi_k^L =& \frac{1}{2\sinh(\pi\omega/a)}\left(\tilde{\phi}_k^{(2)} - (\tilde{\phi}_{-k}^{(1)})^*\right) \\ \chi_k^R =& \frac{1}{2\sinh(\pi\omega/a)}\left(e^{\pi\omega/a}\tilde{\phi}_k^{(1)} - e^{-\pi\omega/a}(\tilde{\phi}_{-k}^{(2)})^*\right).\end{aligned}$$

The modes $\tilde{\phi}_k^{(1,2)}$ share the same positive frequency properties and accordingly also define the same Minkowski vacuum state. These modes are referred to as Unruh modes to provide an intermediate step between Minkowski and Rindler mode expansions. We can expand the scalar quantum field in terms of these Unruh modes $\tilde{\phi}_k^{(1,2)}$:

$$\hat{\phi} = \int_{-\infty}^{\infty} dk\left(\tilde{\phi}_k^{(1)}\hat{d}_k^{(1)} + \tilde{\phi}_k^{(2)}\hat{d}_k^{(2)} + (\tilde{\phi}_k^{(1)})^*(\hat{d}_k^{(1)})^\dagger + (\tilde{\phi}_k^{(2)})^*(\hat{d}_k^{(2)})^\dagger\right)$$

with

$$\hat{d}_k^{(1)}\left|\Omega_M\right\rangle = \hat{d}_k^{(2)}\left|\Omega_M\right\rangle = 0$$

The Bogoliubov transformation relating the creation and annihilation operators corresponding to the Rindler and Unruh modes, as calculated in appendix B.3, is

$$\begin{aligned}\hat{b}_k^L =& \frac{1}{\sqrt{2\sinh(\pi\omega/a)}}\left(e^{\pi\omega/(2a)}\hat{d}_k^{(2)} + e^{-\pi\omega/2a}(\hat{d}_k^{(1)})^\dagger\right) \\ \hat{b}_k^R =& \frac{1}{\sqrt{2\sinh(\pi\omega/a)}}\left(e^{\pi\omega/(2a)}\hat{d}_k^{(1)} + e^{-\pi\omega/2a}(\hat{d}_k^{(2)})^\dagger\right).\end{aligned}$$

The Rindler observer measures the following particles when seeing the Minkowski vacuum state:

$$\left\langle\Omega_M\right|(\hat{b}_k^L)^\dagger\hat{b}_k^L\left|\Omega_M\right\rangle = \frac{e^{-\pi\omega/a}}{2\sinh(\pi\omega/a)} = \frac{1}{e^{2\pi\omega/a}-1}$$

and similarly

$$\langle\Omega_M|\,(\hat{b}_k^R)^\dagger \hat{b}_k^R\,|\Omega_M\rangle = \frac{1}{e^{2\pi\omega/a}-1}.$$

The expectation value of measuring Rindler particles in the Minkowski vacuum equals that of a thermal bath with temperature $T = a/2\pi$ where the particle number measured in the left and right Rindler wedge is identical.

$$\left((\hat{b}_k^L)^\dagger \hat{b}_k^L - (\hat{b}_k^R)^\dagger \hat{b}_k^R\right)|\Omega_M\rangle = 0 \tag{3.13}$$

In order to see that the Minkowski vacuum state perceived by the Rindler observer in the right Rindler wedge is a thermal state, we need to express the Minkowski vacuum state in terms of Rindler modes (see appendix B.4)

$$|\Omega_M\rangle = \prod_k \left(\sqrt{1-e^{-2\pi\omega_k/a}}\sum_{n_k=0}^{\infty} e^{-\pi n_k\omega_k/a}\,|n_k,R\rangle\otimes|n_k,L\rangle\right)$$

The density matrix associated with a Rindler observer in the right wedge is obtained as follows:

$$\rho_R = \mathrm{tr}_L(|\Omega_M\rangle\langle\Omega_M|) = \prod_k\left(1-e^{-2\pi\omega_k/a}\right)\sum_{n_k=0}^{\infty} e^{-2\pi n_k\omega_k/a}\,|n_k,R\rangle\langle n_k,R|\,. \tag{3.14}$$

For comparison, the density matrix for free bosons with temperature $T = 1/\beta$ is

$$\rho_{\text{thermal}} = \sum_i e^{-\beta E_i}\,|\psi_i\rangle\langle\psi_i| = e^{-\beta\mathcal{H}}.$$

This result matches the form of the thermal density matrix in eq. (3.14) of the Rindler observer in the right wedge with a temperature

$$T = \frac{a}{2\pi}$$

where a is the acceleration of the Rindler observer, and the boost generator is the Hamiltonian.

3.3. Quantization of the massless scalar field: flat spacetime coordinates and the conformal vacuum state

In this chapter, we exploit that de Sitter spacetime can be expressed using the metric of a spatially flat FLRW metric introduced in eq. (2.8) where we largely follow [PT09]:

$$\mathrm{d}s^2 = -\mathrm{d}t^2 + a(t)^2(\mathrm{d}x^2+\mathrm{d}y^2+\mathrm{d}z^2)$$

with the scale factor

$$a(t) = \exp\left(\frac{t}{\ell}\right). \tag{3.15}$$

We consider the $3+1$ dimensional case here since this is the most relevant case for our universe and the most commonly studied case in the literature. It is straightforward to reduce this to the two-dimensional case we use in large parts of the rest of this thesis, but this indicates that many calculations can equally be performed in four dimensions. The calculations for the intermediate steps are detailed in appendix B.5. Firstly, we will provide a concise overview of the general spatially flat Friedmann-Lemaître-Robertson-Walker (FLRW) case. Later in this chapter, we will substitute the scale factor from de Sitter spacetime. To comprehend the behavior of the scalar

field, we examine the equation of motion from eq. (3.2). We specifically consider the conformally invariant case with the massless scalar field ($m = 0$) and $\xi = \frac{1}{6}$. In the spatially flat FLRW spacetime, the Ricci curvature scalar R is given by

$$R = 6\left(\frac{\dot{a}^2}{a^2} + \frac{\ddot{a}}{a}\right) = \frac{12}{\ell^2}..$$

The d'Alembert operator is defined in eq. (3.3). When expanded in FLRW coordinates, we obtain[4]

$$\Box\hat{\phi}(t,\vec{x}) = -\,a^{-3}\partial_t\big(a^3\partial_t\phi(t,\vec{x})\big) + a^{-2}(\partial_x^2+\partial_y^2+\partial_z^2)\hat{\phi}(t,\vec{x}). \tag{3.16}$$

With this, the field equation from eq. (3.2) takes the form

$$-a^{-3}\partial_t\big(a^3\partial_t\phi(t,\vec{x})\big) + a^{-2}(\partial_x^2+\partial_y^2+\partial_z^2)\phi(t,\vec{x}) - \left(\frac{\dot{a}^2}{a^2} - \frac{\ddot{a}}{a}\right)\phi(t,\vec{x}) = 0. \tag{3.17}$$

We introduce the conformal time η which is related to the physical time t as:

$$\eta(t) = \int^t \frac{\mathrm{d}t'}{a(t')}. \tag{3.18}$$

The introduction of this new temporal coordinate transforms the metric such that it is conformally equivalent to the Minkowski metric:

$$\mathrm{d}s^2 = a(\eta)^2\big(-\mathrm{d}\eta^2 + \mathrm{d}x^2 + \mathrm{d}y^2 + \mathrm{d}z^2\big). \tag{3.19}$$

The field equation with the conformal time η is

$$\frac{1}{a^2}\left[\partial_\eta^2 + 2\frac{a'}{a}\partial_\eta - (\partial_x^2+\partial_y^2+\partial_z^2) + \frac{a''}{a}\right]\phi(\eta,\vec{x}) = 0. \tag{3.20}$$

The metric and scalar field can be obtained directly by a conformal transformation of the Minkowski metric with the conformal factor $\Omega = a(\eta)^{-1}$ and the known scalar field in Minkowski spacetime we denote as $\chi(x)$:

$$\begin{aligned}\eta_{\mu\nu} =& \Omega^2(x)g_{\mu\nu} = a^{-2}(\eta)g_{\mu\nu}\\ \chi(x) =& \Omega^{-1}\phi(\eta,\vec{x}) = a(\eta)\phi(\eta,\vec{x}).\end{aligned} \tag{3.21}$$

The conformally transformed field equation is the well-known field equation for flat Minkowski spacetime, which in the massless case reads $\eta^{\mu\nu}\partial_\mu\partial_\nu\chi(x) = 0$. The conformal invariance implies that $\phi(t,\vec{x})$ is a solution to the field equation from eq. (3.19) given that $\chi(x)$ is a valid solution to the field equation in Minkowski spacetime, which is detailed in the appendix (proof 4).

The massless quantum scalar field in Minkowski spacetime is well known. We use its representation in the Schrödinger picture with time-independent creation and annihilation operators:

$$\hat{\chi}(\eta,\vec{x}) = \int \mathrm{d}^3k\Big(\hat{a}_{\vec{k}}f^M_{\vec{k}}(\eta,\vec{x}) + (\hat{a}_{\vec{k}})^\dagger f^M_{\vec{k}}(\eta,\vec{x})^*\Big)$$

with the positive frequency mode functions

$$f^M_{\vec{k}}(\eta,\vec{x}) = \frac{1}{(2\pi)^3\sqrt{2k}}e^{\mathrm{i}\vec{k}\cdot\vec{x}-\mathrm{i}k\eta}.$$

[4] As expected, this expression of the d'Alembert operator simplifies to the known case of flat spacetime for the scale factor $a = 1$.

The mode functions of the quantum scalar field ϕ can be directly obtained with the conformal factor:

$$f_{\vec{k}}(\eta,\vec{x}) = \Omega f^M_{\vec{k}}(\eta,\vec{x}) = a^{-1}(\eta) f^M_{\vec{k}}(\eta,\vec{x}).$$

With this the quantum scalar field $\hat{\phi}$ can be expanded as

$$\hat{\phi}(\eta,\vec{x}) = \int \mathrm{d}^3k \Big(\hat{a}_{\vec{k}} f_{\vec{k}}(\eta,\vec{x}) + (\hat{a}_{\vec{k}})^\dagger f_{\vec{k}}(\eta,\vec{x})^* \Big).$$

Since the mode functions $f_{\vec{k}}(\eta,\vec{x})$ and $f^M_{\vec{k}}(\eta,\vec{x})$ which are related by a conformal transformation are both positive frequency solutions, they generate the same vacuum state. This vacuum state is called the *conformal vacuum state*. The conformal vacuums state is defined as

$$\hat{a}_{\vec{k}} \left|\Omega_k\right\rangle = 0 \qquad \forall \vec{k}$$

This typically also is the chosen vacuum state for a massless de Sitter field.

3.4. Quantization of the massive scalar field: flat spacetime coordinates and the Bunch Davies vacuum state

We can now take a look at the massive quantum scalar field for de Sitter spacetime, which again follows [PT09]. First, we take a closer look at the scale factor from eq. (3.15). We will also explore how this scale factor transforms upon the introduction of conformal time η, which runs from $-\infty < \eta < 0$, as given in eq. (3.18).

$$\eta(t) = \int^t \frac{\mathrm{d}t'}{\exp\left(\frac{t'}{\ell}\right)} = -\ell \exp\left(-\frac{t}{\ell}\right) \qquad \Leftrightarrow \qquad t(\eta) = -\ell \log\left(-\frac{\eta}{\ell}\right)$$

For the scale factor, it follows that

$$a = \exp\left(\frac{t}{\ell}\right) = \exp\left(-\log\left(-\frac{\eta}{\ell}\right)\right) = -\frac{\ell}{\eta}.$$

These coordinates only cover half of de Sitter spacetime. We can cover the other half of the spacetime by extending the conformal time to positive η (with a coordinate singularity at $\eta = 0$). The line element of the metric takes the form

$$\mathrm{d}s^2 = \frac{\ell^2}{\eta^2}\left(-\mathrm{d}\eta^2 + \mathrm{d}x^2 + \mathrm{d}y^2 + \mathrm{d}z^2\right).$$

We take the general form of the field equation from eq. (3.2), where we substitute the known d'Alembert operator and scale factor. We obtain the following equation of motion for the massive de Sitter case:

$$-\partial_t^2\phi(t,\vec{x}) - \frac{3}{\ell}\partial_t\phi(t,\vec{x}) + e^{-2t/\ell}(\partial_x^2 + \partial_y^2 + \partial_z^2)\phi(t,\vec{x}) - \left(m^2 + \frac{2}{\ell^2}\right)\phi(t,\vec{x}) = 0. \tag{3.22}$$

We introduce a new parameter which acts as the effective mass that absorbs the curvature term:

$$M^2 = m^2 + \frac{1}{6}R = m^2 + \frac{2}{\ell^2}. \tag{3.23}$$

The quantum scalar field is expanded using mode functions and creation/annihilation operators:

$$\hat{\phi}(t,\vec{x}) = \int \mathrm{d}^3k \Big(\hat{a}_{\vec{k}} f_{\vec{k}}(t,\vec{x}) + (\hat{a}_{\vec{k}})^\dagger f_{\vec{k}}(t,\vec{x})^* \Big)$$

For the mode functions, we make the following product ansatz where we introduce the scale factor $a(t)$ in the normalization:

$$f_{\vec{k}}(t,\vec{x}) = \frac{1}{(2\pi)^3\sqrt{2a(t)^3}} \exp\left[\mathrm{i}\vec{k}\cdot\vec{x}\right] v_k(t).$$

The equation of motion from eq. (3.22) has to be valid for all mode functions. We introduce a new time coordinate, which increases as t decreases to transform the differential equation to a known form:

$$\tau = k\ell \exp(-t/\ell).$$

Upon substitution of the new time coordinate, we get the following equation of motion:

$$\tau^2\partial_\tau v_k(\tau) + \tau\partial_\tau v_k(\tau) + (\tau^2 - \nu^2)v_k(\tau) = 0 \tag{3.24}$$

with

$$\nu = \sqrt{\frac{17}{4} - m^2\ell^2} = \sqrt{\frac{9}{4} - M^2\ell^2}$$

where M is the effective mass from eq. (3.23). This is solved for $v_k(\tau)$ by the Bessel equation of first and second kind:

$$v_k(\tau) = a_k J_\nu(\tau) + b_k Y_\nu(\tau)$$

The normalization of the mode functions and the asymptotic behavior is discussed in detail in the appendix (proof 7 and proof 8). We can write the mode functions as

$$v_k(\tau) = \sqrt{\frac{\pi\ell}{2}}(J_\nu(\tau) + \mathrm{i}Y_\nu(\tau)) = \sqrt{\frac{\pi\ell}{2}}H_\nu^{(1)}(\tau),$$

, which can be expressed with the Hankel function of the first kind. With respect to the time t, this results in the following solution for the mode functions:

$$f_{\vec{k}}(t,\vec{x}) = \frac{1}{2}\frac{\sqrt{\pi\ell}\, e^{\mathrm{i}\vec{k}\cdot\vec{x}}}{(2\pi)^3\sqrt{a(t)^3}} H_\nu^{(1)}(k\ell\exp(-t/\ell)). \tag{3.25}$$

These mode functions determine the creation and annihilation operators that define a vacuum state known as the *Bunch-Davies vacuum*.

$$\hat{a}_{\vec{k}}\,|0_{BD}\rangle = 0 \qquad \forall\vec{k}$$

Due to the restrictions on the mode functions, this vacuum state is derived by considering the high-frequency asymptotic behavior of the quantum scalar field and imposing de Sitter invariance. It is worth noting that while the Bunch-Davies vacuum is not de Sitter invariant in the specific characterization of de Sitter invariance found in [All85], where a certain class of space- and time-reflections must map the full de Sitter group into itself, it is still often regarded as the most natural vacuum state for de Sitter spacetime. We cannot claim full invariance under the de Sitter group, as only seven out of the ten local isometry transformations are used to characterize this state.

It is interesting to highlight that when the Bunch-Davies state is restricted to the massless case, it is identical to the conformal vacuum state from the previous section. A detailed derivation of this equivalence can be found in [PT09].

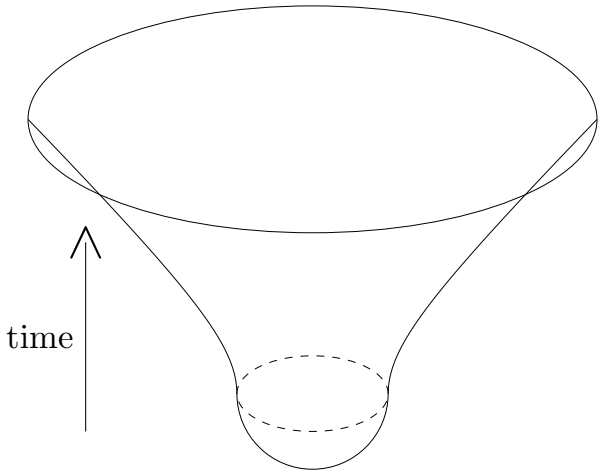

Figure 12.: Schematic depiction of the Hartle-Hawking state where the dashed circles mark $\tau = 0$.

3.5. Euclidean coordinates and the Hartle Hawking state

For many years, physicists have tried to find the *wave function of the universe*, which is often considered to be the solution to understanding quantum gravity. In 1983, Hartle and Hawking suggested a wave function that describes the quantum state of a spatially closed universe as a functional on the geometries of compact three-manifolds which obeys the Wheeler-DeWitt second-order functional differential equation [HH83]. The ground state of this wave function is called the *Hartle-Hawking state* and can be derived using path integral methods. Finding the wave function of the universe as the solution of the Wheeler-DeWitt equation and rigorously defining the Hartle-Hawking state as its ground state has many intricacies. It has been discussed in detail by Hartle and Hawking and in many follow-up publications such as [AHM21, BCT21, BH99, GH93, GS16, HHH19, HHH14, KPY22, Wal88]. We restrict our attention to a simplified definition of the most natural interpretation of the Hartle-Hawking state. In the original paper [HH83], the Hartle-Hawking state is defined by a path integral over the class of paths whose action vanishes in the far past. This is made more rigorous by a rotation to Euclidean time. One important physical property is that the Euclidean region of the HH state has no notion of time as we know it. Since time in its original sense did not exist then, it is not possible to answer the question of what happened before the big bang in this context.

For a more detailed discussion of the definition of Hartle-Hawking states, the reader is referred to the literature [HH83]. For our purposes, we consider a vacuum state where the Wick rotation of the time coordinate in the past is the defining property. The Wick rotation $\tau \to -\mathrm{i}\beta$ transforms the Lorentzian geometry of the hyperbolic spacetime in the past to Euclidean geometry as schematically depicted in figure 12. Due to the transformation to the Euclidean geometry, we will refer to the vacuum state defined by this Wick rotation as the *Euclidean vacuum state*. The resulting vacuum state acts on de Sitter spacetime at $\tau = 0$ (the bottleneck area).

Due to the geometry after the Wick rotation, we can construct the Euclidean vacuum state $|\Omega_E\rangle$ on the basis of spherical modes where we consider positive frequency modes to be the modes that are regular when analytically continued to the lower Euclidean hemisphere. The positive frequency Euclidean modes annihilate the Euclidean vacuum state. The explicit construction of these modes can be found in [BMS01], where we choose the regular solutions of the Klein-Gordon

equation on Euclidean de Sitter space. Here, we will sketch the basic idea of the construction.

For the construction of the modes annihilating the Euclidean vacuum state, we start with the two-dimensional de Sitter metric in global coordinates

$$\mathrm{d}s^2 = -\mathrm{d}\tau^2 + \ell^2 \cosh^2(\tau/\ell)\mathrm{d}\theta^2$$

and perform the Wick rotation $\tau \to -\mathrm{i}\beta$. The resulting metric is equivalent to the metric of a two-sphere in spherical coordinates with a constant radius ℓ:

$$\mathrm{d}s^2 = -\mathrm{d}(-\mathrm{i}\beta)^2 + \ell^2 \cosh^2(-\mathrm{i}\beta/\ell)\mathrm{d}\theta^2 = \mathrm{d}\beta^2 + \ell^2 \cos^2(\beta/\ell).\mathrm{d}\theta^2$$

The positive frequency Euclidean modes are the modes that are regular when analytically continued to the lower Euclidean hemisphere as described above. The explicit expression of the mode functions is derived in appendix B.6. In order to argue that the Euclidean vacuum state can be considered a state, we look at the time evolution of the system with Hamiltonian H:

$$U_\tau = e^{-\mathrm{i}H\tau} \mapsto e^{-\beta H}$$

under the Wick rotation $\tau \to -\mathrm{i}\beta$. We get an exponential function with a real exponent, which resembles the partition function from statistical mechanics. The imaginary time β appears in the same way as it does in statistical mechanics, where it is interpreted as the inverse temperature (where we set the Boltzmann constant $k_B = 1$). This makes it plausible that the vacuum state has thermal properties, which will be employed further later on in this thesis.

It was shown in [BMS01] that the Euclidean vacuum state and rescaled vacua acting at the past boundary of de Sitter spacetime are related via a Bogoliubov transformation. It was shown in [All85] that a family of de Sitter-invariant vacuum states, often referred to as α vacua, can be obtained from the Euclidean vacuum state. These α vacua are all related via Bogoliubov transformations, which yield physically equivalent vacuum states.

3.6. Quantization scalar field in static patch

The physics accessible to a local observer is best described in a static patch because there exists a Killing field in a static patch which is completely timelike. We consider static patches, which we call static patches I and II, which lie on opposing sites of the spacetime and therefore cover the entire spacetime at $t = 0$. Due to the rotational invariance, there is no preferred set of static patches. To obtain a description that is best suited for a local observer, we consider the static patch with the observer located at $r = 0$ as static patch I and the static patch on the antipodal side of the spacetime as static patch II. This allows for a description that is very well suited for a local observer rather than for global de Sitter spacetime. In this section, we will derive the quantum scalar field in the de Sitter static patches I and II. The metric tensor for de Sitter in a static patch is (see eq. (2.6))

$$g_{\mu\nu} = \begin{pmatrix} -1 + \frac{r^2}{\ell^2} & 0 \\ 0 & \frac{\ell^2}{\ell^2 - r^2} \end{pmatrix}.$$

The field equation of a quantum scalar field is given as

$$\left(\Box - m^2\right)\hat{\phi} = 0$$

where the d'Alembert operator in static coordinates can be expanded as

$$\Box = -\frac{\ell^2}{\ell^2 - r^2}\partial_t^2 - \frac{2r}{\ell^2}\partial_r + \left(1 - \frac{r^2}{\ell^2}\right)\partial_r^2.$$

This gives us the field equation in static coordinates:

$$\left(-\frac{\ell^2}{\ell^2-r^2}\partial_t^2-\frac{2r}{\ell^2}\partial_r+\left(1-\frac{r^2}{\ell^2}\right)\partial_r^2-m^2\right)\hat{\phi}=0. \tag{3.26}$$

This equation of motion has to be satisfied for all mode functions $\phi_\omega(t,r)$. The solutions to this field equation are derived using the product ansatz $\phi_\omega(t,r)=e^{-\mathrm{i}\omega t}f_\omega(r)$ in appendix B.7. There are two linearly independent solutions to the radial field equation:

$$\begin{aligned} f_\omega^1(r) =& P_l^n(r/\ell)=P_{-h_\pm}^{\pm\mathrm{i}\ell\omega}(r/\ell)\\ f_\omega^2(r) =& Q_l^n(r/\ell)=Q_{-h_\pm}^{\pm\mathrm{i}\ell\omega}(r/\ell)\end{aligned}$$

where we introduced the parameter

$$h_\pm=\frac{1}{2}\pm\sqrt{\frac{1}{4}-\ell^2m^2}.$$

For the two linearly independent solutions it follows that

$$\begin{aligned}\phi_\omega^1(t,r)=Ne^{-\mathrm{i}\omega t}f_\omega^1(r) =& Ne^{-\mathrm{i}\omega t}P_{-h_\pm}^{\mathrm{i}\ell\omega}\left(\frac{r}{\ell}\right)\\ \phi_\omega^2(t,r)=Ne^{-\mathrm{i}\omega t}f_\omega^2(r) =& Ne^{-\mathrm{i}\omega t}Q_{-h_\pm}^{\mathrm{i}\ell\omega}\left(\frac{r}{\ell}\right).\end{aligned} \tag{3.27}$$

The hypergeometric functions are a generalization of Legendre functions where we have imaginary orders. Especially for higher dimensions, the Hypergeometric functions are necessary to describe the de Sitter mode functions in static patches. Legendre functions and Hypergeometric functions can be related using identities from [AS64]. A substitution to transform the associated Legendre equation to the Hypergeometric equation is described in appendix proof 9. This allows us to express the mode functions as

$$\phi_\omega(t,r)=Ne^{-\mathrm{i}\omega t}\left(1-\frac{r^2}{\ell^2}\right)^{\mathrm{i}\ell\omega/2}{}_2F_1\left(\frac{1}{2}(h_++\mathrm{i}\ell\omega),\frac{1}{2}(h_-+\mathrm{i}\ell\omega),\frac{1}{2},\frac{r^2}{\ell^2}\right) \tag{3.28}$$

up to the normalization constant N. The normalization constant can be determined with the Klein-Gordon inner product.

To include the simplest possible case, we also look at the massless scalar field. For the massless scalar field, the radial equation of motion reduces to

$$\left(\left(1-\frac{r^2}{\ell^2}\right)\partial_r^2-\frac{2r}{\ell^2}\partial_r+\frac{\ell^2}{\ell^2-r^2}\omega^2\right)f_\omega(r)=0$$

which is solved by the two linearly independent solutions $f_\omega^1(r)$ and $f_\omega^2(r)$ which leads to the following solutions of mode functions:

$$\begin{aligned}\phi_\omega^1(t,r)=Ne^{-\mathrm{i}\omega t}f_\omega^1(r) =& \gamma e^{-\mathrm{i}\omega t}\exp(\mathrm{i}\ell\omega\,\mathrm{arctanh}(r/\ell))\\ \phi_\omega^2(t,r)=Ne^{-\mathrm{i}\omega t}f_\omega^2(r) =& \gamma e^{-\mathrm{i}\omega t}\exp(-\mathrm{i}\ell\omega\,\mathrm{arctanh}(r/\ell)).\end{aligned}$$

These also need to be normalized with respect to the Klein-Gordon inner product.

The field equation is identical in different static patches, which is why we have a quantization with the same mode functions in different static patches. To distinguish these, we add a label to denote in which patch the mode function lives. Following basic rules of quantizing scalar fields,

we introduce creation and annihilation operators that satisfy the usual canonical commutation relations

$$\left[\hat{a}_n^{\mathrm{I}}, (\hat{a}_m^{\mathrm{I}})^\dagger\right] = \delta_{mn} \qquad \left[\hat{a}_n^{\mathrm{II}}, (\hat{a}_m^{\mathrm{II}})^\dagger\right] = \delta_{mn}$$

to fully quantize the scalar field in the static patches I and II:

$$\hat{\phi}_{\mathrm{I}}(t,r) = \int_0^\infty d\omega \left[\hat{a}_\omega^{\mathrm{I}} \phi_\omega(r,t) + (\hat{a}_\omega^{\mathrm{I}})^\dagger \phi_\omega^*(r,t)\right]$$
$$\hat{\phi}_{\mathrm{II}}(t,r) = \int_0^\infty d\omega \left[\hat{a}_\omega^{\mathrm{II}} \phi_\omega(r,-t) + (\hat{a}_\omega^{\mathrm{II}})^\dagger \phi_\omega^*(r,-t)\right].$$

It needs to be noted that the time direction is imposed by the Killing field, which has opposite signs in two static patches on opposite sides of the spacetime. This is why we need to take into account that the time in the mode functions of static patch I and II has a relative negative sign. For the static patches, we define vacuum states with the following condition:

$$\begin{aligned} \hat{a}_n^{\mathrm{I}} \left|\Omega_{\mathrm{I}}\right\rangle &= 0 \\ \text{and} \qquad \hat{a}_n^{\mathrm{II}} \left|\Omega_{\mathrm{II}}\right\rangle &= 0 \qquad \forall n. \end{aligned}$$

It must be pointed out that these vacuum states, which are the vacuum states naturally associated with the static patches, are not de Sitter invariant, as described in [CT68]. In [BD82], it is even shown that the expectation value of the quantum field stress-tensor in this vacuum state diverges at the static patch boundary at $\ell = r$. This makes it necessary to associate a vacuum state to each observer in de Sitter such that the observer is located at $r = 0$.

3.7. Euclidean vacuum as linear combination of static patch modes

One compelling reason for utilizing the Euclidean vacuum stems from the convenience of expressing its modes as linear combinations of those derived in section 3.6 from the static patches I and II. In this section, we will review the construction of a linear superposition of the static patch modes, which covers the global de Sitter spacetime and can be identified with the Euclidean modes. For this, we follow the approach presented in [BMS01] (here, we simplify dS_3 to dS_2 and the generalization to arbitrary de Sitter radii ℓ). The intermediate steps are elaborated in appendix B.9. This expression of the vacuum state can also be found in [HY18], where the vacuum state is referred to as the Bunch-Davies vacuum.

To construct a solution across the entire spacetime, we need to match static patch solutions across the horizons between the regions inside and outside the static patches. To do this, we need to match the mode functions across the horizons. This is easiest done in *Kruskal coordinates* where we have no coordinate singularity. In the static patches, the relation between static and Kruskal coordinates is defined as

$$\frac{r}{\ell} = \frac{1+UV}{1-UV}$$
$$\frac{t}{\ell} = \frac{1}{2}\log\left(-\frac{U}{V}\right).$$

An overview of the different regions and the respective values and signs the Kruskal coordinates take is depicted in figure 13. The most crucial regions for combining different solutions are the horizons of the static patch at $r^2 = \ell^2$ (which in Kruskal coordinates implies $UV = 0$). We can directly calculate the metric inside the static patch in Kruskal coordinates (see proof 12)

$$\mathrm{d}s^2 = -4\ell^2 \frac{\mathrm{d}U\,\mathrm{d}V}{(UV-1)^2}. \tag{3.29}$$

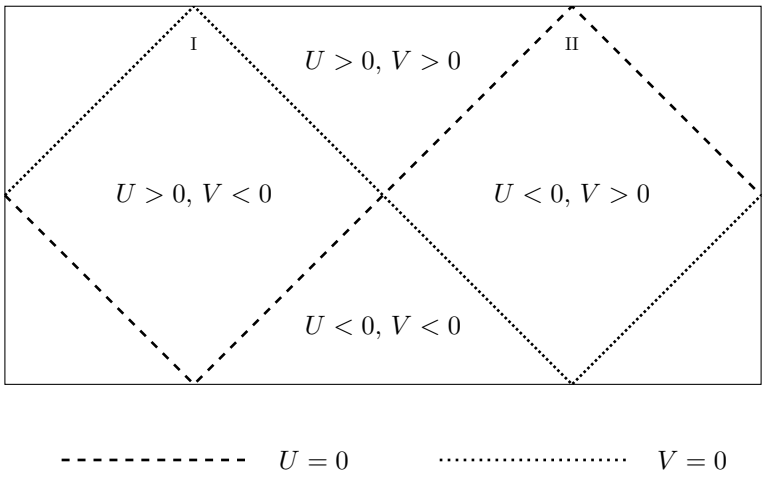

Figure 13.: Overview on different regions and the corresponding values of the Kruskal coordinates U and V inside the static patches ($r < \ell$), at the horizon ($r^2 = \ell^2$) and in the future (includes $\mathcal{I}^+$) and past (includes $\mathcal{I}^-$) region

We will now express the static patch mode functions from eq. (3.28) in Kruskal coordinates:

$$\begin{aligned}\phi_\omega(U,V) =& N\left(-\frac{U}{V}\right)^{-\mathrm{i}\omega\ell/2}\left(-\frac{4UV}{(UV-1)^2}\right)^{\mathrm{i}\ell\omega/2} {}_2F_1\left(\tfrac{1}{2}(h_+ + \mathrm{i}\ell\omega), \tfrac{1}{2}(h_- + \mathrm{i}\ell\omega), \frac{1}{2}, \left(\tfrac{1+UV}{1-UV}\right)^2\right)\\ =& N\left(-\frac{U}{V}\right)^{-\mathrm{i}\omega\ell/2} f_\omega(UV)\end{aligned} \tag{3.30}$$

The modes in static patch I and II are related by

$$\phi^{\mathrm{I}}_\omega(U,V) = \phi^{\mathrm{II}}_\omega(-U,-V).$$

As the signs of U and V cancel, the mode functions of the different static patches have the same form, but their area of support is different.

This section aims to write the Euclidean modes as a linear combination of modes from static patches I and II. For this, we need to define a linear combination of functions with different support regions, which can be related through an analytic continuation. One condition is that the positive frequency mode function is analytic in the lower complex U and V planes; this way, we get modes that are regular on the lower Euclidean hemisphere as shown in [BMS01]. This is achieved by analytically continuing the modes $\phi^{\mathrm{I}}_\omega(U,V)$ to the static patch II along the following contour:

$$\begin{aligned}U \to& e^{-\mathrm{i}\gamma}U,\\ V \to& e^{\mathrm{i}\gamma}V\end{aligned}$$

where γ runs from 0 to π. We can plug this into the mode functions from eq. (3.30) to get a continuation of the mode $\phi^{\mathrm{I}}_\omega(U,V)$. It needs to be noted that the product UV is independent of γ and, therefore, independent of the continuation performed above. We get

$$\phi_\omega(U,V) = N\left(-\frac{e^{-\mathrm{i}\gamma}U}{e^{\mathrm{i}\gamma}V}\right)^{-\mathrm{i}\omega\ell/2} f_\omega(UV) = Ne^{-\gamma\omega\ell}\left(-\frac{U}{V}\right)^{-\mathrm{i}\omega\ell/2} f_\omega(UV).$$

Using this analytic continuation where γ runs from 0 to π, the mode functions from the different static patches can be combined as follows to obtain mode functions with support in the same static patch, which are analytic in the lower Euclidean hemisphere:

$$\begin{aligned}\phi_\omega^{E1} =& \phi_\omega^{\mathrm{I}} + e^{-\pi\omega\ell}(\phi_\omega^{\mathrm{II}})^* \\ \phi_\omega^{E2} =& \phi_\omega^{\mathrm{II}} + e^{-\pi\omega\ell}(\phi_\omega^{\mathrm{I}})^*.\end{aligned}$$

These are both positive frequency Euclidean mode functions for $\omega > 0$, even though this is a linear combination of the positive frequency mode functions from one static patch and the negative frequency mode functions from the other patch. The reason for this is the different notions of time in the different static patches. These mode functions can be used to write down the expansion of the quantum scalar field

$$\hat{\phi} = \int_0^\infty d\omega \Big[\hat{a}_\omega^{E1}\phi_\omega^{E1} + \hat{a}_\omega^{E2}\phi_\omega^{E2} + (\hat{a}_\omega^{E1})^\dagger(\phi_\omega^{E1})^* + (\hat{a}_\omega^{E2})^\dagger(\phi_\omega^{E2})^*\Big] \tag{3.31}$$

where the Euclidean annihilation operators are related to the static patch operators via a Bogoliubov transformation as follows (this relation also is derived in [FPST94, (A.10)] for $\ell = 1$):

$$\begin{aligned}\hat{a}_\omega^{E1} =& \frac{1}{\sqrt{1-e^{-2\pi\omega\ell}}}\Big(\hat{a}_\omega^{\mathrm{I}} - e^{-\pi\omega\ell}(\hat{a}_\omega^{\mathrm{II}})^\dagger\Big) \\ \hat{a}_\omega^{E2} =& \frac{1}{\sqrt{1-e^{-2\pi\omega\ell}}}\Big(\hat{a}_\omega^{\mathrm{II}} - e^{-\pi\omega\ell}(\hat{a}_\omega^{\mathrm{I}})^\dagger\Big).\end{aligned} \tag{3.32}$$

The annihilation operators $\hat{a}_\omega^{E1}$ and $\hat{a}_\omega^{E2}$ as well as the mode functions ϕ_ω^{E1} and ϕ_ω^{E2} are identical except for the exchange of the labels for static patch I and II. Together with the corresponding creation operators $(\hat{a}_\omega^{E1})^\dagger$ and $(\hat{a}_\omega^{E2})^\dagger$ these operators satisfy the usual commutation relations (see proof 14)

$$\Big[\hat{a}_\omega^{E1}, (\hat{a}_{\omega'}^{E1})^\dagger\Big] = \delta_{\omega,\omega'}, \qquad \Big[\hat{a}_\omega^{E2}, (\hat{a}_{\omega'}^{E2})^\dagger\Big] = \delta_{\omega,\omega'} \tag{3.33}$$

with all other commutators vanishing.

The Euclidean vacuum state can be expressed as a linear combination of static patch modes as follows:

$$|\Omega_E\rangle = \prod_{\omega=0}^{\infty} \sqrt{1-e^{-2\pi\omega\ell}}\, e^{e^{-\pi\omega\ell}(\hat{a}_\omega^{\mathrm{I}})^\dagger(\hat{a}_\omega^{\mathrm{II}})^\dagger} |\Omega_{\mathrm{I}}\rangle \otimes |\Omega_{\mathrm{II}}\rangle = \prod_{\omega=0}^{\infty} U_\omega |\Omega_{\mathrm{I}}\rangle \otimes |\Omega_{\mathrm{II}}\rangle \tag{3.34}$$

where U_ω is a two-mode transformation acting on the modes ω in the static patches I and II. This vacuum state is also referred to as the Bunch-Davies vacuum state in [HY18, eq. (88)] (with some restrictions as we considered a lower dimensional case). It is shown that the Euclidean annihilation operators annihilate the Euclidean vacuum state in proof 15:

$$\hat{a}_\omega^{E1} |\Omega_E\rangle = \hat{a}_\omega^{E2} |\Omega_E\rangle = 0.$$

The generator of time evolution for a Euclidean vacuum state is easiest written down in terms of static patch creation and annihilation operators since the time runs forward in static patch I and backward in static patch II:

$$\mathcal{H}_E = \int_0^\infty d\omega\, \omega \Big[(\hat{a}_\omega^{\mathrm{I}})^\dagger \hat{a}_\omega^{\mathrm{I}} - (\hat{a}_\omega^{\mathrm{II}})^\dagger \hat{a}_\omega^{\mathrm{II}}\Big].$$

The Hamiltonian generating time translations can be expressed (see proof 16) using the Euclidean creation and annihilation operators as follows:

$$\mathcal{H}_E = \int_0^\infty d\omega\, \omega \Big[(\hat{a}_\omega^{E1})^\dagger \hat{a}_\omega^{E1} - (\hat{a}_\omega^{E2})^\dagger \hat{a}_\omega^{E2}\Big]. \tag{3.35}$$

When the Hamiltonian acts on the Euclidean vacuum state, we get the known relation for Hamiltonians acting on the ground state:

$$\mathcal{H}_E \left|\Omega_E\right\rangle = 0 \tag{3.36}$$

In this form, it is easy to see that the Euclidean vacuum has thermal properties as described in numerous references such as [EL03, BMS01]. We obtain a thermal density matrix in static patch I when taking the trace over the Hilbert space of static modes in patch II of the Euclidean vacuum state.

3.8. Wightman function

Wightman functions are correlation functions fundamental to QFT. An introduction can be found in [BD82]. The *Wightman function* is a tool to describe the propagation of field disturbances due to boundary conditions. One area where Wightman functions are of particular relevance to us is to see how well a vacuum state agrees with the no-particle state of a co-moving detector. We are interested in the Wightman function because it represents the bath of 'particles' that the detector effectively experiences as a result of its motion.

We want to derive the Wightman function, which is the positive frequency part of the Green's function given by

$$G^+(x,y) = W(x,y) = \langle\Omega|\, \hat{\phi}(x)\hat{\phi}(y)\, |\Omega\rangle$$

where the entire Green's function $\mathrm{i}G(x,y)$ and the Feynman propagator $\mathrm{i}G_F(x,y)$ are defined as

$$\begin{aligned}
\mathrm{i}G(x,y) &= \langle\Omega|\left[\hat{\phi}(x), \hat{\phi}(y)\right]|\Omega\rangle = G^+(x,y) - G^-(x,y) \\
\mathrm{i}G_F(x,y) &= \langle\Omega|\,\mathcal{T}\Big(\hat{\phi}(x)\hat{\phi}(y)\Big)\,|\Omega\rangle = \Theta(t_x - t_y)G^+(x,y) - \Theta(t_y - t_x)G^-(x,y)
\end{aligned}$$

with $\mathcal{T}$ being the time ordering operator and Θ the Heaviside function.As we consider the conformal vacuum state, we are interested in the massless case, where the Green functions are denoted by D instead of G. The Wightman function is obtained by inserting the mode decomposition for the quantum scalar field into the vacuum expectation value.

For a conformally coupled massless scalar field with the conformal vacuum state from section 3.3, the positive frequency Wightman function is evaluated to (see [BD82, eq. (3.59)])

$$D^+(x,x') = -\frac{1}{4\pi^2}\frac{1}{(x^0 - (x')^0 - \mathrm{i}\varepsilon)^2 - |\vec{x} - \vec{x}'|^2} \tag{3.37}$$

where $\vec{x}$ refers to the spatial part. The Wightman function up to first-order perturbations in ε of two observers following Killing trajectories is derived in appendix B.10:

$$W_{m,n}(s) = -\frac{\kappa_m\kappa_n}{16\pi^2}\frac{1}{\sinh^2(s/2 - \mathrm{i}\varepsilon) - b_{mn}}$$

with the new time variable $s = \kappa_m\tilde{\tau} - \kappa_n\tau$, the proper acceleration $\kappa_i = 1/\sqrt{\ell^2 - r_i^2}$ and the parameter

$$b_{mn} = -\frac{1}{2}\big(1 + \kappa_m r_m \kappa_n r_n - \kappa_m\kappa_n\ell^2\big) = \frac{1}{2}\Big(\kappa_m\kappa_n l^2 - \sqrt{\kappa_m^2\ell^2 - 1}\sqrt{\kappa_n^2\ell^2 - 1} - 1\Big) \tag{3.38}$$

The Wightman function takes the following form when expressed in terms of its Fourier modes (as derived in the appendix B.11):

$$W_{m,n}(s) = \frac{1}{\sqrt{2\pi}} \int_{-\infty}^{\infty} \widetilde{\mathcal{W}}_{m,n}\,(\omega) e^{\mathrm{i}\omega s} \mathrm{d}\omega = -\int_{-\infty}^{\infty} \frac{2a \sin\big(2\lambda \operatorname{arcsinh}\big(\sqrt{b_{mn}}\big)\big)}{\sqrt{b_{mn}(b_{mn}+1)}(e^{2\pi\lambda}-1)} e^{\mathrm{i}\lambda s} \mathrm{d}\lambda \tag{3.39}$$

Wightman functions are correlation functions between field operators at different points in spacetime. Using Bogoliubov transformations, the calculation of Wightman functions can be simplified by changing the Fock representation of the quantum scalar field and then calculating the correlation function of an easier (maybe trivial) quantum scalar field. Depending on the particular setup, it can have advantages to use either Bogoliubov transformations to relate different Fock representations or Wightman functions to calculate the correlation function between field operators directly.

In this chapter we reviewed the quantization of the scalar field in de Sitter spacetime and the corresponding vacuum state whose different Fock quantizations are related by Bogoliubov transformations. Together with the Wightman function, this provides a basis for part III of this thesis, where we discuss several aspects of the Unruh effect in the setting of de Sitter spacetime.

Chapter 4

Quantum Information methods

In this chapter, we will introduce some quantum information properties that will be relevant for the rest of this thesis. First, we review some basic material on tensors and tensor network notation in section 4.1 where we largely follow Bridgeman and Chubb [BC17]. In section 4.2, we review a holographic toy model that captures the AdS/CFT correspondence introduced by Pastawski, Yoshida, Harlow, and Preskill introduced in [PYHP15]. This toy model largely motivates the construction of the holographic toy model in de Sitter spacetime discussed in chapter 6. We also give a short review on quantum error correction and approximate cloning in sections 4.3 and 4.4.

4.1. Basics on tensor network notation

This section provides a brief review of tensors, tensor networks, and tensor network notation, which largely follows the paper by Bridgeman and Chubb [BC17]. A tensor is a fundamental building block of any tensor network. One important defining property of any *tensor* is its rank: The basic examples are a d-dimensional vector $v \in \mathbb{C}^d$ which is a rank-1 tensor and a $m \times n$ matrix $M \in \mathbb{C}^{m\times n}$ which is a rank-2 tensor. These motivate a more general definition of a rank-r tensor:

Definition 4.1 (tensor of rank r)
A tensor with dimensions $d_1 \times \cdots \times d_r$ which is element of $\mathbb{C}^{d_1\times\cdots\times d_r}$ is a rank-r tensor.

The rank of a tensor equals the number of indices of that tensor in index notation. In tensor network notation a single tensor is represented by some shape with legs sticking out the tensor. Each leg is associated with an index. Accordingly, the number of legs of the tensor also corresponds to the rank of the tensor. We will illustrate this with an example of a rank-4 tensor $X^{\rho}_{\sigma\mu\nu}$ which has the following representation in tensor network notation:

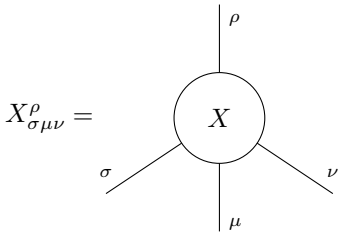

Here, we distinguish between lower and upper tensor legs similarly as we distinguish co- and contravariant indices in the Einstein index notation. We interpret lower tensor legs as incoming and upper tensor legs as outgoing tensor legs, which implies that the direction of time in tensor

network notation is upwards. The incoming and outgoing tensor legs are now associated with different Hilbert spaces, which we denote as $\mathfrak{h}_{\text{in}}$ and $\mathfrak{h}_{\text{out}}$. Each tensor is proportional to a map from $\mathfrak{h}_{\text{in}}$ to $\mathfrak{h}_{\text{out}}$.

This way, we can also interpret a *linear map* $T : \mathcal{H}_A \to \mathcal{H}_B$ as a tensor, which we can express both in index notation and tensor network notation. The linear map T takes the following form in index notation

$$T : |a\rangle \mapsto \sum_b T_{ba} |b\rangle$$

where $\{|a\rangle\}$ is a complete orthonormal basis of $\mathcal{H}_A$ and $\{|b\rangle\}$ is a complete orthonormal basis of $\mathcal{H}_B$.

In the rest of the chapter, we will introduce some basic properties and tensor operations relevant to the construction of the holographic network.

Definition 4.2 (Adjoint tensor)
A tensor $X^\dagger$ is adjoint to the tensor X and can be expressed in tensor network notation as follows: The upper and lower legs are flipped, such that the tensor is mirrored along the constant time slice it sits on.

$(X^\rho_{\sigma\mu\nu})^\dagger = X^{\sigma\mu\nu}_\rho =$ 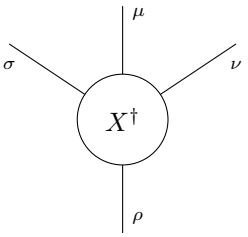

Definition 4.3 (Isometry)
An *isometry* is a linear map $V : \mathcal{H}_A \to \mathcal{H}_B$ between the Hilbert spaces $\mathcal{H}_A$ and $\mathcal{H}_B$ which preserves the inner product. A linear map is an isometry if and only if

$$\sum_b V^\dagger_{a'b} V_{ba} = \delta_{a'a}$$

Graphically, this can be expressed as

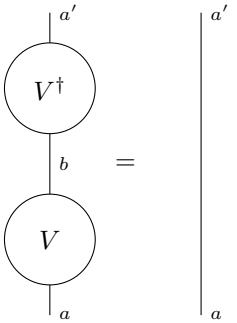

Definition 4.4 (Unitary)
A *unitary* is a linear map $U : \mathcal{H}_A \to \mathcal{H}_B$ between the Hilbert spaces $\mathcal{H}_A$ and $\mathcal{H}_B$ which is an isometry that satisfies the following condition:

$$U^\dagger U = U U^\dagger = \mathbb{1}$$

Definition 4.5 (Perfect tensor)
Perfect tensors are a special class of isometric tensors. A tensor $T_{a_1 \cdots a_n}$ with n indices is a *perfect tensor* if it is proportional to an isometric tensor from A to A^C for *any* bipartition of its indices into a set A and its complementary set A^C with $|A| \leq |A^C|$. This way, a perfect tensor is a special type of tensor with maximal entanglement along any bipartition. On an intuitive level, perfect tensors capture a discrete version of rotation invariance.

Definition 4.6 (Tensor product)
The *tensor product* is defined as the element-wise product of the values of each tensor component:

$$[A \otimes B]_{i_1,\cdots,i_r,j_1,\cdots,j_s} := A_{i_1,\cdots,i_r} \cdot B_{j_1,\cdots,j_s}$$

This is a generalization of the outer product of vectors. In tensor network notation, the tensor product is represented by placing two tensors next to each other:

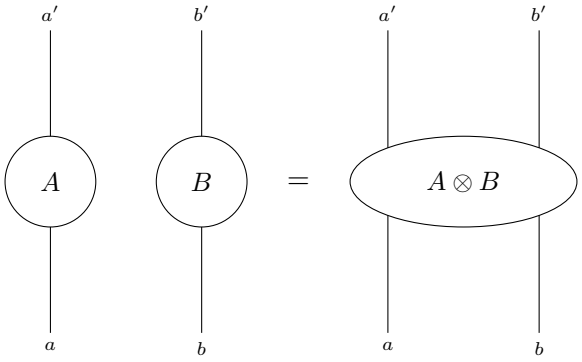

Definition 4.7 (Trace)
The (partial) *trace* is a joint summation over two indices of a given tensor that have the same dimension. The following example shows the trace operation for a tensor T where the dimensions d_x and d_y are equal:

$$\begin{aligned}&[\mathrm{tr}_{x,y}(A)]_{i_1,\cdots,i_{x-1},i_{x+1},\cdots i_r,j_1,\cdots,j_{y-1},j_{y+1},\cdots j_s} \\ &= \sum_{\alpha}^{d_x} A_{i_1,\cdots,i_{x-1},\alpha,i_{x+1},\cdots i_r,j_1,\cdots,j_{y-1},\alpha,j_{y+1},\cdots j_s}\end{aligned}$$

In tensor network notation, this is represented by joining the corresponding tensor legs:

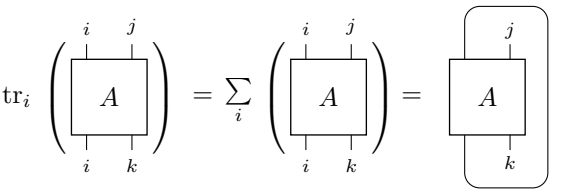

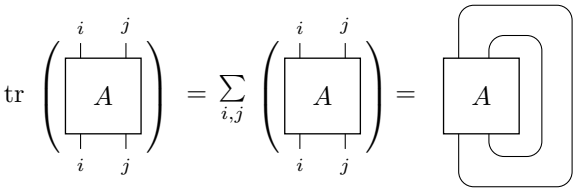

Definition 4.8 (Contraction)
A *contraction* is a tensor product followed by a trace between corresponding indices of the two tensors. In tensor network notation, this can be represented as follows:

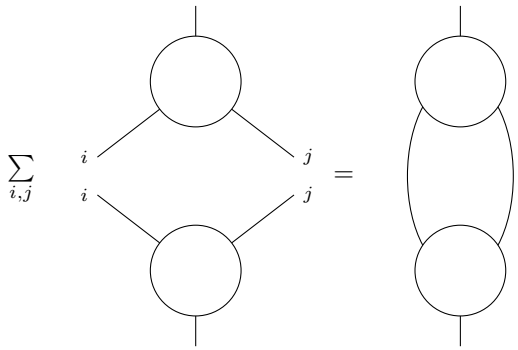

For the rest of this thesis, two particular tensors are most relevant for us: a 3-leg tensor $V_{\alpha}^{\beta\gamma}$ and a 4-leg perfect tensor $U_{\alpha\beta}^{\gamma\delta}$:

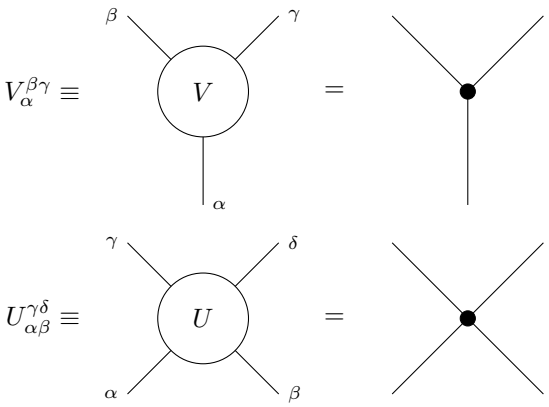

We require the 4-leg tensor to be a unitary transformation

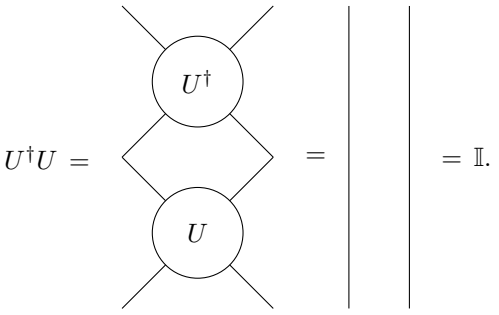

(4.1)

and the 3-leg tensor to be an isometry

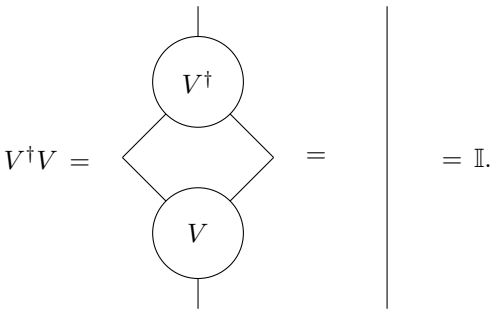

(4.2)

For simplicity, we assume that the indices of both U and V run over a set of size d. Thus, U and V are the following two maps:

$$U : \mathbb{C}^d \otimes \mathbb{C}^d \to \mathbb{C}^d \otimes \mathbb{C}^d, \quad \text{and} \quad V : \mathbb{C}^d \to \mathbb{C}^d \otimes \mathbb{C}^d.$$

Indeed, this assumption does not imply a loss of generality: It is possible (with a small amount of work) to allow for the dimension d of the tensor legs to vary for different spacetime locations.

In the following, the tensor-network labels U and V, as well as the index labels for the legs, are suppressed to keep the notation clean.

In the context of tensor network models, tensors or tensor networks are sometimes interpreted as quantum states. If tensor networks cannot be interpreted directly as quantum states, they often describe the time evolution of a quantum state.

4.2. Review: Toy model of AdS/CFT correspondence

In this section, we want to review a family of toy models, which is an exact model of the AdS/CFT correspondence. The *holographic toy model* was introduced by Pastawski, Yoshida, Harlow, and Preskill [PYHP15] and is here referred to as the AdS toy model. This toy model largely motivates the construction of our holographic model in the de Sitter setting. Accordingly, we will review some basic properties of anti-de Sitter spacetime as well as the corresponding tessellations and the basic construction of the toy model in this section.

Anti-de Sitter spacetime is the constant curvature solution to Einstein's field equations with constant negative curvature schematically depicted in figure 14. AdS_{2+1} can be embedded in four-dimensional flat space with the following coordinates [Hol95]

$$\begin{aligned} X &= \sinh r \cos \phi \\ Y &= \sinh r \sin \phi \\ Z &= \cosh r \cos t \\ T &= \cosh r \sin t \end{aligned}$$

which results in the following metric

$$\mathrm{d}s^2 = \mathrm{d}X^2 + \mathrm{d}Y^2 - \mathrm{d}Z^2 - \mathrm{d}T^2 = -\cosh^2 r \mathrm{d}t^2 + \mathrm{d}r^2 + \sinh^2 r \mathrm{d}\phi^2$$

The coordinates r and ϕ are interpreted as polar coordinates, and t is the time coordinate. It needs to be noted that the time t is 2π periodic in AdS spacetime. For a fixed timeslice, we obtain the two-dimensional hyperbolic plane, which can be identified with the Poincaré disc [And07]. The Poincaré disc is a model of the hyperbolic plane where all points of the hyperbolic plane are identified with points inside the unit disk $\mathbb{D}$. In this setting, straight lines are circular arcs that are perpendicular to the boundary $\partial\mathbb{D}$ (which includes the diameter of the disk).

4.2.1. Uniform tessellations in flat and hyperbolic space

Tessellations are coverings of a surface with geometric shapes (tiles) that are not allowed to overlap or have gaps. A *uniform tiling* is a tessellation that has to satisfy the following additional conditions. All tiles are regular polygons, the pattern around all vertices has to be identical (up to a mirror image), and the tiling has to be vertex-transitive [Max23]. In particular, it follows that there are no preferred tiles of the uniform tessellation. A *polygon* in flat space is defined as a closed convex set that is bounded by Euclidean line segments. A polygon is regular if the

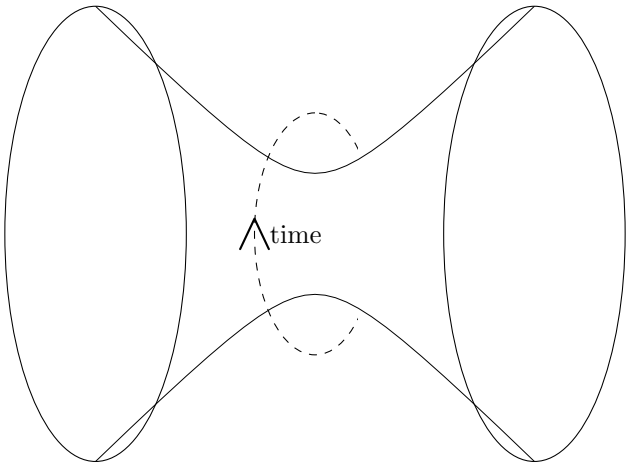

Figure 14.: Schematic depiction of $2+1$ dimensional anti-de Sitter spacetime

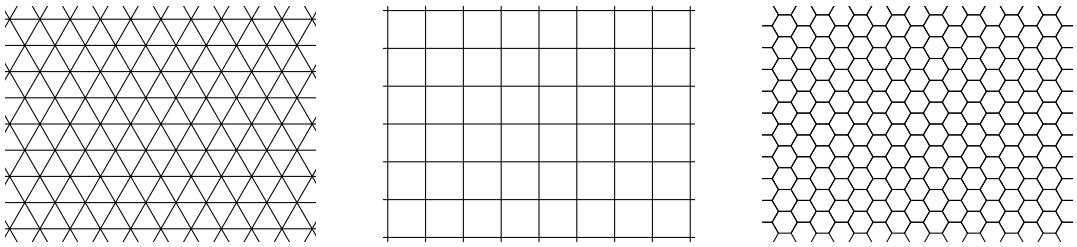

(a) (b) (c)

Figure 15.: Uniform tilings in the Euclidean plane using triangles (a), squares (b), or hexagons (c)

sides have equal length and the interior angles are equal. Uniform tessellations are well known from flat spacetime, for example, in the form of mosaics; examples of uniform triangular and hexagonal tessellation are depicted in figure 15. Tilings reduce the symmetry group from a continuous translation and rotation symmetry to their discrete equivalents: uniform tilings are vertex-transitive and only rotation invariant for discrete angles.

Such uniform tilings can also be defined for hyperbolic space where a hyperbolic tiling is the tessellation of a Poincaré disc $\mathbb{D}$. The definition of polygons can be translated directly to the hyperbolic setting. Hyperbolic polygons are bounded by hyperbolic line segments, which are segments of circular arcs. Hyperbolic tessellations are less common in our everyday lives but make their appearances in a series of artworks of the Dutch artist Maurits Cornelis Escher called *circle limits*[1].

Hyperbolic tessellations are made of tiles, which are hyperbolic polygons. They are often referred to as (p, q) tessellations, which are made of tiles that are regular hyperbolic polygons with p sides where q polygons are adjacent to each vertex. This is a generalization to the Euclidean tiling, where the choice of polygon uniquely characterizes the number of tiles adjacent to each vertex. In hyperbolic geometry, the angle sum of a regular polygon with p sides is smaller than $(p-2)\cdot\pi$ (which would be the exact angle sum for a regular Euclidean polygon). For a (p, q) tessellation

[1] M.C Escher: Circle Limit with Butterflies (1950), Circle limit I (1958), Circle Limit II (1959), Circle Limit III (1959), Circle Limit IV *Heaven and Hell* (1960)

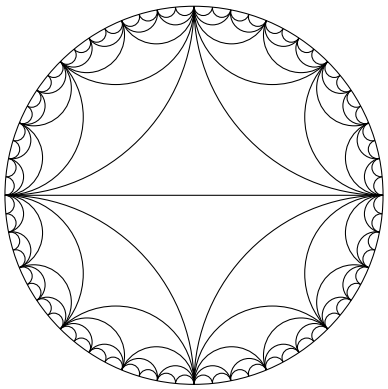

Figure 16.: tessellation of the Poincaré disc using ideal triangles

with hyperbolic polygons with inner angle α we get the following relation:

$$2\pi = \alpha \cdot q < \frac{(p-2)\cdot\pi}{p} \cdot q$$

The more the inner angle α differs from $(p-2)\cdot\pi/p$, the bigger the curvature in the hyperbolic plane. This allows for a large family of *hyperbolic tessellations*, hyperbolic (p, q) tessellations can be constructed interactively on the web page [Chr] which also describes the explicit construction[2]. We mostly refer to tessellations using ideal triangles bounded by geodesics where all vertices lie on the boundary of the Poincaré disc as depicted in figure 16.

The hyperbolic tilings are discretely scale-invariant, and there exists a graph isomorphism that maps any point of the graph to its center while preserving the local structure of the tiling.

4.2.2. AdS toy model

Here, we describe the construction and fundamental properties of the family of AdS toy models introduced in [PYHP15]. The AdS toy model acts on the Poincaré disc, which is a constant time slice of anti-de Sitter spacetime. It models a connection between bulk locality in AdS/CFT and quantum error correcting codes, which has been proposed in [ADH15]. The language of quantum error correction gives a natural interpretation to local bulk operators of the Poincaré disc as logical operators on certain subspaces in the CFT. The model combines this with the suggestion of Swingle [Swi12b, Swi12a] to implement the holographic model using tensor networks, which have been used as a tool to represent quantum many-body states [VCM09].

The foundation of the AdS toy models are uniform tilings of the Poincaré disc. Different choices of tilings result in different models, which is why we get a family of toy models. We will consider the model based on a tessellation comprised of ideal triangles, which also can be referred to as the standard dyadic tessellation of the Poincaré disc shown in figure 14(b), which was also considered in [OS20]. For the construction of an AdS toy model, the fundamental building blocks are perfect tensors, which are placed at each tile. The open legs of the perfect tensors are contracted with the legs of tensors placed at neighboring tiles (which have shared edges), which gives rise to a *tensor network*. As perfect tensors, in general, are not symmetric under all permutations of tensor legs, the ordering of the tensor legs needs to be specified in the construction. Physical spins are associated with the uncontracted tensor legs at the boundary of the tiling.

The resulting tensor network, which only has uncontracted legs at the boundary, is called a *holographic state* (see figure 17(a)) and corresponds to a pure state of these boundary spins. The

[2]Constructions or transformations of such tessellations can be visualized in [Wee] which is an open source software.

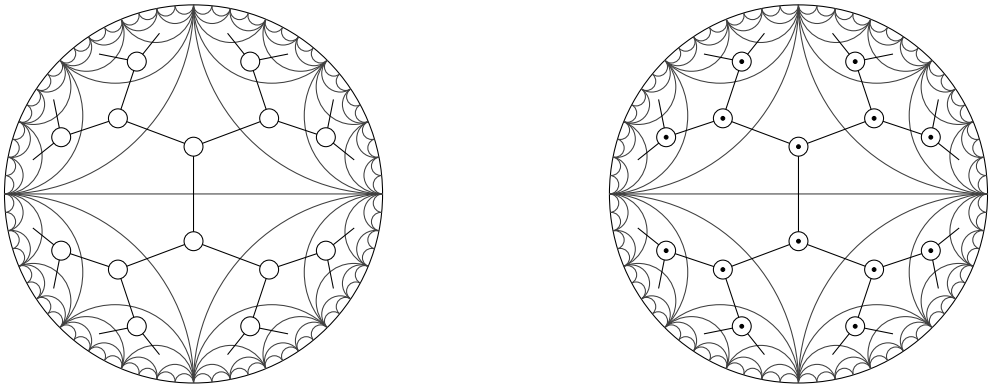

(a) (b)

Figure 17.: Depiction of holographic state (a) and holographic code (b) for the standard dyadic tessellation of the Poincaré disc. Uncontracted tensor legs represent physical legs on the boundary, and black dots in the tensor represent logical input legs associated with each perfect tensor in the bulk.

physical degrees of freedom of the holographic state are associated with the uncontracted tensor legs at the boundary of the Poincaré disc.

The code corresponding to the AdS toy model is obtained by a generalization of the holographic state, which is called *holographic quantum code* in the original paper. The construction is similar to the holographic state, but a tensor with one additional leg is placed at each tile such that each tensor has an uncontracted leg in the bulk. This additional uncontracted bulk leg can be interpreted as a logical input for the tensor network (see figure figure 17(b)). The tensor network is referred to as a holographic code if this tensor network generates an isometry from the uncontracted bulk legs to the uncontracted boundary legs. For the construction described above, the tensor network generates an isometry from the logical indices in bulk to the physical indices on the boundary because each perfect tensor is an isometry. Due to the construction with the underlying tessellation, it cannot have more input than output legs. The tensor network is an isometry as we can apply the perfect tensors layer by layer, and we know that the product of isometries again is an isometry. This isometry then can be viewed as the encoding transformation of a *quantum error-correcting code*. The choice of tessellation, perfect tensor, and the shape of the cutoff[3] determine which code from the family of codes corresponding to the AdS toy model is constructed. Tensor networks with uncontracted bulk legs have been considered before [Vid08, Qi13]. What was new in the AdS toy model is that the states are protected against erasure due to the implementation of quantum error correction.

The code of the AdS toy model comprises the following desirable properties: It provides an exactly solvable toy model for the AdS/CFT correspondence with an exact prescription for the map from bulk to boundary operators. AdS toy models are quantum error-correcting codes and, therefore, realize the proposal from [ADH15] to characterize the AdS/CFT correspondence using quantum error correction. The models also have bulk uniformity since the tensor networks are supported on hyperbolic tessellations, which have no preferred direction if extended to an infinite system.

The holographic states constructed above also reproduce other important properties of the

[3]The concept of taking a cutoff of a tessellation is made precise in the construction of the holographic model in de Sitter spacetime.

AdS/CFT correspondence. One important duality between geometry and entanglement captured by the AdS toy model is that the corresponding code reproduces the relation between the entanglement entropy of a boundary and the corresponding minimal area in the bulk described by the Ryu-Takayanagi formula [RT06]. In AdS, the minimal area can be obtained directly with the minimal bulk geodesic, which encloses the boundary area. The boundary of this minimal area is modeled with a certain cut through the tensor network where one of the disjoint sets of perfect tensors is identified with minimal area.

4.3. Basics on quantum error correction

For many areas in quantum physics, *quantum error correction* (QEC) is a crucial concept to reduce the effect of quantum noise and errors. In classical computing, error correction is usually achieved through redundant bits and error-detection codes. However, the quantum realm presents a more complex landscape. The qubits can not be copied directly due to the no-cloning theorem [WZ82]. A continuum of different errors can occur on a single qubit, and the measuring process disturbs a quantum state. Despite these difficulties, many protocols can successfully perform quantum error correction. One of many other areas in physics where QEC is used is holographic quantum gravity, where quantum error correction is a tool used for bulk reconstruction [PYHP15].

There exists a wide variation of QEC protocols which often are referred to as quantum error correction codes (QECC). The fundamental idea is that logical qubits, abstract representations of quantum information, are encoded into larger sets of physical qubits. This creates a redundancy in the quantum information, making it possible to detect errors without disturbing the quantum state. QEC only works up to certain bounds imposed by *quantum error-correction conditions* that depend on the particular protocol and error operators. A more general introduction to quantum computing can be found in [NC00].

A quantum error correction follows a systematic three-phase process: The initial phase involves encoding, where the quantum information is encoded using a specific protocol that introduces redundancy with additional physical qubits. In the second phase, syndrome measurement is performed which identifies if errors have occurred. This phase requires additional ancillary qubits, which are entangled with the logical qubits. The syndrome measurement can determine the type and location of errors in the encoded quantum state. The number of detectable errors depends on the protocol used. The final phase, recovery, involves error correction based on the syndrome measurement.

One way to describe the protocols for encoding, syndrome measurement, and recovery is to use a quantum circuit, which is comprised of quantum gates and unitary operations. These quantum circuits can also be expressed in terms of one isometry.

For the encoding of the original state, this isometry can also be chosen to be a random isometry as described in [FNA+20]. This is referred to as *randomized quantum error correction*. The well-defined circuits from more traditional quantum error correction codes are replaced with randomized encoding schemes. Random isometries are used to map the initial quantum state to a higher-dimensional space. The use of random isometries simplifies the encoding process and mitigates certain types of errors. The simplification of the encoding process does not translate to the computational cost, but they provide a universal approach that can be applied to a wide range of scenarios.

4.4. Optimal cloning

In general, cloning refers to the process of creating identical copies of an arbitrary unknown state. When translating this to quantum mechanics, we are faced with the difficulty that it is fundamentally impossible to create a perfect copy of an arbitrary unknown quantum state due to the *no-cloning theorem*, which was initially presented by Wootters and Zurek [WZ82]. It is, however, possible to make imperfect quantum copies of quantum states. This was first shown by Bužek and Hillery in [BH96], where a transformation was introduced, which created two approximate copies of an arbitrary input state of a two-level system. The transformation is generally known as a *quantum cloning machine* and was shown to be optimal in the following years [GM97, BDE$^+$98]. A quantum cloning machine acts on an unknown quantum state and generates identical, approximate copies of that state. As we know, perfect cloning is impossible in quantum mechanics; we always refer to *optimal cloning* when talking about cloning channels that map from the input state to the approximated copies.

Cloning machines have been generalized in [BH98], which allowed for higher dimensional systems as input states. The cloning machine is an additional quantum system that interacts with the unknown input state and the (approximate) copy, which is specified by the following conditions:

1. The state of the original system and its copy are identical after applying the cloning machine.

2. All pure states have to be copied equally well. The quality of the copy is specified by the distance between the density operators of the input state and one output (note: this does not depend on the choice of the measure).

3. To obtain an optimal result, the output copies should be as close to the initial state as possible, which means that the distance from 2 has to be minimized.

This transformation is explicitly given for an d dimensional quantum system. The cloning machine is prepared in the state $|X\rangle_c$ with respect to the orthonormal basis $\{|x_i\rangle_c\}$ and the original quantum state is $|\psi_i\rangle_a$. The cloning transformation acts as a unitary transformation on the product space of the original quantum system $|\psi_i\rangle_a$, the quantum cloner $|X\rangle_c$ and a d-dimensional quantum system prepared as $|0\rangle_b$ which will become the copy. The transformation acts as follows (see [BH98, eq. (9)])

$$|\psi_i\rangle_a |0\rangle_b |X\rangle_c \xrightarrow{U} \alpha |\psi_i\rangle_a |\psi_i\rangle_b |x_i\rangle_c + \beta \sum_{j\neq i}^{d} \big(|\psi_i\rangle_a |\psi_j\rangle_b + |\psi_j\rangle_a |\psi_i\rangle_b\big) |x_j\rangle_c$$

The output states $\hat{\rho}_a^{(\text{out})}$ and $\hat{\rho}_b^{(\text{out})}$ after applying the cloning transformation are identical and take the following form (see [BH98, eq. (11)]):

$$\hat{\rho}_a^{(\text{out})} = \sum_{i=1}^{d} |\gamma_i|^2 \big(\alpha^2 + (d-2)\beta^2\big) |\psi_i\rangle \langle\psi_i| + \sum_{\substack{i,j=1 \\ i\neq j}}^{d} \gamma_i \gamma_j^* \big(2\alpha\beta + (d-2)\beta^2\big) |\psi_i\rangle \langle\psi_j| + \beta^2 \mathbb{1}$$

The condition $\alpha^2 + 2(d-1)\beta^2 = 1$ on the real coefficients α and β directly follows from the unitarity of the transformation. The cloning transformation satisfies this relation and the required optimality condition for the following choice of parameters:

$$\alpha^2 = \frac{2}{d+1} \qquad\qquad \beta^2 = \frac{1}{2(d+1)}$$

With these parameters, the cloning channel takes the following form:

$$\hat{\rho}_a^{(\text{out})} = \frac{1}{d+1}\left[\sum_{i=1}^{d} |\gamma_i|^2 \frac{2+d}{2} |\psi_i\rangle\langle\psi_i| + \sum_{\substack{i,j=1 \\ i\neq j}}^{d} \gamma_i\gamma_j^* \frac{d-2}{d+1} |\psi_i\rangle\langle\psi_j| + \frac{1}{2}\mathbb{1}\right] \tag{4.3}$$

The independence of the copies from the input states is determined by the scaling factor s and the following relation [BH98, eq. (8)]:

$$\hat{\rho}_{a,b}^{(\text{out})} = s\hat{\rho}_a^{(\text{in})} + \frac{1-s}{d}\mathbb{1}$$

Where the scaling factor determines the quality of the clones. For this transformation, the scaling factor is

$$s = \alpha^2 + (d-2)\beta^2 = \frac{2+d}{2(d+1)}$$

With that, it is easy to see that the quality of the clones decreases with higher dimensional quantum systems. For the two-dimensional cases, this reproduces known results [BH96, Wer98] of $s = \frac{2}{3}$. For increasingly large dimensions, the scaling factor approaches a finite bound of $s = \frac{1}{2}$ for infinite dimensional systems.

A further generalization of quantum cloning machines was introduced with the $1 \to N$ cloning channel suggested in [GM97], which was able to create N as opposed to two copies of the original state. This $1 \to N$ cloning channel can then be interpreted as an approximated N-fold tensor product of the original state. Optimal cloning is of great interest in various areas of quantum information, including quantum communication and quantum key distribution [Wol21] and cryptography [DKSW07, SIGA05]. Achieving optimal cloning has practical implications for secure communication protocols and understanding the limits of manipulating quantum information. As a result, it has been subject to research in a variety of contexts: A generalization unifying various cloning machines is published in [WSX+11], continuous-variable optimal cloning in infinite dimensions has been studied in [CDPC05] and in the context of quantum information optimal cloning of unitary transformations instead of qubits [CDP08] as well as relation between quantum cloning and quantum state estimation [CY14] has been studied. Optimal cloning also has a wide range of applications in quantum optics, such as in the optimal cloning of coherent states presented in [BCI+01, LLCJ21]. A broad review on optimal cloning can be found in [FWJ+14].

Quantum information properties discussed in this chapter will provide a foundation for the holographic toy model we develop in chapter 6. Later in this thesis, optimal cloning channels will be relevant when studying the channel describing the expansion of de Sitter in chapter 8. There, we will identify properties of an optimal cloning channel in the channel we derive to characterize how a local observer experiences the global expansion of spacetime.

Part II.

Holographic network

Chapter 5

Symmetry groups of de Sitter spacetime

In this chapter, we discuss the symmetries of de Sitter spacetime. Symmetries are isometric transformations mapping the space to itself, which leaves the space invariant. The ultimate goal is to apply isometric transformations to the holographic model, which we develop in the following chapter. Here, we focus on understanding isometries on the Hilbert spaces associated with the temporal past and future boundaries of dS_2 which we refer to as $\mathcal{H}_{\text{in}}$ and $\mathcal{H}_{\text{out}}$. To make the isometry transformations compatible with the holographic toy model, we consider the discretization of the isometry actions at the de Sitter boundaries. This chapter is a combination of a review of well-known symmetry properties of de Sitter spacetime and a more detailed elaboration on the results from [NO22]. We start with a general introduction of the de Sitter symmetry group $SO(2,1)$ and null geodesics in section 5.1. In section 5.2, we introduce an isomorphism to relate the de Sitter symmetry group with the modular group $\mathrm{PSL}(2,\mathbb{R})$. Next, we identify the modular group with the Möbius group acting on the de Sitter future boundary in section 5.3. The rest of the chapter focuses on the discretization of the isometry group, which starts in section 5.4. Next, we introduce Thompson's group F and T, which are groups of piecewise linear homeomorphisms in section 5.5. A subgroup of Thompson's group T is identified with the discretized isometry group $\mathrm{PSL}(2,\mathbb{Z})$ in section 5.6. We relate this discussion to the de Sitter past boundary in section 5.7. The chapter is concluded by a discussion of the asymptotic symmetry group in section 5.8.

5.1. de Sitter symmetry group and null geodesics

The *de Sitter symmetry group* $\mathrm{SO}(1,2)$ whose isometries are generated by the Killing fields derived in 2.3. We can also derive the isometries of dS_2 by considering its embedding in three-dimensional Minkowski spacetime $\mathbb{R}^{1,2}$. We know that the transformations generated by the Lorentz group $O \in \mathrm{O}(1,2)$ preserve the three-dimensional Minkowski metric [Nom82]:

$$\eta = O^T \eta O.$$

The transformations $O \in \mathrm{O}(1,2)$ also induce a symmetry transformation in dS_2 because it preserves the hyperboloid condition (its matrix form can be found in eq. (2.14)) of the embedding coordinates:

$$x^T \eta x = x^T O^T \eta O x = (Ox)^T \eta O x = y^T \eta y = 1.$$

The action of isometries generated by the Lorentz group $\mathrm{SO}(1,2)$ can also be specified in terms of its action on the null geodesics in de Sitter. In section 2.4.1, null geodesics are defined with respect to the parameters u and v. Null geodesics allow us to characterize the isometry action of every point in dS_2 for the following reason: Every point in de Sitter is uniquely determined by

the intersection of one left-moving and one right-moving geodesic. In turn, geodesics are specified by a point on the boundary when remembering the corresponding direction of the geodesic. An isometry action applied to the boundary accordingly can fully specify the isometry action in the entire bulk of the spacetime.

To simplify the discussion below, we restrict our attention to the subgroup $\mathrm{SO}(1,2)$ of proper isometries preserving orientation, which also is called proper Lorentz group (or indefinite special orthogonal group in a more mathematical setting).

5.2. Isomorphism between proper Lorentz group and special linear group

In this section, we will describe the relation between the de Sitter symmetry group $\mathrm{SO}(1,2)$ and the special linear group $\mathrm{SL}(2,\mathbb{R})$. The special linear group $\mathrm{SL}(2,\mathbb{R})$ is the group of all 2×2 matrices over the real numbers $\mathbb{R}$ with determinant 1, with the group operations being matrix multiplication and matrix inversion. We characterize the relation between the proper Lorentz group and the special linear group with a sporadic 2-to-1 homomorphism following [Gar15].[1] We characterize an element from the special linear group as

$$g = \begin{pmatrix} a & b \\ c & d \end{pmatrix}, \quad g \in \mathrm{SL}(2,\mathbb{R}),$$

where the parameters satisfy $ad - bc = 1$. We map this to the isometry group $\mathrm{SO}(1,2)$ via

$$h : \mathrm{SL}(2,\mathbb{R}) \to \mathrm{SO}(1,2) \tag{5.1}$$

This homeomorphism h characterises the relation between the groups $\mathrm{SL}(2,\mathbb{R})$ and $\mathrm{SO}(1,2)$. For defining this homomorphism, we introduce an auxiliary vector space $\mathcal{V}$ defined by the space of real-valued 2×2 matrices with vanishing trace and the symmetric bilinear form

$$\langle x, y\rangle = \frac{1}{2}\operatorname{tr}(xy) \quad \text{with } x, y \in \mathcal{V}.$$

This vector space is equivalent to the Minkowski spacetime $\mathbb{R}^{1+2}$ whose metric has the matrix representation $\eta = \mathrm{diag}(-1,1,1)$ if we choose the basis vectors of $\mathcal{V}$ to be the following Pauli-like matrices: $e_1 = \mathrm{i}\sigma_y$, $e_2 = \sigma_x$ and $e_3 = \sigma_z$. This, as well as an explicit matrix representation of $h(g)$, is explicitly detailed in appendix C.1.

The action of $\mathrm{SL}(2,\mathbb{R})$ on the vector space $\mathcal{V}$ for an element $x \in \mathcal{V}$ is defined by

$$V : \mathcal{V} \to \mathcal{V}, \quad x \mapsto g \cdot x = gxg^{-1}$$

, which is preserved by the bilinear form since the trace is cyclic and the product of g with its inverse yields the identity:

$$\langle x, y\rangle = \frac{1}{2}\operatorname{tr}(xy) \mapsto \frac{1}{2}\operatorname{tr}\big(gxg^{-1}gyg^{-1}\big) = \langle g\cdot x, g\cdot y\rangle = \langle x, y\rangle.$$

Every $x \in \mathcal{V}$ can be expressed as a linear combination of the basis vectors e_1, e_2 and e_3. The explicit matrix representation can be derived by applying the action V on the basis elements as

$$e_j \mapsto g e_j g^{-1} \equiv h_{1j}\, e_1 + h_{2j}\, e_2 + h_{3j}\, e_3$$

[1] Note that the difference between $\mathrm{SO}(1,2)$ and $\mathrm{SO}(2,1)$ in [Gar15] is just a change of the metric signature.

(the explicit derivation can be found in the appendix). As a result, the special linear group $\mathrm{SL}(2,\mathbb{R})$ is a double cover of the special orthogonal group $\mathrm{SO}(1,2)$ through the homomorphism $h : \mathrm{SL}(2,\mathbb{R}) \to \mathrm{SO}(1,2)$.

The kernel of this action is characterized as follows:

$$\ker V = \{g \in \mathrm{SL}(2,\mathbb{R}) : g \cdot x = x\} = \{\mathbb{1}, -\mathbb{1}\}$$

This condition is equivalent to $gxg^{-1} = x$, which is the set of all matrices g commuting with *all* element $x \in \mathcal{V}$ which is only true for $g = \pm\mathbb{1}$. This way, we have a double covering, which means that this correspondence is 2 to 1: the element $g' = -g$ yields the same transformation as g. To compensate for this, we take the set difference with the elements of the kernel. In this way, the *projective special linear group*

$$\mathrm{PSL}(2,\mathbb{R}) = \mathrm{SL}(2,\mathbb{R}) \setminus \{\pm\mathbb{I}\} \tag{5.2}$$

emerges as the natural subgroup to identify with the isometries of dS.

In order to analyze the action of the isometry group $\mathrm{SO}(1,2)$ in dS, we use that an isometry is completely specified by its action on the null geodesics. The action on a null geodesic can be obtained by applying the action imposed by the homeomorphism h to a null geodesic $x(s)$ (which is explicitly done in appendix C.2):

$$x(s) = \begin{pmatrix} s \\ u + vs \\ v - us \end{pmatrix} \quad \xrightarrow{h} \quad x'(s') = h(g)x(s) = \begin{pmatrix} s' \\ u' + v's' \\ v' - uss' \end{pmatrix} = \begin{pmatrix} x'_0 \\ x'_1 \\ x'_2 \end{pmatrix}$$

With the asymptotic limit of large times ($s' \to \infty$), we obtain the isometry action imposed by the homeomorphism h on the temporal future boundary:

$$\frac{x'(s)}{s'} \xrightarrow{s' \to \infty} \begin{pmatrix} 1 \\ v' \\ -us \end{pmatrix}$$

where the parameter u' and v' defining the transformed geodesic are derived in appendix C.2.

5.3. Identify PSL(2,R) with the Möbius group

In $n+1$ dimensional de Sitter spacetime, the temporal boundaries are n-spheres, which reduce to circles in the $1+1$ dimensional case. Accordingly, it can be helpful to describe the symmetry action of an isometry O on the boundary using the *Möbius transformation*, which is a linear fractional transformation of the complex plane that maps straight lines to straight lines and circles to circles. In section 5.2, we argued that $\mathrm{PSL}(2,\mathbb{R})$ is a natural group that can be identified with the isometries of dS. In this section, we will elaborate on the identification between elements of $\mathrm{PSL}(2,\mathbb{R})$ and elements of the *Möbius group*. The Möbius transformation is given by

$$f : \mathbb{C} \to \mathbb{C}, \;\; z \mapsto \frac{\alpha z + \beta}{\gamma z + \delta}, \tag{5.3}$$

where α, β, γ and δ are complex coefficients satisfying the condition $\alpha\delta - \beta\gamma = 1$. We will focus on real Möbius transformations where the domain and range, as well as the parameters, are real numbers. The set of all Möbius transformations forms the Möbius group as both the composition of two Möbius transformations as well as the inverse of a Möbius transformation yields a Möbius transformation. The group of real Möbius transformations can be identified with

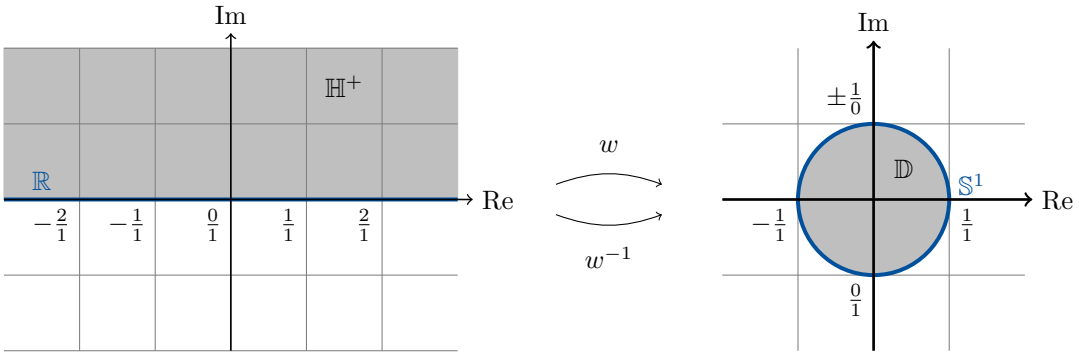

Figure 18.: Schematic depiction of Cayley transformation

the group $\mathrm{PSL}(2,\mathbb{R})$. It can accordingly be identified with the action of $\mathrm{SO}(1,2)$ on the temporal boundaries $\mathcal{I}^{\pm}$. In the following, we will elaborate on this.

We can identify a temporal boundary of de Sitter spacetime with a circle which can be rescaled to the unit circle $\mathbb{S}^1$. This can be understood as the boundary of the unit disk

$$\mathbb{D} = \{z \in \mathbb{C} : |z| \leq 1\}$$

in the complex plane. The Cayley transform is a conformal transformation that maps points from the upper half of the complex plane $\mathbb{H}^+$

$$\mathbb{H}^+ = \{z \in \mathbb{C} : \mathrm{Im}(z) > 0\}$$

to the unit disk $\mathbb{D}$. The following function describes the Cayley transform:

$$\begin{aligned} w : \mathbb{H}^+ &\to \mathbb{D}, \quad z \mapsto \mathrm{i}\frac{z-\mathrm{i}}{z+\mathrm{i}} \\ w^{-1} : \mathbb{D} &\to \mathbb{H}^+, \quad z \mapsto \frac{z+\mathrm{i}}{1+\mathrm{i}z}. \end{aligned} \tag{5.4}$$

For the boundary case, this reduces to a map from the real numbers to the unit circle $w : \mathbb{R} \to \mathbb{S}^1 = \partial\mathbb{D}$ as depicted in figure 18.

We now use the Cayley transform to describe the action of a boundary point of de Sitter spacetime. The boundary action is obtained by identifying a de Sitter boundary point with a complex number

$$z = u + \mathrm{i}v \quad \text{where} \quad u, v \in \mathbb{R}.$$

with the condition $u^2 + v^2 = 1$, we ensure that it lies on a circle embedded in the complex plane. Using the Cayley transform and its inverse, we can define the action induced by the Möbius transformation on the temporal boundary $\mathcal{I}^+$ as

$$t = w \circ f \circ w^{-1} : \mathbb{D} \to \mathbb{H}^+ \to \mathbb{H}^+ \to \mathbb{D}.$$

The induced image of a point z on the temporal boundary under f is thus

$$z' = t(z) = u' + \mathrm{i}v' \quad \Rightarrow \quad \begin{matrix} u' = \mathrm{Re}\, p(z) \\ v' = \mathrm{Im}\, p(z) \end{matrix}.$$

An explicit computation yields:

$$u' = \frac{4\alpha\delta u + 2\beta\delta(1-v) - 2u + 2\alpha\gamma(v+1)}{2u(\alpha\beta+\gamma\delta) + (\alpha^2+\gamma^2)(v+1) - (\beta^2+\delta^2)(v-1)}$$

$$v' = \frac{4\alpha\beta u + 2\alpha^2(v+1) - 2\beta^2(v-1)}{2u(\alpha\beta+\gamma\delta) + (\alpha^2+\gamma^2)(v+1) - (\beta^2+\delta)^2(v-1)} - 1$$

These transformed parameters are identical to the parameters of the action of null geodesics on the temporal boundary derived in appendix C.1 using the matrix representation.

5.4. Discretization of the isometry group: PSL(2,Z)

In the next chapter, we will introduce a tessellation for $1+1$ dimensional de Sitter spacetime. One fundamental principle to selecting a tessellation is the aim to preserve as much of the isometry group of the spacetime to be tessellated as possible. General isometries are, in general, incompatible with a grid because they send points from the tessellation to points lying outside the tessellation. A natural thing to do is to look at the discretized version of the isometry group. The *discretized isometry group* is a subgroup of the isometry group compatible with the tessellation in the sense that it leaves the set of boundary points invariant. In the following, we will consider the group $\mathrm{PSL}(2,\mathbb{R})$ characterized in the previous sections as a subgroup of the isometry group:

$$\mathrm{PSL}(2,\mathbb{Z}) \simeq \mathrm{PSL}(2,\mathbb{Q})$$

Both groups are the groups generated by Möbius transformations where the parameters are integer in $\mathrm{PSL}(2,\mathbb{Z})$ and rational in $\mathrm{PSL}(2,\mathbb{Q})$. It is easy to see that these groups are equivalent:

$$f(z) = \frac{\frac{a_1}{a_2}\,z + \frac{b_1}{b_2}}{\frac{c_1}{c_2}z + \frac{d_1}{d_2}} = \frac{a_1b_2c_2d_2\,z + a_2b_1c_2d_2}{a_2b_2c_1d_2z + a_2b_2c_2d_1}.$$

Here the parameters a_1, a_2, b_1, b_2, c_1, c_2, d_1 and d_2 as well as their product are integers. Thus any transformation in $\mathrm{PSL}(2,\mathbb{Q})$ is equivalent to a corresponding transformation in $\mathrm{PSL}(2,\mathbb{Z})$. This justifies only considering $\mathrm{PSL}(2,\mathbb{Z})$ as the group of isometries for the rest of this section. The projective special linear group $\mathrm{PSL}(2,\mathbb{Z})$ has the following presentation:

$$\langle a, b | a^2 = b^3 = 1 \rangle,$$

The image of the following 2×2 matrices

$$a = \begin{pmatrix} 0 & -1 \\ 1 & 0 \end{pmatrix} \quad \text{and} \quad b = \begin{pmatrix} -1 & 1 \\ -1 & 0 \end{pmatrix}. \tag{5.6}$$

can be chosen as these generators when considering the equivalence relation from eq. (5.2).

5.5. Thompson's group F and T

Both Thompson's group F and T are groups of piecewise linear homeomorphisms. They are finitely presented as infinite groups, where T is a simple group. The review in this chapter is largely based on [CFP96] as well as the theses [Bel04] and [Sti19]. The group elements are characterized as follows:

Definition 5.1 (Thompson's group F)
Thompson's group F is the group of piecewise linear homeomorphisms on the unit interval. The homeomorphisms are differentiable except at finitely many points which lie at dyadic rational numbers. When the functions are differentiable, the derivatives are powers of two.

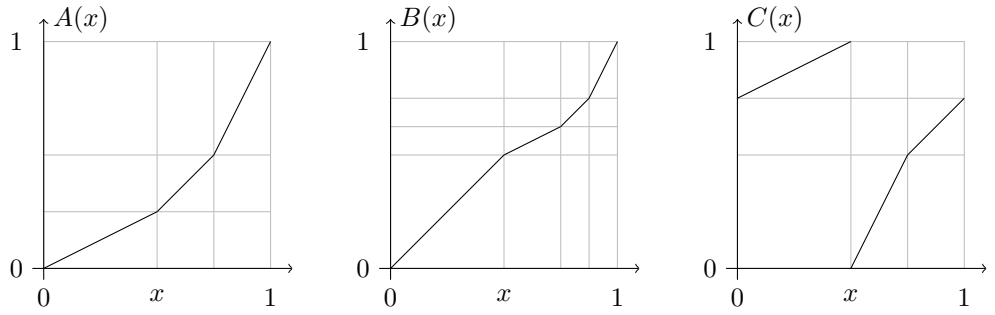

Figure 19.: Graphs of Thompson group elements A, B and C which are generators of Thompson's group F and T

Thompson's group T, which is the *circular* version of Thompson's group F, is comprised of homeomorphisms of the circle. Elements of Thompson's group F can directly be identified with elements of Thompson's group T via a map from the unit interval to the unit circle where the endpoints are identified.

Definition 5.2 (Thompson's group T)
Thompson's group T is the group of piecewise linear homeomorphisms from $\mathbb{S}^1$ to itself (which can be represented as the unit interval with the endpoints identified). The homeomorphisms are differentiable except at finitely many points which lie at dyadic rational numbers. When the functions are differentiable, the derivatives are powers of two.

The *dyadic rational numbers* are defined as

$$\mathbb{Z}_{1/2} = \left\{ \frac{a}{2^n} : a \in \mathbb{Z} \text{ and } n \in \mathbb{Z}_+ \right\}$$

We denote dyadic rational numbers restricted to the unit interval as $\mathbb{Z}_{1/2}^{[0,1]}$. It is shown in [CFP96] that Thompson's groups T is generated with the elements $A(x)$, $B(x)$, and $C(x)$ which have to satisfy the following relations (with $[x, y] = xyx^{-1}y^{-1}$):

$$\begin{aligned}
&1) \quad \left[AB^{-1}, A^{-1}BA\right] = 1 \\
&2) \quad \left[AB^{-1}, (A^{-1})^2BA^2\right] = 1 \\
&3) \quad C = B(A^{-1}CB) \\
&4) \quad (A^{-1}CB)(A^{-1}BA) = B((A^{-1})^2CB^2) \\
&5) \quad CA = (A^{-1}CB)^2 \\
&6) \quad C^3 = 1
\end{aligned}$$

The graphs of the generators A, B, and C are depicted in figure 19. For a presentation of Thompson's group F, the first two conditions suffice.

The elements of Thompson's group can be understood as *dyadic rearrangements*, which are mappings between *dyadic subdivitions* of the unit interval or circle. The fundamental concept is identical for elements of Thompson's group F, and T. We will illustrate the concept of dyadic subdivisions and rearrangements for unit intervals. A dyadic subdivision of a unit interval is obtained by taking the interval $[0, 1]$ and applying the only allowed operation repeatedly: cut the interval in half and then again cut (some) of the resulting intervals in half. One example of a dyadic subdivision is

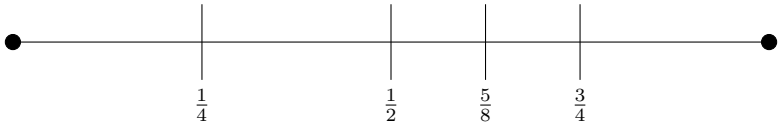

which can be mapped to a different dyadic subdivision, such as

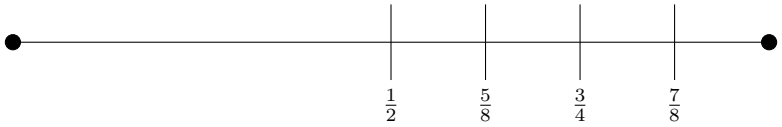

with a dyadic rearrangement.

There are three different ways to define this dyadic rearrangement, which will be introduced in this chapter: The piecewise linear function as depicted in figure 19 for $A(x)$, B and $C(x)$, rectangle diagrams and tree diagrams. We will illustrate these for the Thompson group elements $S(x) = (C^{-1} \circ A^{-1})(x)$ and C, which generate a subgroup of Thompson's group T which is equivalent to the group $\mathrm{PSL}(2, \mathbb{Z})$ as shown in [Fos10] and further discussed in the next section.

In a *rectangle diagram*, we identify the top of the rectangle with the initial dyadic subdivision, which is the domain of the function, and the bottom of the rectangle with the final subdivision which is identified to the functions range [CFP96].[2] A straight line indicates which point is mapped to which element of the dyadic subdivision. The areas in between are interpolated linearly. The use of rectangle diagrams makes it easy to look at compositions of functions, which are represented as stacked rectangle diagrams read from top to bottom. The elements S and C are represented by the following rectangle diagrams:

$S(x) =$ 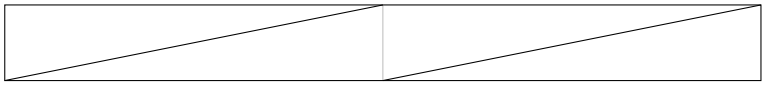

$C(x) =$ 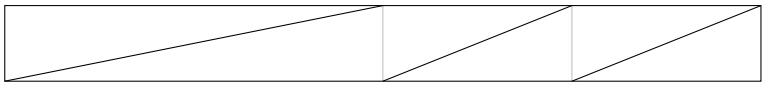

For the composition of several functions we can stack different rectangle diagrams. This way, we can see that S can be generated with the inverses of Thompson group elements A and C:

$S(x) = C^{-1}(A^{-1}(x))$

$=$ 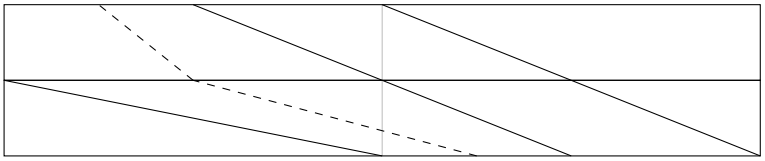

$=$ 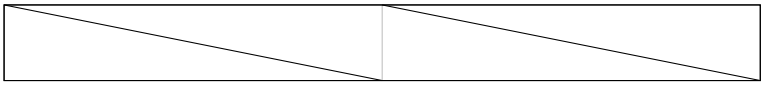

For the representation with *tree diagrams*, we need to associate a tree to both the initial and final subdivision [Bel04, Sti19]. For this, we start with the standard dyadic intervals from a binary tree:

[2] Note, that the direction of time is different here with respect to the rest of the thesis (usually we read diagrams from bottom to top). We stick to this, nevertheless, to follow the standard notation in the literature.

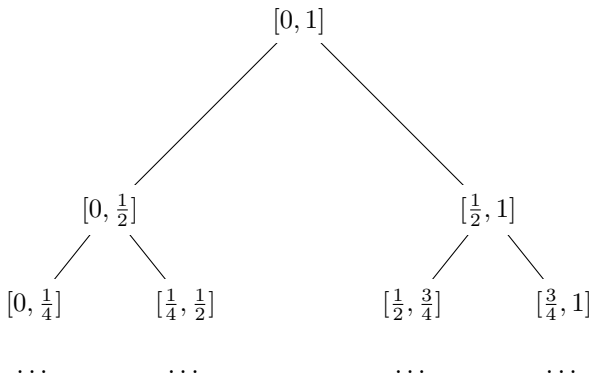

Dyadic subdivisions then correspond to finite rooted subtrees of the infinite binary tree where each leaf of the tree represents an interval of the subdivision. To describe a dyadic rearrangement that corresponds to an element of Thompson's group F, we need a pair of finite binary trees, which we refer to as a *pairs of tree diagrams* or *fraction of binary trees*. The tree at the top represents the initial and the tree at the bottom the final subdivision corresponding to a Thompson's group element. Both trees must have the same number of leaves. For a description of elements of Thompson's group T, we need to associate the trees with a circle. The resulting circular trees are usually referred to as *annular binary trees* where the circle at one of the leaves indicates which leaves belong together according to the cyclic permutation. The tree diagrams of the elements $S(x)$ and $C(x)$ are depicted below:

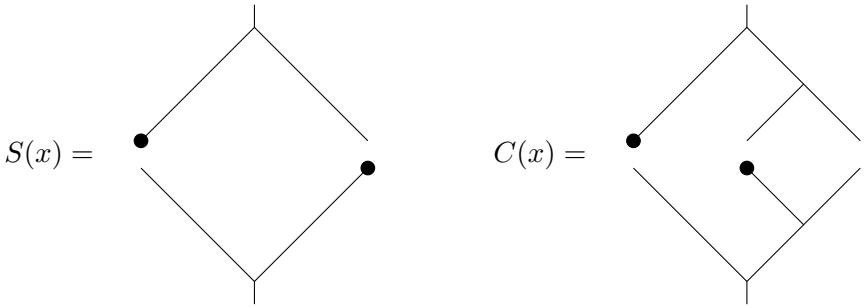

We denote two pairs of tree diagrams to be *equivalent* if one can be generated from the other by removing a pair of opposite carets as depicted in bold below:

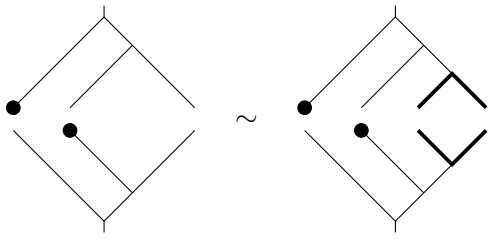

The fractions of binary trees can be extended or reduced by adding or removing opposing carets to both trees in the fraction. This way, every equivalence class of fractions of binary trees has a reduced fraction representative, where no pairs of carets can be removed without changing the equivalence class.

Thompson's group is of high relevance to this problem because its elements can be used to approximate diffeomorphisms on the circle arbitrarily well [BS14, Sti18, Zhu07]. A diffeomorphism on the circle $\mathrm{diff}(S^1)$ is a bijective map from the circle to itself where both the function and its inverse are continuously differentiable. Even though Thompson's group T cannot be identified with $\mathrm{diff}_+(\mathbb{S}^1)$ directly as its elements are not differentiable, there always exists an element $g \in T$

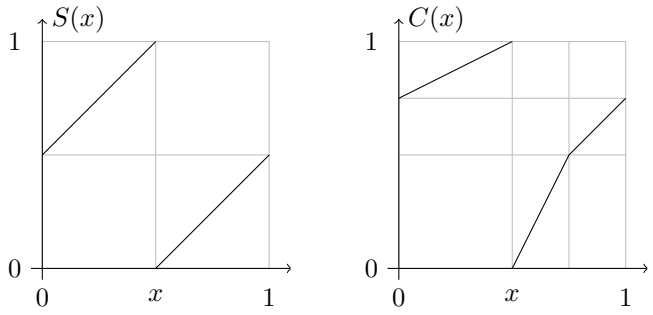

Figure 20.: Graphs of Thompson group elements S and C which are generators of $\mathrm{PSL}(2,\mathbb{Z})$

which approximates an arbitrary diffeomorphism $f \in \mathrm{diff}_+(\mathbb{S}^1)$ arbitrarily well such that the following holds with arbitrary $\varepsilon > 0$:

$$||f - g|| < \varepsilon$$

As a result, Thompson's group T is considered to be the discretized analog of $\mathrm{diff}(\mathbb{S}^1)$ as emphasized by Jones [Jon14].

5.6. Identify PSL(2,Z) with a subgroup of Thompson's group T

Thompson's group T has been studied to create algebraic quantum field theories on the circle [Jon14] as they can be considered to be the discretized analog of the diffeomorphisms $\mathrm{diff}(\mathbb{S}^1)$ on the circle. Thompson's group T proved to be an important tool in characterizing the AdS/CFT correspondence [OS19, OS20]. Following these proposals, we introduce Thompson's group in the de Sitter context.

We can identify $\mathrm{PSL}(2,\mathbb{Z})$ with a subgroup of Thompson's group T by identifying the generators of $\mathrm{PSL}(2,\mathbb{Z})$ with elements of Thompson's group: the two piecewise functions $S(x)$ and $C(x)$ depicted in figure 20:

$$\begin{aligned} S(x) =& \begin{cases} x + \frac{1}{2},\ x < \frac{1}{2} \\ x - \frac{1}{2},\ \frac{1}{2} \leq x \end{cases} \\ C(x) =& \begin{cases} \frac{1}{2}\,x + \frac{3}{4},\ x \leq \frac{1}{2} \\ 2x - 1,\ \frac{1}{2} \leq x \leq \frac{3}{4} \\ x - \frac{1}{4},\ \frac{3}{4} \leq x \end{cases} \end{aligned} \tag{5.7}$$

The functions S and C are elements of *Thompson's group F*. It is straightforward to see that the functions $S(x)$ and $C(x)$ satisfy the relations the generators in the presentation of $\mathrm{PSL}(2,\mathbb{Z})$ have to satisfy using the rectangle diagrams:

$(S \circ S)(x) =$ 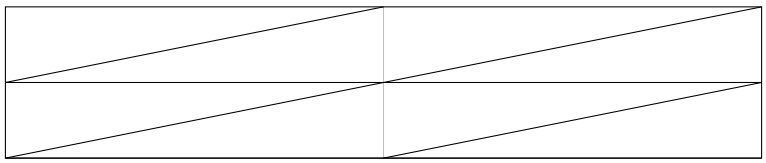

$=$ 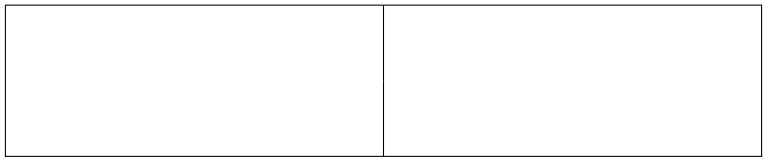 $= x$

$(C \circ C \circ C)(x) =$

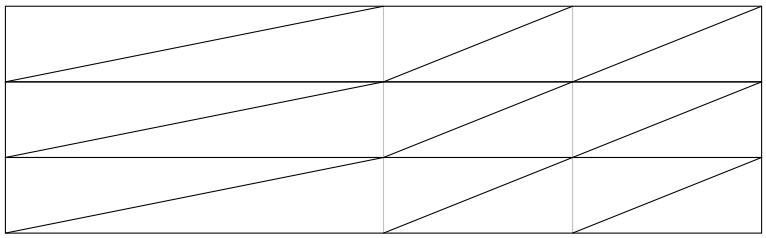

$=$

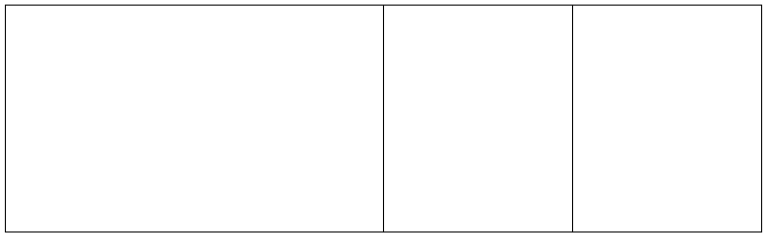

$= x$

As a result, the generators $S(x)$ and $C(x)$ generate a subgroup of Thompson's group T, which is isomorphic to $\mathrm{PSL}(2,\mathbb{Z})$.

We want to directly identify the generators of $\mathrm{PSL}(2,\mathbb{Z})$ as 2×2 matrices as introduced in eq. (5.6) with the elements of Thompson's group T introduced in eq. (5.7). We achieve this by identifying both expressions with the Möbius functions from eq. (5.3). First, we directly identify the parameter from the 2×2 matrix and the Möbius function as follows:

$$g = \begin{pmatrix} \alpha & \beta \\ \gamma & \delta \end{pmatrix} \in \mathrm{SL}(2,\mathbb{Z}) \qquad \Leftrightarrow \qquad f(x) = \frac{\alpha x + \beta}{\gamma x + \delta}$$

Here, we consider the parameters α, β, γ, and δ to be integer numbers in order to stay in the discretized regime of $\mathrm{PSL}(2,\mathbb{Z})$.

The remaining task is to relate these Möbius functions to the elements of Thompson's group. To do this, we need to perform two steps: We need to map the rational numbers from the Möbius function to the unit interval and then map the resulting points to dyadic rational numbers.

In the remainder of this section, we will look at the Möbius functions $a(x)$ and $b(x)$ associated with the generators a and b given in eq. (5.6) as 2×2 matrices:

$$a(x) = -\frac{1}{x}$$
$$b(x) = -\frac{1-x}{x}$$

Mapping the rational numbers to the dyadic rational numbers is achieved by applying the *Minkowski question mark function* $?(x)$ — a homeomorphism of $\mathbb{S}^1$, which is introduced in more detail in [VPB98]. First, we look at the unit interval, where the question-mark function can be defined recursively with the following base cases:

$$?(0) = 0 = \frac{0}{1} \quad \text{and} \quad ?(1) = 1 = \frac{1}{1}.$$

This definition is recursively extended to all rational numbers $\frac{p+r}{q+s}$ in the unit interval which satisfy $|ps - qr| = 1$ following the rule

$$?\left(\frac{p+r}{q+s}\right) = \frac{1}{2}\,?\left(\frac{p}{q}\right) + \frac{1}{2}\,?\left(\frac{r}{s}\right). \tag{5.8}$$

This defines a correspondence between the rational numbers on the unit interval and the dyadic rational numbers, which is illustrated for the first generations:

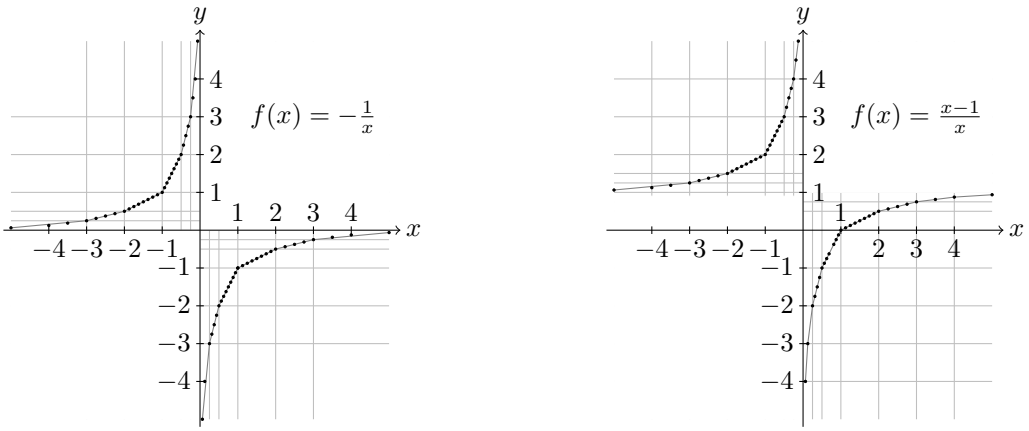

Figure 21.: Different symmetry transformations $(?\circ f\circ ?^{-1})(x)$ with Möbius functions f, which act on the dyadic rational numbers of the real axis.

0								1
0				$?(\frac{1}{2}) = \frac{1}{2}$				1
0			$?(\frac{1}{3}) = \frac{1}{4}$		$\frac{1}{2}$		$?(\frac{2}{3}) = \frac{3}{4}$	1
0	$?(\frac{1}{4}) = \frac{1}{8}$	$\frac{1}{4}$	$?(\frac{2}{5}) = \frac{3}{8}$	$\frac{1}{2}$	$?(\frac{3}{5}) = \frac{5}{8}$	$\frac{3}{4}$	$?(\frac{3}{4}) = \frac{7}{8}$	1

The Minkowski question mark function can be extended to $\mathbb{Q}$ as

$$?(x+1) = ?(x) + 1 \tag{5.9}$$

In order to map the Möbius function to the dyadic rational numbers, we need to apply the Minkowski question mark function ? and its inverse to the Möbius function as follows:

$$f_{\frac{1}{2}} = ? \circ f \circ ?^{-1} : \mathbb{Z}_{1/2} \to \mathbb{Q} \to \mathbb{Z}_{1/2}$$

The easiest way to realize this is to apply the Minkowski question mark function both to the domain and the range of the Möbius transformation to avoid working with the inverse Minkowski question mark function. Mapping the domain of the function to the dyadic rational numbers with ? effectively applies the inverse Minkowski question mark function to the dyadic rational numbers:

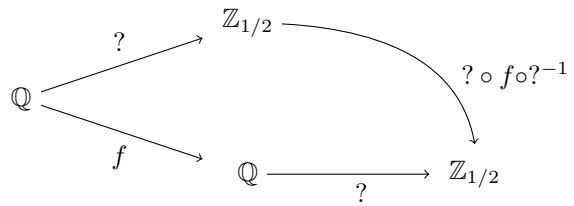

The result is depicted in figure 21. Mapping the dyadic rational numbers to the unit interval is achieved with the function ψ. First, we define ψ for the integer input values:

$$\psi_{\mathbb{Z}} : \mathbb{Z} \to \mathbb{Z}_{1/2}^{[0,1]}, \quad n \mapsto \begin{cases} \dfrac{1}{2^{|n|+1}}, & n < 0 \\ \dfrac{1}{2}, & n = 0 \\ \dfrac{2^{n+1}-1}{2^{n+1}}, & n > 0, \end{cases}$$

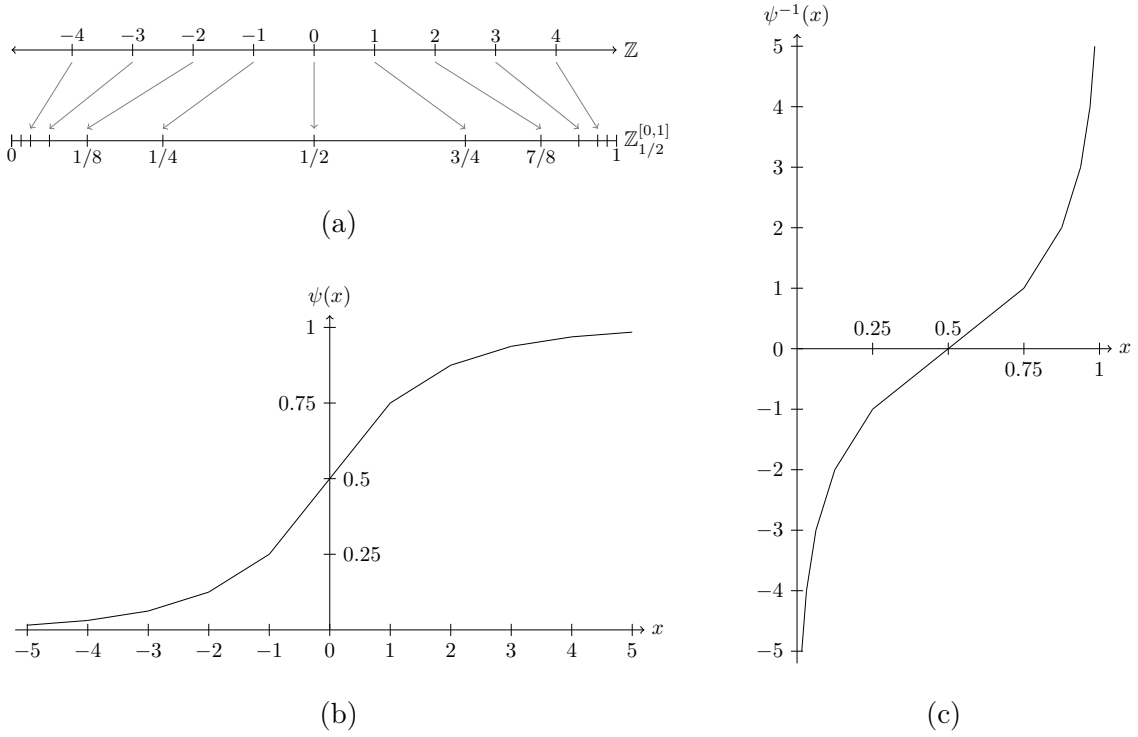

Figure 22.: depiction of the function $\psi(x)$ which maps dyadic rational numbers from the real axis to the unit interval and its inverse.
(a) definition of the mapping from integer to rational numbers
(b) $\psi(x)$ as the generalization to a continuous piecewise linear function
(c) inverse function $\psi^{-1}(x)$ mapping the unit interval to $\mathbb{Q}$

where we refer to the dyadic rational numbers on the unit interval with $\mathbb{Z}^{[0,1]}_{1/2}$. The definition of the function $\psi(x)$ can easily be generalized to all dyadic rational numbers by requiring that the function interpolates linearly between the points defined by $\psi_{\mathbb{Z}}$:

$$\psi : \mathbb{Z}_{1/2} \to \mathbb{Z}^{[0,1]}_{1/2}, \quad x \to \psi_{\mathbb{Z}}(\lfloor x \rfloor) + \frac{\psi_{\mathbb{Z}}(\lceil x \rceil) - \psi_{\mathbb{Z}}(\lfloor x \rfloor)}{\lceil x \rceil - \lfloor x \rfloor}(x - \lfloor x \rfloor) \tag{5.10}$$

where $\lceil x \rceil$ is the smallest integer number greater and $\lfloor x \rfloor$ is the greatest integer numbers smaller than x. The function $\psi(x)$ resulting from this definition is plotted in figure 22.

In order to identify the Möbius transformation with the elements of Thompson's group, we need to map the Möbius function at dyadic rational numbers defined by $(? \circ f \circ ?^{-1})(x)$ to the dyadic rational numbers on the unit interval using the piecewise-linear function ψ. The resulting function is

$$(\psi \circ ? \circ f \circ ?^{-1} \circ \psi^{-1})(x).$$

The result is plotted in figure 23. The transformations considered in this section correspond precisely to the generators of $\mathrm{PSL}(2, \mathbb{Z})$. By composing these two functions (and their inverses), we hence obtain a representation of the action of $\mathrm{PSL}(2, \mathbb{Z})$ on the circle via piecewise-linear functions compatible with the dyadic rationals.

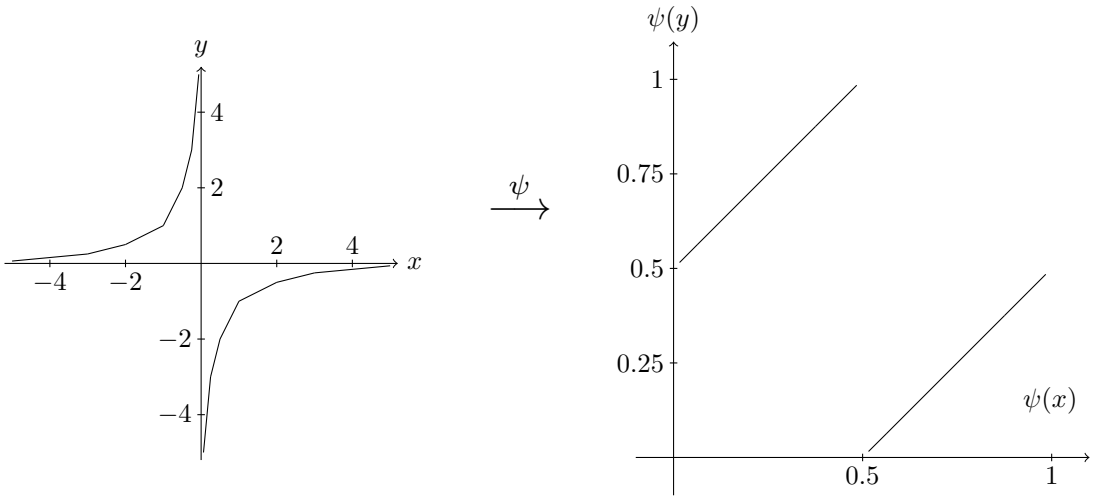

(a)

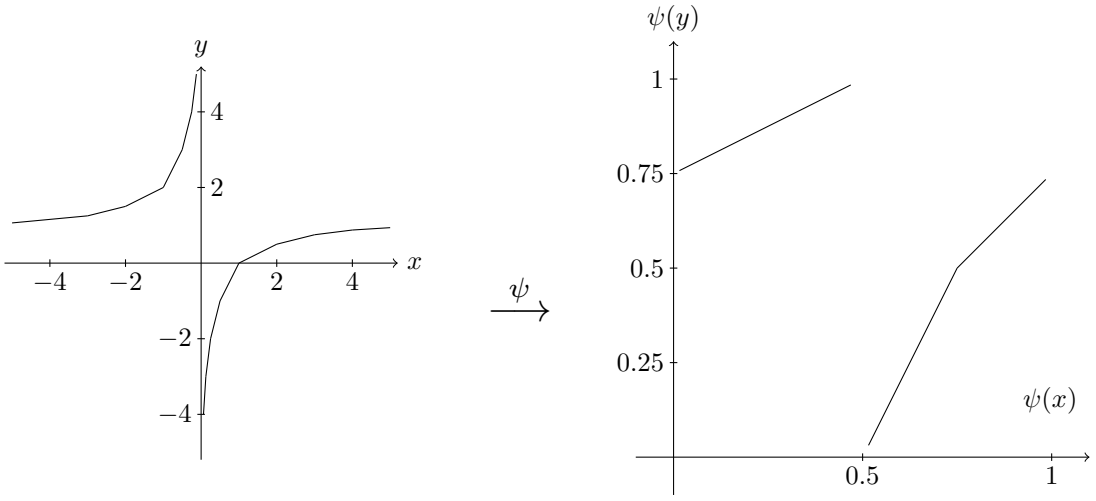

(b)

Figure 23.: Symmetry transformations $(? \circ f \circ ?^{-1})(x)$ for different Möbius functions f mapped to the unit interval using $\psi(x)$: (a) $f(x) = -1/x$ and (b) $f(x) = (x-1)/x$.

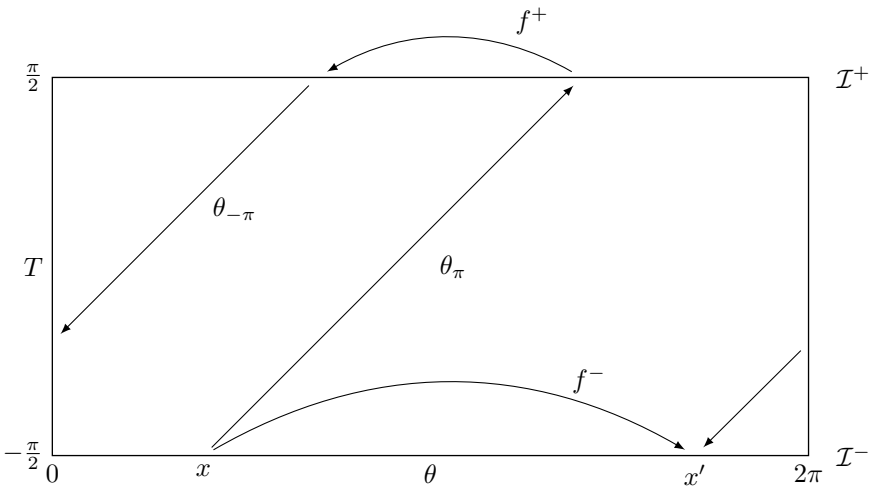

Figure 24.: Symmetry action f^- on the past boundary $\mathcal{I}^-$ of dS_2

5.7. Action on past boundary

The action of an isometry on the (discretized) future boundary $\mathcal{I}^+$ of de Sitter spacetime is given by elements of the group $\mathrm{PSL}(2,\mathbb{Z})$ as discussed in depth in the previous sections. We can use this to immediately obtain an action on the past boundary $\mathcal{I}^-$. In order to do so, we identify a point x in $\mathcal{I}^-$ with a point $x^+ \in \mathcal{I}^+$ by transporting it along a null geodesic.[3] The symmetry action is applied to x^+ and the result transported back to $\mathcal{I}^-$ via a null geodesic. This action is well defined because null geodesics traveling in either direction between $\mathcal{I}^+$ and $\mathcal{I}^-$ transport a past boundary point to the same future boundary point. Explicitly, the maps $\theta_{\pm\pi} : \mathcal{I}^\mp \to \mathcal{I}^\pm$ transporting points between the temporal boundaries are given by $\theta_{\pm\pi}(x) = x \pm \pi$. Hence, we obtain for an isometry $f^+ : \mathcal{I}^+ \to \mathcal{I}^+$ on the future boundary the induced action on the past boundary $\mathcal{I}^-$, depicted in figure 24, via

$$f^- : \mathcal{I}^- \to \mathcal{I}^-, x \to (\theta_{-\pi} \circ f^+ \circ \theta_\pi)(x)$$

When we identify the boundary with the unit interval, the maps $\theta_{\pm\theta}$ are precisely given by Thompson's group element $S(x)$. Accordingly, the action on the de Sitter past boundary rescaled to a unit interval is given by

$$f^- : \mathcal{I}^-_{[0,1]} \to \mathcal{I}^-_{[0,1]}, \quad x \mapsto (S \circ f^+ \circ S)(x) \tag{5.11}$$

5.8. Asymptotic symmetry group

Here, we describe how to extend the action of $\mathrm{PSL}(2,\mathbb{Z})$ described above to an action of Thompson's group T. Since Thompson's group T is the discretized analog to the diffeomorphisms on the circle, we propose that it should be thought of as the discretized symmetry group of asymptotic de Sitter spacetime.

The definition of an asymptotic symmetry of a spacetime, such as dS_2, is nontrivial. Heuristically, we can interpret *asymptotic symmetries* as maps that preserve the intrinsic geometric structure of the asymptotic spacetime. For a definition, we broadly follow [Jäg08, Wal84] who provide a more detailed discussion. As we use their description merely as a motivation for our definition,

[3] As the points are transported along the null geodesics from the past to the future infinity it gets transported to the antipodal point of space and we get the same result for both left- and right-moving geodesics.

the reader is referred to the literature for more details.

Diffeomorphisms determine one important property of asymptotic symmetries of nearly dS_2

$$\psi : \mathcal{I}^{\pm} \to \mathcal{I}^{\pm}$$

of the boundaries, which are conformal with respect to the induced boundary metric h_{ab}. As detailed in [Jäg08], the conformality condition requires that the induced boundary metric only changes up to a conformal factor under the diffeomorphism[4]:

$$\psi^* h_{ab} = \Omega^2 h_{ab}$$

This condition is trivial in our case since the boundary manifolds are one-dimensional. Accordingly, we understand the asymptotic symmetries as diffeomorphisms of the past and future boundaries. We find the group of asymptotic symmetries by taking the set difference with $\mathrm{PSL}(2,\mathbb{Z})$, which is the group of isometries:

$$\mathrm{diff}(S^1) \times \mathrm{diff}(S^1) / \mathrm{PSL}(2,\mathbb{R})$$

The isometries induced by $\mathrm{PSL}(2,\mathbb{Z})$ leave the metric invariant but act non-trivially on the boundary, which is why we obtained the asymptotic symmetries that are truly nontrivial.

The main result of this chapter is that we can use the group $\mathrm{PSL}(2,\mathbb{Z})$ to describe the discretized isometry group of the boundaries in de Sitter spacetime. The modular group $\mathrm{PSL}(2,\mathbb{Z})$ can be identified with a subgroup of Thompson's group T. This will be of importance in chapter 6, where we use results from this chapter to derive isometry transformations of the holographic toy model of de Sitter.

[4]Here ψ^* denotes, that this is the pullback by ψ.

Chapter 6

Holographic Network for de Sitter spacetime

Holographic models have proven very valuable in gaining more insights into the quantum theory of gravity in the AdS case. The fundamental idea is that the information about spacetime can be encoded in its lower-dimensional boundary, which is often referred to as the bulk-boundary correspondence. There are profound reasons to believe that holography can be a tool to also gain insights into some principles in quantum gravity in a more general setting [Raa16]. In the literature, this is known as the *holographic principle*, which was first discussed in [Bou02b, Hoo93, Sus95] and further investigated in the literature in a wide variety of settings such as [BKSS22, CD18, GGK$^+$22, Sal19, Yan17]. In the setting of anti-de Sitter spacetime, toy models of quantum gravity are well established, such as the AdS model described in 4.2. Our goal in this chapter is to further investigate toy models of holographic formulations in the context of de Sitter. We want to transfer some of the ideas and properties of the known AdS toy model to the de Sitter setting to explore its holographic formulations further. The approach which is presented in this chapter is to develop a tensor network that is associated with a de Sitter tessellation, which we interpret as a holographic toy model for two-dimensional de Sitter spacetime. It should be noted, however, that the model we construct here differs drastically from the AdS model reviewed in section 4.2 because de-Sitter spacetime has two temporal boundaries, as opposed to anti-de Sitter spacetime, which only has one temporal boundary. The fundamental difference in boundaries induces profound changes in the physical setup. It is the main reason the toy model we constructed does not directly fit the definition of either a holographic code or state, which is why we tentatively denote it as a *holographic network*. We ultimately interpret the network as the *propagator* from the past boundary of de Sitter spacetime to its future boundary. The construction of the holographic network presented in this chapter largely follows [NO22].

First, we discuss the causal structure of de Sitter spacetime in section 6.1 and introduce causal diamonds. Next, we construct a tessellation in section 6.2, which provides the foundation of our toy model. In section 6.3, we construct the holographic model as a *tensor network* and associate corresponding Hilbert spaces. The construction of the holographic model is generalized in section 6.4 for different curvatures of de Sitter spacetime. In section 6.5, we consider isometry transformations of the holographic model and check the invariance of the vacuum state. The chapter is concluded in section 6.6 by a short discussion of the manipulation of the spacetime achieved by applying transformations, which are discrete approximations of diffeomorphisms but no isometry transformations.

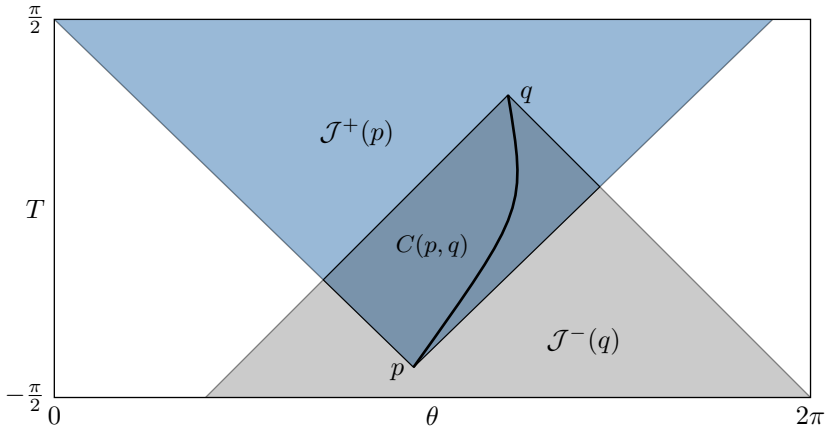

Figure 25.: A causal diamond is the intersection of the causal future of point p and the causal past of point q. It encloses all non-spacelike worldlines from p to q where one of these is depicted here exemplary.

6.1. Causal structure and causal diamonds

Causality and the accessibility of information are important physical properties of any spacetime. In this section, we will discuss causality relations in de Sitter spacetime and introduce a special subset of de Sitter spacetime we refer to as *causal diamonds*. The relevance of such a causal diamond can be seen when considering an experiment moving along a worldline that starts at a spacetime location p and terminates at location q. The subset of spacetime, which both can be influenced by an experiment starting at p and influence an experiment ending at q, will from now on be referred to as a causal diamond. A more detailed review can be found in [HE75]. In a more mathematical sense, this can be translated to two restrictions a point has to fulfill to lie inside a causal diamond spanned by the two points p and q. A point lies in the causal diamond $C(p,q)$ if

1. The point lies in the causal future $\mathcal{J}^+(p)$ of point p.
2. The point lies in the causal past $\mathcal{J}^-(q)$ of point q.

With this, a causal diamond is defined only using the endpoints p and q of the experiment without knowing anything about the experiment's worldline:

$$C(p,q) = \mathcal{J}^+(p) \cap \mathcal{J}^-(q).$$

This causal diamond determines everything an observer following the experiment can do and observe and comprises *all* possible worldlines between the points p and q. A graphical illustration of this can be found in figure 25. Such a causal diamond encloses all continuous non-spacelike world lines from spacetime location p to q.

The area causally related to a local experiment in de Sitter spacetime can be maximized when sending its start and endpoint to the temporal infinities:

$$p \to x_- \in \mathcal{I}^- \qquad q \to x_+ \in \mathcal{I}^+.$$

Such a causal diamond is of maximal size if the defining points have the same spatial coordinate (in this case, θ). These causal diamonds are a central building block in section 6.2, where a tessellation for a two-dimensional de Sitter spacetime is constructed. The static patches we discussed when introducing static coordinates (see definition 2.3) are also causal diamonds of

maximal size.

It is noteworthy that even with a causal diamond of maximal size, it is impossible to cover the entirety of de Sitter spacetime with just one causal diamond. Consequently, no single observer can acquire information about any arbitrary point in de Sitter spacetime, even in principle! This is different in flat Minkowski spacetime, where any local experiment, in principle, is causally connected with any (spatial) point within the spacetime.

Accordingly, everything an observer can do and observe is determined by just these two points $x_\pm$ lying within the temporal boundaries which define the causal diamond $C(x_-, x_+)$. The conclusion is that the observables of quantum gravity in dS live on the temporal boundaries $\mathcal{I}^\pm$. The fact that observables live on the temporal boundaries marks a striking difference from the AdS case, where the observables live on the spatial boundary, which we can identify with observables of a conformal field theory on the holographic boundary. This stark contrast makes reasoning about quantum gravity in dS very different from its AdS counterpart.

One crucial feature of the causal structure of de Sitter spacetime manifests in the fact that there is no globally timelike Killing field in de Sitter spacetime (we derived all allowed Killing fields of dS_2 in section 2.3), which is why there is no global generator of time translation symmetry. It was already emphasized by Witten [Wit01] that there is no global conserved positive energy quantity in de Sitter. The result is that it is impossible to define a global quantum gravity Hamilton operator, which generates a unitary time evolution. Not having a globally defined Hamilton operator is the main reason we focus on the quantum mechanics of the boundary of de Sitter spacetime. The model we construct is defined on a Hilbert space attached to temporal past infinity and describes the (non-unitary) evolution to the temporal future infinity. Working on the boundaries is a key feature of a holographic model. As a result, our model gives us only indirect insight into events within de Sitter spacetime at finite times, which must be holographically reconstructed.

6.2. A tessellation for de Sitter spacetime

The foundation of the holographic network we construct in the remaining chapter is a tessellation. A *tessellation* breaks the spacetime up into smaller pieces, while a good tessellation preserves the isometry group of the spacetime as much as possible. Note that, unlike uniform tessellations of the Euclidean or hyperbolic space as introduced in section 4.2.1, this tessellation is *not* invariant under a discrete subgroup of the group of spacetime isometries. In particular, not all the tiles of the tessellation are identical, and we have two distinguished tiles we will refer to as fundamental regions. We will work with the tessellation proposed by Aicardi [Aic07b, Aic07a] and describe its construction in this section. The tessellation is comprised of causal diamonds whose endpoints lie on the temporal infinities. These points defining the causal diamonds define the entire tessellation. The set of all these endpoints defining the tessellation is identified with the circle $\mathbb{S}^1 \subset \mathbb{C}$. Due to the construction rules of the tessellation, tiles will only be defined on rational numbers on the boundary, which is why we can identify the boundary of the tessellation with $\mathbb{Q}$. To provide a visual representation, figure 26 depicts the resulting tessellation.

The tessellation is defined recursively, starting with two distinguished tiles defining the *fundamental regions* and adding the other tiles recursively. The fundamental tiles are distinguished in the sense that these are the only tiles that extend all the way between the temporal boundaries. Also, the two fundamental tiles cover the entire space at the bottleneck of the spacetime ($t = 0$). We

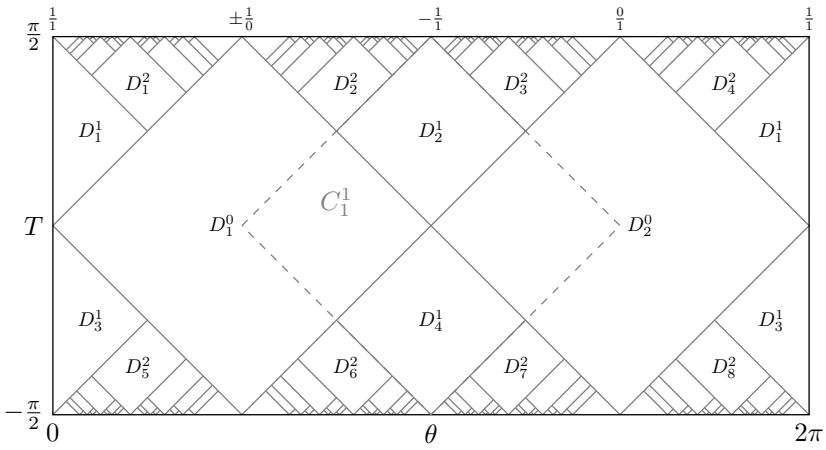

Figure 26.: Recursive construction of a Farey tessellation of dS_2 with causal diamonds.

define the two fundamental tiles, which we denote D_1^0 and D_2^0 as follows:

$$\begin{aligned} D_1^0 &= C\big(\big(\tfrac{\pi}{2}+\gamma, -\tfrac{\pi}{2}\big), \big(\tfrac{\pi}{2}+\gamma, \tfrac{\pi}{2}\big)\big) \\ D_2^0 &= C\big(\big(\tfrac{3\pi}{2}+\gamma, -\tfrac{\pi}{2}\big), \big(\tfrac{3\pi}{2}+\gamma, \tfrac{\pi}{2}\big)\big) \end{aligned} \tag{6.1}$$

The endpoints of these two fundamental regions lie on the temporal infinities $\mathcal{I}^+$ and $\mathcal{I}^-$ and have to be on opposite spatial parts of the spacetime. Due to de Sitter's symmetry properties, there is no preferred position for the fundamental regions, which is captured in the parameter γ (which can also be absorbed by a re-definition of the coordinates). For the rest of the construction, we will consider the case $\gamma = 0$. As all causal diamonds are defined by one spatial coordinate (i.e., the angle θ) and have one defining point on $\mathcal{I}^\pm$ respectively, we will focus on the spatial coordinate for the rest of the construction.

We use the *Cayley transform* to identify the temporal boundaries (which are circles $\mathbb{S}^1$) with the rational numbers. The Cayley transform is a conformal transformation that maps points from the upper half of the complex plane $\mathbb{H}^+$ to the unit disk $\mathbb{D}$, which was introduced in eq. (5.4). For the boundary case, this reduces to a map from the axis of the rational numbers to the unit circle $w : \mathbb{Q} \cup \{\pm\infty\} \to \mathbb{S}^1 = \partial\mathbb{D}$.

With the argument function, we can map the elements of the circle to the interval $[0, 2\pi)$, which we identify with the θ coordinate. This way, we can express the fundamental regions defined in eq. (6.1) as follows:

$$\begin{aligned} D_1^0 =& C\big[\big(\arg\big(w(\pm\tfrac{1}{0})\big), -\tfrac{\pi}{2}\big), \big(\arg\big(w(\pm\tfrac{1}{0})\big), \tfrac{\pi}{2}\big)\big] \\ D_2^0 =& C\big[\big(\arg\big(w(\tfrac{0}{1})\big), -\tfrac{\pi}{2}\big), \big(\arg\big(w(\tfrac{0}{1})\big), \tfrac{\pi}{2}\big)\big] \end{aligned}$$

The following generations of tiles are defined recursively by adding in more tiles. The position of the new tiles is generated with the *Farey mediant* of the points defining the tiles of the previous tessellations. The Farey mediant is an operation to generate all rational numbers, which is defined as

$$\frac{p}{q} \oplus \frac{r}{s} = \frac{p+r}{q+s}.$$

The rational numbers induce the new boundary points on $\mathbb{S}^1$ via the Cayley transformation. To illustrate the construction of new generations of tiles in the tessellation, we will describe this construction in detail for the first generation of tiles; this procedure is similar for higher

generations. The existing tiles are associated with the rational numbers $0/1$ and $\pm 1/0$, which are taken as base cases to construct the new points via the Farey mediant:

$$-\frac{1}{0} \oplus \frac{0}{1} = -\frac{1}{1} \quad \text{and} \quad \frac{0}{1} \oplus \frac{1}{0} = \frac{1}{1}.$$

With the Cayley transform, we can map these rational numbers to points on the circle (or to the interval corresponding to the angle θ). These points define the new causal diamonds necessary to construct the tiles of the first generation:

$$C_1^1 = C\big(\big(\arg(w(1)), -\tfrac{\pi}{2}\big), \big(\arg(w(1)), \tfrac{\pi}{2}\big)\big) = C\big(\big(\tfrac{3\pi}{2}, -\tfrac{\pi}{2}\big), \big(\tfrac{3\pi}{2}, \tfrac{\pi}{2}\big)\big)$$
$$C_2^1 = C\big(\big(\arg(w(-1)), -\tfrac{\pi}{2}\big), \big(\arg(w(-1)), \tfrac{\pi}{2}\big)\big) = C\big(\big(\tfrac{\pi}{2}, -\tfrac{\pi}{2}\big), \big(\tfrac{\pi}{2}, \tfrac{\pi}{2}\big)\big)$$

The tiles for the first generation are defined as the set difference from the causal diamonds C_1^1 and C_2^1 defined above and the tiles of previous generations:

$$D^1 = \big(C_1^1 \cup C_2^1\big) \setminus \big(D_1^0 \cup D_2^0\big) = D_1^1 \cup D_2^1 \cup D_3^1 \cup D_4^1.$$

The first generation is comprised of four tiles where each tile D_k^1 can be interpreted as an individual causal diamond. This procedure is repeated recursively to define tiles of higher generations. For higher generations, we need to take the set difference of the new causal diamonds and *all* pre-existing tiles. The tiles below are the Farey numbers describing the first three generations of tiles (the black numbers correspond to new tiles, and gray numbers represent tiles of previous generations):

$$\begin{array}{ccccccccccccccccc}
-\frac{1}{0} & & & & & & & & \frac{0}{1} & & & & & & & & \frac{1}{0} \quad \mathcal{F}_1 \\
-\frac{1}{0} & & & & -\frac{1}{1} & & & & \frac{0}{1} & & & & \frac{1}{1} & & & & \frac{1}{0} \quad \mathcal{F}_2 \\
-\frac{1}{0} & & -\frac{2}{1} & & -\frac{1}{1} & & -\frac{1}{2} & & \frac{0}{1} & & \frac{1}{2} & & \frac{1}{1} & & \frac{2}{1} & & \frac{1}{0} \quad \mathcal{F}_3 \\
-\frac{1}{0} & -\frac{3}{1} & -\frac{2}{1} & -\frac{3}{2} & -\frac{1}{1} & -\frac{2}{3} & -\frac{1}{2} & -\frac{1}{3} & \frac{0}{1} & \frac{1}{3} & \frac{1}{2} & \frac{2}{3} & \frac{1}{1} & \frac{3}{2} & \frac{2}{1} & \frac{3}{1} & \frac{1}{0} \quad \mathcal{F}_4
\end{array}$$

The recursive application of the Farey mediant generates the *Farey sequence* $\mathcal{F}_n$, which is a sequence of *completely reduced* rational numbers. Two fractions $\frac{p}{q}$ and $\frac{r}{s}$ which are neighboring Farey numbers in a Farey sequence, satisfy $|ps - qr| = 1$, which is equivalent to their difference being equal to $\frac{1}{qs}$. Eventually (in the limit of very high generations), the Farey series generates the entire set of rational numbers $\mathbb{Q}$.

Each Farey number defines a causal diamond by mapping it onto the circle with the Cayley transformation. The points on the future and past boundary associated with the Farey number then define the new causal diamond. Due to the identification with the Farey series, the temporal boundaries of the tessellation can be identified with the rational numbers. The tiles of the new generation are obtained by taking the set difference of the new causal diamond with the tiles of previous generations. The causal diamonds of the nth generation are constructed as

$$C_j^n \equiv C\Big(\Big(\arg(w(\tilde{\mathcal{F}}_n[j])), -\tfrac{\pi}{2}\Big), \arg(w(\tilde{\mathcal{F}}_n[j], \tfrac{\pi}{2}))\Big).$$

where we denote $\tilde{\mathcal{F}}_n[j]$ to be the jth element of $\tilde{\mathcal{F}}_n = \mathcal{F}_n \setminus \mathcal{F}_{n-1}$ which are the Farey numbers new to the nth generation Farey sequence. The tiles of the nth generation are defined as follows:

$$D^n \equiv \left(\bigcup_{j=1}^{2^n} C_j^n\right) \setminus \left(\bigcup_{k=1}^{n-1} D^k\right) = \bigcup_{j=1}^{2^{n+1}} D_j^n,$$

An important aspect in choosing the Farey numbers to generate the tessellation is that it naturally admits the action of the modular group $\mathrm{PSL}(2,\mathbb{Z})$. The group $\mathrm{PSL}(2,\mathbb{Z})$ is the group of isometries

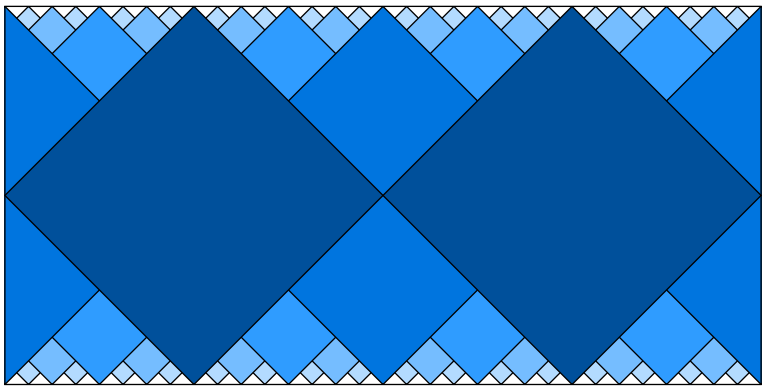

Figure 27.: Dyadic tessellation of dS_2 (colors indicate the generation tiles belong to)

best compatible with this tessellation. We discussed this group of linear fractional transformations in detail in 5.4 and 5.6.

Even though the *Farey tessellation* constructed above is best suited to analyze the group of isometries, it is more convenient to work with a tessellation where the tiles are evenly distributed across the boundary. This has no mathematical or physical reasons and is purely done because the human brain prefers working with apparently evenly distributed tiles. We can evenly distribute the tiles by identifying the Farey numbers with the dyadic rational numbers using the Minkowski question mark function introduced in eq. (5.8). The dyadic rational numbers define the boundary points of the *dyadic tessellation* in the same way the Farey numbers did before. For this, we apply the Minkowski question mark function $?(x)$ to the boundary points of the tessellation, which maps the Farey numbers to the dyadic rational numbers.

The numbers defining the dyadic tessellation lie on the real axis (and accordingly are distributed from $-\infty$ to ∞), which is naturally identified with the unit circle. We can identify the points defining the Farey tessellation with those defining the dyadic tessellation with the generalization of the Minkowski question mark function from eq. (5.9). We can then map the dyadic rational numbers distributed over the real axis to the unit interval using the piecewise linear function ψ introduced in eq. (5.10). The dyadic tessellation, again, is only defined with points on the boundary of spacetime. The points defining the tiles of generations 0 and 1 in the dyadic tessellation are identical to the Farey generation, and the points defining tiles of higher generations are defined as

$$\mathcal{P}_n = \left\{ \frac{2\pi j}{2^{n+1}} \middle| j \in \{1, ..., 2^{n+1}\} \right\} \setminus \left\{ \frac{2\pi j}{2^n} \middle| j \in \{1, ..., 2^n\} \right\}$$

The tessellation is constructed in a similar way to the Farey case, where we construct causal diamonds and take the set difference with tiles of previous tessellations to get the new tiles. The resulting tessellation is depicted in figure 27.

It should be noted that (unlike in the Farey tessellation) the endpoints p and q of the tiles of the same generation $D_j^n \equiv C(p, q)$ (after taking the set difference with pre-existing tiles) lie on *constant time slices* which depend on the generation as depicted in figure 28. We denote the timeslice T_n to be the timeslice which cuts all tiles of generation n:

$$T_n = \text{sgn}(T)\frac{\pi}{2}\frac{2^n - 1}{2^n}$$

The timeslices T_n have an additional interesting interpretation: In the limit of large times, the size of de Sitter spacetime doubles between T_n and T_{n+1}. The doubling of spacetime for consecutive

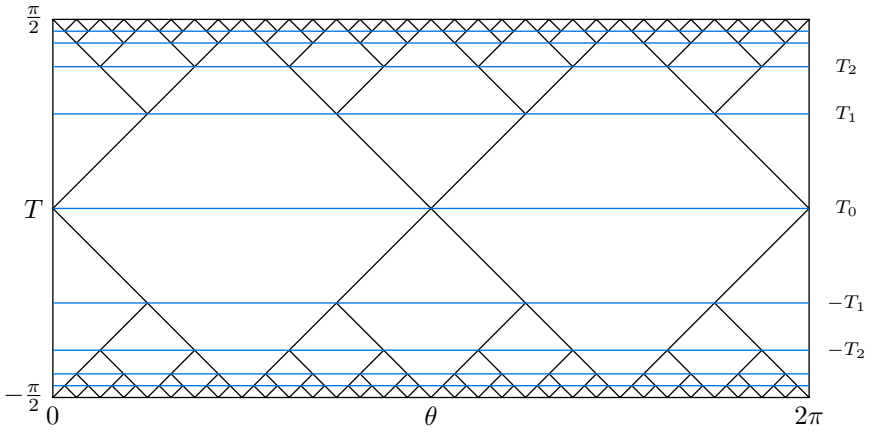

Figure 28.: Dyadic tessellation of dS_2 with constant time slices (blue)

timeslices in the asymptotic limit is explicitly derived in appendix D.1. As a result, in the limit of large times, both the number of tiles and the size of spacetime doubles for consecutive generations. Accordingly, the width of the tiles in the tessellation close to the boundary is approximately constant. This is most clearly observed in the tessellation when embedding de Sitter in Minkowski spacetime as shown in figure 29.

Any tessellation of a given area needs to cover this area with tiles without overlaps or gaps. In order to tessellate the entire $1+1$ dimensional de Sitter spacetime, we need infinitely many generations of tiles to avoid gaps close to the temporal boundaries of the spacetime. To avoid always working with infinitely many tiles, we introduce cutoffs of the tessellation, which are defined by a finite set of tiles. The definition of cutoffs will be made mathematically rigorous in the next section.

6.3. Construction of a holographic toy model

In this section, we construct a *holographic toy model* corresponding to $(1+1)$-dimensional de Sitter spacetime with de Sitter radius $\ell = 1$. For the construction of the holographic toy model, we use a family of tensor networks, which is why we also refer to the holographic toy model as a holographic network. On a technical level, the basic idea follows the tensor network constructions in the anti-de Sitter setting presented in [PYHP15], where the basic ideas relevant to our construction are described in section 4.2.

However, there are some fundamental differences as de Sitter spacetime has, unlike AdS, no spatial but two temporal boundaries. The fundamental structure of de Sitter spacetime is characterized by an initial contraction (for $T < 0$) and a subsequent expansion (for $T > 0$). With the holographic network, we want to model these epochs at a microscopic quantum level. Intuitively, we directly associate these epochs with a fundamental behavior of quantum information: A contracting spacetime should imply the reduction of quantum information as there is less volume and, thus, fewer quantum degrees of freedom to store information. At the same time, we expect the creation of new quantum degrees of freedom for the expanding spacetime.

There are many ways to model processes of loss or deletion as well as creation in quantum mechanics. The strategy employed here is to model the processes as an *isometry*. This way, we obtain an *isometric time evolution* with the consequence that we have to accept that the time evolution is non-unitary. The idea of time evolution being "only" isometric was established

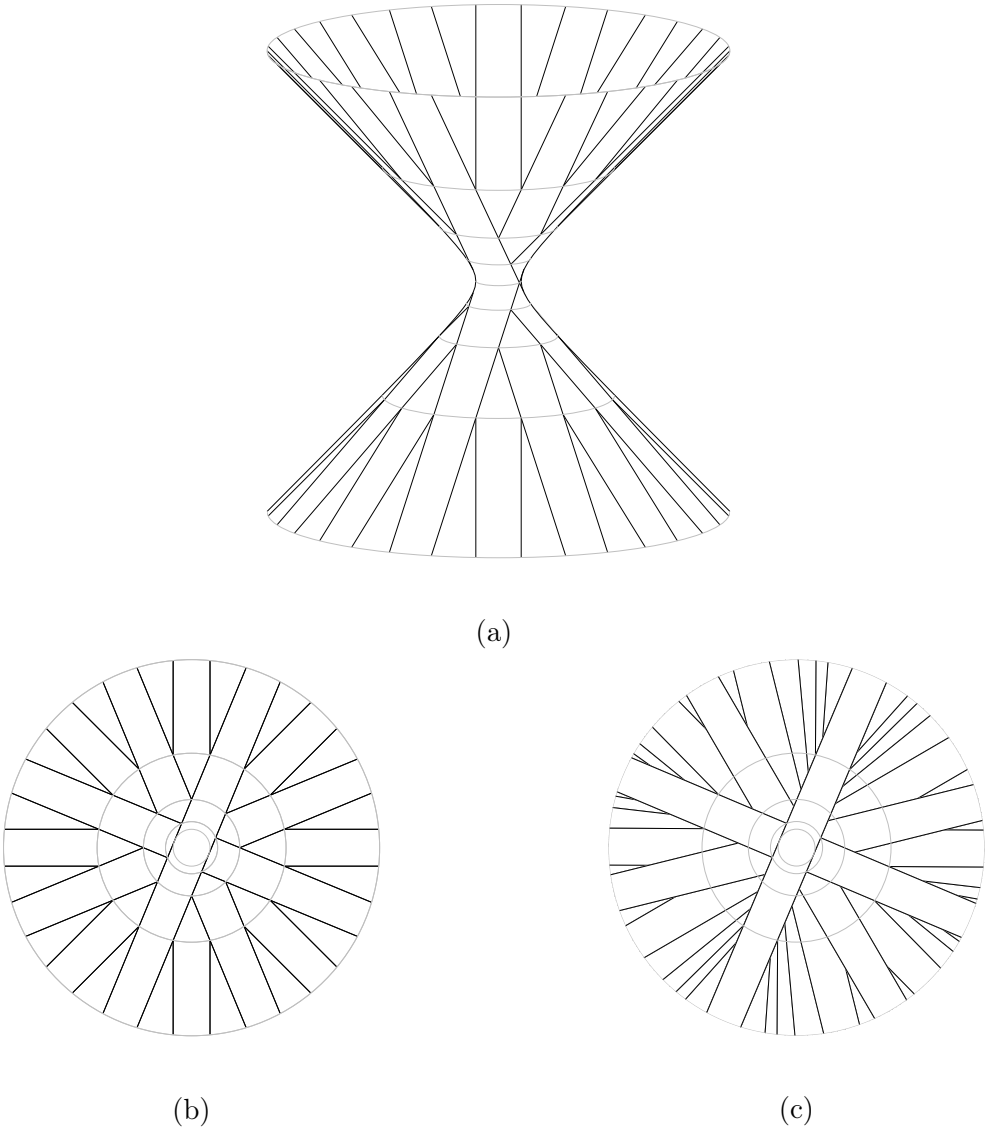

Figure 29.: Tessellations of dS_2 on the hyperbolic sheet embedded in Minkowski spacetime. Depiction of the dyadic tessellation (a) from the side and the dyadic (b) and Farey tessellation (c) from the top.

when we first published the tensor network model in [NO22] and discussed further by Cotler and Strominger in [CS22]. An alternative option that would preserve unitary time evolution is to model the process using *completely positive maps* (CP-maps), which gives rise to a new question: Where does the lost information go, and who can access it? For the construction of the holographic model, we model the time evolution using isometries. The time evolution then manifests in a branching of the spacetime characterized by the type of isometry.

To construct our holographic tensor network M for de Sitter spacetime with radius $\ell = 1$, we adapt the tensor network construction known from the AdS case [PYHP15] and associate tensors with the corners of the tiles as depicted in figure 30. The tensor network structure is obtained by contracting the legs of tensors corresponding to *consecutive generations* of tiles along their edges. Note that the rank of a tensor placed at the corner of a tile corresponds to the number of neighboring tensors. In this way, we have associated 4-leg tensors with only the initial generation and 3-leg tensors everywhere else. Later, we consider the construction of holographic tensor networks corresponding to de Sitter spacetimes with radius $\ell > 1$, which feature a greater number of 4-leg tensors.

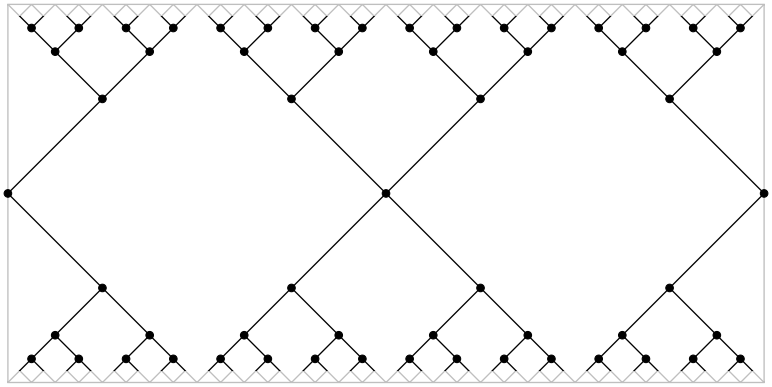

Figure 30.: Holographic tensor network M corresponding to the dyadic tessellation of $\mathrm{dS}_2(\ell = 1)$. This network should be understood as an infinite network extending between the temporal boundaries.

The only uncontracted legs of the resulting *infinite* tensor network are associated with the temporal boundaries of the tensor network. The uncontracted legs are equivalent to the physical degrees of freedom of the model we can access directly. The tensor network can be interpreted as a *propagator* or channel between the Hilbert spaces associated with the temporal boundaries.

With the tensor network M, we have not constructed a quantum gravity solution. Rather, we provide a toy model for quantum gravity in de Sitter spacetime that relates quantum gravity in de Sitter spacetime to quantum information theory. This way, we can learn more about the properties of de Sitter spacetime and have a tool to describe a microscopic realization of a $\mathrm{dS}_{1+1}/\mathrm{TN}_1$ correspondence.

6.3.1. Kinematical Hilbertspaces

One of the most important features of de Sitter spacetime is that all the observables live on the temporal boundaries $\mathcal{I}^{\pm}$. We associate the degrees of freedom at the boundaries with Hilbert spaces: the Hilbert space $\mathcal{H}_{\mathrm{in}}$ for the degrees of freedom at $\mathcal{I}^-$ and the Hilbert space $\mathcal{H}_{\mathrm{out}}$ for the degrees of freedom at $\mathcal{I}^+$. The Hilbert spaces are associated with the uncontracted tensor legs at the boundary, where we again assume the dimension d of the Hilbert spaces associated with the individual tensor legs. We define a Hilbert space of an uncontracted leg at the boundary to be $\mathfrak{h} = \mathbb{C}^d$. This way, the Hilbert spaces at the boundaries are

$$\mathcal{H}_{\mathrm{in}} = \mathfrak{h}^{\otimes\infty} \qquad\qquad \mathcal{H}_{\mathrm{out}} = \mathfrak{h}^{\otimes\infty}$$

The *kinematical states*, which determine the expectation values of the observables, are also associated with the temporal boundaries and thus also live in the *boundary Hilbert spaces*:

$$|\psi_{\mathrm{in}}\rangle \in \mathcal{H}_{\mathrm{in}} \qquad\qquad |\psi_{\mathrm{out}}\rangle \in \mathcal{H}_{\mathrm{out}}$$

We can reduce the description to finite-dimensional Hilbert spaces by introducing a cutoff for the tessellation, which directly relates the tensor network to a finite-dimensional one in the way described below.

Definition 6.1 (Cutoff)
The *cutoff* $\mathfrak{c}$ of a tessellation is a rule to produce a tessellation with only finitely many tiles. Since de Sitter has two boundaries, we consider a cutoff both for the past and the future boundary. The cutoff of a tessellation is defined by the n-tuple of boundary points associated with the tiles

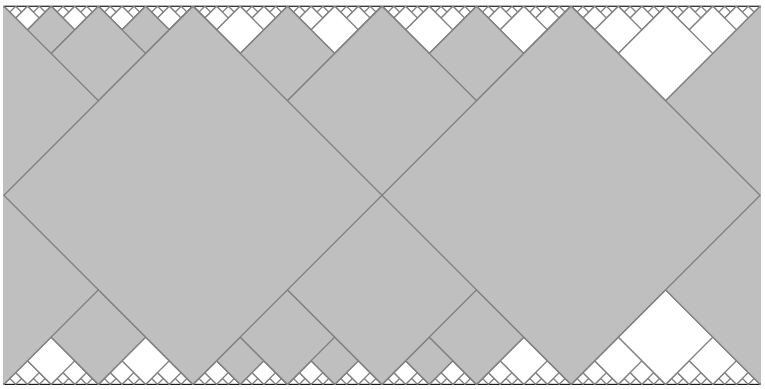

Figure 31.: Cutoff of the dyadic tessellation depicted as the gray area defined by $\mathfrak{c}_+ = \{0, \frac{1}{16}, \frac{1}{8}, \frac{3}{16}, \frac{1}{4}, \frac{3}{8}, \frac{1}{2}, \frac{5}{8}, \frac{3}{4}\}$ and $\mathfrak{c}_- = \{0, \frac{1}{8}, \frac{1}{4}, \frac{5}{16}, \frac{3}{8}, \frac{7}{16}, \frac{1}{2}, \frac{9}{16}, \frac{5}{8}, \frac{3}{4}, \frac{7}{8}\}$

included in the cutoff. For the dyadic tessellation, these points need to be dyadic rational numbers. The boundary is associated with the unit interval where the endpoints are identified. We will refer both to the rule defining the cutoff as well as the area covered by the finite tessellation as a cutoff.

The cutoff generates a tessellation that does not cover the entire spacetime close to the boundary and restricts the system to a finite size. An example of a cutoff is depicted in figure 31. We denote by $\mathcal{C}$ to be the set of all cutoffs, which is a *directed set* with a partial order $\mathfrak{c} \leq \mathfrak{c}'$ imposed by the inclusion of cutoff areas. We can directly associate a tensor network and, with this, a boundary Hilbert space to each cutoff:

$$\mathcal{H}_{\text{in}}^{\mathfrak{c}_-} = \mathfrak{h}^{\otimes 2|\,\mathfrak{c}_-\,|} \qquad\qquad \mathcal{H}_{\text{out}}^{\mathfrak{c}_+} = \mathfrak{h}^{\otimes 2|\,\mathfrak{c}_+\,|}$$

$|\,\mathfrak{c}_\pm\,|$ is the number of tiles on the respective boundary included in the cutoff, and $2|\,\mathfrak{c}_\pm\,|$ is the number of uncontracted legs for a given cutoff on that boundary. The number of uncontracted legs determines the dimension of the boundary Hilbert space.

Any kinematical state $|\psi_{\text{in/out}}\rangle \in \mathcal{H}_{\text{in/out}}^{\mathfrak{c}}$ can be conceptualized as a vector represented with a tensor network with $2|\,\mathfrak{c}\,|$ uncontracted legs. To make physical sense of the states with the imposed cutoff, each kinematical state must be equivalent to the state on a larger cutoff. This equivalence relation to compare states from different Hilbert spaces is characterized below. For this, we need an operation to relate different cutoffs with one another.

The partial ordering of the set of all cutoffs $\mathcal{C}$ allows for a *fine graining* operation: we can always find a cutoff to cover a larger part of the spacetime than the previous cutoff. This has the consequence, that for any two cutoffs $\mathfrak{c}$ and $\mathfrak{c}'$ there always exists a cutoff $\mathfrak{c}''$ which covers an area larger than both initial cutoffs:

$$\mathfrak{c} \leq \mathfrak{c}'' \qquad \text{and} \qquad \mathfrak{c}' \leq \mathfrak{c}''$$

In particular, it is always possible to find such a cutoff $\mathfrak{c}''$ where the boundary points match a regular dyadic subdivision as depicted in figure 32. In practice, we will work with this class of cutoffs. We define the set of all cutoffs producing a standard dyadic tessellation to be $\mathcal{C}_d$.

We now define the *fine graining* operation as a linear map between the cutoff-Hilbert spaces, which relates different cutoffs without adding any further information

$$T_{\mathfrak{c}'}^{\mathfrak{c}} : \mathcal{H}^{\mathfrak{c}} \to \mathcal{H}^{\mathfrak{c}'} \tag{6.2}$$

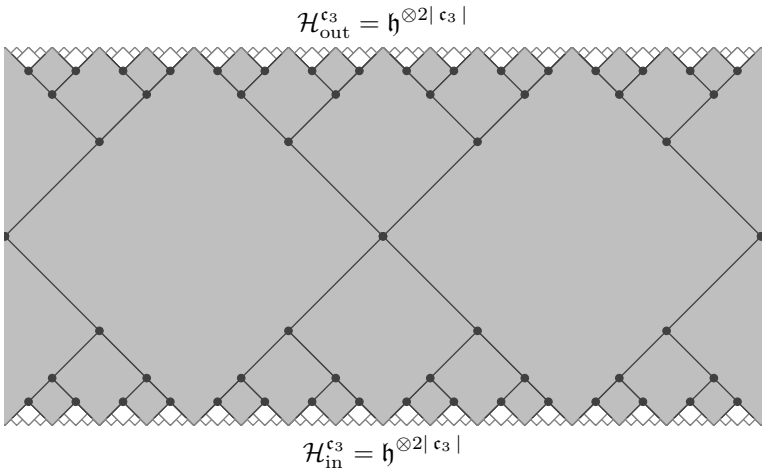

Figure 32.: Hilbert spaces of the future and past boundary associated to the cutoff $\mathfrak{c}_3$ of the dyadic tessellation, the dimension of the Hilbert spaces is determined by $|\,\mathfrak{c}_3\,| = 2^4$ which equals the number of uncontracted legs at the boundary

The fine-graining operation has to satisfy the following properties to be well-defined:

- The fine-graining operation between two identical cutoffs is the identity: $T_{\mathfrak{c}}^{\mathfrak{c}} = \mathbb{1}$
- The fine-graining operation is transitive: $T_{\mathfrak{c}''}^{\mathfrak{c}} = T_{\mathfrak{c}''}^{\mathfrak{c}'} T_{\mathfrak{c}'}^{\mathfrak{c}}$

With this method, we can compare states from different Hilbert spaces: both states are fine-grained to a common Hilbert space and compared in that mutual Hilbert space. The overlap between different states can be determined as follows:

$$\langle \phi_{\mathfrak{c}}| \, (T_{\mathfrak{c}''}^{\mathfrak{c}})^{\dagger} T_{\mathfrak{c}''}^{\mathfrak{c}'} \, |\psi_{\mathfrak{c}'}\rangle$$

We use this fine-graining operation to define an equivalence relation between kinematical states from Hilbert spaces associated with different cutoffs.

Lemma 6.2
Two states $|\psi^{\mathfrak{c}}\rangle \in \mathcal{H}_{\text{in}}^{\mathfrak{c}}$ and $|\psi^{\mathfrak{c}'}\rangle \in \mathcal{H}_{\text{in}}^{\mathfrak{c}'}$ are *physically equivalent* $|\psi^{\mathfrak{c}}\rangle \sim |\psi^{\mathfrak{c}'}\rangle$ if there exists a cutoff $\mathfrak{c}''$ such that the following fine graining operations are equal:

$$T_{\mathfrak{c}''}^{\mathfrak{c}} \, |\psi^{\mathfrak{c}}\rangle = T_{\mathfrak{c}''}^{\mathfrak{c}'} \, |\psi^{\mathfrak{c}'}\rangle$$

With this equivalence relation, we can characterize if two states are physically equal even if they are different on a mathematical level. We can now define a Hilbert space representing *all* states from Hilbert spaces with different cutoffs:

$$\hat{\mathcal{H}} = \biguplus_{\mathfrak{c}\in\mathcal{C}} \mathcal{H}^{\mathfrak{c}} = \bigcup_{\mathfrak{c}\in\mathcal{C}} \{(x, \mathfrak{c}) : x \in \mathcal{H}^{\mathfrak{c}}\}$$

Here, $\uplus$ is the disjoint union defined as the union of subsets where each subset is indexed with its original set. With that, we define the *semicontinuous limit* as the space of equivalence classes of physical states with finite cutoff:

$$\mathcal{H} = \varinjlim \mathcal{H}^{\mathfrak{c}} = \left(\biguplus_{\mathfrak{c}\in\mathcal{C}} \mathcal{H}^{\mathfrak{c}} \Big/ \sim \right)^{\|\cdot\|}$$

The semicontinuous limit is the disjoint union of Hilbert spaces with different cutoffs modulo the equivalence relation completed with respect to the standard norm.

With the Hilbert spaces at the cutoffs $\mathcal{H}_{\text{in}}^{\mathfrak{c}}$ and $\mathcal{H}_{\text{out}}^{\mathfrak{c}'}$, we can relate the infinite tensor network M to a finite tensor network representing an operator acting between the finite cutoff Hilbert spaces at the boundaries. With the equivalence relation, we can directly see that the finite tensor network is physically equivalent to the infinite tensor network. The tensor network defined by our tessellation induces a *family* of linear maps, which is defined by drawing the tensor network up to the given cutoffs

$$M_{\mathfrak{c},\mathfrak{c}'} : \mathcal{H}_{\text{in}}^{\mathfrak{c}} \to \mathcal{H}_{\text{out}}^{\mathfrak{c}'}$$

The open legs act on the respective input and output spaces $\mathcal{H}_{\text{in}}^{\mathfrak{c}}$ and $\mathcal{H}_{\text{out}}^{\mathfrak{c}'}$. Due to the equivalence relation and the semicontinuous limit, we can interpret the tensor network to act in the limit where the boundary Hilbert spaces have infinite size. Effectively, we work in the smallest Hilbert space necessary to represent a state from a certain equivalence class and can use the physical equivalence to all other Hilbert spaces, including $\mathcal{H}_{\text{in}}$ and $\mathcal{H}_{\text{out}}$.

6.3.2. Physical Hilbertspace

We also introduce a Hilbert space $\mathcal{H}_0$, which is associated with the bottleneck ($T = 0$) of the spacetime. As argued above, we model the contraction process with an isometry $A^\dagger$ and the expansion process by an isometry B.

$$A^\dagger : \mathcal{H}_{\text{in}} \to \mathcal{H}_0 \qquad\qquad B : \mathcal{H}_0 \to \mathcal{H}_{\text{out}}$$

Consequently, the evolution of the entire spacetime is represented by the following operator:

$$W = BA^\dagger : \mathcal{H}_{\text{in}} \to \mathcal{H}_{\text{out}}.$$

This operator W, which captures the evolution of de Sitter spacetime, can be described with the tensor network M. We can directly see that this is not a unitary operator:

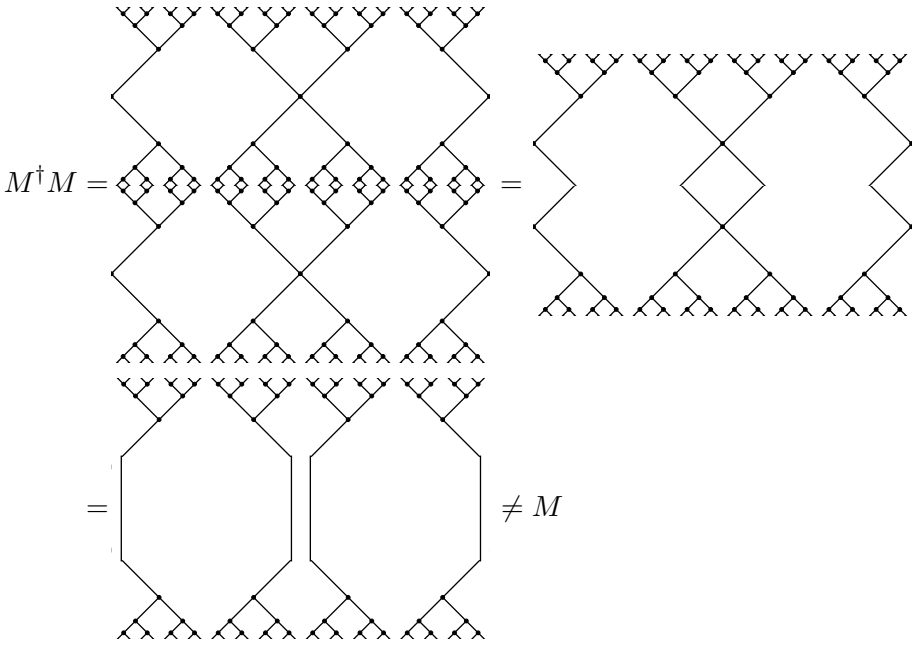

Compositions of isometries such as W are partial isometries. Partial isometries can be defined in several equivalent ways. Here, we define a *partial isometry* as a bounded linear transformation

$C : \mathcal{H}_1 \to \mathcal{H}_2$ where $P = C^\dagger C$ is a projection. It is straightforward to see that $W^\dagger W = AB^\dagger BA^\dagger = AA^\dagger$ is a projection, which implies that W is a partial isometry. This can be directly translated to the tensor network M where we exploit the identities (4.2) and (4.1):

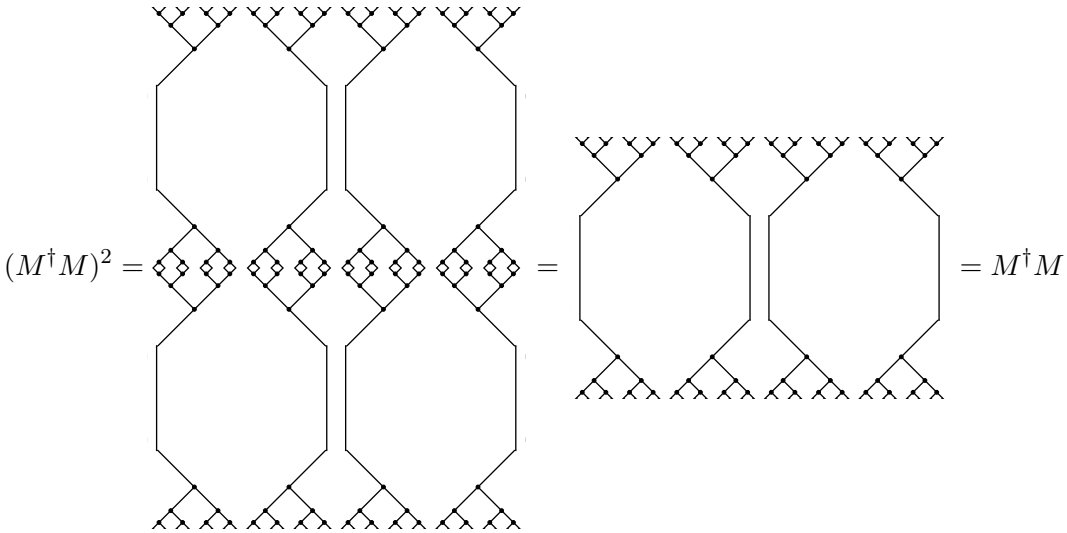

Since $M^\dagger M$ is a projection, the tensor network, indeed, is a partial isometry. As a result, we can identify the operator W with the tensor network M. We can see that the tensor network M fails to be a unitary propagator, as $W^\dagger W$ is a projection and not the identity that would be required for a unitary operation. Consequently, we interpret the operator W as well as the tensor network M as a kind of *restricted propagator* from the Hilbert space $\mathcal{H}_{\text{in}}$ to the Hilbert space $\mathcal{H}_{\text{out}}$.

One important resulting physical feature is that the projection $P = M^\dagger M$ arising from the tensor network singles out a particular subspace of $\mathcal{H}_{\text{in}}$. We denote this subspace to be the *physical Hilbertspace*

$$\mathcal{H}_{\text{phys}} \equiv (M^\dagger M)\mathcal{H}_{\text{in}} \subset \mathcal{H}_{\text{in}}$$

which is the subspace comprised of *physical states*. A physical state $|\phi_{\text{phys}}\rangle \in \mathcal{H}_{\text{phys}}$ hereby is interpreted to be a state which propagates through the network, simulating spacetime without loss of norm.

One fundamental property of the tensor network M is, that the physical Hilbert space $\mathcal{H}_{\text{phys}} \equiv (M^\dagger M)\mathcal{H}_{\text{in}}$ which is a subspace of $\mathcal{H}_{\text{in}}$ is *finite dimensional*. The finite dimensionality can be interpreted as an information bottleneck at $T = 0$. A finite-dimensional quantum Hilbert space in de Sitter spacetime was already suggested by Witten [Wit01]. This tensor network model and, in particular, the subspace $\mathcal{H}_{\text{phys}}$ can be thought of as a microscopic realization of the nonperturbative finite-dimensional Hilbert space introduced by Witten in 2001. Further, we can interpret the tensor network M, which is a partial isometry, as a microscopic realization of the matrix M constructed by Witten. The fact that a finite-dimensional subspace canonically emerges from an infinite dimensional ambient Hilbert space is quite counter-intuitive and easiest to grasp in the tensor network representation. We later connect this observation with the Λ-N correspondence, which characterizes the relation between the curvature of the spacetime and the dimension of the Hilbert space. To do this, we will generalize the here constructed tensor networks from de Sitter radius $\ell = 1$ to larger de Sitter radii.

In the AdS setting, fundamental building blocks of the tensor network are *perfect tensors*, which are useful because they are isometric encoding maps of quantum error-correcting codes [PYHP15]. Also, they ensure that the microscopic quantum tensor network inherits a residual rotation

invariance. The fact that perfect tensors are used for the construction of holographic models in the AdS case creates the motivation to use them here as well. We will see that for most of our observations, we do not actually need our tensors to obey all of the conditions required of a perfect tensor. Indeed, only the condition that they are isometries in the usual sense is necessary for a majority of our results.

Tensor network models, in general, often have the drawback that they are limited to low-dimensional settings, as it is often difficult to define the underlying tessellation in higher dimensions properly. This is also true for the tessellation presented in this context. This abstract structure, which makes use of isometries to describe the evolution, is not necessarily restricted to $(1+1)$ dimensions.

6.4. Holographic networks for different curvatures

We have, so far, only considered tessellations and tensor networks corresponding to a $(1+1)$-dimensional de Sitter spacetime with de Sitter radius $\ell = 1$. The size of the physical Hilbert space is directly related to the number of legs in the bottleneck area of the tensor network. The size of this physical subspace $\mathcal{H}_{\text{phys}}$ limits the information capacity of the tensor network.

In this section, we introduce a generalization of the construction of the holographic model to describe de Sitter spacetime in $(1+1)$ dimensions for various de Sitter radii $\ell > 1$, which yields a correspondence between the curvature of the spacetime and the quantum information capacity of the network. According to this definition, one obtains a correspondence between the quantum information capacity Q of the network and the cosmological constant Λ, which is directly related to the de Sitter radius ℓ. This can be interpreted as a model of the Λ-N *correspondence* introduced by Banks [Ban01] and Bousso [Bou99a, Bou99b, Bou00]. Ultimately, we get a description of the continuous and infinite de Sitter spacetime with a finite-dimensional physical Hilbert space. At the time, this was a striking and counter-intuitive result. This tensor network model captures the finite dimensionality of the Hilbert space in a way that is much more approachable on both a mathematical and intuitive level.

The argument of the Λ-N correspondence builds on the observation that the area of the corresponding causal diamond bounds the total entropy perceived by an observer. This can be understood in the context of associating a local laboratory with an experiment starting at p and ending at q to the observer where the observer can only perform local unitary operations. When assuming that the observer $\mathcal{O}$ initializes their laboratory in a pure state $|\phi\rangle$ at the beginning of the experiment, $\mathcal{O}$ can create entropy by losing halves of entangled pairs before the experiment ends. This creation of entropy is limited by the number of qubits that cross the boundary of the causal diamond $C(p,q)$ before the experiment ends. This way, the flux of qubits through the boundary of the causal diamond limits the total amount of entropy that can be created. The direct relation to the boundary area motivates the use of holographic models. The covariant entropy bound introduced by Bousso in [Bou99a] characterizes an upper bound for the amount of information that can pass a causal diamond. With this, it was argued in [Bou00] that the entropy of a causal diamond is bounded by its area, which is proportional to $1/\Lambda$. This imposes a direct correlation between the cosmological constant Λ and the number of quantum degrees of freedom N.

Here, we describe how the construction of the holographic model directly generalizes to models corresponding to de Sitter spacetimes where the de Sitter radius doubles and construct a description for all de Sitter radii $\ell = 2^n$ with $n \in \mathbb{N}$. We illustrate this in detail for de Sitter radii $\ell = 2$ and $\ell = 4$. With the generalization of the construction, we want to preserve the causal structure of the tensor network for de Sitter spacetime with $\ell = 1$. For the de Sitter radius $\ell = 2$, this can

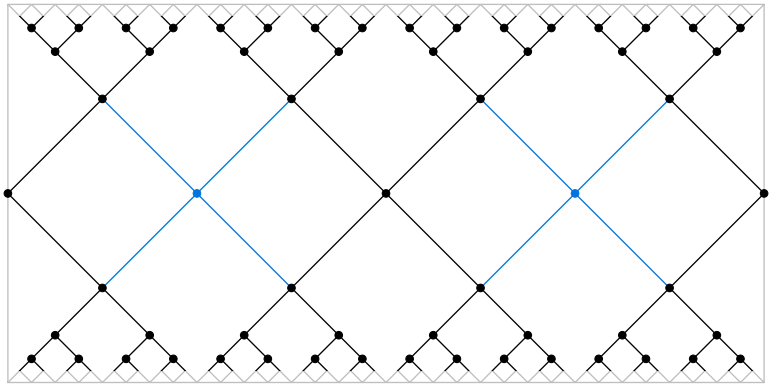

Figure 33.: Tessellation and holographic network M_2 for dS_2 with $\ell = 2$. The blue lines divide the initial causal diamonds of M_1 and are added to the new tensor network.

be achieved by dividing the two fundamental tiles at the bottleneck into four smaller tiles each, which only modifies the tensor network in the bottleneck area. This is plausible from a physical perspective, as the finiteness of the de Sitter radius is most relevant in this part of the spacetime. On the basis of this modified tessellation, the tensor network is constructed in the same way as the original tensor network. The resulting tensor network M_2 is shown in figure 33. Similar to the original tensor network M, the generalized tensor network M_2 is a partial isometry which also implies a finite dimensional physical Hilbert space. It is shown in appendix D.2 that the tensor network corresponding to de Sitter spacetime with de Sitter radius $\ell = 2$ and $\ell = 4$ also are partial isometries. From this, we can directly see that $M_2^\dagger M_2$ is a projection of the input Hilbert space $\mathcal{H}_{\text{in}}$ to the physical Hilbert, which is a subspace with the dimension

$$\dim(\mathcal{H}^2_{\text{phys}}) = \dim(\mathfrak{h})^8.$$

For spacetimes with de Sitter radii $\ell = 4$ and larger, the construction proceeds iteratively: tiles in the bottleneck area are divided into smaller tiles, and a tensor network is associated with the new tessellation. For each doubling of the de Sitter radius (i.e., each iteration step for the construction of a network with a large de Sitter radius), one more generation of tiles is divided into smaller pieces. In the tessellation, this is all the tiles that only cover a finite time interval, plus the first generation of tiles that extend to a temporal boundary. The tessellation corresponding to $\ell = 4$ has four times as many tiles in the bottleneck area compared to the original tessellation M ($\ell = 1$). The corresponding tensor network is depicted in figure 34. The resulting network is also a partial isometry. The partial isometry $M_4^\dagger M_4$ is a projection from $\mathcal{H}_{\text{in}}$ to the corresponding physical Hilbert space with dimension

$$\dim(\mathcal{H}^4_{\text{phys}}) = \dim(\mathfrak{h})^{16}.$$

An analogous calculation can be carried out for larger values of ℓ. For all these tensor networks constructed this way, which are associated with de Sitter spacetimes with $\ell \neq 1$, it holds that they are partial isometries. The corresponding physical Hilbert spaces have the dimension

$$\dim(\mathcal{H}^\ell_{\text{phys}}) = \dim(\mathfrak{h})^{4\ell} = d^{4\ell}.$$

For increasing de Sitter radii, we get a tensor network, which is comprised of a regular grid of unitary operators around the bottleneck area and tree tensor networks in the past and future. In the limiting case of $\ell \to \infty$, the regular grid of unitary operators gets larger, and with this, the tensor network approaches that of Minkowski spacetime. The regular grid of unitary operators describing Minkowski spacetime is called a *quantum cellular automaton* (QCA), which is widely

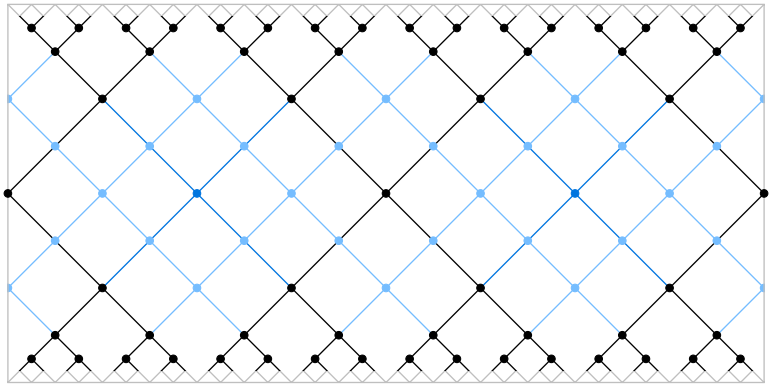

Figure 34.: Tessellation and holographic network M_4 for dS_2 with $\ell = 4$. The blue (edges of D^1) and light blue (edges of D^2) lines divide the initial causal diamonds from M_1 and M_2.

discussed in the literature (see, for example, [AP03, ABF20, BDBD$^+$15, BDP17, Deb19, SW04]). Since QCA has a natural causal structure where information propagates along light rays, they are a natural candidate for a tensor network description of Minkowski spacetime as argued in the literature in various settings [Bén13, dBHMN16, CHQY19, CLMS16, KB17, MV18b, YBC$^+$19]. The emergence of a tensor network structure of Minkowski spacetime in the limit $\ell \to \infty$ further supports this construction and the tensor network as a microscopic model of de Sitter spacetime.

With the dimension of the physical Hilbert space $\mathcal{H}^\ell_{\text{phys}}$ for de Sitter radii $\ell > 1$, we can directly derive a fundamental relation between the cosmological constant Λ and the quantum information capacity Q_ℓ of the corresponding tensor network M_ℓ. The tensor network M_ℓ is a partial isometry and, with that, directly generates a corresponding completely positive map (which is not necessarily trace-preserving!) in the following way:

$$\mathcal{E}_\ell(\rho) \equiv M_\ell \rho M_\ell^\dagger.$$

This CP-map acts as a global operator on the temporal boundary of the spacetime and takes density operators from the Hilbertspace $\mathcal{H}_{\text{in}}$ to density operators in the Hilbertspace $\mathcal{H}_{\text{out}}$. One way to interpret a CP-map is that it represents a communication process between two observers taking the roles of sender and receiver. The question arising here is what the corresponding quantum capacity of the communication process is. In other words, How many qubits of quantum information can be stored in the CP map in a single use and without error? This can be directly answered using the tensor network. In the physical Hilbert space $\mathcal{H}^\ell_{\text{phys}}$ we can encode $2^{Q^{(1)}_\ell}$ qubits, which directly gives us the number of qubits which we denote as *quantum capacity*

$$Q^{(1)}_\ell = \lfloor \log_2(\dim(\mathcal{H}^\ell_{\text{phys}})) \rfloor.$$

with the dimension of the physical Hilbert space being $\mathcal{H}^\ell_{\text{phys}} = d^{4\ell}$. We obtain this quantum capacity because M_ℓ is a partial isometry, and it is possible to directly encode $2^{Q^{(1)}_\ell}$ qubits into the subspace $\mathcal{H}_{\text{phys}}$ which is then transmitted noiselessly. Note that

$$Q^{(1)}_\ell \lesssim 4\ell \log_2 d.$$

The physical interpretation of this quantity is the number of qubits that can be sent through the bottleneck of the tensor network without disturbance. The quantum capacity is directly proportional to the vertices in the tensor network depicted in figure 35. The direct relation between the de Sitter radius and the quantum information capacity directly implies a correspondence between the cosmological constant Λ and the quantum information capacity of the tensor network:

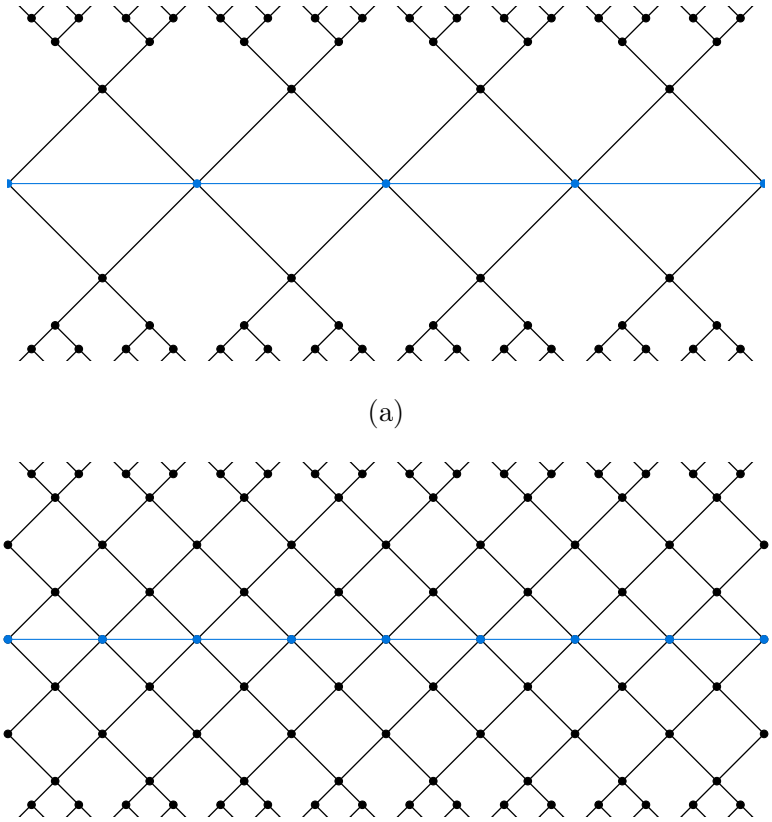

(a)

(b)

Figure 35.: Visual interpretation of the quantum information capacity of the tensor networks related to the number of tensors at the bottleneck which is directly proportional to the dimension of $\mathcal{H}^{\ell}_{\text{phys}}$ for (a) M_2 with $\ell = 2$ and (b) M_4 with $\ell = 4$

$$Q^{(1)} \propto \frac{1}{\sqrt{\Lambda}}. \tag{6.3}$$

In the case of two-dimensional de Sitter spacetime and Jackiw-Teitelboim gravity, the relation between the scalar curvature R and the cosmological constant is characterized in eq. (2.1):

$$\Lambda = \frac{R}{2} = \frac{1}{\ell^2}$$

For $3+1$ dimensional de Sitter spacetime, which is the dimension usually studied in the literature, the relation between de Sitter radius and cosmological constant is the same up to a proportionality factor (see for example [Bou02a]):

$$\frac{\ell}{\sqrt{3}} = \sqrt{\frac{1}{\Lambda}}$$

From the correspondence in eq. (6.3), we can conclude that a positive cosmological constant sets an upper bound on the information capacity of a spacetime. We can also make the reverse statement: a spacetime with finite quantum capacity implies that a spacetime has a positive cosmological constant. This relation also illustrates how the entire spacetime can be characterized with a finite-dimensional Hilbert space. Still, it needs to be noted that this result needs to be treated with some caution: It is presently not clear how a negative cosmological constant (AdS)

influences the quantum capacity. We will not go further into this here, also because the structure of observables in AdS spacetimes is radically different to the dS case.

Holographic models have been studied in the context of de Sitter spacetime, and one well-known tensor network that needs to be mentioned is *MERA*: the multiscale entanglement renormalization ansatz. The fundamental idea of MERA is to disentangle the system at various length scales and, with that, perform a type of coarse-graining, which is introduced in detail in [Hau13]. MERA tensor network representations have been introduced in [MV18a, MV18b] where a correspondence between path integrals in de Sitter geometries and Lorentzian MERA tensor networks has been established. As MERA implements an entanglement evolution, it is naturally equipped with a causal structure [Vid07, Vid08]. MERA tensor networks have been used successfully to capture dualities in the AdS/CFT correspondence [Swi12b]. There have been attempts to explore generalizations of MERA in the context of de Sitter, such as [KB17] where MERA was constructed on a thermal state instead of a pure state as in the initial formulation. This generalization of MERA captures causality relations in de Sitter spacetime. It has a notion of time evolution and is comprised of unitaries and isometries. Within the framework given by the generalization of MERA, it is possible to calculate local observables in the ground state. However, it is not possible yet to fully describe dynamics in this framework. There have been similar works on holographic models in de Sitter spacetime, such as [BCCM17]. The causal structure can be confirmed in a more rigorous manner using various notions of *quantum causal influence* as it was discussed in [Bén13, CHQY19] and references therein. One way to recover the causal structure of de Sitter spacetime is to use the notion of *pure causality* introduced by Bény in [Bén13]. A tensor network, which can be interpreted as a channel, is defined to be *purely causal* if it can be expressed in terms of a unitary map, which is causal where auxiliary input or output systems can be introduced to get a unitary map.

In the limiting case of small curvature $\ell \to \infty$, which we can consider with the construction performed in this chapter, we obtain the structure of a quantum cellular automaton. Together with the connection to Lorentzian MERA models, the QCA structure provides further evidence that our tensor network is a microscopic model for de Sitter spacetime.

If we consider a local observer in de Sitter spacetime, its worldline evolves from the past boundary of the spacetime to its future boundary. We can interpret the tensor network M to be a superposition of *all* possible world lines of local observers.

6.5. Isometry transformations of the holographic model

The isometry group of de Sitter can be reduced to its action on the degrees of freedom on the future and past boundary. One way to characterize the quality of a tessellation is that it is invariant under the actions of transformations from the isometry group as much as possible. One restriction we inevitably have to make when considering a tessellation is that continuous isometries reduce to their discrete analogs. The discretized isometry actions of the de Sitter boundaries are described by $\mathrm{PSL}(2,\mathbb{Z})$, which is a subgroup of Thompson's group, which is described in section 5.6. In this section, we will describe how to apply the isometry action to the tessellation and eventually to the tensor network.

6.5.1. Transformation of the tessellation

The isometry action of the tessellation is generated by applying the action to all the causal diamonds defining out tessellation on the defining points on the future and past boundary (see

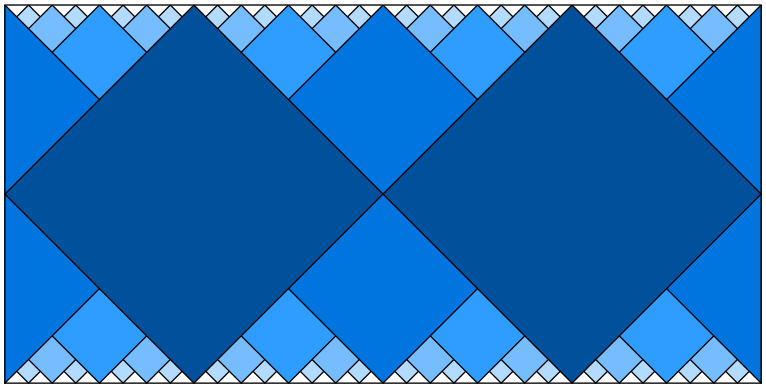

(a)

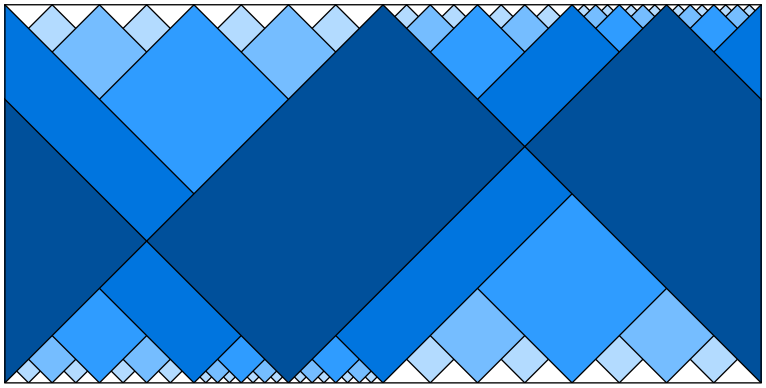

(b)

Figure 36.: Tessellations after the action of transformations from the subgroup $\mathrm{PSL}(2,\mathbb{Z})$ with its generators: (a) tessellation transformed with $S(x)$ and (b) tessellation transformed with $C(x)$.

eq. (5.11)):

$$\begin{aligned} f^+ &: \mathcal{I}^+ \to \mathcal{I}^+, \quad x_+ \mapsto f^+(x_+) \qquad \text{with } f^+ \in \mathrm{PSL}(2,\mathbb{Z}) \\ f^- &: \mathcal{I}^- \to \mathcal{I}^-, \quad x_- \mapsto (S \circ f^+ \circ S)(x_-) \end{aligned}$$

In this section, we will focus on the action of S and C, which generate the group $\mathrm{PSL}(2,\mathbb{Z})$. The tessellations after applying the isometry action imposed by S and C are shown in figure 36. The full action of $\mathrm{PSL}(2,\mathbb{Z})$ is obtained analogously. Although the generator $S(x)$ seemingly does not affect the initial tessellation, this is not the case: it acts as an involution by mapping each point to the opposite side of the spacetime.

The action of the generator $C(x)$ on our tessellation is depicted in figure 36b, where we have restricted the tessellation to a certain cutoff. The resulting tessellation is distorted in the direction of the null geodesics because the actions at the temporal boundaries $\mathcal{I}^+$ and $\mathcal{I}^-$ are not identical. This distortion leads to a translation and distortion along the null geodesics of the diamonds. This distortion also seems to affect the cutoff, but it is always possible to consider an equivalent standard dyadic cutoff using fine graining. This way, one can see that the tiles close to the boundary are left (physically) invariant, and the transformation only distorts a *finite* number of tiles. The remaining tiles are left invariant, which is why the tessellation is *almost* invariant under the isometry action. For our criteria, that a good tessellation should be invariant under isometry actions this is as good as we can get.

We interpret the tessellation itself as the foundation of the description of information propagating along null geodesics through dS_2 from the past to the future boundaries. This process can be modeled as a function M

$$M : \mathcal{I}^- \to \mathcal{I}^+.$$

This characterization of the process helps us to understand how applying the isometry changes the propagation of the function. We denote M to be the entire propagation process and M' the process only induced by the transformed tensor network:

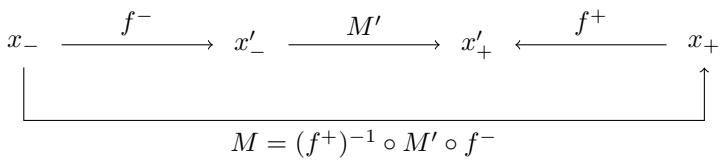

It directly follows that the isometry action on the tessellation can be described with the following function:

$$M \mapsto M' = f^+ \circ M \circ (S \circ (f^+)^{-1} \circ S) \tag{6.4}$$

In the case $f^+ = S$, the transformation of the function from eq. (6.4) is trivial. However, in general (and in particular for $f^+ = C$), the transformation is non-trivial.

As a finite amount of tiles is distorted under the isometry action, we have a residual action when comparing the propagation of information of the tesselation with or without isometry transformation. This residual action has consequences for the construction of the physical Hilbertspace. It imposes additional constraints on the model we construct to ensure the resulting quantum system is invariant under the full isometry group $\mathrm{PSL}(2, \mathbb{Z})$.

We use that the group of diffeomorphisms on the circle $\mathrm{diff}(S^1)$ can be approximated arbitrarily well with Thompson's group T. With this, the asymptotic symmetry group of the tessellation can be described as

$$G \equiv (T \times T)/\,\mathrm{PSL}(2, \mathbb{Z}).$$

This group acts as follows. We consider f and g to be elements of Thompson's group T and $h \in \mathrm{PSL}(2, \mathbb{Z})$. Given a representative $(f, g) \star (h, S \circ h \circ S)$, where the group operation $\star$ is elementwise composition we obtain a new tessellation by applying $f \circ h$ to the future boundary and $S \circ g \circ h \circ S$ to the past boundary:

$$(f, S \circ g \circ S) \star (h, S \circ h \circ S) \equiv (f \circ h, S \circ g \circ h \circ S),$$

This operation generates a new tessellation by shifting the endpoints of causal diamonds. With the original tessellation and this group of actions, we generate a family of tessellations corresponding to the elements of the asymptotic symmetry group, which directly translates to the tensor networks.

6.5.2. Isometric transformations of holographic networks

Given a symmetry-transformed tessellation, one can directly construct the corresponding holographic network: tensors are placed at the corners, and legs from neighboring generations are contracted to build a tensor network. We write M^f for the tensor network arising in this way from the action of $f \in \mathrm{PSL}(2, \mathbb{Z})$. We will see, that the tensor network after the isometric transformation is not invariant. This has important consequences for the interpretation of our

tensor network as will be discussed later.

We illustrate the construction of the transformed tensor network M^f for the example $f = C \in \mathrm{PSL}(2,\mathbb{Z})$. Remember that each tensor network is representative of an equivalence class of physically equivalent tensor networks with different cutoffs. We refer to this equivalence class as a family of tensor networks that represent linear operators $M_{\mathfrak{c}_m,\mathfrak{c}_n}$ from the standard dyadic cutoff at timeslice T_m to the standard dyadic cutoff at timeslice T_n. We consider the explicit example of the tensor network with de Sitter radius $\ell = 2$.

$M_{\mathfrak{c}_{-3},\mathfrak{c}_3} =$

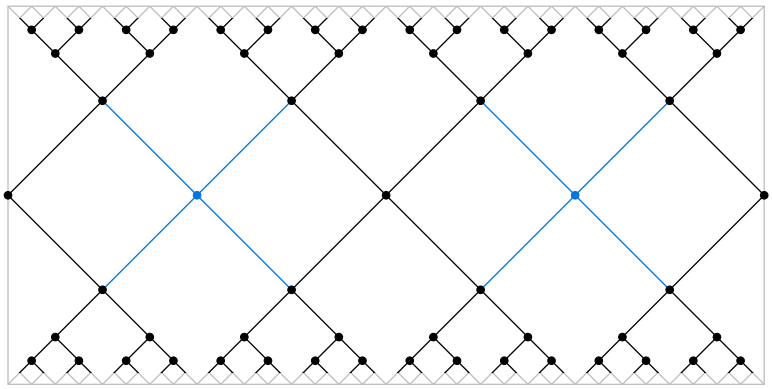

The input and output Hilbert space both have 2^5 uncontracted legs: $\mathcal{H}_{\mathrm{in/out}} = \mathfrak{h}^{\otimes 2^5}$. After the isometry transformation of the tessellation with $C \in \mathrm{PSL}(2,\mathbb{Z})$ and constructing the corresponding tensor network, we get the following operator:

$C\big(M_{\mathfrak{c}_{-3},\mathfrak{c}_3}\big) =$

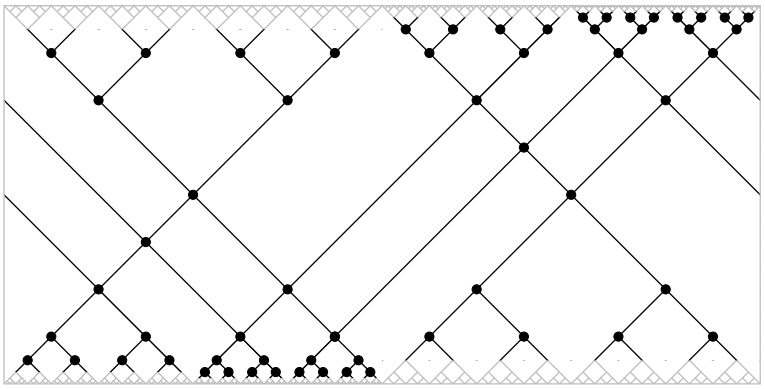

While this isometry transformation does not change the number of input and output legs, the distortion induced by C pushed the legs closer together in some places and further apart in others. This way, we no longer have a standard dyadic cutoff. We can change to a physically equivalent input and output state by applying the fine-graining operation at the future and past Hilbert space. This way, we obtain a tensor network from the infinite family of physically equivalent operators, which acts on standard dyadic cutoffs. This modification of the cutoff can be interpreted as a *partial UV completion*.

$M^C_{\mathfrak{c}_{-4},\mathfrak{c}_4} =$ 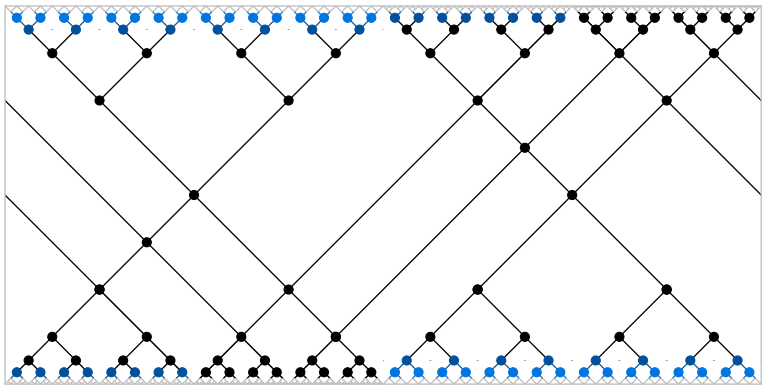

This way we get the input Hilbert space $\mathcal{H}_{\text{in}}^{\mathfrak{c}_{-4}}$ and the output Hilbert space $\mathcal{H}_{\text{out}}^{\mathfrak{c}_4}$. It is always possible to reduce the tensor network to the smallest possible cutoff, which results in a physically equivalent network. In this case this would be $M^C_{\mathfrak{c}_{-2},\mathfrak{c}_2}$. Also, we can obtain the infinite tensor network, which describes the entire system by taking the semicontinuous limit, which shifts the cutoffs into the far past and future.

An alternative way (see also section 4.4 in [OS20]) to formally express the symmetry transformed operator M^f is to write it with the unitary operator $U(f)$:

$$M^f \equiv U(f) M U^\dagger (S \circ f \circ S),$$

Intuitively, the operator $U(f) : \mathcal{H}_{\text{in}} \to \mathcal{H}_{\text{in}}$ is an operator that shifts around the qudits comprising $\mathcal{H}_{\text{in}}$ according to the function f. To formally describe the action of $U(f)$ we consider a physical state $|\psi_{\mathfrak{c}}\rangle \in \mathcal{H}_{\text{in}}^{\mathfrak{c}}$. To describe the transformation explicitly we consider the transformation $f = C$ and the cutoff $\mathfrak{c} = \mathfrak{c}_{-1}$ which results in the cutoff Hilbertspace $\mathcal{H}_{\text{in}}^{\mathfrak{c}} = \mathfrak{h}^{\otimes 2^3}$. The initial state $|\psi_{\mathfrak{c}}\rangle$ is interpreted as a quantum spin system where the 8 spins corresponding to uncontracted legs evenly distributed around the circle:

$|\psi_{\mathfrak{c}}\rangle =$ 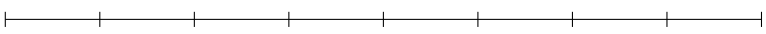

The action of $U(f)$ can be constructed for both boundary Hilbert spaces and all elements $\mathrm{PSL}(2,\mathbb{Z})$ in the same fashion. Here, we detail the example of the action C on the past boundary. The application of the isometry action C moves the spins around on the boundary: they are contracted in some places and dilated in others. This new state is the cyclically permuted version of the physical state $|\psi_{\mathfrak{c}}\rangle$.

$|\psi'_{\mathfrak{c}}\rangle =$ 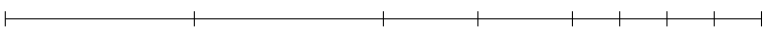

This new state $|\psi'_{\mathfrak{c}}\rangle$ needs to be assigned to spins on a nonregular grid. The dyadic subdivision of this grid corresponds to the following tree diagram:

$|\psi'_{\mathfrak{c}}\rangle =$ 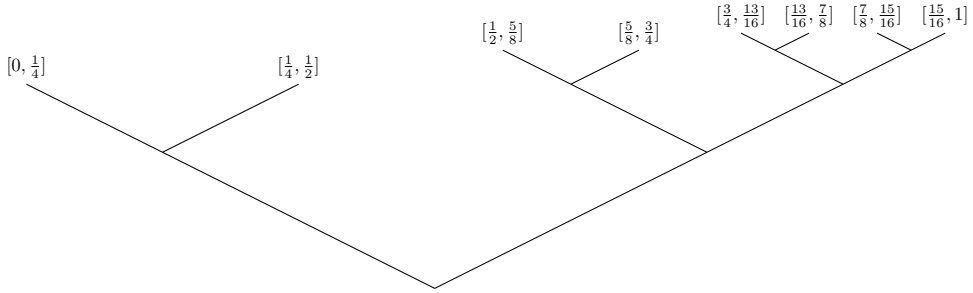

We can find an equivalent state using the fine-graining operation introduced in eq. (6.2):

$$|\psi\rangle \xrightarrow{U(C)} T^{\mathfrak{c}}_{\mathfrak{c}'} |\psi'_{\mathfrak{c}}\rangle = |\psi'_{\mathfrak{c}'}\rangle$$

The fine-graining operation can be written down explicitly using the V tensor:

$$|\psi'_{\mathfrak{c}'}\rangle = [(V \otimes V)V \otimes (V \otimes V)V \otimes V \otimes V \otimes \mathbb{1} \otimes \mathbb{1} \otimes \mathbb{1} \otimes \mathbb{1}] \, |\psi'_{\mathfrak{c}}\rangle$$

In tensor network language, this can be depicted as follows:

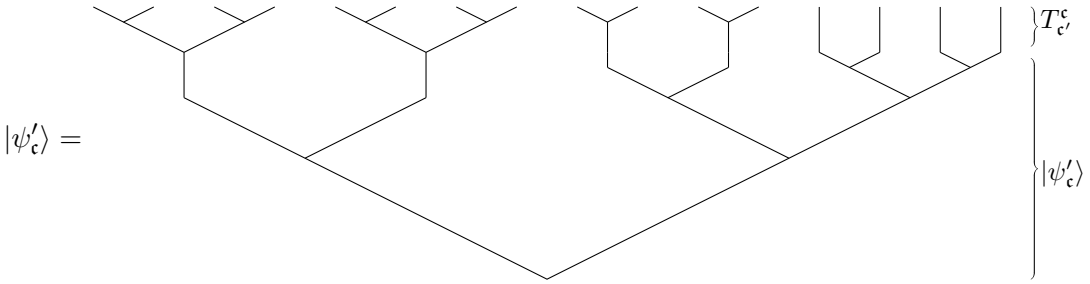

The fine-grained state then is associated with a grid, which equals a standard dyadic subdivision with 16 intervals:

$|\psi'_{\mathfrak{c}'}\rangle =$ 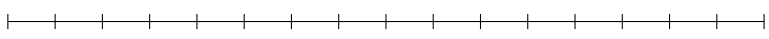

The isometry action induced by $U(f)$ is, in general, not trivial which can be seen by computing the overlap of the initial and cyclically permuted state. To do this, we need to look at the physically equivalent fine-grained states that live in the same cutoff Hilbert space:

$$\begin{aligned}\langle \psi_{\mathfrak{c}'} | \psi'_{\mathfrak{c}'} \rangle =& \Big(\langle \psi_{\mathfrak{c}} | \, (V^\dagger)^{\otimes 8} \Big) \Big([(V \otimes V)V]^{\otimes 2} \otimes V^{\otimes 2} \otimes \mathbb{1}^{\otimes 4} U(C) \, |\psi_{\mathfrak{c}}\rangle \Big) \\ =& \langle \psi_{\mathfrak{c}} | \left(V \otimes V \otimes \mathbb{1} \otimes \mathbb{1} \otimes V^\dagger \otimes V^\dagger \right) |\psi'_{\mathfrak{c}}\rangle \end{aligned} \tag{6.5}$$

In tensor network notation, the isometries describing the fine-graining simplify as follows:

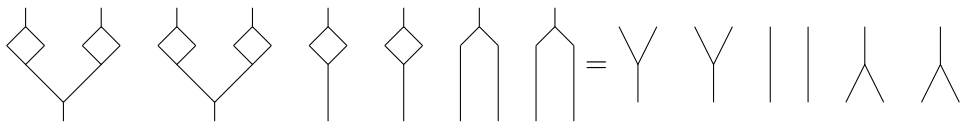

The overlap from eq. (6.5) depends on the initial state $|\psi_{\mathfrak{c}}\rangle$ and the tensor V. It is straightforward to see that this overlap need not be trivial. For a non-trivial overlap, the action also is non-trivial. This way, we obtained a unitary representation of Thompson's group T on the boundary Hilbert spaces. With this unitary representation, we can write the transformation of the tensor network with the action $f \in T$ as follows:

$$M^f \equiv U(f) M U(S)^\dagger U(f)^\dagger U(S)^\dagger.$$

where we used, that $U(f \circ g) = U(f)U(g)$. With this representation, we can easily see that the transformed tensor network is also a partial isometry from $\mathcal{H}_{\text{in}}$ to $\mathcal{H}_{\text{out}}$ (see appendix D.3). For arbitrary tensors U and V, which make our building blocks of the tensor network, we get a family of projections that are, in general, not identical:

$$P_f \equiv (M^f)^\dagger M^f$$

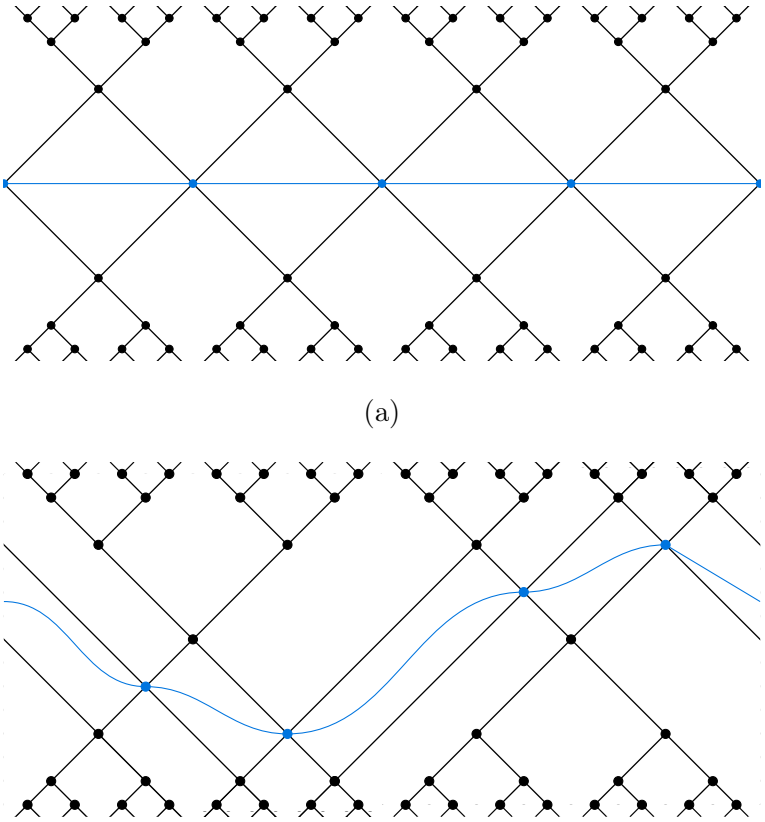

Figure 37.: Identical quantum information capacity for the tensor networks (a) M_2 and (b) M_2^C

One crucial consequence is that this also affects the physical subspaces the boundary Hilbert space $\mathcal{H}_{\text{in}}$ are projected into:

$$\mathcal{H}^f_{\text{phys}} = P_f \mathcal{H}_{\text{in}}$$

We will interpret this as a gauge degree of freedom in the sense that we consider the different physical subspaces to be gauge equivalent. This equivalence is also true for the corresponding quantum information capacity as depicted in figure 37. An alternative approach would be to demand that the different physical subspaces are mathematically equal for all $f \in \text{PSL}(2, \mathbb{Z})$. This equality would impose further conditions on the tensors U and V, which are currently not formulated in detail.

In the following, we will consider the conditions imposed by asking that the tensors V and U are perfect. This way, the tensor V as a rank-3 tensor has to satisfy the *pivotality condition*

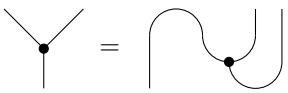

(6.6)

which can be interpreted as some rotational invariance of the tensor, and the rank-4 tensor U has to satisfy the *braiding operation*

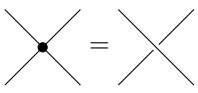

(6.7)

This choice of perfect tensors for the tensor network results in a class of tensor networks where the physical subspaces corresponding to different transformations have non-vanishing overlap:

$$\mathcal{H}'_{\text{phys}} \equiv \bigcap_{f \in \text{PSL}(2,\mathbb{Z})} \mathcal{H}^f_{\text{phys}} \neq \emptyset.$$

We show below that this set is non-empty by showing that the vacuum state is invariant under the action of the tensor network as well as the tensor network transformed with $f \in \text{PSL}(2,\mathbb{Z})$.

6.5.3. Vacuum state

In this section, we construct a *vacuum state* $|\Omega\rangle \in \mathcal{H}_{\text{in}}$ which is invariant under all M^f. We use the class of tensor networks where the tensors U and V satisfy the conditions in eq. (6.6) and eq. (6.7). This vacuum state is the infinite regular binary tree (or the regular binary tree with a certain cutoff that is physically equivalent)

$|\Omega\rangle =$

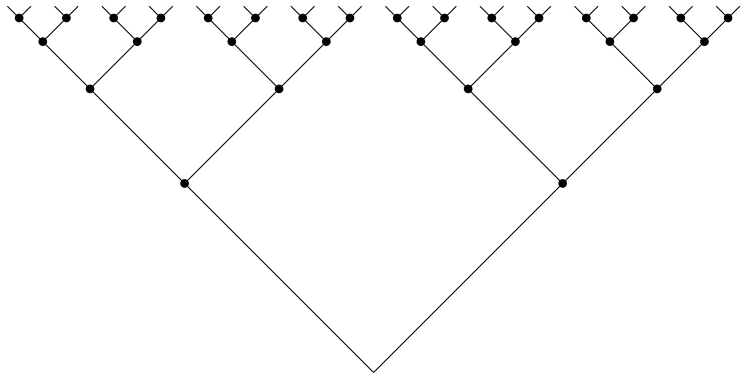

The invariance of $|\Omega\rangle$ under the tensor network M follows directly from the isometry conditions for U and V and the pivotality condition for V. To show the vacuum state is invariant under all M^f with $f \in \text{PSL}(2,\mathbb{Z})$ we show that it is invariant under the generators S and C:

$M\,|\Omega\rangle =$

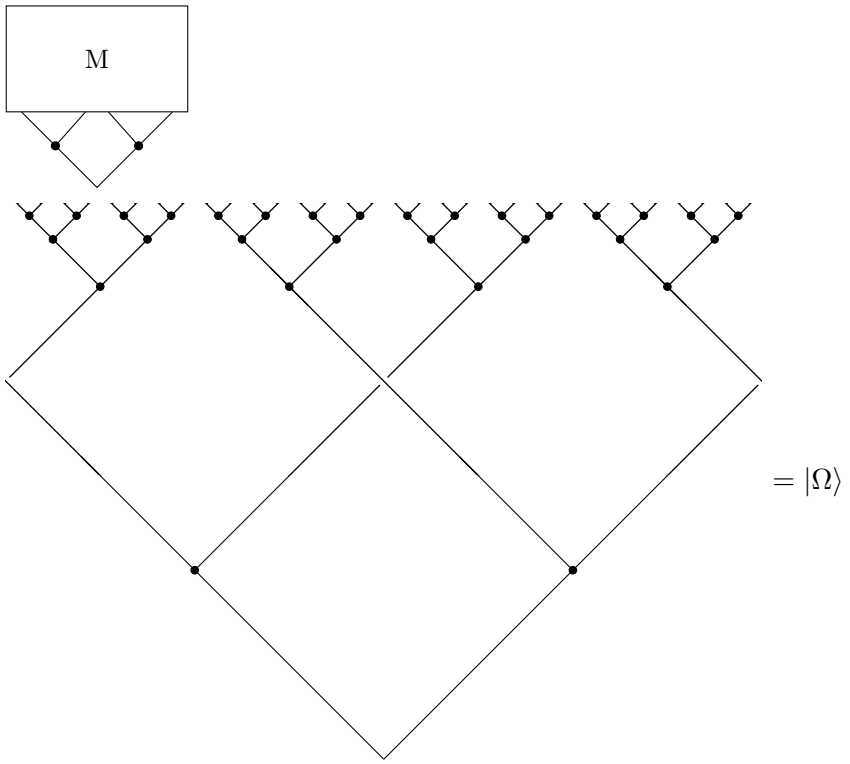

$= \qquad\qquad = |\Omega\rangle$

The initial simplification steps are detailed in appendix D.4. The same invariance holds for $M^S |\Omega\rangle = |\Omega\rangle$ since the action of S does not change the shape of the tensor network. To show the invariance of the vacuum state under the action of C, we need both the pivotality and braiding conditions:

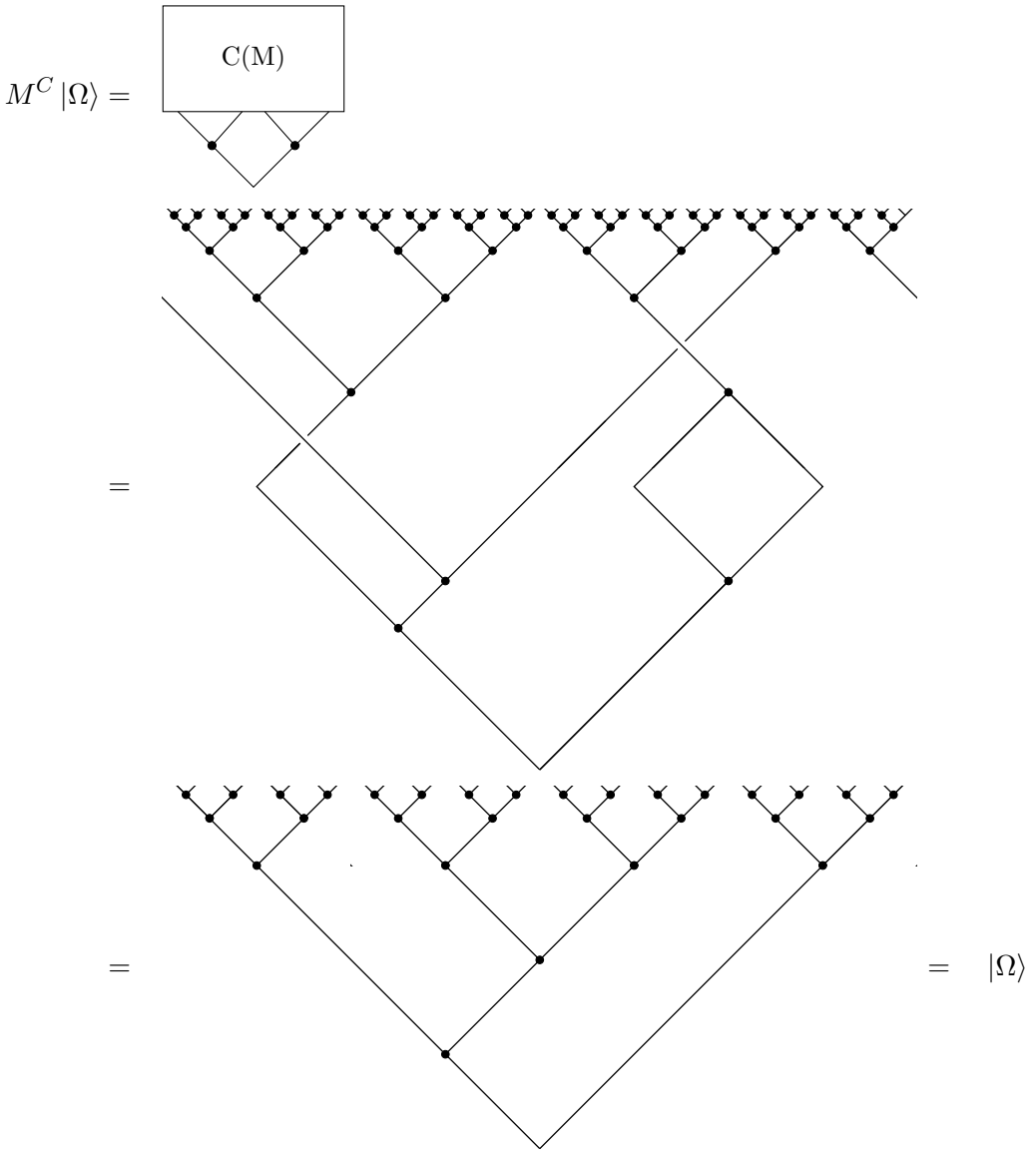

6.6. Manipulation of the spacetime

It is also possible to apply transformations to the tensor network, which are elements of Thompson's group T, but not in $\mathrm{PSL}(2,\mathbb{Z})$. Thompson's group elements are approximating diffeomorphisms on the circle arbitrarily well, but in the case where they are not elements of $\mathrm{PSL}(2,\mathbb{Z})$, they are not isometries of the spacetime. One such candidate is $B(x)$, which is one of the generators of Thompson's group T but not in its subgroup $\mathrm{PSL}(2,\mathbb{Z})$. The other generators of Thompson's group T are also elements of $\mathrm{PSL}(2,\mathbb{Z})$. The tessellation after the transformation with Thompson's group element B is depicted in figure 38. The transformation of the tessellation is performed following the procedure described in section 6.5.1 where the future boundary is On the basis of this transformed tessellation, we can construct the tensor network M^B.

We can see that the vacuum state is *not* invariant under diffeomorphisms, which are no isomor-

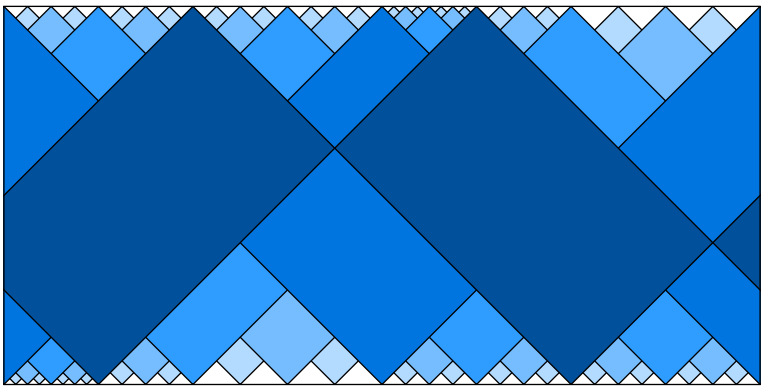

Figure 38.: Symmetry transformation $B(x)$ of the tensor network M.

phisms using the representative B:

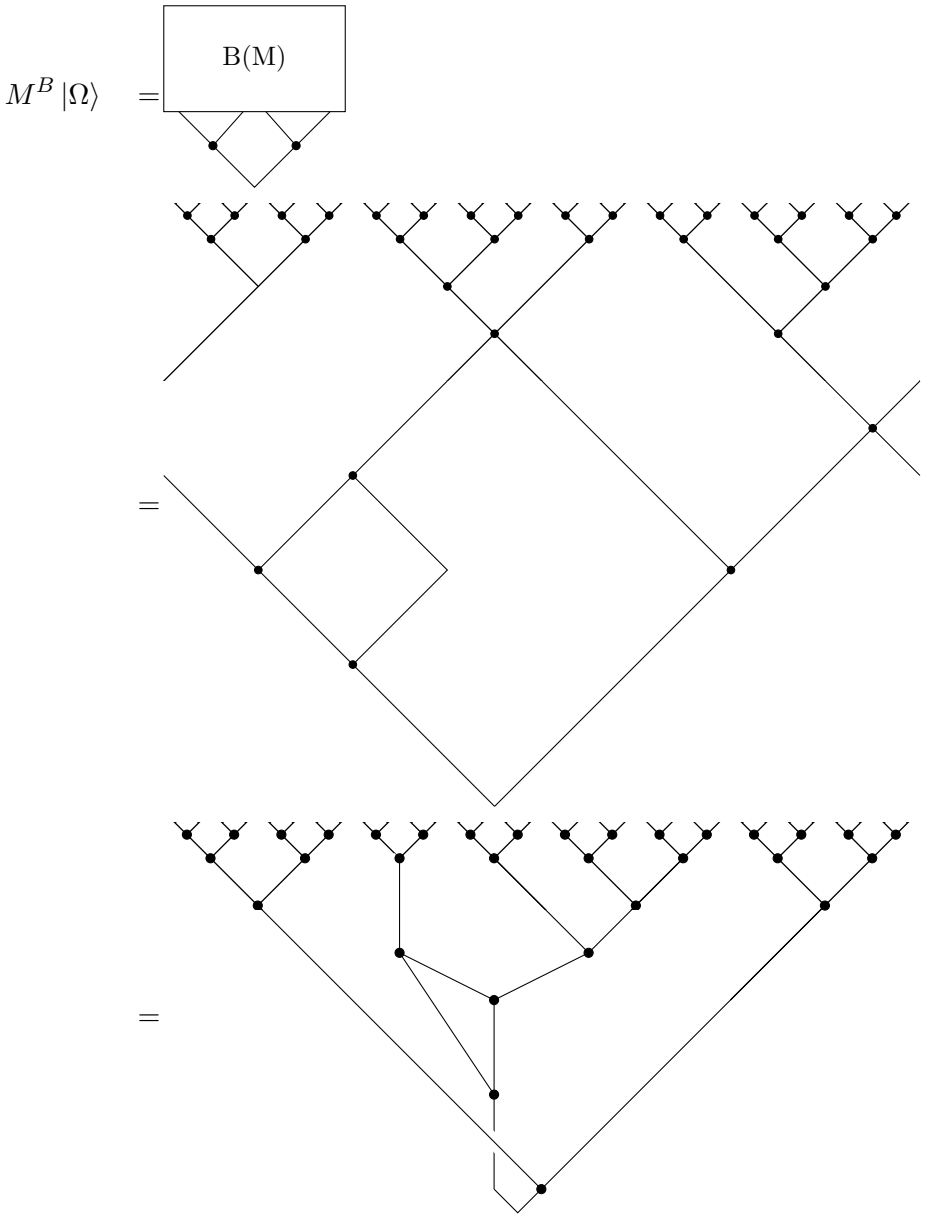

The resulting state $M^B\,|\Omega\rangle$ is *not* equal to the vacuum state, as there is no possibility to eliminate

the loop in the state.

The fact that the vacuum state is not invariant under M^B can be interpreted in a way that the resulting state $M^B |\Omega\rangle$ corresponds to a different spacetime. Since B is not an isometry, it distorts the underlying spacetime. With the tensor network M and the family of tensor networks M^f with $f \in \mathrm{PSL}(2, \mathbb{Z})$, we have constructed a tensor network that describes the spacetime with a vanishing energy-momentum tensor. We suggest that the transformation of the tensor network with B and the corresponding distortion of the tensor network can be interpreted as a change in the energy-momentum tensor of the underlying spacetime.

In this chapter, we have developed a holographic toy model that captures the dS/CFT correspondence. In the following chapter, we will relate the language used to characterize this holographic toy model to quantities known from quantum mechanics. In particular, we will discuss properties of physical states that live in the boundary Hilbert space $\mathcal{H}_{\mathrm{in}}$ and allow transformations to generate new physical states from the vacuum state. This discussion is intimately tied to further characterizing the properties of the tensors forming the holographic model.

Chapter 7

States of the kinematical Hilbertspace

In this section, we attempt to characterize further the allowed set of physical states in the kinematical Hilbert space constructed in the previous section. We already have a vacuum state $|\Omega\rangle$ of the Hilbertspace and interpret physical states to be all states $|\psi\rangle \in \mathcal{H}_{\text{in}}$ that can be generated with feasible transformations of the vacuum state. Only the vacuum state is necessarily invariant under isometry transformations. All other physical states can be affected by isometry transformations of the tensor network. We describe how to generate a physical state from the vacuum state in section 7.1. The way in which the physical states are affected by the tensor network characterizes the *dynamical Hilbertspace*, which captures the time evolution of the states.

Fully characterizing the set of physical states is a very challenging task because the characterization is directly linked to the properties of the tensors. Accordingly, we need to fully characterize the properties of the tensors comprising the tensor network to characterize the set of physical states. In this chapter, we will elaborate on this and consider different properties of the tensors and the effects this has on the set of physical states.

Depending on the concrete properties of the tensor network, different things could characterize the set of physical states and influence under which transformations they are invariant. In the AdS toy model described in section 4.2, which motivated the construction of our tensor network model, the tensor network comprised properties of a quantum error correcting code [PYHP15] where the bulk and boundary legs of the tensor network respectively correspond to the input and outputs of the encoding quantum circuit. We transfer this idea to the de Sitter setting and want to answer the following question in section 7.2:

Are quantum error correction codes compatible with local operators in de Sitter spacetime?

In section 7.3, we will discuss some aspects of the interpretation of local quantum mechanics in the context of the holographic model. Here, the focus lies on the allowed application of operators at the boundary and how the information propagates through the tensor network. We also briefly comment on some properties of entropy in de Sitter spacetime, which will not be made rigorous in this thesis.

7.1. Physical states: Manipulate the boundary

We have seen in the previous chapter that de Sitter spacetime can be modeled with a tensor network M comprised of isometries and unitaries. We denote $|\psi\rangle$ to be a global state in the boundary Hilbertspace of the far past:

$$|\psi\rangle \in \mathcal{H}_{\text{in}}$$

This state gets transported to the Hilbert space of the future boundary with the tensor network:

$$M\,|\psi\rangle \in \mathcal{H}_{\text{out}}$$

With the cutoff introduced in 6.1, we can find physically equivalent states that are defined on a different Hilbert space, which is associated with a finite timeslice if we choose a standard dyadic cutoff. This way, states in the boundary Hilbert spaces corresponding to that cutoff effectively lie in the bulk of the spacetime but are physically equivalent to the corresponding states on the boundary:

$$|\psi\rangle \sim |\psi_{\mathfrak{c}}\rangle \in \mathcal{H}_{\text{in}}^{\mathfrak{c}} = \bigotimes_{j=1}^{n} \mathfrak{h}_j$$

The cutoff Hilbertspace $\mathcal{H}_{\text{in}}^{\mathfrak{c}}$ as well as $\mathcal{H}_{\text{out}}$ is comprised of many subsystems $\mathfrak{h}_j$ which can be interpreted as local laboratories where the observables live. The partial trace over all other subsystems of the Hilbert space obtains the reduced density matrix corresponding to the subsystem $\mathfrak{h}_j$

$$\rho_j = \text{tr}_{\hat{j}}(|\psi\rangle\langle\psi|) \tag{7.1}$$

The state $|\psi^{\mathfrak{c}}\rangle$ lies in $\mathcal{H}_{\text{in}}^{\mathfrak{c}}$ which is the Hilbertspace associated with a certain timeslice and lies in the bulk of dS for a finite cutoff. Therefore, $|\psi^{\mathfrak{c}}\rangle$ cannot be accessed directly. In order for $|\psi^{\mathfrak{c}}\rangle$ to be a valid physical state, we require that we can generate the state by only accessing/modifying the boundaries.

In the following, we consider $|\psi^{\mathfrak{c}}\rangle$ to be an arbitrary valid initial state and analyze if it is possible to generate a different state by modifying the boundary. In the easiest case, we start with the vacuum state, which we know to be a valid physical state. The boundary on which we apply the *local operator* is associated with Hilbert space $\mathcal{H}_{\text{out}}$ where we again introduce a cutoff. Since the equivalence between states was made precise in the previous chapter, we will sometimes not explicitly mention that we always work at a finite cutoff at the future boundary.

We consider an operator $\mathcal{W} : \mathcal{H}_{\text{out}} \to \mathcal{H}_{\text{out}}$ that acts on a local subsystem on the boundary:

$$\mathcal{W} = \mathbb{1}_1 \otimes \cdots \otimes \mathbb{1}_{j-1} \otimes W_j \otimes \mathbb{1}_{j+1} \otimes \cdots \otimes \mathbb{1}_n$$

where we consider the local operator W_j to be unitary. For the arbitrary state $|\psi\rangle \in \mathcal{H}_{\text{in}}$, the spacetime dynamics that describe the evolution of the state from the far past to the far future is modeled by the tensor network M. The question of the initial state $|\psi\rangle$ can be transformed to a different state $|\psi'\rangle \in \mathcal{H}_{\text{in}}^{\mathfrak{c}}$ only by modifying the boundary can be formulated as follows:

$$\mathcal{W}M\,|\psi\rangle = M\,|\psi'\rangle \tag{7.2}$$

We want to evaluate if it is possible to simulate a valid state $|\psi'\rangle \in \mathcal{H}_{\text{in}}^{\mathfrak{c}}$ by applying a local operator at the future boundary. This way, we want to find a state which satisfies the following two conditions:

1. The state $|\psi'\rangle$ is a valid state that satisfies the condition from eq. (7.2).

2. The state $|\psi'\rangle$ is normalized and therefore satisfies $\langle\psi'|\psi'\rangle = 1$.

The possibility to simulate a state $|\psi'\rangle$ in such a way depends on the properties of the tensor network.

7.2. Simulate a physical state using quantum error correction?

In this section, we specify the properties of the tensor network and consider quantum error correction as it has been used in the toy model for the AdS/CFT correspondence. We evaluate if it is possible to simulate a physical state $|\psi'\rangle$ starting with a physical state $|\psi\rangle$ only manipulating the boundary of a tensor network, which has the properties of an encoding map of a quantum error correcting code. We choose the isometries in the tensor network to be isometries characterizing the encoding operation of quantum error correction as described in section 4.3. On a local scale, we are interested in how these individual subsystems from eq. (7.1) can evolve.

It is possible to consider three different cases that model parts of de Sitter spacetime: The past, which is a contraction of spacetime; the future, which is an expansion; and the limiting case, which is a small curvature that is almost flat. For our purposes, we are primarily interested in the expanding and the flat case as we apply the operators to manipulate the physical states at the future boundary.

A flat spacetime is the limit of de Sitter spacetime with very small curvature. For a flat spacetime, the universe has constant size, and thus the dimensions of $\mathcal{H}_{\text{in}} = \mathfrak{h}^{\otimes n}$ and $\mathcal{H}_{\text{out}} = \mathfrak{h}^{\otimes n}$ and accordingly also the number of input and output legs of the tensor network are identical. We again consider the dimension of one tensor leg to be $\mathfrak{h} = \mathbb{C}^d$. The tensor network M is a regular grid of unitaries in the flat spacetime limit, which we can describe as one unitary operator[1]

$$U : \mathcal{H}_{\text{in}} \to \mathcal{H}_{\text{out}} = \mathfrak{h}^{\otimes n} \to \mathfrak{h}^{\otimes n}$$

For any unitary operator U, we can choose the state $|\psi'\rangle \in \mathcal{H}_{\text{in}}$ such that it is a valid normalized state which satisfies the condition (7.2) in the following way:

$$\begin{aligned} |\psi'\rangle =& U^\dagger \mathcal{W} U |\psi\rangle \\ U|\psi'\rangle =& U U^\dagger \mathcal{W} U |\psi\rangle = \mathcal{W} U |\psi\rangle \\ \langle\psi'|\psi'\rangle =& \Big(\langle\psi| U^\dagger \mathcal{W}^\dagger U\Big)\Big(U^\dagger \mathcal{W} U |\psi\rangle\Big) = \langle\psi|\psi\rangle = 1 \end{aligned}$$

This shows that it is possible to generate a physical state in $\mathcal{H}_{\text{in}}$ by applying a local operator at the boundary $\mathcal{H}_{\text{out}}$. $\mathcal{H}_{\text{in}}$ is physically equivalent to a state on a chosen cutoff, which corresponds to any timeslice of flat spacetime that can lie within the bulk. The same thing would hold in contracting spacetime as detailed in appendix D.5.

For an expanding universe, the spacetime dynamics can be described and identified with the encoding map of a quantum error correction code. As discussed in section 4.3, we can characterize this encoding map with a *random isometry* V, which captures the encoding of *randomized quantum error correction*. The dimension of $\mathcal{H}_{\text{in}} = \mathfrak{h}^{\otimes k}$ is smaller than the dimension of $\mathcal{H}_{\text{out}} = \mathfrak{h}^{\otimes n}$ such that more physical qubits are used to encode the quantum state:

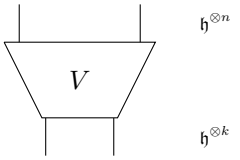

$$V : \mathcal{H}_{\text{in}} \to \mathcal{H}_{\text{out}} = \mathfrak{h}^{\otimes k} \to \mathfrak{h}^{\otimes n} \quad \text{with } k < n$$

We have seen that it is possible to modify a valid physical state by applying a local operator at the future boundary to obtain a new valid physical state in the case of flat and contracting

[1] Note that this unitary operator is not the encoding of a QECC, as it does not map the physical state into a bigger space. It is also considered here for completeness.

spacetime. In expanding spacetime, the condition from eq. (7.2) is solved by the following state:

$$|\psi'\rangle = V^\dagger \mathcal{W} V |\psi\rangle$$

It remains to be checked if this is a valid state. This is the case if it is normalizable:

$$\langle\psi'|\psi'\rangle = \Big(\langle\psi| V^\dagger \mathcal{W}^\dagger V\Big)\Big(V^\dagger \mathcal{W} V |\psi\rangle\Big) = \langle\psi| V^\dagger \mathcal{W}^\dagger V V^\dagger \mathcal{W} V |\psi\rangle \tag{7.3}$$

Different from the previous cases, it is not trivial to evaluate this expression. In order to evaluate this expression further, we express the random isometry V as a random unitary U by adding ancillary qubits in the following way:

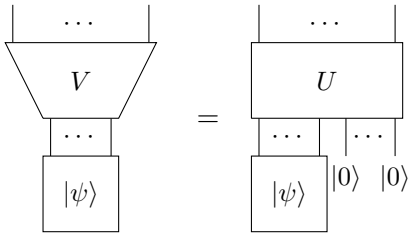

$$V : \mathfrak{h}^{\otimes k} \to \mathfrak{h}^{\otimes n}$$

$$U : \mathfrak{h}^{\otimes k} \otimes |0\rangle^{\otimes (n-k)} \to \mathfrak{h}^{\otimes n}$$

To evaluate the expression eq. (7.3) and check if the state is normalized, we express it in tensor network notation:

$$1 = \langle\psi'|\psi'\rangle = \langle\psi| V^\dagger \mathcal{W}^\dagger V V^\dagger \mathcal{W} V |\psi\rangle \quad =$$

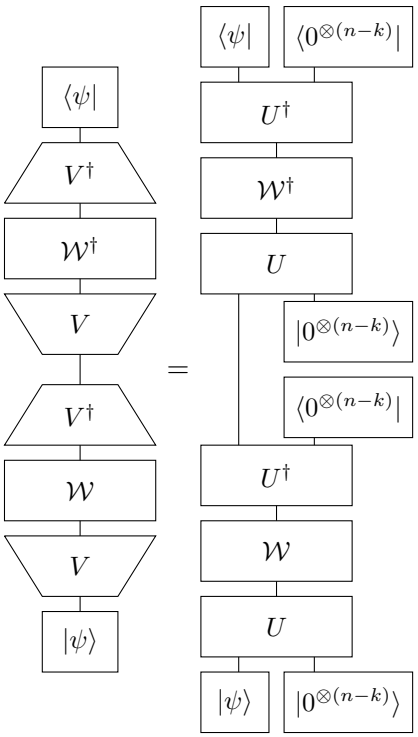

$$= \tag{7.4}$$

This can be solved by calculating the *Haar integral* over the group of random unitaries.

In mathematics, measures are a tool studied in a wide variety of contexts. One familiar example of a measure is the probability measure, which characterizes the distribution of a set of given objects. The measure needed to evaluate eq. (7.4) is the *Haar measure*, which is used to transfer results from measure theory to group theory [Die14]. For a matrix-valued function $f(U)$ on the unitary group $\mathcal{U}$, we can write the integral with respect to the Haar measure as

$$I = \int dU f(U). \tag{7.5}$$

A discussion of the *unitary group* in more detail than necessary in this context can be found in [Dui00]. The defining property of the Haar measure is left- or right-invariance with respect to shifts via multiplications with a fixed unitary operator $V \in \mathcal{U}(d)$:

$$\int dU\, f(UV) = \int d(U'V^\dagger) f(U') = \int dU' f(U')$$

The right-invariance of the Haar measure imposes a similar condition. The Haar measure allows us to sample unitary operations and, with that, check if the new physical state $|\psi'\rangle$ is normalized. The approach presented here to calculate Haar measures was inspired by Aram Harrow and Matt Hastings and was also described in [PBO20].

In order to calculate the Haar Integral over the random unitaries, we rearrange the expression in eq. (7.4) in the following way:

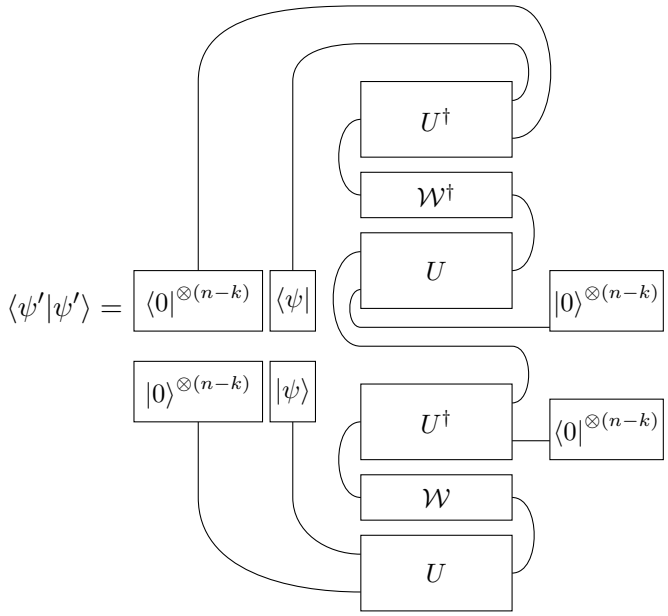

(7.6)

To solve this, we need the Haar integral identity, which is derived in the appendix D.6:

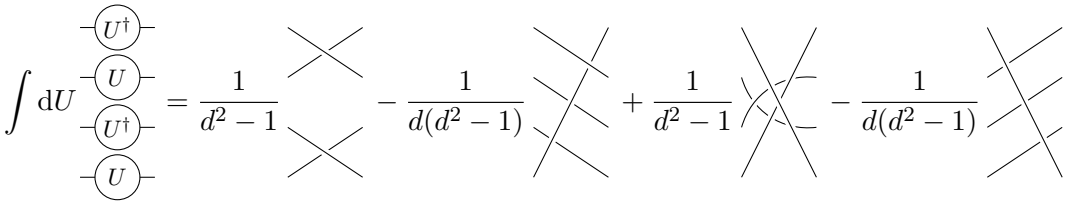

(7.7)

Using this identity, we can directly calculate the Haar integral corresponding to eq. (7.6), which is detailed in appendix D.7. We obtain the following result:

$$\langle\psi'|\psi'\rangle = \frac{|\operatorname{tr}(W)|^2\left(1 - d^k d^{-n}\right)}{d^2(1 - d^{-2n})} + \frac{d^{-n}\left(d^k - d^{-n}\right)}{1 - d^{-2n}}. \tag{7.8}$$

If it were possible to generate a new state $|\psi'\rangle$ by applying a local operator on the boundary, the state $|\psi'\rangle$ would have to be normalized. In order to simplify (7.8) we use, that the following holds for any d-dimensional unitary operator W (see appendix D.8) where the equality only holds if W is the identity:

$$|\operatorname{tr} W|^2 \leq d^2 \tag{7.9}$$

$$\langle\psi'|\psi'\rangle \leq \frac{d^2\left(1-d^k d^{-n}\right)}{d^2(1-d^{-2n})} + \frac{d^{-n}\left(d^k - d^{-n}\right)}{1-d^{-2n}}$$

We can now relate these considerations to the tensor network for de Sitter spacetime. The local operator is applied to $\mathcal{H}_{\text{out}}$, which can be identified with the temporal future boundary for the expanding case. At the temporal boundaries, spacetime has infinite size, and therefore, the number of sites goes towards infinity:

$$\lim_{n\to\infty} \langle\psi'|\psi'\rangle = \frac{|\operatorname{tr} W|^2}{d^2} \leq 1$$

As the equality only holds if the local operator W is the identity, we can conclude that the only local operator that can be applied to the tensor network comprised of random unitaries is the identity.

Similar results directly transfer to local operators ρ_j at a subsystem j and how their properties are influenced by applying an operator $\mathcal{W}$ at the future boundary. It is shown in appendix D.9 that for non-trivial $\mathcal{W}$, the operator ρ_j is maximally mixed. This translates to the fact that any local operator we could model by applying $\mathcal{W}$ as a super-operator at the boundary would be very close to the boundary, and no local operations would be possible. This only allows for one physical state, which is identical to the vacuum state. This does not lead to a reasonable physical theory. Therefore, it is not reasonable to describe the de Sitter tensor network with random isometries, although this approach was very successful for anti-de Sitter spacetime.

7.3. Various aspects of local quantum mechanics

With the given tensor network construction, we still need to describe the local quantum mechanics of an observer at finite time. What we discussed so far is the application of an operator acting globally at the future infinity. We will refer to this as a *super-operator*. In local quantum mechanics, an observer is not able to apply such a super-operator. However, this is the only allowed operation in the context of holography. Here, we will look into how the application of a super-operator can simulate the application of *local operators* at finite times.

We start with considering the application of a super-operator $\mathcal{W}$, which is comprised of many operators acting locally on the open tensor legs at the boundary. For our considerations, the super-operator acts as the identity except for one boundary leg where it applies the local operator W:

$$\mathcal{W} = \mathbb{1} \otimes \cdots \otimes \mathbb{1} \otimes W$$

In the depiction below where the operator W is identified with the rectangle $W = \blacksquare$. We look at the action of the super-operator $\mathcal{W}$ on the physical state $|\psi\rangle$:

$\mathcal{W}|\psi\rangle =$ 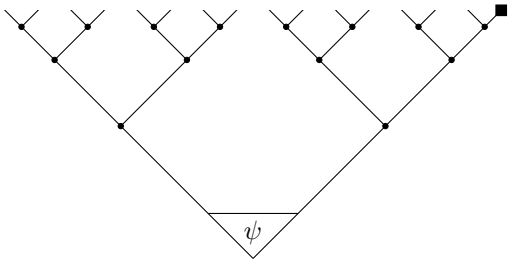

The properties of the tensors highly influence how the operator W and the information it carries propagates through the tensor network corresponding to the evolution of the physical state and influences the state for finite times. Accordingly, different properties of the tensors in the tensor

network generate different sets of allowed local operations, which can be simulated with the application of super-operators. We consider the local algebra of observables at a finite time is interpreted to be the algebra of all allowed local operations. The local algebra of observables in de Sitter spacetime has recently been discussed by Chandrasekaran, Longo, Penington, and Witten in [CLPW23] in a different setting.

This relationship between the vacuum state, the algebra of observables, and the properties of the tensors is reminiscent of the *Reeh-Schlieder theorem* in quantum field theory, which was originally published in [RS61]. The theorem characterizes the structure of the vacuum state and the algebra of observables in a quantum field theory. Entanglement properties in quantum field theory are studied to this day. Witten emphasized in [Wit18] that entanglement in quantum field theory is often a property of the algebra of observables and not only of the quantum states. In the following, we will investigate some approaches to describe the algebra of observables; it needs to be noted that this still needs to lead to a final characterization at this point.

In analogy to the AdS toy model from [PYHP15], we choose that the tensor network is comprised of perfect tensors (introduced in definition 4.5). These are tensors with maximal entanglement along any bipartition. A review of various properties of maximally entangled states can be found in [EWŻ16]. For us, the following definition will suffice:

$$|\psi_{AB}\rangle = \frac{1}{\sqrt{d}} \sum_{j=1}^{d} |j\rangle_A |j\rangle_B$$

We can push W past tensors in this tensor network if the tensors represent maximally entangled states as shown in appendix D.10:

$$(M \otimes N) |\psi_{AB}\rangle = (MN^{-1} \otimes \mathbb{1}) |\psi_{AB}\rangle$$

The tensor product structure we obtain through the tensor network can be interpreted as a choice of a basis. This way we can push the local operator past the perfect tensors as follows where $W^{-1} = \blacklozenge$:

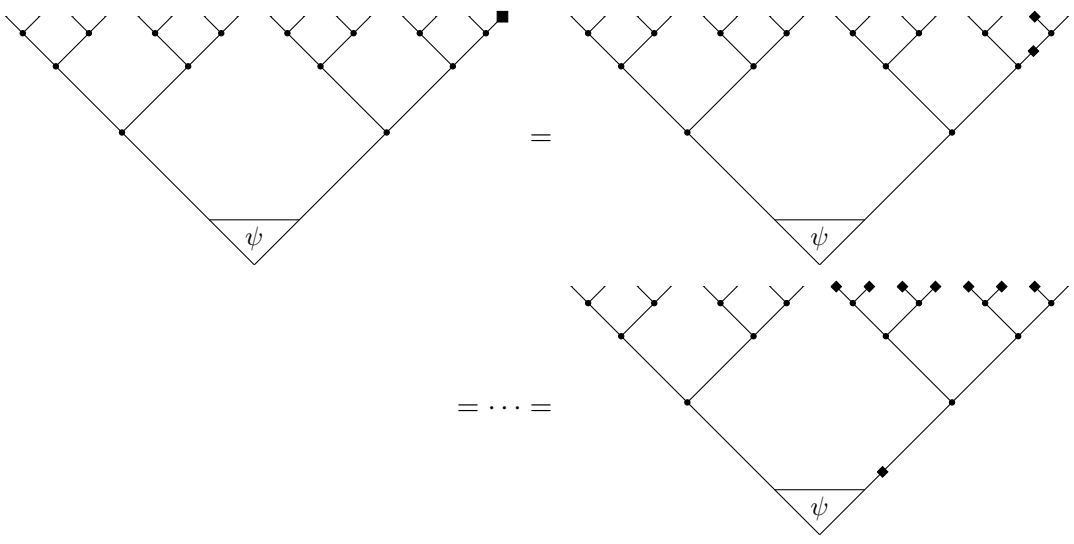

If the physical state $|\psi\rangle$ is maximally entangled, we can push the operator W through the entire

network:

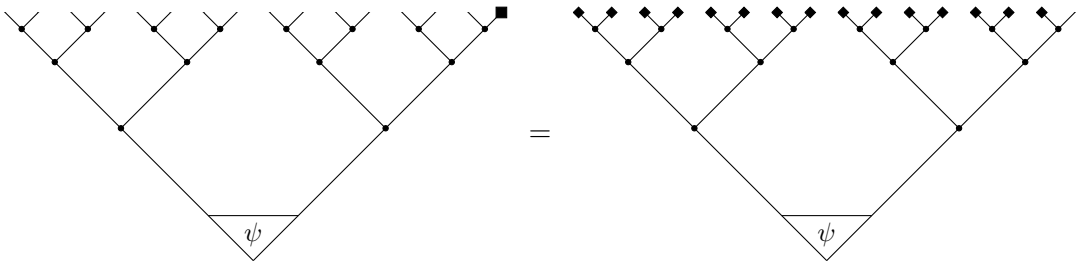

(7.10)

It remains an open question if this is a desirable property. Thinking of quantum physics on a local scale, the property from eq. (7.10) seems unphysical because it contradicts the rules of causality. Various aspects of quantum causal influence in the context of quantum states which encode spacetime dynamics are discussed in [CHQY19]. From this point of view, we must require that the physical state $|\psi\rangle$ is *not* maximally entangled.

On the other hand, we already established that the application of a super-operator at the temporal boundary is not an action allowed to any local observer, which is why causality relations might not be a crucial physical property in this case. The relation displayed in eq. (7.10) is reminiscent of optimal cloning in quantum mechanics. In the following chapter, we will investigate cloning properties of the tensor network further.

Another prominent research topic that is closely related is the de Sitter entropy. Attempts to characterize the entropy in de Sitter spacetime range from discussions in early publications [BHM01, Bou01] and is not fully resolved to this day: "It seems fair to say that although black hole entropy remains highly enigmatic to this day, the entropy of a cosmological horizon, such as the de Sitter horizon, is only more mysterious" [CLPW23, p. 2]. It is understood that the entropy of a black hole can be related to its horizon [Bek72, Haw75] which was soon generalized to a wider context with a positive cosmological constant [GH77b]: the event horizon perceived by a local observer is directly tied to the entropy. It needs to be noted that the horizon now is observer-dependent, and thus, the entropy can vary locally. The possible variation of entropy does not affect de Sitter spacetime, where all observers perceive the same entropy since de Sitter spacetime is maximally symmetric. To this date, there exists a wide variety of definitions of entropy in de Sitter space, and work has to be done to unify these in *one* rigorous definition. Balasubramanian and Hořava have provided a list of various possible interpretations of entropy in de Sitter spacetime in [BHM01, 2.2]. The main interpretations of entropy in de Sitter spacetime are the following: dS entropy is related to the degrees of freedom which are associated with the horizon, hidden behind the horizon or arise from the quantization of gravity in general. Another interpretation is that dS entropy corresponds to the number of initial conditions that can evolve into empty de Sitter space, or dS entropy is correlated to the finite size of the physical Hilbert space.

We argue that entropy can also be considered in the context of the holographic tensor network model we developed in chapter 6. Qualitatively, we can directly characterize de Sitter entropy in this context:

De Sitter entropy corresponds to the number of operators we can locally apply in a static patch corresponding to a local observer.

This way, the upper bound on entropy is directly imposed by the number of tensor legs cutting the boundary of the static patch. The local algebra of observables can impose further restrictions on the number of allowed local operations, and this reduces the entropy. This way, we need a full characterization of the local algebra of observables to characterize the entropy in de Sitter

rigorously. It remains an open question how the entropy perceived this way by a local observer is related to the finite dimension of the physical Hilbert space. A direct relation between the entropy characterized by the number of allowed local operations and the finite dimension of the Hilbert space seems likely (but has not been proven at this point).

Part III.

Unruh effect

Chapter 8

Unruh effect in de Sitter spacetime

The Unruh effect has been studied in a wide variety of settings and was originally formulated in flat spacetime as reviewed in section 3.2. A result of the Unruh effect, which is less known, was presented in the paper series [BHP09, BHTW10, BHP12] where the vacuum state of the original formulation from the Unruh effect was replaced with a different state. This new state is referred to as the *multi-rail state*, which is the Minkowski vacuum state with some excited modes. The multi-rail state is interpreted as one possible method to encode a logical qubit. The Unruh channel hereby is the channel mapping the initial state to the state perceived by the accelerated observer. In this framework, the Unruh channel has properties of a cloning channel as described in [BHTW10]. It needs to be clarified how to interpret this result in flat spacetime physically. We argue that the physically more interesting setting to consider a similar setup is de Sitter spacetime.

The reason for that is that the acceleration central to the Unruh effect is a fundamental property of de Sitter spacetime. The Unruh effect in de Sitter spacetime bears close similarities to cosmological particle creation, which describes the effect that freely falling particle detectors in expanding spacetime still register particles even if the global state is a vacuum state. Initially, this phenomenon was discussed by Parker in [Par67, Par68, Par69] and Sexl and Urbantke in [SU69]; now, it is part of the standard literature such as [BD82]. One important paper where cosmological particle creation was studied in de Sitter spacetime is [Mot85]. The intrinsic acceleration makes de Sitter spacetime a natural place to study the Unruh effect, which has already been done in the past: De Sitter space was assigned a characteristic temperature in [FHKN75] and in [GH77a] the temperature of a cosmological horizon in de Sitter was calculated. It was shown in [BB99] that the global structure of algebras of observables has a similar structure in de Sitter spacetime and their Minkowski counterpart. The Unruh effect in the context of de Sitter spacetime was early discussed in [Laf89, DL97, NPT96] and still finds interest in more recent publications such as [CCO$^+$11, GP04, SUFK21]. One key feature that is employed is that curved spacetimes inherit the thermal properties known from flat spacetime through appropriate embeddings [DL99]. More examples of the Unruh effect being studied in the context of de Sitter spacetime are by Jennings in the context of de Sitter as a brane universe [Jen05, Jen10] or by Padmanabhan with more focus on the cosmological horizon and an explicit value for the cosmological constant [Pad03, Pad05]. We will review the basics of the Unruh effect in the context of de Sitter spacetime in section 8.1.

In this chapter, we combine these fields of study and introduce an alternative initial state for the Unruh effect in de Sitter spacetime. For this alternative initial state, which we interpret as the initial state of de Sitter spacetime, we derive the corresponding Unruh channel by following the computations outlined in [BHP12]. From a mathematical perspective, these calculations bear close similarities to those previously undertaken in the Minkowski setting. The noteworthy aspect lies in their execution within the framework of de Sitter spacetime and the new physical interpretation that comes with that. This setting is more natural for this consideration than

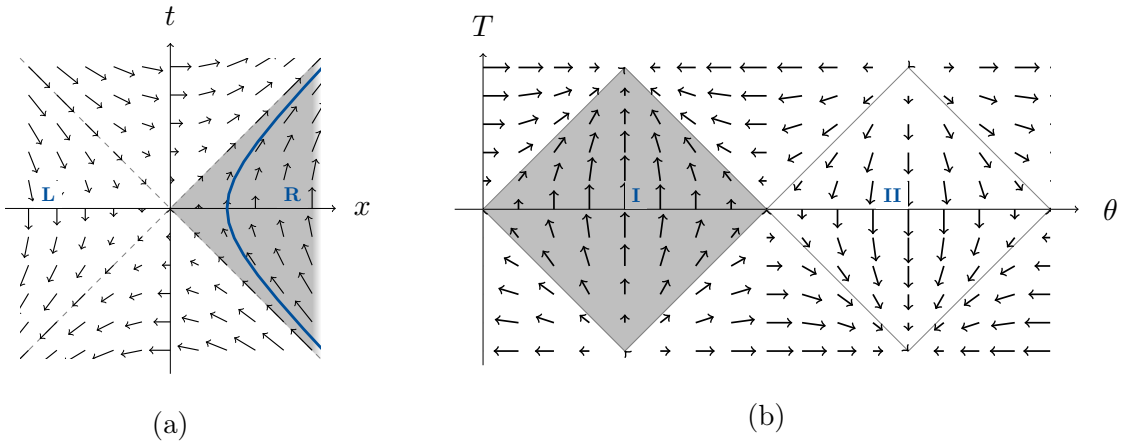

(a) (b)

Figure 39.: Comparision of Killing fields
(a) Lorentz boost in Minkowski spacetime and
(b) de Sitter Killing field which is timelike in one static patch

Minkowski spacetime, given the intrinsic connection between the cloning properties of the channel and the fundamental nature of the expansion of spacetime. The relation between the Unruh channel and the cloning channel allows for a meaningful relationship to be established between the cloning properties and the spacetime's expansion features. In section 8.1, we give a short review of the Unruh effect in de Sitter spacetime and characterize the notions of acceleration and temperature. This is followed by an introduction of the initial state of de Sitter spacetime in section 8.2. The chapter is concluded by section 8.3 where we derive the Unruh channel in de Sitter spacetime and relate this to properties of cloning channels introduced in section 4.4. The content of this chapter largely follows [NO24]. To follow the rest of the thesis, we perform the calculations in $1+1$ dimensional de Sitter spacetime. This calculation can easily be generalized to a higher dimensional de Sitter spacetime. In [NO24], we perform the calculations in the $2+1$ dimensional case, which gives rise to an extra quantum number but does not change the essence of the result.

8.1. Unruh effect in de Sitter

Similar to the Unruh effect in flat spacetime, thermodynamic properties can be assigned to cosmological models in curved spacetimes. It was already argued in [GH77b] that there is a connection between event horizons in spacetimes, which are asymptotic de Sitter, and thermodynamics. This way, the thermal nature of de Sitter spacetime is intimately connected to its expansion, which gives rise to a horizon and a temperature associated with it. This relation manifests in the fact that a freely falling detector indeed measures a background from thermal radiation coming from the cosmological event horizon. This effect is also referred to as *cosmological particle creation*.

On a more technical level this can be explained by the fact that there does not exist a globally timelike Killing field in de Sitter spacetime. The possible Killing fields for de Sitter are derived in section 2.3. There is a Killing field in de Sitter, which is timelike in one static patch that exhibits close similarities with the Lorentz boost in flat spacetime as shown in figure 39. The similarity in the Killing field induces properties in de Sitter spacetime that are similar to the accelerated frame in the Unruh effect in flat spacetime without adding an external acceleration. Rather, acceleration is a fundamental component of spacetime in the de Sitter setting. As we are interested in the experience of a local observer and the Killing field in one static patch is timelike, we use static coordinates.

In flat spacetime, the Killing field generating time translations in inertial frames is always identical to geodesics. An observer following a Killing field accordingly experiences no proper acceleration. This is different in the de Sitter case, where the proper acceleration of Killing trajectories (see appendix eq. (A.9)) is

$$a_\mu a^\mu = \frac{1}{\ell^2}\frac{r^2}{\ell^2 - r^2}$$

The proper acceleration only vanishes for the trajectory following the radial variable $r = 0$, which is the trajectory identified by a local observer. Any detector that is in the same static patch following the Killing trajectory $r \neq 0$ experiences a proper acceleration. As a result, local observers following different Killing trajectories keep a finite distance between each other. This acceleration compensates for the expansion of the spacetime, which is different for each Killing trajectory.

We can study the thermal properties of de Sitter spacetime by embedding it in a higher dimensional Minkowski spacetime as described by Deser and Levin [DL98, DL99]. The proper acceleration in embedding static coordinates is derived in appendix eq. (A.10):

$$\kappa_\mu \kappa^\mu = \frac{1}{\ell^2 - r^2} \tag{8.1}$$

The proper acceleration of the Killing trajectory with respect to the embedded space never vanishes. It takes its minimal value $\kappa_\mu \kappa^\mu = 1/\ell$ for the radial variable $r = 0$. This proper acceleration is used to characterize the *de Sitter temperature*:

$$T_{\mathrm{dS}} = \lim_{r\to 0}\frac{\kappa}{2\pi} = \lim_{r\to 0}\frac{1}{2\pi\sqrt{\ell - r^2}} = \frac{1}{2\pi\ell} \tag{8.2}$$

As mentioned in [HY18], thermal properties that appear in vacuum states in curved spacetime are interpreted as the result of the entanglement of states in causally disconnected regions. The *Unruh effect* is used to make sense of the expansion from a physical perspective. The relation between the expansion of spacetime and its thermal properties manifests in the Euclidean vacuum state from eq. (3.34), which is a vacuum state invariant under the full de Sitter group acting globally on de Sitter spacetime expressed with a linear combination of static patch modes:

$$|\Omega_E\rangle = \prod_{\omega=0}^{\infty} \sqrt{1 - e^{-2\pi\omega\ell}}\, e^{e^{-\pi\omega\ell}(\hat{a}^{\mathrm{I}}_\omega)^\dagger(\hat{a}^{\mathrm{II}}_\omega)^\dagger} |\Omega_{\mathrm{I}}\rangle \otimes |\Omega_{\mathrm{II}}\rangle$$

Even though there is an ambiguity in the choice of vacuum states in de Sitter spacetime, it is reasonable to work with the Euclidean vacuum state as its response to a de Sitter Unruh detector is thermal. This vacuum state takes the role of the Minkowski vacuum state expressed with Rindler modes in flat spacetime. The density matrix perceived by a local observer in static patch I matches the following thermal density matrix:

$$\rho_I = \mathrm{tr}_{\mathrm{II}}[|\Omega_E\rangle\langle\Omega_E|] = \prod_{\omega=0}^{\infty}\left(1 - e^{-2\pi\omega\ell}\right)\sum_{n_\omega=0}^{\infty} e^{-\pi\omega n_\omega \ell}\, |n_\omega, \mathrm{I}\rangle\langle n_\omega, \mathrm{I}|\,.$$

Here, we can see that changing the Fock representation to capture the properties of the static patch also changes the interpretation of particles. With the new Fock representation, we obtain thermal properties perceived by a local observer.

8.2. Initial state of de Sitter universe

We consider the *initial state of de Sitter spacetime* to be the global Euclidean vacuum state defined in eq. (3.34) with added quantum perturbations. The vacuum state is referred to as the Bunch-Davies vacuum state in [HY18]. The quantum fluctuations are modeled as d excited particles with different frequencies, which are created globally in the vacuum state. This initial state is also referred to as a *multi-rail state*, which is a state with d distinguishable excited modes. The paper [BHP09, BHP12, BHTW10] follows a similar approach in flat spacetime where they use an encoded logical qubit instead of the vacuum as an initial state to calculate the Unruh channel, which also takes the form of the multi-rail state. The initial state of de Sitter spacetime takes the following form:

$$|\psi\rangle = \sum_{j=1}^{d} c_j (\hat{a}^E_{\omega_j})^\dagger |\Omega_E\rangle \tag{8.3}$$

The relation between the static patch creation and annihilation operator and the Euclidean ones, which act globally on de Sitter, is described in eq. (3.32):

$$\begin{aligned}\hat{a}^{E1}_\omega =& \frac{1}{\sqrt{1-e^{-2\pi\omega\ell}}}\left(\hat{a}^{\mathrm{I}}_\omega - e^{-\pi\omega\ell}(\hat{a}^{\mathrm{II}}_\omega)^\dagger\right)\\ \hat{a}^{E2}_\omega =& \frac{1}{\sqrt{1-e^{-2\pi\omega\ell}}}\left(\hat{a}^{\mathrm{II}}_\omega - e^{-\pi\omega\ell}(\hat{a}^{\mathrm{I}}_\omega)^\dagger\right)\end{aligned}$$

The creation (and annihilation) operators $\hat{a}^{E1}_\omega$ and $\hat{a}^{E2}_\omega$ are obtained by swapping the static patches. Here, we will only consider the operators $\hat{a}^{E1}_\omega$, the operators $\hat{a}^{E2}_\omega$ yield similar results.

In the next section, we derive how a local observer who, in principle, cannot access the entire spacetime perceives the global expansion of de Sitter. To study this, we express the entire initial state of the universe $|\psi\rangle$ only with static patch modes. The initial state of the universe takes the following form (see appendix E.1):

$$|\psi\rangle = \sum_{j=1}^{d} c_j \sqrt{1-e^{-2\pi\omega_j}} (\hat{a}^{\mathrm{I}}_j)^\dagger |\Omega_E\rangle \tag{8.4}$$

It needs to be noted that the Euclidean vacuum state entails an infinite product, which is why the transformation from the global description with Euclidean modes to the description with static patch modes is not unitary in a mathematically rigorous sense [Wal94]. This is similar to the Minkowski vacuum state expressed in Rindler modes. To get a unitary transformation, we use the approximation with the two-mode unitary transformation U_ω which is detailed in appendix E.2:

$$|\Omega_E\rangle = \prod_{\omega=0}^{\infty} \sqrt{1-e^{-2\pi\omega\ell}} e^{e^{-\pi\omega\ell}(\hat{a}^{\mathrm{I}}_\omega)^\dagger(\hat{a}^{\mathrm{II}}_\omega)^\dagger} |\Omega_{\mathrm{I}}\rangle \otimes |\Omega_{\mathrm{II}}\rangle = \prod_{\omega=0}^{\infty} U_\omega |\Omega_{\mathrm{I}}\rangle \otimes |\Omega_{\mathrm{II}}\rangle$$

The two-mode transformation can be expanded as

$$\begin{aligned}U_\omega =& \exp\left[\theta\left((\hat{a}^{\mathrm{I}}_\omega)^\dagger(\hat{a}^{\mathrm{II}}_\omega)^\dagger - \hat{a}^{\mathrm{I}}_\omega\hat{a}^{\mathrm{I}}_\omega\right)\right] \qquad \text{with } 1/\cosh\theta = \sqrt{1-e^{-2\pi\omega}}\\ =& \sqrt{1-e^{-2\pi\omega}} e^{e^{-\pi\omega}(\hat{a}^{\mathrm{I}}_\omega)^\dagger(\hat{a}^{\mathrm{II}}_\omega)^\dagger} e^{\frac{1}{2}\ln(1-e^{-2\pi\omega})((\hat{a}^{\mathrm{I}}_\omega)^\dagger\hat{a}^{\mathrm{I}}_\omega + (\hat{a}^{\mathrm{II}}_\omega)^\dagger\hat{a}^{\mathrm{II}}_\omega)} e^{-e^{-\pi\omega}\,\hat{a}^{\mathrm{I}}_\omega\hat{a}^{\mathrm{II}}_\omega}\end{aligned} \tag{8.5}$$

The last exponentials in eq. (8.5) are absorbed in the static patch vacuum states with $\hat{a}^{\mathrm{I(,II)}}_\omega |\Omega_{\mathrm{I(,(II))}}\rangle$ which is how we obtain the initial form of the Euclidean vacuum state. In appendix E.3, the transformation between the expressions of the initial state of de Sitter spacetime from eq. (8.3) and eq. (8.4) is derived using the two-mode transformation. For this calculation, the introduction

of the two-mode transformation is a generalization that is not necessary. For more general cases with fewer simplifications where the vacuum state annihilates terms, this provides a detailed mathematical foundation. The calculation with the two mode transformation also shows, more explicitly, that the different modes do not influence each other in the transformation. The fact that only a finite number of modes take an active part in the transformation justifies that we restrict the infinite product to a finite number of modes to obtain a unitary transformation. When considering the transformation of a d-rail state, we only allow for d input modes and restrict our attention to d output modes. Physically, this can be interpreted as if the detector is tuned to this finite number of output modes, and only the excited modes participate in the transformation. Mathematically, we have restricted the size of the input and output Fock space such that they are finite and unitarily equivalent. This approach is also well known when transforming states from the Minkowski to the Rindler setting.

The expression of the state $|\psi\rangle$ can be further simplified by expressing the initial state of de Sitter spacetime we obtained with multi-index notation and using the multinomial theorem (for more details, see appendix E.4). For this, we introduce the abbreviation $z = e^{-\pi\omega}$.

$$|\psi\rangle = \sum_{k=1}^{d} c_k \sqrt{1-z_k^2} \sum_{n=0}^{\infty} \left(\prod_{\omega} \sqrt{1-z^2} z^n \right) \cdot \sum_{L_n} \sqrt{l_k+1}\, |L^{(k)}\rangle_{\mathrm{I}}\, |L\rangle_{\mathrm{II}}$$

The multi-index notation we used here is defined as follows:

$$\begin{aligned} |L\rangle &= |l_1 l_2 \dots l_d\rangle \\ |l_i\rangle &= \frac{1}{\sqrt{l_i!}} (\hat{a}^\dagger_{\omega_i})^{l_i} |\Omega\rangle \\ |L^{(i)}\rangle &= \frac{1}{\sqrt{l_i+1}} (\hat{a}^{\mathrm{I}}_{\omega_i})^\dagger |L\rangle \\ \sum_{L_n} &= \sum_{l_1+\dots+l_d=n} \end{aligned}$$

Under the assumption that we consider sufficiently large frequencies, we can consider the z in the product of frequencies to be equal. Together with the restriction to d frequencies contributing to the transformation, the expression simplifies as follows:

$$|\psi\rangle \approx \left(1-z^2\right)^{\frac{d+1}{2}} \sum_{k=1}^{d} c_k \sum_{n=0}^{\infty} z^n \sum_{L_n} \sqrt{l_k+1}\, |L^{(k)}\rangle_{\mathrm{I}}\, |L\rangle_{\mathrm{II}} \tag{8.6}$$

8.3. de Sitter Unruh channel with cloning properties

In this section, we derive the channel that describes how the evolution of the initial state of global de Sitter spacetime, and with that, the expansion of spacetime is perceived by a local observer in a static patch. We choose the observer to be located in static patch I. In the previous section, we have derived the initial state of the universe $|\psi\rangle$ expressed with static modes. For the derivation of the density matrix of the global state we need to restrict the density of the global state to the static patch accessible to a local observer. To restrict the density matrix to the space accessible to a local observer in static patch I, we trace out all modes from static patch II. Static patch II is the region that is causally disconnected from static patch I. Therefore, these are the modes that cannot influence what an inertial observer in this static patch perceives. To calculate the *Unruh channel*, we take the initial state from eq. (8.6). The resulting channel is

$$\mathcal{E}(\psi) = \mathrm{tr}_{\mathrm{II}}(|\psi\rangle\langle\psi|) = \mathrm{tr}_{\mathrm{II}}[\rho] = \rho_{\mathrm{I}} \otimes \rho_{\mathrm{I}}^{\mathrm{residual}}. \tag{8.7}$$

We will put our focus on ρ_{I} and neglect the residual part $\rho_{\mathrm{I}}^{\mathrm{residual}}$ of the cloning channel. The residual part $\rho_{\mathrm{I}}^{\mathrm{residual}}$ satisfies the following condition: $\omega \neq \omega_k$ and with that is composed of all modes which do not take an active part in the transformation from global to static modes. Neglecting the residual part is equivalent to only considering a finite number of modes. The density operator ρ_{I} is the main part of the Unruh channel, which comprises all modes participating in the transformation. The detailed calculated of ρ_{I} is detailed in appendix E.5:

$$\rho_{\mathrm{I}} = (1-z^2)^{d+1} \bigoplus_{n=0}^{\infty} z^{2n} \sigma_{\mathrm{I}}^{(n)}$$

with

$$\sigma_{\mathrm{I}}^{(n)} = \sum_{k=1}^{d} |c_k|^2 (l_k+1) \sum_{L_n} |L^{(k)}\rangle \langle L^{(k)}|_{\mathrm{I}} + \sum_{\substack{k,\tilde{k}=1 \\ k\neq\tilde{k}}}^{d} c_k c_{\tilde{k}} \sqrt{l_k+1}\sqrt{l_{\tilde{k}}+1} \sum_{L_n} |L^{(k)}\rangle \langle L^{(\tilde{k})}|_{\mathrm{I}} \tag{8.8}$$

The structure of $\sigma_{\mathrm{I}}^{(n)}$ is that of a n-dimensional *optimal cloning channel* introduced in eq. (4.3) which is of the following form:

$$\hat{\rho}_a^{(\mathrm{out})} = \frac{1}{n+1} \left[\sum_{i=1}^{n} |\gamma_i|^2 \frac{2+n}{2} |\psi_i\rangle \langle\psi_i| + \sum_{\substack{i,j=1 \\ i\neq j}}^{n} \gamma_i \gamma_j^* \frac{n-2}{n+1} |\psi_i\rangle \langle\psi_j| + \frac{1}{2}\mathbb{1} \right]$$

The identity from the d-dimensional cloning channel $\hat{\rho}_a^{(\mathrm{out})}$ is contained in the diagonal part of $\rho_{\mathrm{I}}^{(n)}$. The explicit factors to identify $\rho_{\mathrm{I}}^{(n)}$ with an n-dimensinal cloning channel can be obtained by rewriting the multi-index notation. The Unruh channel $\rho_{\mathrm{I}}^{(n+1)}$ and the d-dimensional cloning channel $\hat{\rho}_a^{(out)}$ are of the same form. The coefficients of the respective diagonal and off-diagonal parts are explicitly compared in appendix E.6 and match up to the leading order.

A similar result was obtained in Rindler spacetime for the Unruh channel [BHTW10, BHP12]. The resulting channel is also a block diagonal density matrix where each block can be interpreted as an instance of a $1 \to n$ cloning channel. Both in the Rindler setting studied in [BHTW10] as well as in the de Sitter framework studied in this thesis, the cloning channel and its properties are a result of the acceleration. While the same phenomenon can be studied in flat spacetime, one needs to keep in mind that acceleration is always added as an external acceleration because we *choose* to study an accelerated observer. The mathematical aspects of the calculation are very similar in both cases, but we would like to highlight the novelty of the physical interpretation. We argue that de Sitter is the more natural place to study this because, here, acceleration is a fundamental property that is not to be avoided. With that, the result that the Unruh channel has properties of a cloning channel is even more compelling in the de Sitter framework, where cloning properties can be directly associated with the spacetimes expansion.

At the current stage it needs to be clarified what implications this has. However, the connection between the expansion of spacetime and the properties of a cloning channel is a novel result that opens many opportunities to gain a deeper understanding of quantum mechanics in de Sitter spacetime. In particular, the cloning properties of this channel can be used to further characterize the properties of the tensors in the holographic model discussed in part II of this thesis. Furthermore, the general setup using the Unruh effect opens many possibilities to study the evolution of local observers in de Sitter spacetime. In the next section, we will focus on the Unruh effect, where the detector follows a quantum superposition of trajectories.

Chapter 9

Superposition of static trajectories in de Sitter spacetime

In the study of quantum field theory in curved spacetime, the particle content of a field is usually determined with a *particle detector* which probes the particle content perceived as by a local observer [DeW80, BD82]. A particle detector hereby is considered to be a localized system that has internal degrees of freedom that couple to the background field. This way, the state of the detector provides information on what particles are perceived by a local observer following the trajectory of the detector in a given spacetime geometry. It is well-established that reading out the state of these degrees of freedom provides information about the particle perception by the observers following the trajectory of the detector. Typically, we consider particle detectors that follow well-defined classical trajectories. This can be generalized to consider a detector that follows a quantum superposition of trajectories.

Different scenarios of a detector following a quantum superposition of trajectories have been considered in the past [FOZ20, WVCZ21, GZ22, FAZM23, FZ23, FMZ23]. In the context of de Sitter spacetime different scenarios of quantum superposition of trajectories have been considered recently in [FMZ20] where a Unruh-de Witt detector which followed a quantum superposition of trajectories was studied. The authors considered both the superposition of different spatially translated trajectories in one de Sitter geometry as well as the superposition corresponding to de Sitter spacetime with different curvatures. The main result of the work is that the response functions of the detectors for these setups are calculated, which is considered to provide information about the particle detection rate of a detector. They find that the setups are not diffeomorphic to each other. In expanding spacetimes, local observers whose trajectories follow the timelike Killing vector field in one de Sitter static patch keep a fixed distance from one another. We refer to these trajectories as *static trajectories*. Keeping a fixed distance from one another is only possible because local observers following the Killing field experience proper acceleration.

In this chapter, we follow our work from [NB24], where we generalize the approach from [FMZ20] by considering the particle detector to be a multi-level particle detector as introduced in [BCRAvB20]. As this detector can be in more than two energy states, we can perform a more in-depth discussion of the final state of the detector. We consider the setup, where the multi-level particle detector follows a quantum superposition of static trajectories. This setup is detailed in section 9.1 including the interaction between the detector, its trajectories, and the background field. This follows an approach which already been employed to study the quantum superposition of the detector's trajectories in other contexts of quantum field theory in curved spacetime: the Unruh effect in flat spacetime [BCRAvB20] and in measuring Hawking radiation [PB23].

The main result of this chapter is the derivation and discussion of the final state of the detector

in section 9.2. We find that there is interference between the different trajectories in quantum superposition, therefore the resulting state of the detector goes beyond being a thermal mixture of states. We relate these additional coherence terms to the properties of the particle absorbed by the detector. This is a novel result in the context of cosmological particle creation in de Sitter spacetime. A similar effect was detected in the flat spacetime Unruh effect [BCRAvB20] and in measuring Hawking radiation [PB23] when considering a quantum superposition of trajectories. We discuss the physical interpretation of the final state of the detector in section 9.3.

9.1. Description of the initial state

In this section, we fully characterize the initial state of the considered problem. This includes the state of the background field, the initial state of the detector, the characterization of the quantum superposition of trajectories and how they interact.

We consider the global background field $\hat{\phi}(\hat{x}_r(\tau))$ to be initiated in the Euclidean vacuum state introduced in eq. (3.34) which is expressed as a linear combination of static patch modes

$$|0\rangle_{\mathrm{F}} = \prod_{\omega=0}^{\infty} \sqrt{1-e^{-2\pi\omega\ell}}\, e^{e^{-\pi\omega\ell}(\hat{a}^{\mathrm{I}}_{\omega})^{\dagger}(\hat{a}^{\mathrm{II}}_{\omega})^{\dagger}} |\Omega_{\mathrm{I}}\rangle \otimes |\Omega_{\mathrm{II}}\rangle \,.$$

Here, $|\Omega_{\mathrm{I}}\rangle$ and $|\Omega_{\mathrm{II}}\rangle$ are the vacuum states of the static patches I and II respectively. The positive frequencies of the background field $\hat{\phi}(\hat{x}_r(\tau))$ are annihilated by the vacuum state $|0\rangle_{\mathrm{F}}$. As the field is constructed from modes in the static patches as described in section 3.7, its quantization is based on static coordinates.

We also use static coordinates to characterize the trajectories, where each trajectory has a fixed spatial coordinate r. These trajectories follow the de Sitter Killing vector field and keep a fixed distance from one another (see section 2.4.3). We can express the trajectory directly in static coordinates with respect to the proper time τ (derived in appendix eq. (A.8)):

$$x_r(\tau) = \begin{pmatrix} t(\tau) \\ r(\tau) \end{pmatrix} = \begin{pmatrix} \tau/\sqrt{1-r_i^2/\ell^2} \\ r_i \end{pmatrix}$$

We need to note here that the relation between the coordinate time t and the proper time τ differs for different r_i and thus different trajectories. We interpret this relation as an operator that acts on the basis states $|i\rangle_{\mathrm{T}}$ of trajectories, as the proper time is dependent on the choice of trajectory and with that elevate the coordinates describing the trajectory to an operator. Each trajectory corresponds to a state of the set $\{|1\rangle_{\mathrm{T}}, |2\rangle_{\mathrm{T}}, \dots\}$ and we require that the trajectories are fully distinguishable. As a result the set of states of trajectories forms an orthonormal basis of the Hilbert space corresponding to the external degrees of freedom of the detector and we have $\langle i|k\rangle_{\mathrm{T}} = \delta_{ik}$. We express the relation between the proper time and the different trajectories with the following operator:

$$\hat{x}_r(\tau)\,|i\rangle_{\mathrm{T}} = \left(\tau/\sqrt{1-r_i^2/\ell^2}, r_i\right)|i\rangle_{\mathrm{T}}$$

To describe the coupling between the state of the field $\hat{\phi}(\hat{x}_r(\tau))$ and the detector we use the interaction picture:

$$\hat{H}_{\mathrm{I}}(\tau) = \chi(\tau)\hat{m}(\tau)\hat{\phi}(\hat{x}_r(\tau)), \tag{9.1}$$

where the switching function $\chi(\tau)$, $\hat{m}$ is the monopole moment characterizing the evolution of the detector and $\hat{\phi}(\hat{x}_r(\tau))$ is the background field. The *switching function* controls the intensity of

the coupling between the field and the detector. On an intuitive level, this can be interpreted as turning the detector on and off. The switching function is a Gaussian function with interaction time T defined as

$$\chi(\tau) = \frac{1}{(2\pi)^{1/4}} \mathrm{e}^{-\tau^2/(4T^2)}.$$

The Gaussian function itself is not normalized in order to capture the duration of the interaction. Under the assumption that we have an *adiabaticity condition* between the field and the detector, we impose the following condition for the interaction time T and the energies ω_i:

$$T \sim \frac{1}{\varepsilon\omega_1} >> \frac{1}{\omega_1} \leq \frac{1}{\omega_i} \tag{9.2}$$

With this condition we ensure, that the interaction time characterizing the switching function is large enough, that no additional transitions in the detector are excited.

The evolution of the multi-level particle detector with the free Hamiltonian is characterized by the *monopole moment* $\hat{m}(\tau)$. The normalization of the state is fixed by the coupling amplitudes ζ_i in the monopole moment. The monopole moment is defined as

$$\hat{m}(\tau) = \sum_i \zeta_i \, \mathrm{e}^{\mathrm{i}\omega_i\tau} \, |\omega_i\rangle \, \langle 0|_{\mathrm{D}} + \mathrm{h.c.}$$

where the coupling amplitudes ζ_i characterize how different excitations of the detector are coupled to its ground state.

We now have all the tools to define the initial state we want to study. We prepare the detector in its ground state $|0\rangle_{\mathrm{D}}$ and the background field in the Euclidean vacuum state $|0\rangle_{\mathrm{F}}$. We consider a quantum superposition of different trajectories where A_n are the normalization amplitudes for the different trajectories. The trajectories $|n\rangle_{\mathrm{T}}$ all follow the constant spatial coordinate r_n:

$$|\Psi(\tau \to -\infty)\rangle = |0\rangle_{\mathrm{D}} \, |0\rangle_{\mathrm{F}} \left(\sum_n A_n \, |n\rangle_{\mathrm{T}} \right),$$

With the interaction model with the Hamiltonian in eq. (9.1), we know how the state evolves and can calculate the state at late times. We consider the evolution of the state describing the field and the detector up to the first order in ε:

$$\begin{aligned} |\Psi(\tau \to \infty)\rangle =& \left(\hat{\mathrm{I}} + \mathrm{i}\varepsilon \int_{-\infty}^{\infty} \mathrm{d}\tau \, \hat{H}_{\mathrm{I}}(\tau) \right) |\Psi(\tau \to -\infty)\rangle \\ =& \, |0\rangle_{\mathrm{D}} \, |0\rangle_{\mathrm{F}} \left(\sum_n A_n \, |n\rangle_{\mathrm{T}} \right) + \mathrm{i}\varepsilon \int_{-\infty}^{\infty} \mathrm{d}\tau \, \chi(\tau) \hat{m}(\tau) \hat{\phi}(\hat{x}_r(\tau)) \, |0\rangle_{\mathrm{D}} \, |0\rangle_{\mathrm{F}} \left(\sum_n A_n \, |n\rangle_{\mathrm{T}} \right) \end{aligned} \tag{9.3}$$

9.2. Final state of the detector after the interaction

In this section, we explicitly calculate the state of the field and the detector from eq. (9.3) after the interaction at late times. The monopole moment $\hat{m}$ describing the evolution of the detector takes the following form:

$$\hat{m}(\tau) \, |0\rangle_{\mathrm{D}} = \left(\sum_i \zeta_i \, \mathrm{e}^{\mathrm{i}\omega_i\tau} \, |\omega_i\rangle \, \langle 0|_{\mathrm{D}} + \mathrm{h.c.} \right) |0\rangle_{\mathrm{D}} = \sum_i \zeta_i \, \mathrm{e}^{\mathrm{i}\omega_i\tau} \, |\omega_i\rangle_{\mathrm{D}}$$

With that, we get the following expression for the state $|\Psi\rangle$ at late times:

$$|\Psi(\tau \to \infty)\rangle = |0\rangle_{\mathrm{D}} \, |0\rangle_{\mathrm{F}} \left(\sum_n A_n \, |n\rangle_{\mathrm{T}} \right) + \mathrm{i}\varepsilon \sum_{i,n} \zeta_i A_n \, |\omega_i\rangle_{\mathrm{D}} \, |\omega_i, n\rangle_{\mathrm{F}} \, |n\rangle_{\mathrm{T}}$$

$$\text{with} \qquad |\omega_i, n\rangle_{\mathrm{F}} = \int_{-\infty}^{\infty} \mathrm{d}\tau \chi(\tau) \mathrm{e}^{\mathrm{i}\omega_i \tau} \hat{\phi}(\hat{x}_r(\tau)) \, |0\rangle_{\mathrm{F}}$$

The state $|\omega_i n\rangle_{\mathrm{F}}$ describes the state of the field and how it is influenced by different trajectories $|n\rangle_{\mathrm{T}}$. It is the state in which the field is left when the detector follows the trajectory $|n\rangle_{\mathrm{T}}$ and gets excited to the state $|\omega_i\rangle_{\mathrm{D}}$. We will focus on this in the upcoming calculations. The state can be expressed in the following equivalent ways:

$$\begin{aligned}
|\omega_i, n\rangle_{\mathrm{F}} =& \int_{-\infty}^{\infty} \mathrm{d}\tau \chi(\tau) \mathrm{e}^{\mathrm{i}\omega_i \tau} \hat{\phi}(\hat{x}_r(\tau)) \, |0\rangle_{\mathrm{F}} \\
=& \frac{1}{\mathrm{i}\varepsilon \zeta_i A_n} \langle \omega_i |_{\mathrm{D}} \langle n |_{\mathrm{T}} \, |\psi(\tau \to \infty)\rangle \\
=& \frac{1}{\zeta_i} \langle \omega_i |_{\mathrm{D}} \langle n |_{\mathrm{T}} \int_{-\infty}^{\infty} \mathrm{d}\tau \hat{H}_{\mathrm{I}}(\tau) \, |0\rangle_{\mathrm{D}} \, |0\rangle_{\mathrm{F}} \, |n\rangle_{\mathrm{T}}
\end{aligned}$$

To obtain the final state of the detector related to the superposition of trajectories, we consider the density matrix where we trace out the background field and its degrees of freedom:

$$\begin{aligned}
\rho_{\mathrm{DT}} =& \mathrm{tr}_{\mathrm{F}}(|\psi(\tau \to \infty)\rangle \langle \psi(\tau \to \infty)|) \\
=& \left(\sum_{m,n} A_m^* A_n \, |n\rangle \langle m|_{\mathrm{T}} \right) |0\rangle \langle 0|_{\mathrm{D}} + \varepsilon^2 \sum_{i,j,m,n} \zeta_j^* \zeta_i A_m^* A_n \, |\omega_i\rangle \langle \omega_j|_{\mathrm{D}} \langle \omega_j, m | \omega_i, n \rangle_{\mathrm{F}} \, |n\rangle \langle m|_{\mathrm{T}}
\end{aligned} \tag{9.4}$$

The first term, which is the term of zeros order in ε, corresponds to the case where we have no detected perticles and describes the state *without* interaction between the detector and the field. The characterizing quantity of the term describing the interaction is the scalar product $\langle \omega_j, m | \omega_i, n \rangle_{\mathrm{F}}$, which is calculated in detail in appendix F.1. Here, we can distinguish between terms we refer to as diagonal and off-diagonal terms: the diagonal terms contain the scalar product of identical trajectories and the off-diagonal terms relate different trajectories. For the diagonal terms, we have shown in appendix F.2 that the scalar product for two identical trajectories reduces to the known result: We get a thermal spectrum described by a Planckian probability distribution with de Sitter temperature weighted with the excitation frequency ω_i of the detector. The off-diagonal terms can be expressed with the normalized inner product Λ_{nm}^{ij} derived in appendix F.3. With that, the state after the interaction takes the following form:

$$\begin{aligned}
\rho_{\mathrm{DT}} =& \left(\sum_{m,n} A_m^* A_n \, |n\rangle \langle m|_{\mathrm{T}} \right) |0\rangle \langle 0|_{\mathrm{D}} + \varepsilon^2 \frac{T}{2\pi} \sum_{j,n} \zeta_j^* \zeta_j A_n^* A_n \, |\omega_j\rangle \langle \omega_j|_{\mathrm{D}} \frac{\omega_j}{e^{2\pi q_{jn}} - 1} \, |n\rangle \langle n|_{\mathrm{T}} \\
&+ \varepsilon^2 \frac{T}{2\pi} \sum_{\substack{i,j \\ i \neq j}} \sum_{\substack{m,n \\ m \neq n}} \zeta_j^* \zeta_i A_m^* A_n \, |\omega_i\rangle \langle \omega_j|_{\mathrm{D}} \Lambda_{nm}^{ij} \frac{\sqrt{\omega_i \omega_j}}{e^{2\pi q_{jn}} - 1} \, |n\rangle \langle m|_{\mathrm{T}}
\end{aligned} \tag{9.5}$$

where the normalized inner product is

$$\Lambda_{ij}^{mn} = \frac{\sqrt{\kappa_m \kappa_n} \sin\big(2 q_{in} \operatorname{arcsinh}\big(\sqrt{b_{mn}}\big)\big)}{\sqrt{2} q_{in} \sqrt{\kappa_n^2 + \kappa_m^2} \sqrt{b_{mn}(b_{mn}+1)}} \tag{9.6}$$

with

$$b_{mn} = \frac{1}{2} \left(\frac{(1 - x_m x_n)}{\sqrt{1 - x_m^2} \sqrt{1 - x_n^2}} - 1 \right).$$

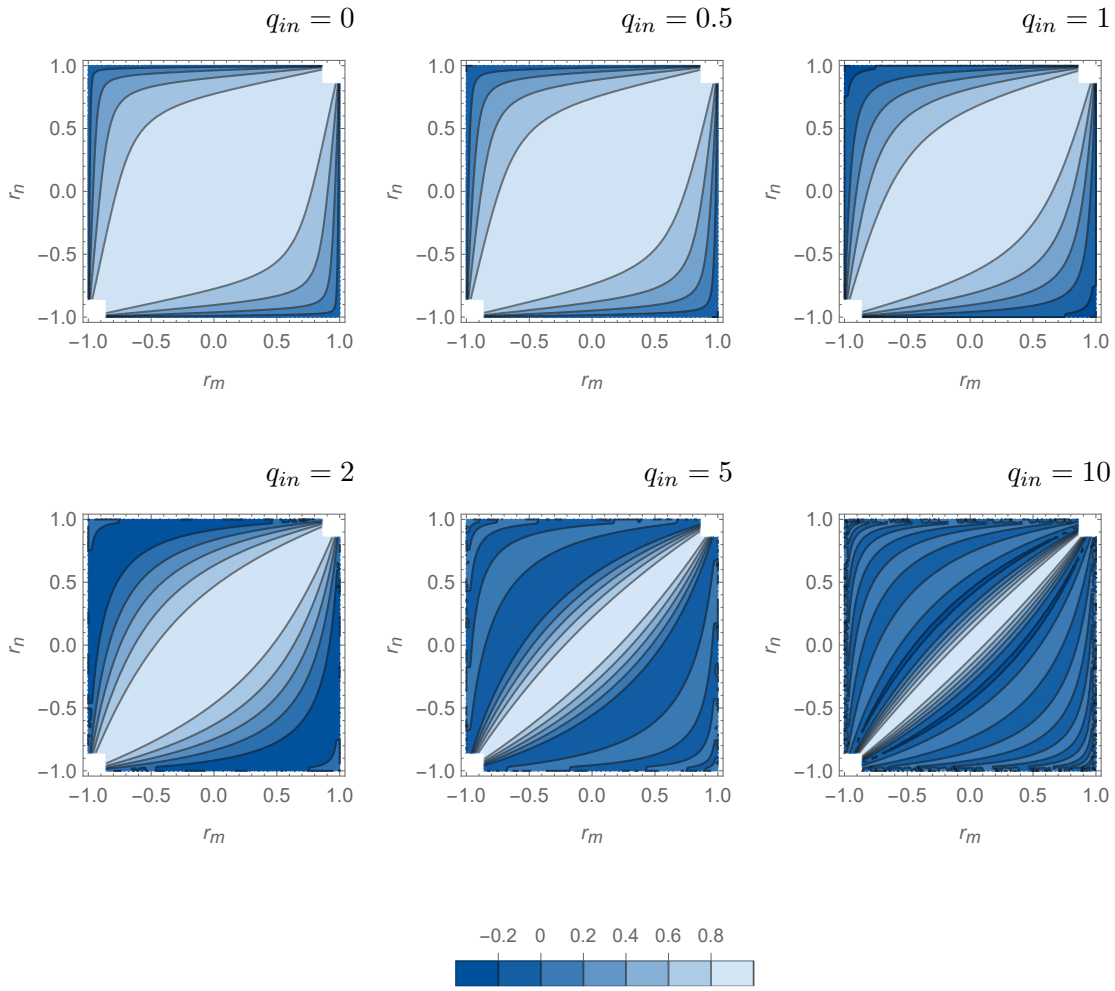

Figure 40.: The normalized inner product Λ^{ij}_{nm} for different values of q_{in} plotted for two trajectories characterized by the radial coordinates r_m and r_n

Here, we introduced the rescaled spatial coordinate $x_i = r_i/\ell$ and the auxiliary parameter b_{mn}. The parameter q_{in} is an auxiliary parameter characterized by the ratio between the energy ω_i and acceleration κ_n (introduced in eq. (8.1)):

$$q_{in} = \frac{\omega_i}{\kappa_n} \tag{9.7}$$

The value of the normalized inner product is plotted in figure 40 for different values of q_{in}. The value of $q_{in} = 0$ is included to describe the limiting behaviour of the normalized inner product for small frequencies. We derived in the appendix eq. (F.3) that the off-diagonal terms up to first order in ε are only non-vanishing if the parameter q_{in} and q_{jm} for the two trajectories in the scalar product satisfy the following condition:

$$q_{in} \approx q_{jm}$$

We obtain this relation because of a product of two sharp Gaussian functions in the calculation of the scalar product. The Gaussians are centered around q_{in} and q_{jm} respectively, and this product vanishes if the peaks are too far apart from one another.

We have derived the state ρ_{DT}, which captures the final state of the detector and the trajectories (eq. (9.5)). Now, we want to explicitly study the internal state of the detector independent of the

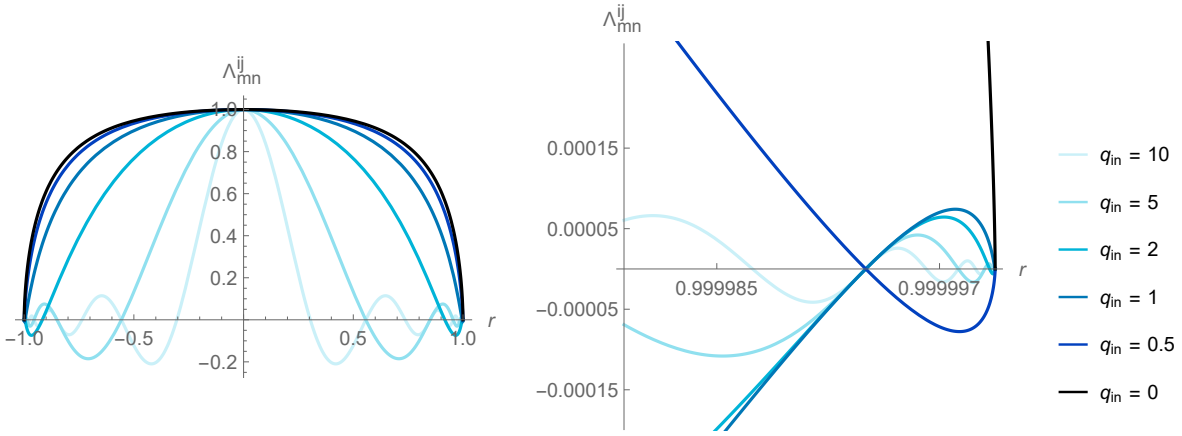

(a) (b)

Figure 41.: Values for the normalized inner product Λ^{ij}_{nm} where the radial coordinate of one trajectory is fixed to $r_n = 0$. This restriction allows us to visualize the oscillations of the value of Λ^{ij}_{mn} close to the boundaries, which increase for larger values of q_{in}. (a) shows the entire range of the spatial variable r of the second trajectory, and (b) only shows the area very close to one boundary. The case $q_{in} = 0$ is the only one without oscillations.

trajectories. With that, we want to associate a temperature with its internal energy levels, as we did for a detector with one well-defined trajectory. For deriving the state of the detector, we need to take a partial trace over the trajectories. By tracing out the trajectories, we eliminate all off-diagonal terms, which decoheres the resulting state completely. As a result, we lose all interference terms between the different trajectories. The resulting state after taking the partial trace over the trajectories would be

$$\rho_{\mathrm{D}} = \mathrm{tr}_{\mathrm{T}}(\rho_{\mathrm{DT}}) = |0\rangle\langle 0|_{\mathrm{D}} + \varepsilon^2 \frac{T}{2\pi} \sum_{j,n} \zeta_j^* \zeta_j A_n^* A_n \, |\omega_j\rangle\langle\omega_j|_{\mathrm{D}} \, \frac{\omega_j}{e^{2\pi q_{jn}} - 1} \tag{9.8}$$

The resulting state is a mixture of thermal states with different temperatures depending on the trajectories. The different trajectories correspond to different temperatures, as we required the trajectories to be fully distinguishable. This result is compatible with the standard result for a detector following a well-defined trajectory, but we have lost all interfering properties between the trajectories in superposition.

One option to keep the interfering property in the resulting state of the detector is to measure its final state on a different basis that does not belong to the well-defined trajectories before taking the partial trace. We construct a new basis $|\tilde{n}\rangle_{\mathrm{T}} := \sum_n B_n \, |n\rangle_T$ in which we measure the state of the detector and get the following result up to first order:

$$\begin{aligned}
\rho_{\mathrm{D}}^{\mathrm{measure}} &= \mathrm{tr}_{\mathrm{T}}(|\tilde{n}\rangle\langle\tilde{n}|_{\mathrm{T}} \, \rho_{\mathrm{DT}}) \\
&= \left(\sum_{m,n} B_m^* A_n^* B_n A_m^* \right) |0\rangle\langle 0|_{\mathrm{D}} + \varepsilon^2 \frac{T}{2\pi} \sum_{j,n} |\zeta_j|^2 |A_n|^2 |B_n|^2 \, |\omega_j\rangle\langle\omega_j|_{\mathrm{D}} \, \frac{\omega_j}{e^{2\pi q_{jn}} - 1} \\
&\quad + \varepsilon^2 \frac{T}{2\pi} \sum_{\substack{i,j \\ i \neq j}} \sum_{\substack{m,n \\ m \neq n}} \zeta_j^* \zeta_i A_m^* B_n^* A_n B_m \, |\omega_i\rangle\langle\omega_j|_{\mathrm{D}} \, \Lambda^{ij}_{nm} \frac{\sqrt{\omega_i \omega_j}}{e^{2\pi q_{jn}} - 1}
\end{aligned} \tag{9.9}$$

This result captures the final state of the detector and its excited internal energy levels.

9.3. Physical interpretation

In this section, we comment on the physical interpretation of the theoretical result of the final state of the detector after the interaction. First, we consider the state ρ_{DT} including both the trajectory and the detector from eq. (9.5). Here, we distinguish the different orders of perturbation: The zeroth order in ε describes the case *without* interaction between the detector and the field. The first order in ε (note, that the term with ε^2 is in fact of order ε, since $T \sim 1/\varepsilon$) describes the interaction between the field and the detector and is comprised of diagonal and off-diagonal terms. The diagonal terms reproduce the known result for detectors following one well-defined trajectory, which is a thermal spectrum with respective temperature described by a Planckian probability distribution weighted with the coupling amplitude ξ_i for each frequency. The temperature $T = \kappa/(2\pi) = 1/(2\pi\sqrt{\ell^2 - r^2})$ is defined by the de Sitter radius ℓ and the proper acceleration κ introduced in eq. (8.1). The diagonal terms, therefore, are the incoherent combination of the contributions of all individual trajectories. With this, the original result that a detector following a trajectory with constant acceleration perceives a thermal bath is contained in our result. In our case, the constant acceleration refers to static trajectories following the Killing field in a de Sitter static patch.

The more interesting result is contained in the off-diagonal terms. The off-diagonal terms are primarily characterized by the normalized inner product Λ_{ij}^{mn} whose behavior is plotted in figure 40. The normalized inner product characterizes transitions between different energy levels of the detector depending on the trajectories and we can see, that the value of Λ_{nm}^{ij} decays to zero the more the trajectories differ. This way, the normalized inner product can be interpreted as the product of two states describing the detector and its trajectory where the particle is absorbed in the state corresponding to one or the trajectory to excite the detector. The value of the normalized inner product has an oscillatory behavior when considering trajectories close to the boundary of the static patch, which characterizes the *coherence of particles* absorbed by detectors on different trajectories. We only get this coherent behavior if the condition eq. (9.7) holds, which means that the ratio between the excitation level ω and the proper acceleration κ has to be similar for different trajectories in quantum superposition. This oscillatory behaviour can best be seen in figure 41, where we have fixed one trajectory to $r = 0$ and plotted the value of the normalized inner product depending on the other trajectory. Here we can see, that the oszillations get more pronounced for higher values of q_{in} and the only case where we have no oscillations at all is the limiting case of small frequencies ($q_{in} = 0$). From this, we can deduce some dispersion relation for a delocalized particle. The off-diagonal terms are characterized by the product of the square root of the thermal spectra for the respective trajectories multiplied with the normalized inner product from eq. (9.6).

During the time of interaction, the detector absorbs particles from the thermal bath perceived by the vacuum state. These absorbed particles are almost delocalized along the interaction period. As a result, the absorbed particles have very little dispersion in frequency due to uncertainty relations. This justifies the condition in eq. (9.7), which is a manifestation of the Tolman factor from a physical perspective: it requires that the particles absorbed along different trajectories are fine-tuned in frequency such that they can still be distinguished, and we would get no off-diagonal terms.

We also considered the state ρ_{D} of the detector independent of the trajectories in eq. (9.8). Here, the first order in ε only has diagonal terms which again directly correspond to the thermal contributions. When measuring the state in a different basis as done in eq. (9.9) the weights of the different temperature terms are modified depending on the new choice of basis. The more important difference is, that we keep the off-diagonal terms characterizing the interference between trajectories in $\rho_{\mathrm{D}}^{\mathrm{measure}}$. Consequently, the state $\rho_{\mathrm{D}}^{\mathrm{measure}}$ is *not* just a mixture of thermal

states with well-defined energy. The coherences from the interference terms in the resulting state are the main result of this chaoter.

There is one special case we want to emphasize: We can choose the new basis such that the state of the trajectory measured in the new basis $|\tilde{n}\rangle_{\mathrm{T}}$ is orthogonal to the initial state of the trajectory. When choosing the new basis in this way, we get, similar to considering a well-defined trajectory, a vanishing off-diagonal term $|0\rangle\langle 0|_{\mathrm{D}}$. Different from the case with a well-defined trajectory, this still is a valid state, as we have additional off-diagonal terms that do not vanish. Physically, this scenario is only possible if the entanglement of the initial trajectory gets entangled with the internal energy levels of the detectors through the background field. Even after taking the partial trace over the trajectories, this entanglement remains in the state of the detector. From this, it is possible to consider the trajectory as a quantum degree of freedom that interacts with the background field and can be influenced by the interaction. This is possible even after the background field is traced out. The only case where the quantum degree of freedom collapses is when we choose a well-defined trajectory. The result bears close similarities to the one of the final state of the detector following a superposition of trajectories in the flat-spacetime Unruh effect discussed in [BCRAvB20].

In this chapter, we have studied the final state of the multi-level particle detector following a quantum superposition of trajectories with a fixed distance in a de Sitter static patch after its interaction with the background field. The result bears close similarities to the Unruh effect in Minkowski spacetime for a quantum superposition of trajectories with fixed distance. For future research, it would be interesting to generalize the setup to also consider a quantum superposition of different de Sitter spacetime geometries. The superposition of conformally equivalent spacetime metrics has already been studied in [KdlHCRB22], which also can be applied to de Sitter geometries with different curvatures. With this and the generalization of a multi-level particle detector considered in this chapter, the results from [FMZ20] where different scenarios of a detector following a quantum superposition of trajectories can be further generalized in the future.

Chapter 10

Conclusion

In this thesis, we investigated different aspects of quantum gravity in de Sitter spacetime with a focus on using holographic models and methods from quantum information theory to characterize the dS/CFT correspondence. Here, we summarize our results and point out ideas for future research questions.

As the centerpiece of this thesis, we developed a *holographic toy model* for $1+1$ dimensional de Sitter spacetime, which is a discrete model that can describe both kinematical as well as dynamical properties of de Sitter spacetime and the dS/CFT correspondence. Part II of this thesis puts focus on the holographic toy model: It was developed in chapter 6, and its properties were studied in this and the following chapter. The holographic toy model is defined as a family of tensor networks associated with a tessellation of de Sitter spacetime, which acts as a propagator from the de Sitter past to the future boundary. The tensor networks can be interpreted as a map from an infinite dimensional kinematical Hilbertspace $\mathcal{H}_{\text{in}}$ associated with the past boundary to the infinite-dimensional kinematical Hilbertspace $\mathcal{H}_{\text{out}}$ associated to the future boundary and takes the form of a partial isometry.

From a physical viewpoint, the holographic toy model has two key properties. First, we find that the time evolution of de Sitter spacetime captured by the holographic toy model is *isometric* and not unitary. This is plausible as the isometry captures that degrees of freedom are added in expanding spacetimes such as de Sitter. Second, we find a direct relation between the effective degrees of freedom allowed by the holographic toy model and the curvature of de Sitter. This manifests as follows: As a partial isometry, the tensor network maps the infinite-dimensional Hilbert space $\mathcal{H}_{\text{in}}$ to a finite-dimensional subspace we refer to as the physical Hilbert space $\mathcal{H}_{\text{phys}}$. The dimension of the physical Hilbertspace is directly related to the de Sitter radius ℓ and, with that, to the de Sitter curvature. The dimension of $\mathcal{H}_{\text{phys}}$ limits the capacity of the channel implemented by the tensor network, which implies a direct relation between the quantum information capacity of the holographic toy model and the curvature of de Sitter spacetime. The quantum information capacity is directly related to the effective degrees of freedom of the holographic model. As a result, we can see Λ-N correspondence, which was already postulated in the early 2000s, as a property in this holographic toy model.

What primarily sets this holographic toy model apart from previous tensor network models is that we get a *dynamical model* since the action of the discretized isometries on the boundary Hilbert spaces is fully characterized as described in chapter 5 of this thesis. To describe the asymptotic de Sitter symmetry group, we have characterized the discretized isometry group at the de Sitter boundaries as a subgroup of Thompson's group T, which we identified with the modular group $\text{PSL}(2,\mathbb{Z})$. With the characterization using Thompson's group T, we were able to identify the circular boundary of $1+1$ dimensional de Sitter spacetime with a conformal field theory (CFT)

and, with that, obtain a notion of a dS/CFT correspondence. We have shown that there is a vacuum state in the physical Hilbertspace which is invariant under isometry transformations when choosing the tensors in the tensor network to be *perfect tensors*. The existence of a vacuum state, other physical states, and a well-defined notion of dynamics gives rise to a reasonable physical model.

We develop the holographic toy model further by characterizing allowed physical states and operations in chapter 7 to generate them from the vacuum state. A central result is that the properties of the physical states of this model highly depend on the properties of the tensors that make up the tensor network. In models capturing the AdS/CFT correspondence, quantum error correcting codes have been the best candidates for the tensor networks. We found that adapting this result to the dS/CFT model does not work because the model gets trivial in this scenario: only the vacuum state is permitted as a physical state, and only the identity is an allowed operation. Even though we were not able to fully characterize the properties of the tensors to produce reasonable physical states, we have provided a formalism to generate physical states from the vacuum state using allowed operations. For the allowed operations, we apply operators at the future boundary, and depending on the tensor properties, this generates different local operations in the bulk and thus also generates different physical states.

Finally, in part III of the thesis, we looked at properties of quantum gravity in de Sitter spacetime from a different point of view. The aim is to gain more insights into the physical properties of the holographic toy model to help further characterize the properties of the tensors in the future and consequently improve our understanding of the dS/CFT correspondence. We follow two different approaches, which are both generalizations of the Unruh effect in the context of de Sitter spacetime. Similar to Minkowski spacetime, there is a global vacuum state in de Sitter, which is perceived as a thermal state whose temperature depends on the de Sitter radius by a local observer following the Killing field. The expansion of spacetime and the acceleration of a Rindler observer have a similar effect, as the local observer experiences a proper acceleration in both cases.

In the first project detailed in chapter 8, we made the generalization that we replaced the vacuum state with a vacuum state with quantum fluctuations. We model the quantum fluctuations with d excited particles with different frequencies and consider this state to be the *initial state of the de Sitter universe*. We derive how this initial state manifests in a static patch accessible by a local observer. This way, we get an understanding of how a local observer experiences the global expansion of spacetime. We find that the channel mapping the initial state of the universe to the state perceived by the local observer has the properties of an *optimal cloning channel*. It needs to be clarified what implications this has. On an intuitive level, it makes sense that an expanding spacetime is associated with a cloning property, as new spacetime regions need to be created as the spacetime expands. One possible interpretation is that the tensors in the holographic toy model should also have properties of optimal cloning channels. This hypothesis needs further clarification in future works.

The second project, which is presented in chapter 9, generalizes the study of the Unruh effect in de Sitter spacetime in a different way. Here, we consider a multi-level particle detector that takes the role of the local observer, which follows a *quantum superposition of trajectories* with a fixed distance. Superposition of trajectories in de Sitter spacetime was already studied in [FMZ20]; here, we generalized this approach by considering a *multi-level particle detector* opposed to a particle detector with two energy levels. In this thesis, we consider the superposition of trajectories, which each follow the Killing field in the de Sitter static patch, and each experiences a different proper acceleration. The focus lies on the derivation of the final state of the excited

particle detector after its interaction with the background field. We find that this final state of the detector contains a coherent superposition of energy levels that correspond to different trajectories. These coherences do not appear when considering a well-defined trajectory of the detector or a two-energy level Unruh-de Witt detector. Similar coherent behavior was found in the context of measuring the Unruh effect [BCRAvB20] or Hawking radiation [PB23], but the result is novel in the context of de Sitter spacetime.

The work in this thesis provides a broad foundation to study the dS/CFT correspondence further using a holographic toy model, but there remain many open questions for future research. Here, we primarily focus on open questions arising directly from the work in this thesis. The arguably most central open problem is a rigorous characterization of the properties of tensors and, with that, a full characterization of the allowed physical states and algebra of observables. From what we found in this thesis in chapter 8, a natural next step for further characterizing the allowed physical states would be to consider tensors with cloning properties for the holographic toy model and clarify how the set of allowed physical states is affected by that. There have been recent studies on the local algebra of observables in de Sitter spacetime in [Wit23], but it needs to be clarified in future studies if that description is compatible with the holographic model studied in this thesis and how it would affect the explicit properties of the tensors.

As the tensor network defining the holographic model can be interpreted as a quantum superposition of all possible world lines in de Sitter spacetime, it seems plausible that results from studying the superposition of trajectories have effects on tensor network properties. This opens many opportunities for new research questions. On the one hand, it is interesting to relate findings from this thesis, such as the interference properties between different trajectories evident in the state of the excited detector, to properties of the tensor network. On the other hand, there is huge potential in studying the superposition of de Sitter geometries with different curvatures as suggested in [FMZ20]. Again, this can be related to the holographic model, where we have different tensor networks for different de Sitter curvatures such that it is possible to consider a quantum superposition of these different tensor networks corresponding to different de Sitter radii and relate this to findings from quantum field theory in curved spacetime.

We are still far from having a completely understood theory of quantum gravity. However, we believe that holography and methods from quantum information theory are central to developing our understanding further in the future.

Appendix

Appendix A

de Sitter basics - calculations

A.1. Action in Jackiw Teitelboim gravity

The general action with a dilaton field looks as follows (see, for example, [CJM20, eq. (2.1)]):

$$S = \frac{1}{16\pi G}\int d^2x\sqrt{-g}(\varphi R + U(\varphi)) + \text{boundary term}$$

In order to find the potential $U(\varphi)$ that describes de Sitter spacetime, we need to vary the Lagrangian in terms of the scalar dilaton field capturing properties of the low dimensional spacetime:

$$0 = \frac{\partial L}{\partial \varphi} - \frac{d}{dt}\frac{\partial L}{\partial \dot{\varphi}} = \frac{\partial L}{\partial \varphi} = \frac{\partial}{\partial \varphi}\sqrt{-g}(\varphi R + U(\varphi)) = \sqrt{-g}\big(R + U'(\varphi)\big)$$

We know that de Sitter spacetime has constant curvature. Accordingly, R is constant. For the potential follows:

$$U'(\varphi) = -R \qquad \Rightarrow \qquad U(\varphi) = -R\varphi + c$$

There are two different lines of argument:

1. We know the constant curvature equation for 1+1 dimensional gravity and use for the potential, that $R - 2\Lambda = 0$.
2. We know the action <u>with</u> the potential and can derive the constant curvature equation from this.

Here, we choose the first line of argument in order to rewrite the potential such that it only depends on the dilaton field and the cosmological constant. For de Sitter spacetime the cosmological constant is $\Lambda = \frac{1}{L^2}$ where L is the de Sitter radius:

$$U(\varphi) = -2\Lambda\varphi + c = -\frac{2}{L^2}\varphi + c$$

In order to get rid of the integration constant, we express the dilaton field as $\varphi = \varphi^0 + \bar{\varphi}$ where φ^0 is a constant satisfying $U(\varphi^0) = 0$:

$$\begin{aligned} U(\varphi^0) =& -\frac{2}{L^2}\varphi^0 + c = 0 \Rightarrow c = \frac{2}{L^2}\varphi^0 \\ U(\varphi) =& U(\varphi^0 + \bar{\varphi}) = U(\varphi^0) + U(\bar{\varphi}) = U(\bar{\varphi}) \\ =& -\frac{2}{L^2}(\varphi^0 + \bar{\varphi}) + c = -\frac{2}{L^2}\varphi^0 - \frac{2}{L^2}\bar{\varphi} + \frac{2}{L^2}\varphi^0 = -\frac{2}{L^2}\bar{\varphi} \end{aligned}$$

For the action in the bulk, we get

$$\begin{aligned}
S =& \frac{1}{16\pi G}\int d^2x\sqrt{-g}\left(\varphi R - \frac{2}{L^2}\bar{\varphi}\right) + \text{boundary term} \\
=& \frac{1}{16\pi G}\int d^2x\sqrt{-g}\left(\varphi^0 R + \bar{\varphi}R - \frac{2}{L^2}\bar{\varphi}\right) + \text{boundary term} \\
=& \underbrace{\frac{1}{16\pi G}\int d^2x\sqrt{-g}\varphi^0 R}_{=S^0} + \underbrace{\frac{1}{16\pi G}\int d^2x\sqrt{-g}\bar{\varphi}\left(R - \frac{2}{L^2}\right)}_{=\bar{S}} + \text{boundary term}
\end{aligned}$$

The resulting $\bar{S}$ is the same as in [Jac85], eq. (3.4) and [CJM20] eq. (2.4).

A.2. Static coordinates embedded in Minkowski space and on the cylinder

Here, we derive the direct relation between the settings of de Sitter spacetime as a hyperboloid embedded in Minkowski spacetime and represented in the conformal setting for static coordinates. We use T as the conformal time for global coordinates and $\tilde{T}$ as the rescaled time for static coordinates:

$$\begin{aligned}
\vec{x}_G(\tau,\theta) &= \begin{pmatrix} \ell\sinh(\tau/\ell) \\ \ell\cos(\theta)\cosh(\tau/\ell) \\ \ell\sin(\theta)\cosh(\tau/\ell) \end{pmatrix} = \begin{pmatrix} \ell(1+\sec T)\tan(T/2) \\ \ell\cos(\theta)\sec(T) \\ \ell\sin(\theta)\sec(T) \end{pmatrix} = \vec{x}_G(T,\theta) \\
\vec{x}_S(r,t) &= \begin{pmatrix} \sqrt{\ell^2-r^2}\sinh(t/\ell) \\ \pm\sqrt{\ell^2-r^2}\cosh(t/\ell) \\ r \end{pmatrix} = \begin{pmatrix} \sqrt{\ell^2-r^2}(1+\sec\tilde{T})\tan(\tilde{T}/2) \\ \pm\sqrt{\ell^2-r^2}\sec(\tilde{T}) \\ r \end{pmatrix} = \vec{x}_S(r,\tilde{T}) \\
\vec{x}_G(T,\theta) &= \begin{pmatrix} \ell(1+\sec T)\tan(T/2) \\ \ell\cos(\theta)\sec(T) \\ \ell\sin(\theta)\sec(T) \end{pmatrix} = \begin{pmatrix} \sqrt{\ell^2-r^2}(1+\sec(\tilde{T}))\tan(\tilde{T}/2) \\ \pm\sqrt{\ell^2-r^2}\sec(\tilde{T}) \\ r \end{pmatrix} = \vec{x}_S(r,\tilde{T})
\end{aligned}$$

This can be solved for T and θ to express the static coordinates in the conformal setting:

$$\begin{aligned}
T &= \pm\,\text{arcsec}\left(\pm\sqrt{r^2-(-1+r^2)\sec^2\tilde{T}}\right) \\
\theta &= \pm\arccos\left(\pm\frac{\sec(\tilde{T})}{\sqrt{\sec^2(\tilde{T})-\frac{r^2}{r^2-1}}}\right)
\end{aligned}$$

This can be expressed as

$$T(\theta) = \pm\,\text{arcsec}\left(\pm\sqrt{r^2\csc(\theta)^2}\right)$$

This can be inverted to

$$\begin{aligned}
r &= \pm\sec T\sin\theta \\
\tilde{T} &= \pm\,\text{arcsec}\left(\pm\frac{\cos\theta}{\sqrt{\cos^2 T-\sin^2\theta}}\right)
\end{aligned}$$

A.3. Induced metric of Cauchy hypersurface

We can obtain the metric intrinsic to the Cauchy surface from eq. (2.7) by a restriction of the metric of the spacetime. This is often referred to as the *induced metric* of the hypersurface [Poi04]. To do so, we first need the unit normal vectors of Σ (n_a) and the vectors tangent to the curves contained in Σ (e^b_a).

$$\begin{aligned}
n^a =& \gamma \begin{pmatrix} 1 \\ 0 \end{pmatrix}, \qquad g_{ab} n^a n^b = g_{tt} n^t n^t = \left(-1 + \frac{r^2}{\ell^2}\right)\gamma^2 = -1 \qquad \Rightarrow \qquad \gamma = \frac{\ell}{\sqrt{\ell^2 - r^2}} \\
n^a =& \frac{\ell}{\sqrt{\ell^2 - r^2}} \begin{pmatrix} 1 \\ 0 \end{pmatrix} \\
n_t =& g_{tb} n^b = \left(-1 + \frac{r^2}{\ell^2}\right) \frac{\ell}{\sqrt{\ell^2 - r^2}} = -\frac{\sqrt{\ell^2 - r^2}}{l}
\end{aligned}$$

For the tangent vector, we need the parametric description of the manifold x^a and the hypersurface y^a. In the case of the de Sitter static patches, this is almost trivial because the parametrization y^a of the hypersurface t is fixed and r unchanged. We get

$$\begin{aligned}
e^\alpha_\mu =& \frac{\partial x^\alpha}{\partial y_\mu} \\
e^r_r =& 1 \\
e^t_r = e^t_t = e^r_t =& 0
\end{aligned}$$

The induced metric of the hypersurface is obtained as follows:

$$h_{\mu\nu} = g_{\alpha\beta} e^\alpha_\mu e^\beta_\nu$$

For static coordinates it follows, that

$$h_{rr} = g_{rr} e^r_r e^r_r = \frac{\ell^2}{\ell^2 - r^2}$$

A.4. Curvature properties in different coordinates

In global coordinates with metric $g = -\mathrm{d}\tau^2 + \ell^2 \cosh^2(\tau/\ell)\mathrm{d}\theta^2$ from eq. (2.3) the only non-vanishing Christoffel symbols are

$$\begin{aligned}
\Gamma^\tau{}_{\theta\theta} =& \ell \cosh(\tau/\ell) \sinh(\tau/\ell) \\
\Gamma^\theta{}_{\tau\theta} =& \Gamma^\theta{}_{\theta\tau} = \tanh(\tau/\ell)/\ell
\end{aligned}$$

The Ricci tensor and scalar are

$$\begin{aligned}
R_{\mu\nu} =& \begin{pmatrix} -\frac{1}{\ell^2} & 0 \\ 0 & \cosh(\tau/\ell)^2 \end{pmatrix} \\
R =& \frac{2}{\ell^2}
\end{aligned}$$

In conformal coordinates with metric $g = \frac{\ell^2}{\cos(T)^2}\left(-\mathrm{d}T^2 + \mathrm{d}\theta^2\right)$ from eq. (2.4) the only non-vanishing Christoffel symbols are

$$\Gamma^T{}_{TT} = \Gamma^T{}_{\theta\theta} = \Gamma^\theta{}_{T\theta} = \Gamma^\theta{}_{\theta T} = \tan(T)$$

The Ricci tensor and Ricci scalar are

$$\begin{aligned} R_{\mu\nu} =& \begin{pmatrix} -\sec(T)^2 & 0 \\ 0 & \sec(T) \end{pmatrix} \\ R =& \frac{2}{\ell^2} \end{aligned}$$

In static coordinates with metric $g = \frac{\ell^2}{\cos(T)^2}\left(-\mathrm{d}T^2 + \mathrm{d}\theta^2\right)$ from eq. (2.6) the only non-vanishing Christoffel symbols are

$$\begin{aligned} \Gamma^t{}_{tr} =& \Gamma^t{}_{rt} = \frac{r}{-\ell^2 + r^2} \\ \Gamma^r{}_{tt} =& \frac{-\ell^2 + r^2}{\ell^4} r \\ \Gamma^r{}_{rr} =& \frac{r}{\ell^2 - r^2} \end{aligned}$$

The Ricci tensor and Ricci scalar are

$$\begin{aligned} R_{\mu\nu} =& \begin{pmatrix} -\frac{\ell^2+r^2}{\ell^4} & 0 \\ 0 & \frac{1}{\ell^2-r^2} \end{pmatrix} \\ R =& \frac{2}{\ell^2} \end{aligned}$$

In FLRW coordinates with metric $g = -\mathrm{d}t^2 + e^{2t/\ell}\left(\mathrm{d}x^2 + \mathrm{d}y^2 + \mathrm{d}z^2\right)$ from eq. (2.8) the only non-vanishing Christoffel symbols are

$$\begin{aligned} \Gamma^t{}_{ii} =& \frac{1}{\ell} e^{2t/\ell} && i \in \{x, y, z\} \\ \Gamma^i{}_{it} =& \Gamma^i{}_{ti} \frac{1}{\ell} \end{aligned}$$

The Ricci tensor and Ricci scalar are

$$\begin{aligned} R_{tt} =& -\frac{3}{\ell^2} \\ R_{ii} =& \frac{3}{\ell^2} e^{2t/\ell} && i \in \{x, y, z\} \\ R =& \frac{12}{\ell^2} \end{aligned}$$

Note that the difference in the scalar curvature only depends on the dimension.
For a d-dimensional de Sitter spacetime the scalar curvature is

$$R = \frac{d(d-1)}{\ell^2}$$

A.5. Killing fields

This appendix covers all supplementary calculations for deriving the Killing fields in de Sitter spacetime.

A.5.1. Equivalence of Killing equation with covariant derivatives and in coordinate form

We want to show that the Killing equation can be expressed in its coordinate form as follows:

$$\xi_{\alpha;\beta} + \xi_{\beta;\alpha} = 0 \tag{2.9}$$

$$\Leftrightarrow \qquad g_{\alpha\beta,\mu}\xi^{\mu} + g_{\delta\beta}\xi^{\delta}{}_{,\alpha} + g_{\alpha\delta}\xi^{\delta}{}_{,\beta} = 0. \tag{2.10}$$

First, we write out the covariant derivatives and use that the covariant derivative of the metric vanishes:

$$\xi_{\alpha;\beta} = \nabla_\beta \xi_\alpha = \nabla_\beta(g_{\alpha\gamma}\xi^\gamma) = g_{\alpha\gamma}\nabla_\beta\xi^\gamma = g_{\alpha\gamma}\Big(\partial_\beta\xi^\gamma + \Gamma^\gamma{}_{\beta\delta}\xi^\delta\Big)$$

it then follows, that

$$\begin{aligned}
0 =& \xi_{\alpha;\beta} + \xi_{\beta;\alpha} = g_{\alpha\gamma}\Big(\partial_\beta\xi^\gamma + \Gamma^\gamma{}_{\beta\delta}\xi^\delta\Big) + g_{\beta\gamma}\Big(\partial_\alpha\xi^\gamma + \Gamma^\gamma{}_{\alpha\delta}\xi^\delta\Big) \\
=& g_{\alpha\gamma}\partial_\beta\xi^\gamma + g_{\beta\gamma}\partial_\alpha\xi^\gamma + g_{\alpha\gamma}\Gamma^\gamma{}_{\beta\delta}\xi^\delta + g_{\beta\gamma}\Gamma^\gamma{}_{\alpha\delta}\xi^\delta \\
=& g_{\alpha\gamma}\partial_\beta\xi^\gamma + g_{\beta\gamma}\partial_\alpha\xi^\gamma + \partial_\delta g_{\alpha\beta}\xi^\delta \\
=& g_{\alpha\gamma}\xi^\gamma{}_{,\beta} + g_{\beta\gamma}\xi^\gamma{}_{,\alpha} + g_{\alpha\beta}{}_{\delta}\xi^\delta
\end{aligned}$$

Where we used that

$$\begin{aligned}
& g_{\alpha\gamma}\Gamma^\gamma{}_{\beta\delta}\xi^\delta + g_{\beta\gamma}\Gamma^\gamma{}_{\alpha\delta}\xi^\delta \\
&= \frac{1}{2}g_{\alpha\gamma}g^{\gamma\lambda}(\partial_\beta g_{\lambda\delta} + \partial_\delta g_{\beta\lambda} - \partial_\lambda g_{\beta\delta}) + \frac{1}{2}g_{\beta\gamma}g^{\gamma\lambda}(\partial_\alpha g_{\lambda\delta} + \partial_\delta g_{\alpha\lambda} - \partial_\lambda g_{\alpha\delta})\xi^\delta \\
&= \frac{1}{2}\Big[\delta^\lambda_\alpha(\partial_\beta g_{\lambda\delta} + \partial_\delta g_{\beta\lambda} - \partial_\lambda g_{\beta\delta}) + \delta^\lambda_\beta(\partial_\alpha g_{\lambda\delta} + \partial_\delta g_{\alpha\lambda} - \partial_\lambda g_{\alpha\delta})\Big]\xi^\delta \\
&= \frac{1}{2}[\partial_\beta g_{\alpha\delta} + \partial_\delta g_{\beta\alpha} - \partial_\alpha g_{\beta\delta} + \partial_\alpha g_{\beta\delta} + \partial_\delta g_{\alpha\beta} - \partial_\beta g_{\alpha\delta}]\xi^\delta \\
&= (\partial_\delta g_{\alpha\beta})\xi^\delta
\end{aligned}$$

A.5.2. de Sitter Killing fields in conformal coordinates

We have shown above that the Killing eq. (2.9) and (2.10) are equivalent. We plug the metric into the Killing eq. (2.10) for the different possible choices of indices:

$$\begin{aligned}
2.11 \qquad & -\partial_T\left(\frac{\ell^2}{\cos^2 T}\right)\xi^T - \frac{\ell^2}{\cos^2 T}\partial_T\xi^T - \frac{\ell^2}{\cos^2 T}\partial_T\xi^T = 0 \\
\Leftrightarrow \quad & -2\frac{\ell^2\tan T}{\cos^2 T}\xi^T - 2\frac{\ell^2}{\cos^2 T}\partial_T\xi^T = 0 \\
\Leftrightarrow \quad & \tan T\xi^T + \partial_T\xi^T = 0 \\
2.12 \qquad & \frac{\ell^2}{\cos^2 T}\partial_T\xi^\theta - \frac{\ell^2}{\cos^2 T}\partial_\theta\xi^T = 0 \\
\Leftrightarrow \quad & \partial_T\xi^\theta - \partial_\theta\xi^T = 0 \\
2.13 \qquad & \partial_T\left(\frac{\ell^2}{\cos^2 T}\right)\xi^T + 2\frac{\ell^2}{\cos^2 T}\partial_\theta\xi^\theta = 0 \\
\Leftrightarrow \quad & 2\frac{\ell^2\tan T}{\cos^2 T}\xi^T + 2\frac{\ell^2}{\cos^2 T}\partial_\theta\xi^\theta = 0 \\
\Leftrightarrow \quad & \tan T\xi^T + \partial_\theta\xi^\theta = 0
\end{aligned}$$

First we want to solve 2.11:

$$\tan T\xi^T + \partial_T\xi^T = 0 \quad \Rightarrow \quad \xi^T = c_1(\theta)\cos T$$

We can use this to plug ξ^T into 2.12:

$$\begin{aligned}
\partial_T\xi^\theta - \partial_\theta\xi^T = 0 \quad & \Rightarrow \quad \partial_T\xi^\theta - \partial_\theta(c_1(\theta)\cos T) = \partial_T\xi^\theta - c_1'(\theta)\cos T = 0 \\
& \Rightarrow \quad \xi^\theta = c_1'(\theta)\sin T + c_2(\theta)
\end{aligned}$$

Now look at 2.13 and plug in the results from above:

$$\begin{aligned} \tan T\xi^T + \partial_\theta \xi^\theta = 0 \quad &\Rightarrow \quad \tan T c_1(\theta)\cos T + \partial_\theta\big(c_1'(\theta)\sin T + c_2(\theta)\big) = 0 \\ &\Leftrightarrow \quad \sin T c_1(\theta) + c_1''(\theta)\sin T + c_2'(\theta) = 0 \\ &\Leftrightarrow \quad \sin T\big(c_1(\theta) + c_1''(\theta)\big) + c_2'(\theta) = 0 \end{aligned} \tag{A.1}$$

To solve eq. (A.1) we need to find time independent solutions for $c_1(\theta)$ and $c_2(\theta)$. When we require this equation to be solvable for all times T, this simplifies to

$$\begin{aligned} c_1(\theta) + c_1''(\theta) &= 0 \\ c_2'(\theta) &= 0 \qquad \Rightarrow \qquad c_2(\theta) = \text{const} \end{aligned} \tag{A.2}$$

We look at possible solutions to eq. (A.2):

$$\begin{aligned} c_1(\theta) &= a\cos\theta + b\sin\theta \\ c_2(\theta) &= c \end{aligned}$$

For the Killing fields, it follows that

$$\begin{aligned} \xi^T(T,\theta) &= (a\cos\theta + b\sin\theta)\cos T \\ \xi^\theta(T,\theta) &= (-a\sin\theta + b\cos\theta)\sin T + c \end{aligned}$$

With the parameters a, b, and c, this is a linear combination of the three independent Killing fields for de Sitter spacetime in conformal coordinates.

A.5.3. de Sitter Killing fields in static coordinates

The Killing equation in coordinate form reads

$$g_{\alpha\beta,\mu}\xi^\mu + g_{\delta\beta}\xi^\delta{}_{,\alpha} + g_{\alpha\delta}\xi^\delta{}_{,\beta} = 0.$$

We use that the de Sitter metric in static coordinates is diagonal with $g_{tt} = -1 + \frac{r^2}{\ell^2}$ and $g_{rr} = \frac{\ell^2}{\ell^2 - r^2}$.

$$\begin{aligned} \alpha{=}\beta{=}t \quad & g_{tt,t}\xi^t + g_{tt,r}\xi^r + g_{tt}\xi^t{}_{,t} + g_{tt}\xi^t{}_{,t} = g_{tt,r}\xi^r + 2g_{tt}\xi^t{}_{,t} = 0 \\ \alpha{=}\beta{=}r \quad & g_{rr,t}\xi^t + g_{rr,r}\xi^r + g_{rr}\xi^r{}_{,r} + g_{rr}\xi^r{}_{,r} = g_{rr,r}\xi^r + 2g_{rr}\xi^r{}_{,r} = 0 \\ \alpha{=}t,\beta{=}r \quad & g_{tr,\mu}\xi^\mu + g_{rr}\xi^r{}_{,t} + g_{tt}\xi^t{}_{,r} = g_{rr}\xi^r{}_{,t} + g_{tt}\xi^t{}_{,r} = 0 \end{aligned}$$

when we plug in the metric, we get the following three equations:

$$\begin{aligned} \frac{2r}{\ell^2}\xi^r + 2\left(-1 + \frac{r^2}{\ell^2}\right)\xi^t{}_{,t} = 0 \quad &\Leftrightarrow \quad r\xi^r + (r^2 - \ell^2)\xi^t{}_{,t} = 0 \\ \frac{2\ell^2 r}{(\ell^2 - r^2)^2}\xi^r + 2\frac{\ell^2}{\ell^2 - r^2}\xi^r{}_{,r} = 0 \quad &\Leftrightarrow \quad r\xi^r + (\ell^2 - r^2)\xi^r{}_{,r} = 0 \\ \frac{\ell^2}{\ell^2 - r^2}\xi^r{}_{,t} + \left(-1 + \frac{r^2}{\ell^2}\right)\xi^t{}_{,r} = 0 \quad &\Leftrightarrow \quad \frac{\ell^2}{\ell^2 - r^2}\xi^r{}_{,t} - \frac{\ell^2 - r^2}{\ell^2}\xi^t{}_{,r} = 0 \end{aligned} \tag{A.3}$$

We can solve (A.3) since it is only dependent on ξ^r and r with

$$\xi^r(t,r) = \sqrt{r^2 - \ell^2}f(t)$$

For the remaining two equations, it follows that

$$\begin{aligned} r\sqrt{r^2-\ell^2}f(t) + (r^2-\ell^2)\xi^t{}_{,t} = 0 \quad &\Leftrightarrow \quad rf(t) + \sqrt{r^2-\ell^2}\xi^t{}_{,t} = 0 \\ \frac{\ell^2}{\sqrt{r^2-\ell^2}}f'(t) + \frac{\ell^2-r^2}{\ell^2}\xi^t{}_{,r} = 0 \quad &\Leftrightarrow \quad \frac{\ell^2}{\sqrt{r^2-\ell^2}}f'(t) + \frac{\ell^2-r^2}{\ell^2}\xi^t{}_{,r} = 0 \end{aligned}$$

We obtain the following general solution of a Killing field:

$$\begin{aligned} \xi^t(t,r) =& c - \frac{\ell^2 r}{\sqrt{r^2-\ell^2}}f_{ab}(t) \\ \xi^r(t,r) =& \sqrt{r^2-\ell^2}f_{ab}(t) \\ \text{with} \quad f_{ab}(t) =& ae^{t/\ell} + be^{-t/\ell} \end{aligned}$$

A.6. Properties of different trajectories

In this section, we further characterize the different properties of the trajectories discussed in section 2.4.

A.6.1. Null geodesics: relation between embedding coordinates and parameters

Here we derive an explicit expression for the parameters s, u, and v defining a null geodesic in terms of the embedding coordinates of the null geodesic (we consider both *anticlockwise* pointing null geodesics $x_{\mathrm{ac}}(s)$ and *clockwise* pointing null geodesics $x_{\mathrm{c}}(s)$):

$$x_{\mathrm{ac}}(s) = \begin{pmatrix} s \\ u+vs \\ v-us \end{pmatrix} \quad \Rightarrow \quad \begin{aligned} x_{\mathrm{ac},0} &= s \\ x_{\mathrm{ac},1} &= u+vs \\ x_{\mathrm{ac},2} &= v-us \end{aligned}$$

Hence we find

$$u = \frac{x_{\mathrm{ac},1} - x_{\mathrm{ac},0}x_{\mathrm{ac},2}}{1+x_{\mathrm{ac},0}^2}, \quad \text{and} \quad v = \frac{x_{\mathrm{ac},2} + x_{\mathrm{ac},0}x_{\mathrm{ac},1}}{1+x_{\mathrm{ac},0}^2}.$$

Similarly, for clockwise pointing null geodesics

$$x_{\mathrm{c}}(s) = \begin{pmatrix} s \\ u-vs \\ v+us \end{pmatrix} \quad \Rightarrow \quad \begin{aligned} x_{\mathrm{c},0} &= s \\ x_{\mathrm{c},1} &= u-vs \\ x_{\mathrm{c},2} &= v+us \end{aligned}$$

we have

$$u = \frac{x_{\mathrm{c},1} + x_{\mathrm{c},0}x_{\mathrm{c},2}}{1+x_{\mathrm{c},0}^2}, \quad \text{and} \quad v = \frac{x_{\mathrm{c},2} - x_{\mathrm{c},0}x_{\mathrm{c},1}}{1+x_{\mathrm{c},0}^2}.$$

A.6.2. Zero momentum geodesics

Here, show that the following family of trajectories with fixed angles are geodesics:

$$\begin{pmatrix} \tau(s) \\ \theta(s) \end{pmatrix} = \begin{pmatrix} \tau(s) \\ \theta_j \end{pmatrix}$$

In order to show this, we need to show that this is a valid solution to the geodesic equation.
To calculate the geodesic equation in global coordinates, we need the non-vanishing Christoffel symbols in global coordinates:

$$\Gamma^{\tau}{}_{\theta\theta} = \ell\cosh(\tau/\ell)\sinh(\tau/\ell)$$

$$\Gamma^{\theta}{}_{\tau\theta} = \Gamma^{\theta}{}_{\theta\tau} = \frac{1}{\ell}\tanh(\tau/\ell)$$

We can write down the geodesic equation for the temporal variable τ

$$\frac{d^2\tau(s)}{ds^2} + \Gamma^{\tau}{}_{\theta\theta}\frac{d\theta(s)}{ds}\frac{d\theta(s)}{ds} = 0 \quad \Rightarrow \quad \tau''(s) + \ell\cosh(\tau/\ell)\sinh(\tau/\ell)\big(\theta'(s)\big)^2 = 0 \tag{A.4}$$

and the spatial variable θ

$$\frac{d^2\theta(s)}{ds^2} + 2\Gamma^{\theta}{}_{\tau\theta}\frac{d\theta(s)}{ds}\frac{d\tau(s)}{ds} = 0 \quad \Rightarrow \quad \frac{d^2\theta(s)}{ds^2} + \frac{2}{\ell}\tanh(\tau/\ell)\frac{d\theta(s)}{ds}\frac{d\tau(s)}{ds} = 0 \tag{A.5}$$

It can directly be shown that (2.15) is a geodesic by plugging it into the geodesic equations:

$$(A.4) = \tau''(s) + \ell\cosh(\tau/\ell)\sinh(\tau/\ell)(0)^2 = \tau''(s) = 0$$

$$(A.5) = 0 + \frac{2}{\ell}\tanh(\tau/\ell)\cdot 0\cdot\tau'(s) = 0$$

This is a valid geodesic for any linear function for τ:

$$\tau(s) = \lambda_1 s + \lambda_2$$

As expected, the proper acceleration along these geodesics vanishes. To see this we need the non-vanishing Christoffel symbols in global coordinates which are $\Gamma^{\tau}{}_{\theta\theta} = \ell\cosh(\tau/\ell)\sinh(\tau/\ell)$ and $\Gamma^{\theta}{}_{\tau\theta} = \Gamma^{\theta}{}_{\theta\tau} = \tanh(\tau/\ell)/\ell$.

$$\begin{aligned}
u^{\mu} =& \frac{\partial x^{\mu}}{\partial\tau} = \begin{pmatrix}\lambda_1\\ 0\end{pmatrix}\\
a^{\mu} =& \frac{\partial u^{\mu}}{\partial\tau} + \Gamma^{\mu}{}_{\lambda\nu}u^{\lambda}u^{\nu} = \Gamma^{\mu}{}_{\lambda\nu}u^{\lambda}u^{\nu}\\
a^{\tau} =& \Gamma^{\tau}{}_{\theta\theta}u^{\theta}u^{\theta} = 0\\
a^{\theta} =& 2\Gamma^{\theta}{}_{\tau\theta}u^{\tau}u^{\theta} = 0\\
|a|^2 =& a_{\mu}a^{\mu} = g_{\mu\nu}a^{\mu}a^{\nu} = 0
\end{aligned}$$

A.6.3. Proper acceleration of Killing trajectories

To calculate the geodesic equation in static coordinates (2.5) we need the non-vanishing Christoffel symbols:

$$\begin{aligned}
\Gamma^{t}{}_{rt} =& \Gamma^{t}{}_{tr} = \frac{r}{r^2-\ell^2}\\
\Gamma^{r}{}_{tt} =& \frac{r}{\ell^4}(r^2-\ell^2)\\
\Gamma^{r}{}_{rr} =& -\frac{r}{r^2-\ell^2}
\end{aligned}$$

We can write down the geodesic equation for the temporal coordinate t

$$\begin{aligned}
&\frac{d^2t(s)}{ds^2} + 2\Gamma^{t}{}_{tr}\frac{dt(s)}{ds}\frac{dr(s)}{ds} = 0\\
\Rightarrow\quad & t''(s) + 2\frac{r}{r^2-\ell^2}t'(s)r'(s) = 0
\end{aligned} \tag{A.6}$$

and the spatial coordinate r

$$\frac{d^2r(s)}{ds^2} + \Gamma^{r}{}_{tt}\frac{dt(s)}{ds}\frac{dt(s)}{ds} + \Gamma^{r}{}_{rr}\frac{dr(s)}{ds}\frac{dr(s)}{ds} = 0$$

$$\Rightarrow \quad r''(s) + \frac{r}{\ell^4}(r^2-\ell^2)to(s)^2 - \frac{r}{r^2-\ell^2}r'(s)^2 = 0 \tag{A.7}$$

When we plug in the trajectory (2.16) with a constant radial coordinate into the geodesic equation, we get the following differential equation:

$$\begin{aligned}(A.6) =& t''(s) + 2\frac{r_i}{r_i^2-\ell^2}t'(s)\cdot 0 = t''(s) = 0\\ (A.7) =& 0 + \frac{r_i}{\ell^4}(r_i^2-\ell^2)\big(t'(s)\big)^2 - \frac{r_i}{r_i^2-\ell^2}(0)^2 = \frac{r_i}{\ell^4}(r_i^2-\ell^2)\big(t'(s)\big)^2 = 0\end{aligned}$$

The only trajectory which yields a valid geodesic is the trajectory for $r_i = 0$.

This family of trajectories is not (in general) a geodesic, as the proper acceleration of a particle following this trajectory does not vanish for all trajectories. We consider the following trajectory, where we interpret the time component to be the coordinate time, which we denote as s:

$$x_r(s) = \begin{pmatrix} t(s) \\ r(s) \end{pmatrix} = \begin{pmatrix} s \\ r_i \end{pmatrix}$$

First, we calculate the proper time of the trajectory where the tangent vector to this trajectory is $T^\mu = \begin{pmatrix} 1 \\ 0 \end{pmatrix}$:

$$\tau = \int \sqrt{-g_{ab}T^aT^b}\mathrm{d}s = \int \sqrt{-g_{tt}}\mathrm{d}s = \int \sqrt{1-\frac{r_i^2}{\ell^2}}\mathrm{d}s = \sqrt{1-\frac{r_i^2}{\ell^2}}s \tag{A.8}$$

The trajectory with constant $r = r_i$ expressed with its proper time τ is

$$x_r(\tau) = \begin{pmatrix} \tau/\sqrt{1-r_i^2/\ell^2} \\ r_i \end{pmatrix}$$

We can now directly calculate the proper velocity and acceleration:

$$\begin{aligned}u^\mu =& \partial_\tau x^\mu = \begin{pmatrix} 1/\sqrt{1-r_i^2/\ell^2} \\ 0 \end{pmatrix}\\ a^\mu =& \partial_\tau u^\mu + \Gamma^\mu{}_{\lambda\nu}u^\lambda u^\nu\\ a^t =& 2\Gamma^t{}_{tr}u^t u^r = 0\\ a^r =& \Gamma^r{}_{tt}u^t u^t + \Gamma^r{}_{rr}u^r u^r = \frac{r_i}{\ell^4}(r_i^2-\ell^2)\frac{1}{1-r_i^2/\ell^2} = -\frac{r_i}{\ell^2}\end{aligned}$$

For the absolute value of the proper acceleration, it follows that

$$|a|^2(r) = a_\mu a^\mu = g_{\mu\nu}a^\mu a^\nu = g_{rr}a^r a^r = \frac{\ell^2}{\ell^2-r^2}\frac{r^2}{\ell^4} \tag{A.9}$$

We can look at the proper acceleration of the same set of trajectories from the embedding space (where all Christoffel symbols vanish identically):

$$x_i^\mu(\tau) = \begin{pmatrix} \sqrt{\ell^2-r_i^2}\sinh(\tau/\sqrt{\ell^2-r_i^2}) \\ \sqrt{\ell^2-r_i^2}\cosh(\tau/\sqrt{\ell^2-r_i^2}) \\ r_i \end{pmatrix}$$

$$
\begin{aligned}
u_i^\mu(\tau) =& \begin{pmatrix} \cosh(\tau/\sqrt{\ell^2 - r_i^2}) \\ \sinh(\tau/\sqrt{\ell^2 - r_i^2}) \\ 0 \end{pmatrix} \\
a_i^\mu(\tau) =& \frac{1}{\sqrt{\ell^2 - r_i^2}} \begin{pmatrix} \sinh(\tau/\sqrt{\ell^2 - r_i^2}) \\ \cosh(\tau/\sqrt{\ell^2 - r_i^2}) \\ 0 \end{pmatrix} \\
a_\mu a^\mu =& \eta_{\mu\nu} a_i^\mu a_i^\nu = \frac{1}{\ell^2 - r_i^2}
\end{aligned}
\tag{A.10}
$$

Appendix B

Quantization of scalar fields

B.1. Principle of least action

Here, we derive eq. (3.2) using the principle of least action.

We have the action $S = \int \mathrm{d}^n \mathcal{L}$ with the generalized Lagrangian

$$\mathcal{L} = \frac{1}{2}\sqrt{-g}\big(g^{\mu\nu}\partial_\mu\phi\partial_\nu\phi + m^2\phi^2 + \xi R\phi^2\big)$$

From the variational principle, it follows (as can be found in any standard literature)

$$0 = \delta S = \int \mathrm{d}^n \delta\mathcal{L} = \int \mathrm{d}^n \left[\frac{\partial\mathcal{L}}{\partial\phi(x)} - \partial_\mu \frac{\partial\mathcal{L}}{\partial(\partial_\mu)}\right]\delta\phi(x)$$

We can plug in our Lagrangian and obtain the following equation of motion:

$$\begin{aligned} 0 =& \frac{\partial\mathcal{L}}{\partial\phi(x)} - \partial_\mu \frac{\partial\mathcal{L}}{\partial(\partial_\mu)} \\ =& \sqrt{-g}\big(m^2\phi + \xi R\phi\big) - \partial_\mu\big[\sqrt{-g}g^{\mu\nu}\partial_\nu\phi\big] \\ =& -\sqrt{-g}\left[\frac{1}{\sqrt{-g}}\partial_\mu\big(\sqrt{-g}\partial^\mu\big) - m^2 - \xi R\right]\phi(x) \end{aligned}$$

with the identity for the d'Alembert operator shown in appendix B.2

$$\Box = \nabla_\mu\nabla^\mu = \frac{1}{\sqrt{-g}}\partial_\mu\big(\sqrt{-g}\partial^\mu\big)$$

it directly follows

$$\big[\nabla_\mu\nabla^\mu - (m^2 + \xi R)\big]\phi(x) = 0$$

B.2. d'Alembert operator in curved spacetime

We want to show that the two expressions for the d'Alembert operator in eq. (3.3) are equivalent:

$$\begin{aligned} \Box =& g^{\mu\nu}\nabla_\mu\nabla_\nu = g^{\mu\nu}\nabla_\mu\partial_\nu = g^{\mu\nu}\partial_\mu\partial_\nu - g^{\mu\nu}\Gamma^\lambda{}_{\mu\nu}\partial_\lambda \\ =& g^{\mu\nu}\partial_\mu\partial_\nu - g^{\mu\nu}\frac{1}{2}g^{\lambda\kappa}(\partial_\mu g_{\kappa\nu} + \partial_\nu g_{\mu\kappa} - \partial_\kappa g_{\mu\nu})\partial_\lambda \\ =& g^{\mu\nu}\partial_\mu\partial_\nu - \frac{g^{\mu\nu}g^{\lambda\kappa}}{2}(g_{\kappa\nu,\mu}\partial_\lambda + g_{\mu\kappa,\nu}\partial_\lambda - g_{\mu\nu,\kappa}\partial_\lambda) \end{aligned}$$

$$
\begin{aligned}
&= g^{\mu\nu}\partial_\mu\partial_\nu + \frac{1}{2}g^{\mu\nu}g^{\lambda\kappa}(-2g_{\mu\kappa,\nu}\partial_\lambda + g_{\mu\nu,\kappa}\partial_\lambda) \\
&= g^{\mu\nu}\partial_\mu\partial_\nu - g^{\mu\nu}g^{\lambda\kappa}g_{\mu\kappa,\nu}\partial_\lambda + \frac{1}{2}g^{\mu\nu}g^{\lambda\kappa}g_{\mu\nu,\kappa}\partial_\lambda \\
&= g^{\mu\nu}\partial_\mu\partial_\nu + (\partial_\nu g^{\nu\lambda})\partial_\lambda + \frac{1}{2}g^{\lambda\kappa}g^{\mu\nu}(\partial_\kappa g_{\mu\nu})\partial_\lambda
\end{aligned}
$$

with $\partial_\alpha g_{\beta\gamma} = g_{\beta\gamma,\alpha}$.

In order to simplify the second expression we use $g = \det g_{\mu\nu}$ and $\partial_\mu g = g g^{ab}\partial_\mu g_{ab}$:

$$
\begin{aligned}
\partial_\mu\sqrt{-g} &= -\frac{\partial_\mu g}{2\sqrt{-g}} = -\frac{g g^{\sigma\rho}\partial_\mu g_{\sigma\rho}}{2\sqrt{-g}} \\
&= \frac{-g}{2\sqrt{-g}} g^{\sigma\rho}\partial_\mu g_{\sigma\rho} = \frac{1}{2}\sqrt{-g} g^{\sigma\rho}\partial_\mu g_{\sigma\rho}
\end{aligned}
$$

we can plug this in and get

$$
\begin{aligned}
\Box &= \frac{1}{\sqrt{-g}}\partial_\mu\big(\sqrt{-g}g^{\mu\nu}\partial_\nu\big) \\
&= \frac{(\partial_\mu\sqrt{-g})g^{\mu\nu}}{\sqrt{-g}}\partial_\nu + \frac{\sqrt{-g}(\partial_\mu g^{\mu\nu})}{\sqrt{-g}}\partial_\nu + \frac{\sqrt{-g}g^{\mu\nu}}{\sqrt{-g}}\partial_\mu\partial_\nu \\
&= \frac{1}{2}(g^{\sigma\rho}\partial_\mu g_{\sigma\rho})g^{\mu\nu}\partial_\nu + (\partial_\mu g^{\mu\nu})\partial_\nu + g^{\mu\nu}\partial_\mu\partial_\nu
\end{aligned}
$$

This directly results in the equality to be shown.

B.3. Bogoliubov transformation from Rindler to Unruh modes

We start with the expansion of the scalar field in Rindler modes $\chi_k^{R,L}$. We plug in the inverted relations from eq. (3.12) to translate the expression to Unruh modes:

$$
\begin{aligned}
\hat\phi &= \int_{-\infty}^{\infty} dk\Big(\hat b_k^L\chi_k^L + (\hat b_k^L)^\dagger(\chi_k^L)^* + \hat b_k^R\chi_k^R + (\hat b_k^R)^\dagger(\chi_k^R)^*\Big) \\
&= \int_{-\infty}^{\infty} dk\frac{\coth(\pi\omega/a)-1}{2}\Big(\hat b_k^R e^{2\pi\omega/a}\tilde\phi_k^{(1)} + (\hat b_k^R)^\dagger e^{2\pi\omega/a}(\tilde\phi_k^{(1)})^* + \hat b_k^L e^{\pi\omega/a}\tilde\phi_k^{(2)} \\
&\qquad + (\hat b_k^L)^\dagger e^{\pi\omega/a}(\tilde\phi_k^{(2)})^* - (\hat b_k^L)^\dagger e^{\pi\omega/a}\tilde\phi_{-k}^{(1)} - \hat b_k^L e^{\pi\omega/a}(\tilde\phi_{-k}^{(1)})^* - (\hat b_k^R)^\dagger\tilde\phi_{-k}^{(2)} - \hat b_k^R(\tilde\phi_{-k}^{(2)})^*\Big) \\
&= \int_{-\infty}^{\infty} dk\frac{\coth(\pi\omega/1)-1}{2}\Big\{\Big(\hat b_k^R e^{2\pi\omega/a} - (\hat b_{-k}^L)^\dagger e^{\pi\omega/a}\Big)\tilde\phi_k^{(1)} + \Big(\hat b_k^L e^{\pi\omega/a} - (\hat b_{-k}^R)^\dagger\Big)\tilde\phi_k^{(2)} \\
&\qquad + \Big((\hat b_k^R)^\dagger e^{2\pi\omega/a} - \hat b_{-k}^L e^{\pi\omega/a}\Big)(\tilde\phi_k^{(1)})^* + \Big((\hat b_k^L)^\dagger e^{\pi\omega/a} - \hat b_{-k}^R\Big)(\tilde\phi_k^{(2)})^*\Big\}
\end{aligned}
$$

With the following relation, we can express the Unruh annihilation operators with Rindler creation and annihilation operators:

$$
\begin{aligned}
\hat d_k^{(1)} &= \frac{1}{2\sinh(\pi\omega/a)}\Big(\hat b_k^R e^{\pi\omega/a} - (\hat b_{-k}^L)^\dagger\Big) \\
\hat d_k^{(2)} &= \frac{1}{2\sinh(\pi\omega/a)}\Big(\hat b_k^L - e^{-\pi\omega/a}(\hat b_{-k}^L)^\dagger\Big).
\end{aligned}
$$

The relation between Unruh and Rindler creation operators can be inverted as follows:

$$
\hat b_k^L = \frac{1}{\sqrt{2\sinh(\pi\omega/a)}}\Big(e^{\pi\omega/(2a)}\hat d_k^{(2)} + e^{-\pi\omega/2a}(\hat d_k^{(1)})^\dagger\Big)
$$

$$\hat{b}_k^R = \frac{1}{\sqrt{2\sinh(\pi\omega/a)}}\left(e^{\pi\omega/(2a)}\hat{d}_k^{(1)} + e^{-\pi\omega/2a}(\hat{d}_k^{(2)})^\dagger\right).$$

We can express this in matrix form as follows:

$$\begin{aligned}\begin{pmatrix}\hat{b}_k^R\\(\hat{b}_k^L)^\dagger\end{pmatrix} &= \frac{1}{\sqrt{2\sinh(\pi\omega/a)}}\begin{pmatrix}e^{\pi\omega/(2a)} & e^{-\pi\omega/(2a)}\\ e^{-\pi\omega/(2a)} & e^{\pi\omega/(2a)}\end{pmatrix}\begin{pmatrix}\hat{d}_k^{(1)}\\(\hat{d}_k^{(2)})^\dagger\end{pmatrix}\\ &= \begin{pmatrix}\cosh r & \sinh r\\ \sinh r & \cosh r\end{pmatrix}\begin{pmatrix}\hat{d}_k^{(1)}\\(\hat{d}_k^{(2)})^\dagger\end{pmatrix}\end{aligned}$$

where the auxiliary variable r and the frequency ω are related as

$$\begin{aligned}\cosh r &= \frac{e^{\pi\omega/(2a)}}{\sqrt{2\sinh(\pi\omega/a)}} = \frac{e^{\pi\omega/(2a)}}{\sqrt{e^{\pi\omega/a}-e^{-\pi\omega/a}}} = \sqrt{\frac{e^{\pi\omega/a}}{e^{\pi\omega/a}-e^{-\pi\omega/a}}}\\ \sinh r &= \frac{e^{-\pi\omega/(2a)}}{\sqrt{2\sinh(\pi\omega/a)}} = \frac{e^{-\pi\omega/(2a)}}{\sqrt{e^{\pi\omega/a}-e^{-\pi\omega/a}}} = \sqrt{\frac{e^{-\pi\omega/a}}{e^{\pi\omega/a}-e^{-\pi\omega/a}}}\end{aligned}$$

This satisfies the relation $\cosh^2 r - \sinh^2 r = 1$. The inverse Bogoliubov transformation is

$$\begin{pmatrix}\hat{d}_k^{(1)}\\(\hat{d}_k^{(2)})^\dagger\end{pmatrix} = \begin{pmatrix}\cosh r & -\sinh r\\ -\sinh r & \cosh r\end{pmatrix}\begin{pmatrix}\hat{b}_k^R\\(\hat{b}_k^L)^\dagger\end{pmatrix}$$

B.4. Minkowski vacuum state as thermal state perceived by Rindler observer

This derivation follows [CHM08]. We know that the particle number measured in the left and right Rindler wedge is identical such that we can write (see eq. (3.13)):

$$\left((\hat{b}_k^L)^\dagger\hat{b}_k^L - (\hat{b}_k^R)^\dagger\hat{b}_k^R\right)|\Omega_M\rangle = 0$$

Since this is the case for *all* frequencies k, we know that the Minkowski vacuum state is proportional to the following expression:

$$|\Omega_M\rangle \propto \prod_k \sum_{n_k}^{\infty} \frac{K_{n_k}}{n!}\left((\hat{b}_k^R)^\dagger(\hat{b}_k^L)^\dagger\right)^{n_k}|\Omega_R\rangle$$

We can derive the relation K_{n_k} has to satisfy knowing that the Unruh modes annihilate the Minkowski vacuum state:

$$\begin{aligned}\hat{d}_k^{(1)}|\Omega_M\rangle &= \frac{1}{2\sinh(\pi\omega/a)}\left(\hat{b}_k^R e^{\pi\omega/a} - (\hat{b}_{-k}^L)^\dagger\right)|\Omega_M\rangle = 0\\ \hat{d}_k^{(2)}|\Omega_M\rangle &= \frac{1}{2\sinh(\pi\omega/a)}\left(\hat{b}_k^L - e^{-\pi\omega/a}(\hat{b}_{-k}^L)^\dagger\right)|\Omega_M\rangle = 0\end{aligned}$$

From this, we directly get the recursion formula

$$K_{n_i+1} - e^{-\pi\omega_i/a}K_{n_i} = 0$$

from which we can derive

$$K_{n_i} = e^{-\pi\omega_i n_i/a}K_0$$

and with that, the expression of the Minkowski vacuum in Rindler modes:

$$|\Omega_M\rangle = \prod_k \left(C_i \sum_{n_k=0}^{\infty} \frac{e^{-\pi n_k \omega_k/a}}{n_k!} \left((\hat{b}_k^R)^\dagger (\hat{b}_k^L)^\dagger \right)^{n_k} \right) |\Omega_R\rangle$$

with the normalization constant $C_i = \sqrt{1 - e^{-2\pi\omega_k/a}}$. This can also be expressed as follows:

$$\begin{aligned}
|\Omega_M\rangle =& \prod_k \left(\sqrt{1 - e^{-2\pi\omega_k/a}} \sum_{n_k=0}^{\infty} \frac{e^{-\pi n_k \omega_k/a}}{n_k!} \left((\hat{b}_k^R)^\dagger (\hat{b}_k^L)^\dagger \right)^{n_k} \right) |\Omega_R\rangle \\
=& \prod_k \left(\sqrt{1 - e^{-2\pi\omega_k/a}} \sum_{n_k=0}^{\infty} e^{-\pi n_k \omega_k/a} \, |n_k, R\rangle \otimes |n_k, L\rangle \right) \\
=& \prod_k \frac{1}{\cosh r} \sum_{m=0}^{\infty} \tanh^m r \, |\Omega_R^L\rangle \, |\Omega_R^R\rangle
\end{aligned}$$

B.5. Field equation in spatially flat FLRW coordinates

This appendix section is a collection of proofs to give a detailed description and derivation of the intermediate steps in section 3.3.

Proof 1: d'Alembert operator in spatially flat FLRW spacetime, eq. (3.16)

$$\begin{aligned}
\Box\phi =& g^{\mu\nu} \left(\partial_\mu \partial_\nu \phi - \Gamma^\lambda_{\mu\nu} \partial_\lambda \phi \right) \\
=& \partial^\mu \partial_\mu \phi - \sum_{i \in \{x,y,z\}} g^{ii} \Gamma^t_{ii} \partial_t \phi - 2 \sum_{i \in \{x,y,z\}} g^{it} \Gamma^i_{ti} \partial_t \phi \\
=& \partial^\mu \partial_\mu \phi - \sum_{i=1}^{3} (a^{-2}) a \dot{a} \partial_t \phi \\
=& \partial^\mu \partial_\mu \phi - 3 \frac{\dot{a}}{a} \partial_t \phi \\
=& \left(-\partial_t^2 + a^{-2} (\partial_x^2 + \partial_y^2 + \partial_z^2) \right) \phi - 3 \frac{\dot{a}}{a} \partial_t \phi \\
=& \left(-\partial_t^2 - 3 \frac{\dot{a}(t)}{a(t)} \partial_t + a(t)^{-2} (\partial_x^2 + \partial_y^2 + \partial_z^2) \right) \phi \\
=& - a^{-3} \partial_t \left(a^3 \partial_t \phi \right) + a^{-2} \sum_{i \in \{x,y,z\}} \partial_i^2 \phi
\end{aligned}$$

□

Proof 2: Transformation of metric to conformal time, eq. (3.19)

We want to introduce the conformal time

$$\eta(t) = \int^t \frac{\mathrm{d}t'}{a(t')}.$$

to transform the spatially flat FLRW metric:

$$\begin{aligned}
\mathrm{d}s^2 =& - \mathrm{d}t^2 + a(t)^2 \left(\mathrm{d}x^2 + \mathrm{d}y^2 + \mathrm{d}z^2 \right) \\
& \tfrac{\mathrm{d}\eta}{\mathrm{d}t} = \tfrac{\mathrm{d}}{\mathrm{d}t} \int^t \tfrac{\mathrm{d}t'}{a(t')} = \tfrac{1}{a(t)} \quad \Leftrightarrow \quad \mathrm{d}t = a(t) \mathrm{d}\eta
\end{aligned}$$

$$= -a(t)^2 \mathrm{d}\eta^2 + a(t)^2\big(\mathrm{d}x^2 + \mathrm{d}y^2 + \mathrm{d}z^2\big) = a(\eta)^2\big(-\mathrm{d}\eta^2 + \mathrm{d}x^2 + \mathrm{d}y^2 + \mathrm{d}z^2\big)$$

□

Proof 3: Transformation of field equation using conformal time, eq. (3.20)

We now need to calculate the coordinate transformation from physical to conformal time (3.18) of the above field eq. (3.17). To do this, we first evaluate the temporal derivatives of the scalar field and the scale factor. We use the shortened notation that $\partial_\eta a = a'$:

$$\begin{aligned}
\dot{\phi} =& \partial_t \phi = \frac{\partial \eta}{\partial t}\partial_\eta \phi = \frac{1}{a}\partial_\eta \phi \\
\ddot{\phi} =& \partial_t^2 \phi = \left(\frac{\partial \eta}{\partial t}\partial_\eta\right)\left(\frac{\partial \eta}{\partial t}\partial_\eta\right)\phi = \left(\frac{1}{a}\partial_\eta\right)\left(\frac{1}{a}\partial_\eta\right)\phi = \left(\frac{1}{a^2}\partial_\eta^2 - \frac{a'}{a^3}\partial_\eta\right)\phi \\
\dot{a} =& \partial_t a = \frac{1}{a}\partial_\eta a = \frac{a'}{a} \\
\ddot{a} =& \partial_t^2 a = \left(\frac{1}{a^2}\partial_\eta^2 - \frac{a'}{a^3}\partial_\eta\right)a = \frac{1}{a}\left(\frac{a''}{a} - \frac{(a')^2}{a^2}\right)
\end{aligned}$$

Plug everything in:

$$\begin{aligned}
-a^{-3}\partial_t\big(a^3\partial_t\phi(t,\vec{x})\big) + a^{-2}(\partial_x^2 + \partial_y^2 + \partial_z^2)\phi(t,\vec{x}) - \left(\frac{\dot{a}^2}{a^2} + \frac{\ddot{a}}{a}\right)\phi(t,\vec{x}) &= 0 \\
-\partial_t^2\phi(t,\vec{x}) - a^{-3}\big(3a^2\partial_t a\big)\partial_t\phi(t,\vec{x}) + a^{-2}(\partial_x^2 + \partial_y^2 + \partial_z^2)\phi(t,\vec{x}) - \left(\frac{\dot{a}^2}{a^2} + \frac{\ddot{a}}{a}\right)\phi(t,\vec{x}) &= 0 \\
\left[-\frac{1}{a^2}\partial_\eta^2 + \frac{a'}{a^3}\partial_\eta + a^{-2}(\partial_x^2 + \partial_y^2 + \partial_z^2) - 3\frac{a'}{a^2}\frac{1}{a}\partial_\eta - \frac{(a')^2}{a^4} - \frac{1}{a^2}\left(\frac{a''}{a} - \frac{(a')^2}{a^2}\right)\right]\phi &= 0 \\
\frac{1}{a^2}\left[-\partial_\eta^2 + \frac{a'}{a}\partial_\eta + (\partial_x^2 + \partial_y^2 + \partial_z^2) - 3\frac{a'}{a}\partial_\eta - \frac{(a')^2}{a^2} - \frac{a''}{a} + \frac{(a')^2}{a^2}\right]\phi &= 0 \\
\frac{1}{a^2}\left[-\partial_\eta^2 - 2\frac{a'}{a}\partial_\eta + (\partial_x^2 + \partial_y^2 + \partial_z^2) - \frac{a''}{a}\right]\phi &= 0
\end{aligned}$$

□

Proof 4: Conformal transformation of the field equation from eq. (3.21)

Due to the conformal transformation, we can introduce the following relation between the scalar field in FLRW spacetime ϕ and Minkowski spacetime χ:

$$\chi(x) = a(\eta)\phi(x)$$

This changes the equation of motion as follows (where both χ and a depend on η - we drop the arguments to have things less cluttered):

$$\begin{aligned}
\partial_\eta \phi &= \partial_\eta \frac{\chi}{a} = \frac{\chi'}{a} - \frac{\chi a'}{a^2} \\
\partial_\eta^2 \phi &= \partial_\eta\left(\frac{\chi'}{a} - \frac{\chi a'}{a^2}\right) = \frac{\chi''}{a} - 2\frac{\chi' a'}{a^2} + 2\frac{a'^2}{a^3}\chi - \frac{a''}{a^2}\chi
\end{aligned}$$

We start with the field equation from eq. (3.20)

$$\frac{1}{a^2}\left[-\partial_\eta^2 - 2\frac{a'}{a}\partial_\eta + (\partial_x^2 + \partial_y^2 + \partial_z^2) - \frac{a''}{a}\right]\phi = 0$$

$$\Leftrightarrow \quad \frac{1}{a^2}\left[-\left(\frac{\chi''}{a} - 2\frac{\chi' a'}{a^2} + 2\frac{a'^2}{a^3}\chi - \frac{a''}{a^2}\chi\right) - 2\frac{a'}{a}\left(\frac{\chi'}{a} - \frac{\chi a'}{a^2}\right) + (\partial_x^2 + \partial_y^2 + \partial_z^2)\frac{\chi}{a} - \frac{a''}{a}\frac{\chi}{a}\right] = 0$$

$$\Leftrightarrow \quad \frac{1}{a^2}\left[-\frac{\chi''}{a} + (\partial_x^2 + \partial_y^2 + \partial_z^2)\frac{\chi}{a}\right] = 0$$

$$\Leftrightarrow \quad \frac{1}{a^3}\big(-\partial_\eta^2 + \partial_x^2 + \partial_y^2 + \partial_z^2\big)\chi = 0$$

Accordingly, the axillary field χ is a solution to the field equation in Minkowski spacetime.

□

Proof 5: Equation of motion of massive scalar field (dS, FLRW coordinates), eq. (3.22)

We start with the field equation from eq. (3.2) and use the expanded d'Alembert operator derived earlier and the scale factor $a(t) = \exp(t/\ell)$ (where we used $\partial_t a = \dot{a} = a/\ell$, $\ddot{a} = a/\ell^2$):

$$\begin{aligned}
&\big(\Box - (m^2 + \xi R)\big)\phi(t,\vec{x}) = 0 \\
&- a^{-3}\partial_t\big(a^3\partial_t\phi(t,\vec{x})\big) + a^{-2}(\partial_x^2 + \partial_y^2 + \partial_z^2)\phi(t,\vec{x}) - \big(m^2 + \xi R\big)\phi(t,\vec{x}) = 0 \\
&- \partial_t^2\phi(t,\vec{x}) - \underbrace{a^{-3}\big(3a^2\dot{a}\big)\partial_t\phi(t,\vec{x})}_{(i)} + a^{-2}(\partial_x^2 + \partial_y^2 + \partial_z^2)\phi(t,\vec{x}) - \Big(\quad m^2 + \underbrace{\frac{\dot{a}^2}{a^2} + \frac{\ddot{a}}{a}}_{(ii)} \quad \Big)\phi(t,\vec{x}) = 0
\end{aligned}$$

$$(i) = a^{-3}\big(3a^2\dot{a}\big)\partial_t\phi(t,\vec{x}) = \exp(-3t/\ell)(3\exp(2t/\ell)\exp(t/\ell)/\ell)\partial_t\phi(t,\vec{x}) = \frac{3}{\ell}\partial_t\phi(t,\vec{x})$$

$$(ii) = \frac{\dot{a}^2}{a^2} + \frac{\ddot{a}}{a} = \frac{(\exp(t/\ell)/\ell)^2}{\exp(t/\ell)^2} + \frac{\exp(t/\ell)/\ell^2}{\exp(t/\ell)} = \frac{2}{\ell^2}$$

$$\Rightarrow \quad - \partial_t^2\phi(t,\vec{x}) - \frac{3}{\ell}\partial_t\phi(t,\vec{x}) + e^{-2t/\ell}(\partial_x^2 + \partial_y^2 + \partial_z^2)\phi(t,\vec{x}) - \left(m^2 + \frac{2}{\ell^2}\right)\phi(t,\vec{x}) = 0$$

where we have again chosen $\xi = \frac{1}{6}$ which results in $\xi R = \frac{2}{\ell^2}$.

□

Proof 6: Equation of motion for massive scalar field, derive Bessel eq. (3.24)

We start with the mode function from eq. (3.22)

$$-\partial_t^2\phi(t,\vec{x}) - \frac{3}{\ell}\partial_t\phi(t,\vec{x}) + e^{-2t/\ell}(\partial_x^2 + \partial_y^2 + \partial_z^2)\phi(t,\vec{x}) - \left(m^2 + \frac{2}{\ell^2}\right)\phi(t,\vec{x}) = 0$$

We make the following ansatz for the mode function with the scale factor $a(t) = \exp(t/\ell)$:

$$f_{\vec{k}}(t,\vec{x}) = \frac{1}{(2\pi)^3\sqrt{2e^{3t/\ell}}}\exp\Big[\mathrm{i}\vec{k}\cdot\vec{x}\Big]v_k(t)$$

We first look at the spatial derivatives to reduce this to a differential equation only dependent on time. These only act on the exponential function as $\partial_x^2 e^{\mathrm{i}\vec{k}\cdot\vec{x}} = -k_x^2$ which leads to:

$$(\partial_x^2 + \partial_y^2 + \partial_z^2)f_{\vec{k}} = -k_x^2 f_{\vec{k}} - k_y^2 f_{\vec{k}} - k_z^2 f_{\vec{k}} = -k^2 f_{\vec{k}}$$

For the equation of motion, it directly follows

$$-\partial_t^2 f_{\vec{k}}(t,\vec{x}) - \frac{3}{\ell}\partial_t f_{\vec{k}}(t,\vec{x}) - e^{-2t/\ell}k^2 f_{\vec{k}}(t,\vec{x}) - \left(m^2 + \frac{2}{\ell^2}\right)f_{\vec{k}}(t,\vec{x}) = 0$$

We then introduce a new time coordinate:

$$\tau = k\ell\exp(-t/\ell) \qquad \Leftrightarrow \qquad t = \ell\log\left(\frac{k\ell}{\tau}\right)$$

The equation of motion after the substitution of the new time coordinate looks as follows:

$$\begin{aligned}\left[\left(-\frac{\tau^2}{\ell^2}\partial_\tau^2 - \frac{\tau}{\ell^2}\partial_\tau\right) + 3\frac{\tau}{\ell^2}\partial_\tau - \frac{\tau^2}{\ell^2} + \left(\frac{2}{\ell^2} - m^2\right)\right] f_{\vec{k}}(\tau,\vec{x}) =& 0 \\ \Leftrightarrow \qquad \left[-\frac{\tau^2}{\ell^2}\partial_\tau^2 + 2\frac{\tau}{\ell^2}\partial_\tau - \frac{\tau^2}{\ell^2} + \left(\frac{2}{\ell^2} - m^2\right)\right] f_{\vec{k}}(\tau,\vec{x}) =& 0\end{aligned}$$

When we plug in the mode function with the new time variable, we need to consider the derivatives (two factors in the mode function are time-dependent):

$$\begin{aligned}f_{\vec{k}}(\tau,\vec{x}) =& \frac{1}{(2\pi)^3\sqrt{2\left(\frac{k\ell}{\tau}\right)^3}} \exp\left[\mathrm{i}\vec{k}\cdot\vec{x}\right] v_k(\tau) = c_{\vec{k}}(\vec{x})\tau^{3/2}v_k(\tau) \\ \partial_\tau f_{\vec{k}}(\tau,\vec{x}) =& c_{\vec{k}}(\vec{x})\left(\tau^{3/2}\partial_\tau + \frac{3}{2}\sqrt{\tau}\right)v_k(\tau) \\ \partial_\tau^2 f_{\vec{k}}(\tau,\vec{x}) =& c_{\vec{k}}(\vec{x})\left(\tau^{3/2}\partial_\tau^2 + 3\sqrt{\tau}\partial_\tau + \frac{3}{4\sqrt{\tau}}\right)v_k(\tau)\end{aligned}$$

We can plug this in and obtain

$$\begin{aligned}&\left[-\frac{\tau^2}{\ell^2}c_{\vec{k}}(\vec{x})\left(\tau^{3/2}\partial_\tau^2 + 3\sqrt{\tau}\partial_\tau + \frac{3}{4\sqrt{\tau}}\right) + 2\frac{\tau}{\ell^2}c_{\vec{k}}(\vec{x})\left(\tau^{3/2}\partial_\tau + \frac{3}{2}\sqrt{\tau}\right)\right. \\ &\qquad \left. -\frac{\tau^2}{\ell^2}c_{\vec{k}}(\vec{x})\tau^{3/2} + \left(\frac{2}{\ell^2} - m^2\right)c_{\vec{k}}(\vec{x})\tau^{3/2}\right] v_k(\tau) = 0 \\ \Leftrightarrow \quad &\left[-\tau^2\left(\tau^{3/2}\partial_\tau^2 + 3\sqrt{\tau}\partial_\tau + \frac{3}{4\sqrt{\tau}}\right) + 2\tau\left(\tau^{3/2}\partial_\tau + \frac{3}{2}\sqrt{\tau}\right) - \tau^2\tau^{3/2} + \left(2 - \ell^2m^2\right)\tau^{3/2}\right] v_k(\tau) = 0 \\ \Leftrightarrow \quad &\left[\tau^2\partial_\tau^2 + \tau 3\partial_\tau - 2\tau\partial_\tau + \frac{3}{4} - 3 + \tau^2 - 2 + \ell^2m^2\right] v_k(\tau) = 0 \\ \Leftrightarrow \quad &\left[\tau^2\partial_\tau^2 + \tau\partial_\tau + \tau^2 - \left(\frac{17}{4} - \ell^2m^2\right)\right] v_k(\tau) = 0\end{aligned}$$

This can be identified with the Bessel equation

$$\tau^2\partial_\tau v_k(\tau) + \tau\partial_\tau v_k(\tau) + (\tau^2 - \nu^2)v_k(\tau) = 0$$

with

$$\nu = \sqrt{\frac{17}{4} - m^2\ell^2}$$

□

Proof 7: Normalization of mode function in eq. (3.25)

$$\begin{aligned}f_{\vec{k}}(t,\vec{x}) =& \frac{\exp\left[\mathrm{i}\vec{k}\cdot\vec{x}\right]}{(2\pi)^3\sqrt{2e^{3t/\ell}}}(a_kJ_\nu(k\ell\exp(-t/\ell)) + b_kY_\nu(k\ell\exp(-t/\ell))) \\ v_k(t) =& a_kJ_\nu(k\ell\exp(-t/\ell)) + b_kY_\nu(k\ell\exp(-t/\ell)) \\ v_k(\tau) =& a_kJ_\nu(\tau) + b_kY_\nu(\tau)\end{aligned}$$

with $\tau = k\ell e^{-t/\ell}$. In order to find conditions for the parameters a_k and b_k, we need to calculate the Wronskian

$$W[v_k, v_k^*] = v_k'v_k^* - v_k(v_k^*)' = 2\mathrm{i}\,\mathrm{Im}(v_k'v_k^*)$$

where the normalization condition imposes

$$\mathrm{Im}(v_k' v_k^*) = -1$$

where$'$ denotes the derivative with respect to t. The Bessel functions have the properties [AS64]

$$\begin{aligned} J_n^*(x) =& J_n(x^*) \\ J_n'(x) =& J_{n-1}(x) - J_{n+1}(x) \\ J_{n+1}(x) =& \frac{2n}{x} J_n(x) - J_{n-1}(x) \end{aligned}$$

$$\begin{aligned} W[v_k, v_k^*] =& v_k' v_k^* - v_k (v_k^*)' = \frac{\partial \tau}{\partial t}(\partial_\tau v_k) v_k^* - v_k \frac{\partial \tau}{\partial t}(\partial_\tau v_k^*) \\ & \frac{\partial \tau}{\partial t} = -k e^{-t/\ell} = -\frac{\tau}{\ell} \\ =& -\frac{\tau}{\ell}(\partial_\tau v_k) v_k^* + \frac{\tau}{\ell} v_k (\partial_\tau v_k^*) \\ =& \frac{\tau}{\ell}\big[(a_k J_\nu(\tau) + b_k Y_\nu(\tau))\big(a_k^* J_\nu'(\tau) + b_k^* Y_\nu'(\tau)\big) - \big(a_k J_\nu'(\tau) + b_k Y_\nu'(\tau)\big)(a_k^* J_\nu(\tau) + b_k^* Y_\nu(\tau))\big] \\ =& -\frac{\tau}{\ell}(a_k b_k^* - a_k^* b_k)\big(J_\nu'(\tau) Y_\nu(\tau) - J_\nu(\tau) Y_\nu'(\tau)\big) \\ =& -\frac{\tau}{\ell}(a_k b_k^* - a_k^* b_k)\bigg(J_{\nu-1}(\tau) Y_\nu(\tau) - \frac{2\nu}{\tau} J_\nu(\tau) Y_\nu(\tau) + J_{\nu-1}(\tau) Y_\nu(\tau) - J_\nu(\tau) Y_{\nu-1}(\tau) \\ & + \frac{2\nu}{\tau} J_\nu(\tau) Y_\nu(\tau) - J_\nu(\tau) Y_{\nu-1}(\tau)\bigg) \\ =& -\frac{\tau}{\ell}(a_k b_k^* - a_k^* b_k)(J_{\nu-1}(\tau) Y_\nu(\tau) - J_\nu(\tau) Y_{\nu-1}(\tau)) \end{aligned}$$

With the identity of Bessel functions

$$J_n(x) Y_{n-n}(x) - J_{n-n}(x) Y_n(x) = \frac{2}{\pi x}$$

this simplifies to the following expression

$$W[v_k, v_k^*] = -\frac{\tau}{\ell}(a_k b_k^* - a_k^* b_k)\frac{2}{\pi\tau} = -\frac{2}{\pi\ell}(a_k b_k^* - a_k^* b_k) = -2\mathrm{i}$$

With the normalization condition, we obtain the following relation for the parameters a_k and b_k:

$$a_k b_k^* - a_k^* b_k = \mathrm{i}\pi\ell \tag{B.1}$$

□

Proof 8: Asymptotic properties Bessel functions

The Bessel functions of the first and second kind have the following asymptotic properties [AS64]:

$$\begin{aligned} J_n(x) &\sim \frac{1}{\Gamma(n+1)}\Big(\frac{x}{2}\Big)^n \qquad x \to 0,\ n \neq -1, -2, \dots \\ Y_n(x) &\sim -\frac{\Gamma(n)}{\pi}\Big(\frac{x}{2}\Big)^{-n} \qquad x \ \to 0,\ \mathrm{Re}(n) > 0 \end{aligned}$$

In the following, we will briefly study the asymptotic form of these mode equations. We focus on the asymptotic behavior of the Bessel functions $v_k(\tau)$. For large times $t \to \infty$, the time coordinate τ, which is the argument of the Bessel function, approaches 0. We are interested in the time-dependent part of the mode functions

$$v_k(\tau) = a_k J_\nu(\tau) + b_k Y_\nu(\tau)$$

In the limiting case $\tau \to 0$ we can neglect $J_\nu(\tau)$ and get the following late time asymptotic behaviour:

$$v_k(\tau) \sim \frac{b_k}{\pi} 2^\nu \tau^{-\nu} \Gamma(\nu)$$

As these modes do not oscillate, the regular notion of a particle is not well-defined.
We look at the asymptotic behavior at early times, which is captured by $\tau \to \infty$:

$$J_n(x) \sim \sqrt{\frac{2}{\pi x}} \cos\Big(x - \frac{n\pi}{2} - \frac{\pi}{3}\Big) \qquad |x| \to \infty$$
$$Y_n(x) \sim \sqrt{\frac{2}{\pi x}} \sin\Big(x - \frac{n\pi}{2} - \frac{\pi}{3}\Big) \qquad |x| \to \infty$$

For the mode function, it follows that

$$v_k(\tau) = a_k \sqrt{\frac{2}{\pi\tau}} \cos\Big(\tau - \frac{\nu\pi}{2} - \frac{\pi}{3}\Big) + b_k \sqrt{\frac{2}{\pi\tau}} \sin\Big(\tau - \frac{\nu\pi}{2} - \frac{\pi}{3}\Big)$$

This can be further simplified by considering the physical wavelength: In the limit of early times ($\tau \to \infty$), the physical wavelength

$$\lambda \sim a(\tau) \sim \frac{k\ell}{\tau}$$

is much smaller than the curvature scale ℓ, which is why mode functions are almost not affected by the curvature. This is why they should behave as they do in flat spacetime. To achieve this, we choose

$$b_k = -\mathrm{i} a_k$$

With the results from the normalization condition from eq. (B.1), we get

$$a_k b_k^* - a_k^* b_k = a_k \mathrm{i} a_k^* + a_k^* \mathrm{i} a_k = 2\mathrm{i}|a_k|^2 = \mathrm{i}\pi\ell \qquad \Rightarrow \qquad a_k = \sqrt{\frac{\pi\ell}{2}}$$

With this, we get the following mode functions (up to first order):

$$\begin{aligned} v_k(\tau) \sim& \sqrt{\frac{\pi\ell}{2}} \sqrt{\frac{2}{\pi\tau}} \Big[\cos\Big(\tau - \frac{\nu\pi}{2} - \frac{\pi}{3}\Big) + \mathrm{i}\sin\Big(\tau - \frac{\nu\pi}{2} - \frac{\pi}{3}\Big)\Big] \\ \sim& \sqrt{\frac{\ell}{\tau}} \exp\Big[\mathrm{i}\tau - \mathrm{i}\frac{\nu\pi}{2} - \mathrm{i}\frac{\pi}{3}\Big] \end{aligned}$$

With the scale factor $a(\tau) = \frac{k\ell}{\tau}$ we get the form familiar from Minkowski spacetime up to a phase factor:

$$v_k(\tau) \sim \frac{1}{\sqrt{a(\tau)k}} \exp\Big[\mathrm{i}\tau - \mathrm{i}\frac{\nu\pi}{2} - \mathrm{i}\frac{\pi}{3}\Big]$$

□

B.6. Euclidean modes in global coordinates

In global coordinates, the field equation is

$$(\Box - m^2)\phi(\tau,\theta) = \left(\ell\partial_\tau^2 + \tanh(\tau/\ell)\partial_\tau + \frac{\partial_\theta^2}{\cosh(\tau/\ell)^2} + \ell m^2\right)\phi(\tau,\theta) = 0$$

With the product ansatz $\phi(\tau,\theta) = f(\tau)h(\theta)$, we get the following decoupled and simplified form of the differential equation:

$$\frac{\ell\cosh(\tau/\ell)^2}{f(\tau)}\big(\ell m^2 + \tanh(\tau/\ell)\partial_\tau + \ell\partial_\tau^2\big)f(\tau) - \frac{\partial_\theta^2 h(\theta)}{h(\theta)} = 0$$

In a more general case considering higher dimensions, the function $h(\theta)$ would be the spherical harmonic functions on a $(d-1)$ dimensional sphere. Since this is only a circle, in our case, this reduces to Fourier modes (where ω is a non-negative integer).

$$h(\theta) = e^{-\mathrm{i}\omega\theta}$$

which satisfy the following relation:

$$\partial_\theta^2 h(\theta) = -\omega^2 h(\theta)$$

For the temporal part of the equation of motion, it follows that

$$\left(\ell^2\partial_\tau^2 + \ell\tanh(\tau/\ell)\partial_\tau + \ell^2 m^2 + \frac{\omega^2}{\cosh(\tau/\ell)^2}\right)f(\tau) = 0$$

we perform the substitution $\sigma = -e^{2\tau/\ell}$ and get the following equation of motion:

$$2\sigma\left(2\sigma f''(\sigma) + f'(\sigma)\left(\tanh\left(\frac{\log(-\sigma)}{2}\right) + 2\right)\right) + f(\sigma)\left(\ell^2 m^2 - \frac{4\sigma\omega^2}{(\sigma-1)^2}\right) = 0$$

We can perform another substitution to the variable $z = 1-\sigma$ and obtain:

$$2(z-1)\big(2(z-1)zf''(z) + (3z-2)f'(z)\big) + f(z)\left(\ell^2 m^2 z + \frac{4\omega^2(z-1)}{z}\right) = 0$$

This is solved by the two linearly independent solutions involving the Hypergeometric functions ${}_2F_1(a,b,c,z)$:

$$f_1(z) = \frac{c_2(-1)^{2\omega}z^\omega(z-1)^{\frac{1}{4}\left(\sqrt{1-4\ell^2m^2}+2\right)}\,{}_2F_1\left(\omega+\frac{1}{2},\omega+\frac{1}{2}\sqrt{1-4\ell^2m^2}+\frac{1}{2};2\omega+1;z\right)}{\sqrt[4]{1-z}}$$

$$f_2(z) = \frac{c_1 z^{-\omega}(z-1)^{\frac{1}{4}\left(\sqrt{1-4\ell^2m^2}+2\right)}\,{}_2F_1\left(\frac{1}{2}\left(-2\omega+\sqrt{1-4\ell^2m^2}+1\right),\frac{1}{2}-\omega;1-2\omega;z\right)}{\sqrt[4]{1-z}}$$

We want to choose a solution that is analytic on the continuation of the Euclidean sphere. For this, we look at the Euclidean pole, which is at $z = 0 - \mathrm{i}\varepsilon$. We consider the easiest case where $\ell = 1$, $m = 0$ and $\omega = 1$ and get the following behaviour:

$$f_1(-\mathrm{i}\varepsilon) \overset{\varepsilon\to 0}{\longrightarrow} 0$$
$$f_2(-\mathrm{i}\varepsilon) \overset{\varepsilon\to 0}{\longrightarrow} \infty$$

We choose the solution $f_1(z)$ as the other one is singular at the Euclidean pole. The resulting mode functions are

$$f(\tau) = \frac{(-1)^{2\omega}\left(e^{\frac{2\tau}{\ell}}\right)^{\frac{1}{4}\left(\sqrt{1-4\ell^2m^2}+2\right)}\left(e^{\frac{2\tau}{\ell}}+1\right)^\omega}{\sqrt[4]{-e^{\frac{2\tau}{\ell}}}}$$

$$\begin{aligned}
&\cdot\ {}_2F_1\left(\omega+\frac{1}{2},\omega+\frac{1}{2}\sqrt{1-4\ell^2m^2}+\frac{1}{2};2\omega+1;1+e^{\frac{2\tau}{\ell}}\right)\\
=&(-1)^{2\omega-\frac{1}{4}}e^{\frac{1}{2}\left(2+\sqrt{1-4\ell^2m^2}-2\omega\right)\tau/\ell}\cosh^{\omega}\left(\frac{\tau}{\ell}\right)\\
&\cdot\ {}_2F_1\left(\omega+\frac{1}{2},\omega+\frac{1}{2}\sqrt{1-4\ell^2m^2}+\frac{1}{2};2\omega+1;1+e^{\frac{2\tau}{\ell}}\right)
\end{aligned}$$

The normalization is fixed by demanding that these modes are orthonormal with respect to the Klein-Gordon inner product. The inner product is easiest evaluated on the temporal past boundary. The exact normalization is not necessary in this context, more details can be found in [BMS01]. The following identity from [AS64, (15.1.20)] is useful

$${}_2F_1(a,b,c,1)=\frac{\Gamma(c)\Gamma(c-a-b)}{\Gamma(c-a)\Gamma(c-b)}$$

B.7. Quantum scalar field in a static patch

The field equation from eq. (3.26) has been solved in the literature before numerous times with slight changes in the definition of coordinates and dimensions [LP78, Pol89a, Pol89b, BMS01]. We make the following product ansatz for the positive frequency mode functions:

$$\phi_\omega(r,t)=f_\omega(r)e^{-\mathrm{i}\omega t}$$

With this ansatz, we obtain the following radial de Sitter field equation

$$\begin{aligned}
\left(-\frac{\ell^2}{\ell^2-r^2}(-\mathrm{i}\omega)^2-\frac{2r}{\ell^2}\partial_r+\left(1-\frac{r^2}{\ell^2}\right)\partial_r^2-m^2\right)f_\omega(r)=&0\\
\left(\left(1-\frac{r^2}{\ell^2}\right)\partial_r^2-\frac{2r}{\ell^2}\partial_r+\frac{\ell^2}{\ell^2-r^2}\omega^2-m^2\right)f_\omega(r)=&0
\end{aligned}$$

with the substitution $x=\frac{r}{\ell}$ we can identify this with the associated Legendre differential equation

$$\left((1-x^2)\partial_x^2-2x\partial_x+\frac{\ell^2}{1-x^2}\omega^2-\ell^2m^2\right)f_\omega(x)=0$$

This equation can be identified with the associated Legendre differential equation

$$\left[(1-x^2)\frac{d^2}{dx^2}-2x\frac{d}{dx}+\left(l(l+1)-\frac{n^2}{1-x^2}\right)\right]P_l^n(x)=0$$

The equation of motion is solved by Legendre functions $P_l^n(r/\ell)$ and $Q_l^n(r/\ell)$ where the orders l and n have to satisfy

$$\begin{aligned}
l=&-\left(\frac{1}{2}\pm\sqrt{\frac{1}{4}-\ell^2m^2}\right)=-h_\pm\\
n=&\pm\,\mathrm{i}\ell\omega
\end{aligned}$$

Proof 9: Relation associated Legendre equation and Hypergeometric equation

The associated Legendre equation is

$$\left[(1-x^2)\frac{d^2}{dx^2}-2x\frac{d}{dx}+\left(\lambda(\lambda+1)-\frac{\mu^2}{1-x^2}\right)\right]f(x)=0$$

, which is solved by the first (or second) order Legendre function $f(x) = P_\lambda^\mu(x)$. We perform the substitution

$$f(x) = (1-x^2)^{\mu/2} w(x^2)$$

, which gives us the following differential equation:

$$\big(1-x^2\big)^{\mu/2}\left[4\big(x^2-1\big)x^2\frac{d^2}{dx^2} + \big((4\mu+6)x^2-2\big)\frac{d}{dx} - (\lambda-\mu)(\lambda+\mu+1)\right]w(x^2) = 0 \tag{B.2}$$

The hypergeometric equation is

$$(1-z)zf''(z) + f'(z)(c-z(a+b+1)) - abf(z) = 0$$

we can identify the parameters as follows

$$\begin{aligned} a &= \frac{1}{2}(1+\mu+\lambda) \\ b &= \frac{1}{2}(\mu-\lambda) \\ c &= \frac{1}{2} \end{aligned}$$

to get this form of the Hypergeometric equation:

$$-4(z-1)zf''(z) - ((4\mu+6)z-2)f'(z) + f(z)(\lambda-\mu)(\lambda+\mu+1) = 0 \tag{B.3}$$

We can directly identify the Hypergeometric equation in eq. (B.3) with eq. (B.2) which is a direct result of the Legendre equation. Accordingly, the function $w(x^2)$ in eq. (B.2) is a function that solves the Hypergeometric equation, and the Legendre function $f(x)$ can be expressed in terms of the Hypergeometric function as follows:

$$f(x) = P_\lambda^\mu(x) = (1-x^2)^{\mu/2} w(x^2) = (1-x^2)^{\mu/2}\, {}_2F_1\left(\frac{1}{2}(1+\mu+\lambda), \frac{1}{2}(\mu-\lambda), \frac{1}{2}, x^2\right)$$

With the parameter from the mode functions of the static patch in eq. (3.27) we get the following mode functions in terms of the Hypergeometric function:

$$f(x) = (1-x^2)^{\mathrm{i}\ell\omega/2}\, {}_2F_1\left(\frac{1}{2}(h_+ + \mathrm{i}\ell\omega), \frac{1}{2}(h_- + \mathrm{i}\ell\omega), \frac{1}{2}, x^2\right)$$

A similar relation between Legendre functions and Hypergeometric functions, including normalization, is described in [AS64, eq. (15.4.23)].

□

In order to calculate the normalization of the mode functions, we need to calculate the Klein-Gordon inner product from eq. (3.4). This is easiest done on a constant time slice of the mode function. As this is not directly relevant to this thesis and has already been done in the past (the normalization is, for example, characterized in [Bou02a]), we will skip this calculation in this context.

B.8. Commutators with exponentials

In this appendix section, we will review the proofs for some commutator identities where the operators are arguments of exponential functions. These will be relevant for upcoming sections in the appendix.

$$\left[e^{\lambda_1 \hat{a}\hat{b}}, \hat{a}^\dagger\right] = \lambda_1 \hat{b} e^{\lambda_1 \hat{a}\hat{b}} \tag{B.4}$$

$$\left[e^{\lambda_2 \hat{a}^\dagger \hat{a}}, \hat{a}^\dagger\right] = (1 - e^{-\lambda_2}) e^{\lambda_2 \hat{a}^\dagger \hat{a}} \hat{a}^\dagger \tag{B.5}$$

$$\left[e^{\lambda_3 \hat{a}^\dagger \hat{b}^\dagger}, \hat{a}^\dagger\right] = 0 \tag{B.6}$$

$$\left[e^{\lambda_1 \hat{a}\hat{b}}, \hat{a}\right] = 0$$

$$\left[e^{\lambda_2 \hat{a}^\dagger \hat{a}}, \hat{a}\right] = \left(1 - e^{\lambda_2}\right) e^{\lambda_2 \hat{a}^\dagger \hat{a}} \hat{a} \tag{B.7}$$

$$\left[e^{\lambda_3 \hat{a}^\dagger \hat{b}^\dagger}, \hat{a}\right] = -\lambda_3 \hat{b}^\dagger \, e^{\lambda_3 \hat{a}^\dagger \hat{b}^\dagger} \tag{B.8}$$

Proof 10: show identity (B.4) and (B.8)

$$[A, e^B] = \int_0^1 ds \, e^{(1-s)B} \, [A, B] \, e^{sB}$$

We use the above identity to prove (B.4). It directly follows, that

$$\begin{aligned}
\left[\hat{a}^\dagger, e^{\lambda \hat{a}\hat{b}}\right] &= \int_0^1 ds \, e^{(1-s)\lambda \hat{a}\hat{b}} \, [\hat{a}^\dagger, \lambda \hat{a}\hat{b}] \, e^{s\lambda \hat{a}\hat{b}} \\
&= \int_0^1 ds \, e^{(1-s)\lambda \hat{a}\hat{b}} \, \lambda(-\hat{b}) \, e^{s\lambda \hat{a}\hat{b}} \\
&= -\lambda \hat{b} \int_0^1 ds \, e^{(1-s)\lambda \hat{a}\hat{b}} \, e^{s\lambda \hat{a}\hat{b}} \\
&= -\lambda \hat{b} \int_0^1 ds \, e^{\lambda \hat{a}\hat{b}} \\
&= -\lambda \hat{b} \, e^{\lambda \hat{a}\hat{b}}
\end{aligned}$$

For (B.8) we get

$$\begin{aligned}
\left[\hat{a}, e^{\lambda \hat{a}^\dagger \hat{b}^\dagger}\right] &= \int_0^1 ds \, e^{(1-s)\lambda \hat{a}^\dagger \hat{b}^\dagger} \, [\hat{a}, \lambda \hat{a}^\dagger \hat{b}^\dagger] \, e^{s\lambda \hat{a}^\dagger \hat{b}^\dagger} \\
&= \int_0^1 ds \, e^{(1-s)\lambda \hat{a}^\dagger \hat{b}^\dagger} \, \lambda \hat{b}^\dagger \, e^{s\lambda \hat{a}^\dagger \hat{b}^\dagger} \\
&= \lambda \hat{b}^\dagger \int_0^1 ds \, e^{(1-s)\lambda \hat{a}^\dagger \hat{b}^\dagger} \, e^{s\lambda \hat{a}^\dagger \hat{b}^\dagger} \\
&= \lambda \hat{b}^\dagger \int_0^1 ds \, e^{\lambda \hat{a}^\dagger \hat{b}^\dagger} \\
&= \lambda \hat{b}^\dagger \, e^{\lambda \hat{a}^\dagger \hat{b}^\dagger}
\end{aligned}$$

□

Proof 11: show identity (B.5) and (B.7)
We want to calculate the commutator $\left[e^{\lambda \hat{a}^\dagger \hat{a}}, \hat{a}\right]$ (B.5). To do this, we first expand the expression and left-multiply with $e^{-\lambda \hat{a}^\dagger \hat{a}}$:

$$\begin{aligned}
\left[e^{\lambda \hat{a}^\dagger \hat{a}}, \hat{a}^\dagger\right] = e^{\lambda \hat{a}^\dagger \hat{a}} \hat{a}^\dagger - \hat{a}^\dagger e^{\lambda \hat{a}^\dagger \hat{a}} &= x(\lambda) \hat{a}^\dagger \\
e^{-\lambda \hat{a}^\dagger \hat{a}} e^{\lambda \hat{a}^\dagger \hat{a}} \hat{a}^\dagger - e^{-\lambda \hat{a}^\dagger \hat{a}} \hat{a}^\dagger e^{\lambda \hat{a}^\dagger \hat{a}} &= e^{-\lambda \hat{a}^\dagger \hat{a}} x(\lambda) \hat{a}^\dagger
\end{aligned}$$

$$\underbrace{e^{-\lambda\hat{a}^\dagger\hat{a}}\hat{a}^\dagger e^{\lambda\hat{a}^\dagger\hat{a}}}_{=f(\lambda)} = -e^{-\lambda\hat{a}^\dagger\hat{a}}x(\lambda)\hat{a}^\dagger + \hat{a}^\dagger = \underbrace{\Big(1 - e^{-\lambda\hat{a}^\dagger\hat{a}}x(\lambda)\Big)\hat{a}^\dagger}_{=g(\lambda)}$$

This also needs to be a valid equation after taking the derivative of λ.

$$\begin{aligned}
f'(\lambda) =& e^{-\lambda\hat{a}^\dagger\hat{a}}(-\hat{a}^\dagger\hat{a})\hat{a}^\dagger e^{\lambda\hat{a}^\dagger\hat{a}} + e^{-\lambda\hat{a}^\dagger\hat{a}}\hat{a}^\dagger e^{\lambda\hat{a}^\dagger\hat{a}}(\hat{a}^\dagger\hat{a}) = e^{-\lambda\hat{a}^\dagger\hat{a}}\Big[\hat{a}^\dagger, a^\dagger\hat{a}\Big]e^{\lambda\hat{a}^\dagger\hat{a}} = -f(\lambda)\\
g'(\lambda) =& e^{-\lambda\hat{a}^\dagger\hat{a}}\hat{a}^\dagger\hat{a}\,x(\lambda)\hat{a}^\dagger - e^{-\lambda\hat{a}^\dagger\hat{a}}\,x'(\lambda)\hat{a}^\dagger = e^{-\lambda\hat{a}^\dagger\hat{a}}\Big(\hat{a}^\dagger\hat{a}\,x(\lambda) - x'(\lambda)\Big)\hat{a}^\dagger
\end{aligned}$$

It is necessary that $g(\lambda)$ satisfies the same relation as $f(\lambda)$. It follows:

$$\begin{aligned}
g'(\lambda) = e^{-\lambda\hat{a}^\dagger\hat{a}}\Big(\hat{a}^\dagger\hat{a}\,x(\lambda) - x'(\lambda)\Big)\hat{a}^\dagger =& -\Big(1 - e^{-\lambda\hat{a}^\dagger\hat{a}}\,x(\lambda)\Big)\hat{a}^\dagger = -g(\lambda)\\
e^{-\lambda\hat{a}^\dagger\hat{a}}\hat{a}^\dagger\hat{a}\,x(\lambda)\hat{a}^\dagger - e^{-\lambda\hat{a}^\dagger\hat{a}}x'(\lambda)\hat{a}^\dagger =& -\hat{a}^\dagger + e^{-\lambda\hat{a}^\dagger\hat{a}}\,x(\lambda)\hat{a}^\dagger\\
\hat{a}^\dagger\hat{a}\,x(\lambda) - x'(\lambda) =& -e^{\lambda\hat{a}^\dagger\hat{a}} + x(\lambda)\\
\Big(\hat{a}^\dagger\hat{a} - 1\Big)x(\lambda) + e^{\lambda\hat{a}^\dagger\hat{a}} =& x'(\lambda)
\end{aligned}$$

The following function solves this first-order differential equation:

$$x(\lambda) = \Big(1 - e^{-\lambda}\Big)e^{\lambda\hat{a}^\dagger\hat{a}}$$

The initial values $f(0) = \hat{a}^\dagger$ and $g(0) = \hat{a}^\dagger$ are identical. The solutions to first-order linear differential equations are unique. Accordingly, we found that the commutator is

$$\Big[e^{\lambda\hat{a}^\dagger\hat{a}}, \hat{a}^\dagger\Big] = (1 - e^{-\lambda})e^{\lambda\hat{a}^\dagger\hat{a}}\hat{a}^\dagger$$

The commutator $\Big[e^{\lambda\hat{a}^\dagger\hat{a}}, \hat{a}\Big]$ from (B.7) is calculated similarly:

$$\begin{aligned}
\Big[e^{\lambda\hat{a}^\dagger\hat{a}}, \hat{a}\Big] = e^{\lambda\hat{a}^\dagger\hat{a}}\hat{a} - \hat{a}e^{\lambda\hat{a}^\dagger\hat{a}} =& x(\lambda)\hat{a}\\
e^{-\lambda\hat{a}^\dagger\hat{a}}e^{\lambda\hat{a}^\dagger\hat{a}}\hat{a} - e^{-\lambda\hat{a}^\dagger\hat{a}}\hat{a}e^{\lambda\hat{a}^\dagger\hat{a}} =& e^{-\lambda\hat{a}^\dagger\hat{a}}x(\lambda)\hat{a}\\
\underbrace{e^{-\lambda\hat{a}^\dagger\hat{a}}\hat{a}e^{\lambda\hat{a}^\dagger\hat{a}}}_{=f(\lambda)} =& -e^{-\lambda\hat{a}^\dagger\hat{a}}x(\lambda)\hat{a} + \hat{a} = \underbrace{\Big(1 - e^{-\lambda\hat{a}^\dagger\hat{a}}x(\lambda)\Big)\hat{a}}_{=g(\lambda)}
\end{aligned}$$

This also needs to be a valid equation after taking the derivative of λ.

$$\begin{aligned}
f'(\lambda) =& e^{-\lambda\hat{a}^\dagger\hat{a}}(-\hat{a}^\dagger\hat{a})\hat{a}e^{\lambda\hat{a}^\dagger\hat{a}} + e^{-\lambda\hat{a}^\dagger\hat{a}}\hat{a}e^{\lambda\hat{a}^\dagger\hat{a}}(\hat{a}^\dagger\hat{a}) = e^{-\lambda\hat{a}^\dagger\hat{a}}\Big[\hat{a}, a^\dagger\hat{a}\Big]e^{\lambda\hat{a}^\dagger\hat{a}} = f(\lambda)\\
g'(\lambda) =& e^{-\lambda\hat{a}^\dagger\hat{a}}\hat{a}^\dagger\hat{a}\,x(\lambda)\hat{a} - e^{-\lambda\hat{a}^\dagger\hat{a}}\,x'(\lambda)\hat{a} = e^{-\lambda\hat{a}^\dagger\hat{a}}\Big(\hat{a}^\dagger\hat{a}\,x(\lambda) - x'(\lambda)\Big)\hat{a}
\end{aligned}$$

It is necessary that $g(\lambda)$ satisfies the same relation as $f(\lambda)$. It follows:

$$\begin{aligned}
g'(\lambda) = e^{-\lambda\hat{a}^\dagger\hat{a}}\Big(\hat{a}^\dagger\hat{a}\,x(\lambda) - x'(\lambda)\Big)\hat{a} =& \Big(1 - e^{-\lambda\hat{a}^\dagger\hat{a}}\,x(\lambda)\Big)\hat{a} = g(\lambda)\\
e^{-\lambda\hat{a}^\dagger\hat{a}}\hat{a}^\dagger\hat{a}\,x(\lambda)\hat{a} - e^{-\lambda\hat{a}^\dagger\hat{a}}x'(\lambda)\hat{a} =& \hat{a} - e^{-\lambda\hat{a}^\dagger\hat{a}}\,x(\lambda)\hat{a}\\
\hat{a}^\dagger\hat{a}\,x(\lambda) - x'(\lambda) =& e^{\lambda\hat{a}^\dagger\hat{a}} - x(\lambda)\\
\Big(\hat{a}^\dagger\hat{a} + 1\Big)x(\lambda) - e^{\lambda\hat{a}^\dagger\hat{a}} =& x'(\lambda)
\end{aligned}$$

This first-order differential equation is solved by

$$x(\lambda) = \Big(1 + c\,e^{\lambda}\Big)e^{\lambda\hat{a}^\dagger\hat{a}}$$

The initial values $f(0) = \hat{a}$ and $g(0) = \hat{a}$ are identical. It follows, that $x(0) = 0$ which is true for $c = -1$. The solutions to first-order linear differential equations are unique. Accordingly, we found that the commutator is

$$\left[e^{\lambda \hat{a}^\dagger \hat{a}}, \hat{a}\right] = \left(1 - e^{\lambda}\right) e^{\lambda \hat{a}^\dagger \hat{a}} \hat{a}$$

□

B.9. Express Euclidean modes with static patch modes

In this appendix, we collect calculations and detailed descriptions of intermediate steps from section 3.7.

Proof 12: Metric in Kruskal coordinates (3.29)

The metric in static coordinates which describes one static patch is

$$\mathrm{d}s^2 = \left(-1 + \frac{r^2}{\ell^2}\right)\mathrm{d}t^2 + \frac{\ell^2}{\ell^2 - r^2}\mathrm{d}r^2$$

The Kruskal coordinates in static patch I are defined as

$$\begin{aligned}\frac{r_\mathrm{I}}{\ell} &= \frac{1 + UV}{1 - UV} \\ \frac{t_\mathrm{I}}{\ell} &= \frac{1}{2}\log\left(-\frac{U}{V}\right)\end{aligned}$$

Substituting this into the metric yields the following metric in Kruskal coordinates:

$$\begin{aligned}\mathrm{d}s^2 =& \left(-1 + \frac{r^2}{\ell^2}\right)\left(\frac{\partial t}{\partial U}\mathrm{d}U + \frac{\partial t}{\partial V}\mathrm{d}V\right)^2 + \frac{\ell^2}{\ell^2 - r^2}\left(\frac{\partial r}{\partial U}\mathrm{d}U + \frac{\partial r}{\partial V}\mathrm{d}V\right)^2 \\ =& -4\ell^2 \frac{\mathrm{d}U\mathrm{d}V}{(UV - 1)^2}\end{aligned}$$

The horizon of the static patch I is at $r_\mathrm{I} = 0$ which imposes the following condition on the coordinates U and V:

$$1 = \frac{1 + UV}{1 - UV} \qquad \Leftrightarrow \qquad 1 - UV = 1 + UV$$

which is true for $U = 0$ or $V = 0$. For the time this has the following implications:

$$\begin{aligned}\lim_{U \to 0} \frac{t_\mathrm{I}}{\ell} &= \lim_{U \to 0} \frac{1}{2}\log\left(-\frac{U}{V}\right) = \infty \\ \lim_{V \to 0} \frac{t_\mathrm{I}}{\ell} &= \lim_{U \to 0} \frac{1}{2}\log\left(-\frac{V}{V}\right) = -\infty\end{aligned}$$

□

Proof 13: Mode expansion Euclidean modes as linear combination static patch modes

We check that the mode expansion from eq. (3.31) yields the same quantum scalar field as the expansion with static patch modes:

$$\hat{\phi^E} = \int_0^\infty d\omega \left[\hat{a}_\omega^{E1}\phi_\omega^{E1} + \hat{a}_\omega^{E2}\phi_\omega^{E2} + (\hat{a}_\omega^{E1})^\dagger(\phi_\omega^{E1})^* + (\hat{a}_\omega^{E2})^\dagger(\phi_\omega^{E2})^*\right]$$

$$
\begin{aligned}
&= \int_0^\infty d\omega \frac{1}{1-e^{-2\pi\omega\ell}} \Big[\Big(\hat{a}^{\mathrm{I}}_\omega - e^{-\pi\omega\ell} (\hat{a}^{\mathrm{II}}_\omega)^\dagger \Big) \Big(\phi^{\mathrm{I}}_\omega + e^{-\pi\omega\ell} (\phi^{\mathrm{II}}_\omega)^* \Big) \\
&\quad + \Big(\hat{a}^{\mathrm{II}}_\omega - e^{-\pi\omega\ell} (\hat{a}^{\mathrm{I}}_\omega)^\dagger \Big) \Big(\phi^{\mathrm{II}}_\omega + e^{-\pi\omega\ell} (\phi^{\mathrm{I}}_\omega)^* \Big) + \Big((\hat{a}^{\mathrm{I}}_\omega)^\dagger - e^{-\pi\omega\ell} \hat{a}^{\mathrm{II}}_\omega \Big) \Big((\phi^{\mathrm{I}}_\omega)^* + e^{-\pi\omega\ell} \phi^{\mathrm{II}}_\omega \Big) \\
&\quad + \Big((\hat{a}^{\mathrm{II}}_\omega)^\dagger - e^{-\pi\omega\ell} \hat{a}^{\mathrm{I}}_\omega \Big) \Big((\phi^{\mathrm{II}}_\omega)^* + e^{-\pi\omega\ell} \phi^{\mathrm{I}}_\omega \Big) \Big] \\
&= \int_0^\infty d\omega \Big[\hat{a}^{\mathrm{I}}_\omega \phi^{\mathrm{I}}_\omega + \hat{a}^{\mathrm{II}}_\omega \phi^{\mathrm{II}}_\omega + (\hat{a}^{\mathrm{I}}_\omega)^\dagger (\phi^{\mathrm{I}}_\omega)^* + (\hat{a}^{\mathrm{II}}_\omega)^\dagger (\phi^{\mathrm{II}}_\omega)^* \Big]
\end{aligned}
$$

□

Proof 14: Euclidean creation/annihilation operators satisfy canonical commutation relations

We check that the commutation relations from eq. (3.33) are satisfied:

$$
\begin{aligned}
\Big[\hat{a}^{E1}_\omega, (\hat{a}^{E1}_\omega)^\dagger \Big] &= \frac{1}{1-e^{-2\pi\omega\ell}} \Big[\hat{a}^{\mathrm{I}}_\omega - e^{-\pi\omega\ell} (\hat{a}^{\mathrm{II}}_\omega)^\dagger, (\hat{a}^{\mathrm{I}}_\omega)^\dagger - e^{-\pi\omega\ell} \hat{a}^{\mathrm{II}}_\omega \Big] \\
&= \frac{1}{1-e^{-2\pi\omega\ell}} \Big(1 + e^{-2\pi\omega\ell} (-1) \Big) = 1 \\
\Big[\hat{a}^{E1}_\omega, (\hat{a}^{E2}_\omega)^\dagger \Big] &= \frac{1}{1-e^{-2\pi\omega\ell}} \Big[\hat{a}^{\mathrm{I}}_\omega - e^{-\pi\omega\ell} (\hat{a}^{\mathrm{II}}_\omega)^\dagger, (\hat{a}^{\mathrm{II}}_\omega)^\dagger - e^{-\pi\omega\ell} \hat{a}^{\mathrm{I}}_\omega \Big] = 0 \\
\big[\hat{a}^{E1}_\omega, \hat{a}^{E2}_\omega \big] &= \frac{1}{1-e^{-2\pi\omega\ell}} \Big[\hat{a}^{\mathrm{I}}_\omega - e^{-\pi\omega\ell} (\hat{a}^{\mathrm{II}}_\omega)^\dagger, \hat{a}^{\mathrm{II}}_\omega - e^{-\pi\omega\ell} (\hat{a}^{\mathrm{I}}_\omega)^\dagger \Big] \\
&= \frac{1}{1-e^{-2\pi\omega\ell}} \Big(\big[\hat{a}^{\mathrm{I}}_\omega, \hat{a}^{\mathrm{II}}_\omega \big] - e^{-\pi\omega\ell} \Big[\hat{a}^{\mathrm{I}}_\omega, (\hat{a}^{\mathrm{I}}_\omega)^\dagger \Big] - e^{-\pi\omega\ell} \Big[(\hat{a}^{\mathrm{II}}_\omega)^\dagger, \hat{a}^{\mathrm{II}}_\omega \Big] + \Big[(\hat{a}^{\mathrm{II}}_\omega)^\dagger, (\hat{a}^{\mathrm{I}}_\omega)^\dagger \Big] \Big) \\
&= \frac{1}{1-e^{-2\pi\omega\ell}} \Big(-e^{-\pi\omega\ell} - e^{-\pi\omega\ell} (-1) \Big) = 0
\end{aligned}
$$

The static patch operators can be expressed with the Euclidean ones as follows:

$$
\begin{aligned}
\hat{a}^{\mathrm{I}}_\omega &= \frac{1}{\sqrt{1-e^{-2\pi\omega\ell}}} \Big(\hat{a}^{E1}_\omega + e^{-\pi\omega\ell} (\hat{a}^{E2}_\omega)^\dagger \Big), \qquad (\hat{a}^{\mathrm{I}}_\omega)^\dagger = \frac{1}{\sqrt{1-e^{-2\pi\omega\ell}}} \Big((\hat{a}^{E1}_\omega)^\dagger + e^{-\pi\omega\ell} \hat{a}^{E2}_\omega \Big) \\
\hat{a}^{\mathrm{II}}_\omega &= \frac{1}{\sqrt{1-e^{-2\pi\omega\ell}}} \Big(\hat{a}^{E2}_\omega + e^{-\pi\omega\ell} (\hat{a}^{E1}_\omega)^\dagger \Big), \qquad (\hat{a}^{\mathrm{II}}_\omega)^\dagger = \frac{1}{\sqrt{1-e^{-2\pi\omega\ell}}} \Big((\hat{a}^{E2}_\omega)^\dagger + e^{-\pi\omega\ell} \hat{a}^{E1}_\omega \Big)
\end{aligned}
$$

□

Proof 15: Annihilation of Euclidean vacuum state

We want to show that

$$
\hat{a}^E_\omega \, |\Omega_E\rangle = 0
$$

for the Euclidean annihilation operators

$$
\begin{aligned}
\hat{a}^{E1}_\omega &= \frac{1}{\sqrt{1-e^{-2\pi\omega\ell}}} \Big(\hat{a}^{\mathrm{I}}_\omega - e^{-\pi\omega\ell} (\hat{a}^{\mathrm{II}}_\omega)^\dagger \Big) \\
\hat{a}^{E2}_\omega &= \frac{1}{\sqrt{1-e^{-2\pi\omega\ell}}} \Big(\hat{a}^{\mathrm{II}}_\omega - e^{-\pi\omega\ell} (\hat{a}^{\mathrm{I}}_\omega)^\dagger \Big)
\end{aligned}
$$

and the Euclidean vacuum state

$$
|\Omega_E\rangle = \prod_{\omega=0}^{\infty} \sqrt{1-e^{-2\pi\omega\ell}} e^{e^{-\pi\omega\ell} (\hat{a}^{\mathrm{I}}_\omega)^\dagger (\hat{a}^{\mathrm{II}}_\omega)^\dagger} \, |\Omega_{\mathrm{I}}\rangle \otimes |\Omega_{\mathrm{II}}\rangle
$$

$$
\hat{a}^{E1}_{\tilde{\omega}} \, |\Omega_E\rangle = \frac{1}{\sqrt{1-e^{-2\pi\tilde{\omega}\ell}}} \Big(\hat{a}^{\mathrm{I}}_{\tilde{\omega}} - e^{-\pi\tilde{\omega}\ell} (\hat{a}^{\mathrm{II}}_{\tilde{\omega}})^\dagger \Big) \prod_{\omega=0}^{\infty} \sqrt{1-e^{-2\pi\omega\ell}} e^{e^{-\pi\omega\ell} (\hat{a}^{\mathrm{I}}_\omega)^\dagger (\hat{a}^{\mathrm{II}}_\omega)^\dagger} \, |\Omega_{\mathrm{I}}\rangle \otimes |\Omega_{\mathrm{II}}\rangle
$$

$$
\begin{aligned}
&= \prod_{\omega=0}^{\infty} \frac{\sqrt{1-e^{-2\pi\omega\ell}}}{\sqrt{1-e^{-2\pi\tilde{\omega}\ell}}} \Bigg\{ \underbrace{e^{e^{-\pi\omega\ell}(\hat{a}^{\mathrm{I}}_{\omega})^\dagger(\hat{a}^{\mathrm{II}}_{\omega})^\dagger}\hat{a}^{\mathrm{I}}_{\omega}}_{=0} - \left[e^{e^{-\pi\omega\ell}(\hat{a}^{\mathrm{I}}_{\omega})^\dagger(\hat{a}^{\mathrm{II}}_{\omega})^\dagger}, \hat{a}^{\mathrm{I}}_{\tilde{\omega}}\right] \\
&\quad - e^{e^{-\pi\omega\ell}(\hat{a}^{\mathrm{I}}_{\tilde{\omega}})^\dagger(\hat{a}^{\mathrm{II}}_{\omega})^\dagger} e^{-\pi\tilde{\omega}\ell}(\hat{a}^{\mathrm{II}}_{\tilde{\omega}})^\dagger \Bigg\} |\Omega_{\mathrm{I}}\rangle \otimes |\Omega_{\mathrm{II}}\rangle \\
&\overset{(B.8)}{=} \prod_{\omega=0}^{\infty} \frac{\sqrt{1-e^{-2\pi\omega\ell}}}{\sqrt{1-e^{-2\pi\tilde{\omega}\ell}}} \Big\{ -\Big[-e^{-\pi\omega\ell}(\hat{a}^{\mathrm{II}}_{\omega})^\dagger \delta(\omega-\tilde{\omega}) e^{e^{-\pi\omega\ell}(\hat{a}^{\mathrm{I}}_{\omega})^\dagger(\hat{a}^{\mathrm{II}}_{\tilde{\omega}})^\dagger}\Big] \\
&\quad - e^{e^{-\pi\omega\ell}(\hat{a}^{\mathrm{I}}_{\tilde{\omega}})^\dagger(\hat{a}^{\mathrm{II}}_{\omega})^\dagger} e^{-\pi\tilde{\omega}\ell}(\hat{a}^{\mathrm{II}}_{\tilde{\omega}})^\dagger \Big\} |\Omega_{\mathrm{I}}\rangle \otimes |\Omega_{\mathrm{II}}\rangle \\
&= \prod_{\omega=0}^{\infty} \frac{\sqrt{1-e^{-2\pi\omega\ell}}}{\sqrt{1-e^{-2\pi\tilde{\omega}\ell}}} \Big\{ e^{-\pi\omega\ell}(\hat{a}^{\mathrm{II}}_{\omega})^\dagger \delta(\omega-\tilde{\omega}) - e^{-\pi\tilde{\omega}\ell}(\hat{a}^{\mathrm{II}}_{\tilde{\omega}})^\dagger \Big\} e^{e^{-\pi\omega\ell}(\hat{a}^{\mathrm{I}}_{\omega})^\dagger(\hat{a}^{\mathrm{II}}_{\omega})^\dagger} |\Omega_{\mathrm{I}}\rangle \otimes |\Omega_{\mathrm{II}}\rangle \\
&= 0
\end{aligned}
$$

similarly, it follows for the second Euclidean annihilation operator

$$
\begin{aligned}
\hat{a}^{E2}_{\tilde{\omega}} |\Omega_E\rangle &= \frac{1}{\sqrt{1-e^{-2\pi\tilde{\omega}\ell}}} \Big(\hat{a}^{\mathrm{II}}_{\tilde{\omega}} - e^{-\pi\tilde{\omega}\ell}(\hat{a}^{\mathrm{I}}_{\tilde{\omega}})^\dagger\Big) \prod_{\omega=0}^{\infty} \sqrt{1-e^{-2\pi\omega\ell}} e^{e^{-\pi\omega\ell}(\hat{a}^{\mathrm{I}}_{\omega})^\dagger(\hat{a}^{\mathrm{II}}_{\omega})^\dagger} |\Omega_{\mathrm{I}}\rangle \otimes |\Omega_{\mathrm{II}}\rangle \\
&= \prod_{\omega=0}^{\infty} \frac{\sqrt{1-e^{-2\pi\omega\ell}}}{\sqrt{1-e^{-2\pi\tilde{\omega}\ell}}} \Big\{ e^{e^{-\pi\omega\ell}(\hat{a}^{\mathrm{I}}_{\omega})^\dagger(\hat{a}^{\mathrm{II}}_{\omega})^\dagger} \hat{a}^{\mathrm{II}}_{\omega} - \left[e^{e^{-\pi\omega\ell}(\hat{a}^{\mathrm{I}}_{\omega})^\dagger(\hat{a}^{\mathrm{II}}_{\omega})^\dagger}, \hat{a}^{\mathrm{II}}_{\tilde{\omega}}\right] \\
&\quad - e^{e^{-\pi\omega\ell}(\hat{a}^{\mathrm{I}}_{\tilde{\omega}})^\dagger(\hat{a}^{\mathrm{I}}_{\omega})^\dagger} e^{-\pi\tilde{\omega}\ell}(\hat{a}^{\mathrm{II}}_{\tilde{\omega}})^\dagger \Big\} |\Omega_{\mathrm{I}}\rangle \otimes |\Omega_{\mathrm{II}}\rangle \\
&\overset{(B.8)}{=} \prod_{\omega=0}^{\infty} \frac{\sqrt{1-e^{-2\pi\omega\ell}}}{\sqrt{1-e^{-2\pi\tilde{\omega}\ell}}} \Big\{ -\Big[-e^{-\pi\omega\ell}(\hat{a}^{\mathrm{I}}_{\omega})^\dagger \delta(\omega-\tilde{\omega}) e^{e^{-\pi\omega\ell}(\hat{a}^{\mathrm{I}}_{\omega})^\dagger(\hat{a}^{\mathrm{II}}_{\tilde{\omega}})^\dagger}\Big] \\
&\quad - e^{e^{-\pi\omega\ell}(\hat{a}^{\mathrm{I}}_{\tilde{\omega}})^\dagger(\hat{a}^{\mathrm{II}}_{\omega})^\dagger} e^{-\pi\tilde{\omega}\ell}(\hat{a}^{\mathrm{I}}_{\tilde{\omega}})^\dagger \Big\} |\Omega_{\mathrm{I}}\rangle \otimes |\Omega_{\mathrm{II}}\rangle \\
&= \prod_{\omega=0}^{\infty} \frac{\sqrt{1-e^{-2\pi\omega\ell}}}{\sqrt{1-e^{-2\pi\tilde{\omega}\ell}}} \Big\{ e^{-\pi\omega\ell}(\hat{a}^{\mathrm{I}}_{\omega})^\dagger \delta(\omega-\tilde{\omega}) - e^{-\pi\tilde{\omega}\ell}(\hat{a}^{\mathrm{I}}_{\tilde{\omega}})^\dagger \Big\} e^{e^{-\pi\omega\ell}(\hat{a}^{\mathrm{I}}_{\omega})^\dagger(\hat{a}^{\mathrm{II}}_{\tilde{\omega}})^\dagger} |\Omega_{\mathrm{I}}\rangle \otimes |\Omega_{\mathrm{II}}\rangle
\end{aligned}
$$

□

Proof 16: express Hamilton operator with static patch operators

We want to show that the Hamiltonian corresponding to the Euclidean vacuum state generating time evolution takes the form in eq. (3.35). For this, we express the static patch creation and annihilation operators with the Euclidean ones:

$$
\begin{aligned}
&(\hat{a}^{\mathrm{I}}_{\omega})^\dagger \hat{a}^{\mathrm{I}}_{\omega} - (\hat{a}^{\mathrm{II}}_{\omega})^\dagger \hat{a}^{\mathrm{II}}_{\omega} \\
=&\frac{1}{1-e^{-2\pi\omega\ell}} \Big[\Big((\hat{a}^{E1}_{\omega})^\dagger + e^{-\pi\omega\ell}\hat{a}^{E2}_{\omega}\Big)\Big(\hat{a}^{E1}_{\omega} + e^{-\pi\omega\ell}(\hat{a}^{E2}_{\omega})^\dagger\Big) \\
&-\Big((\hat{a}^{E2}_{\omega})^\dagger + e^{-\pi\omega\ell}\hat{a}^{E1}_{\omega}\Big)\Big(\hat{a}^{E2}_{\omega} + e^{-\pi\omega\ell}(\hat{a}^{E1}_{\omega})^\dagger\Big)\Big] \\
=&\frac{1}{1-e^{-2\pi\omega\ell}} \Big[(\hat{a}^{E1}_{\omega})^\dagger \hat{a}^{E1}_{\omega} + (\hat{a}^{E1}_{\omega})^\dagger e^{-\pi\omega\ell}(\hat{a}^{E2}_{\omega})^\dagger + e^{-\pi\omega\ell}\hat{a}^{E2}_{\omega}\hat{a}^{E1}_{\omega} + e^{-\pi\omega\ell}\hat{a}^{E2}_{\omega}e^{-\pi\omega\ell}(\hat{a}^{E2}_{\omega})^\dagger \\
&-(\hat{a}^{E2}_{\omega})^\dagger \hat{a}^{E2}_{\omega} - (\hat{a}^{E2}_{\omega})^\dagger e^{-\pi\omega\ell}(\hat{a}^{E1}_{\omega})^\dagger - e^{-\pi\omega\ell}\hat{a}^{E1}_{\omega}\hat{a}^{E2}_{\omega} - e^{-\pi\omega\ell}\hat{a}^{E1}_{\omega}e^{-\pi\omega\ell}(\hat{a}^{E1}_{\omega})^\dagger\Big] \\
=&\frac{1}{1-e^{-2\pi\omega\ell}} \Big[(\hat{a}^{E1}_{\omega})^\dagger \hat{a}^{E1}_{\omega} + e^{-2\pi\omega\ell}\hat{a}^{E2}_{\omega}(\hat{a}^{E2}_{\omega})^\dagger - (\hat{a}^{E2}_{\omega})^\dagger \hat{a}^{E2}_{\omega} - e^{-2\pi\omega\ell}\hat{a}^{E1}_{\omega}(\hat{a}^{E1}_{\omega})^\dagger\Big] \\
=&\frac{1}{1-e^{-2\pi\omega\ell}} \Big[(\hat{a}^{E1}_{\omega})^\dagger \hat{a}^{E1}_{\omega} + e^{-2\pi\omega\ell}\Big(1 + (\hat{a}^{E2}_{\omega})^\dagger \hat{a}^{E2}_{\omega}\Big) - (\hat{a}^{E2}_{\omega})^\dagger \hat{a}^{E2}_{\omega} - e^{-2\pi\omega\ell}\Big(1 + (\hat{a}^{E1}_{\omega})^\dagger \hat{a}^{E1}_{\omega}\Big)\Big] \\
=&(\hat{a}^{E1}_{\omega})^\dagger \hat{a}^{E1}_{\omega} - (\hat{a}^{E2}_{\omega})^\dagger \hat{a}^{E2}_{\omega}
\end{aligned}
$$

□

Proof 17: generator of time translations annihilates Euclidean vacuum state

We want to show the relation from eq. (3.36)

$$\mathcal{H}_E \left|\Omega_E\right\rangle = \int_0^\infty d\tilde{\omega}\, \omega \underbrace{\left[(\hat{a}_{\tilde{\omega}}^{E1})^\dagger \hat{a}_{\tilde{\omega}}^{E1} - (\hat{a}_{\tilde{\omega}}^{E2})^\dagger \hat{a}_{\tilde{\omega}}^{E2}\right]}_{=(\star)} \left|\Omega_E\right\rangle$$

$$\begin{aligned}
(\star) =& \frac{1}{1-e^{-2\pi\tilde{\omega}\ell}} \Big(\Big(\hat{a}_{\tilde{\omega}}^{\mathrm{I}} - e^{-\pi\tilde{\omega}\ell}(\hat{a}_{\tilde{\omega}}^{\mathrm{II}})^\dagger\Big)^\dagger \Big(\hat{a}_{\tilde{\omega}}^{\mathrm{I}} - e^{-\pi\tilde{\omega}\ell}(\hat{a}_{\tilde{\omega}}^{\mathrm{II}})^\dagger\Big) \\
& - \Big(\hat{a}_{\tilde{\omega}}^{\mathrm{II}} - e^{-\pi\tilde{\omega}\ell}(\hat{a}_{\tilde{\omega}}^{\mathrm{I}})^\dagger\Big)^\dagger \Big(\hat{a}_{\tilde{\omega}}^{\mathrm{II}} - e^{-\pi\tilde{\omega}\ell}(\hat{a}_{\tilde{\omega}}^{\mathrm{I}})^\dagger\Big)\Big) \\
=& \frac{1}{1-e^{-2\pi\tilde{\omega}\ell}} \Big((\hat{a}_{\tilde{\omega}}^{\mathrm{I}})^\dagger \hat{a}_{\tilde{\omega}}^{\mathrm{I}} - (\hat{a}_{\tilde{\omega}}^{\mathrm{I}})^\dagger e^{-\pi\tilde{\omega}\ell}(\hat{a}_{\tilde{\omega}}^{\mathrm{II}})^\dagger - e^{-\pi\tilde{\omega}\ell}\hat{a}_{\tilde{\omega}}^{\mathrm{II}}\hat{a}_{\tilde{\omega}}^{\mathrm{I}} + e^{-2\pi\tilde{\omega}\ell}\hat{a}_{\tilde{\omega}}^{\mathrm{II}}(\hat{a}_{\tilde{\omega}}^{\mathrm{II}})^\dagger \\
& - (\hat{a}_{\tilde{\omega}}^{\mathrm{II}})^\dagger \hat{a}_{\tilde{\omega}}^{\mathrm{II}} + (\hat{a}_{\tilde{\omega}}^{\mathrm{II}})^\dagger e^{-\pi\tilde{\omega}\ell}(\hat{a}_{\tilde{\omega}}^{\mathrm{I}})^\dagger + e^{-\pi\tilde{\omega}\ell}\hat{a}_{\tilde{\omega}}^{\mathrm{I}}\hat{a}_{\tilde{\omega}}^{\mathrm{II}} - e^{-2\pi\tilde{\omega}\ell}\hat{a}_{\tilde{\omega}}^{\mathrm{I}}(\hat{a}_{\tilde{\omega}}^{\mathrm{I}})^\dagger\Big)
\end{aligned}$$

We look separately on how the static patch annihilation operators act on the Euclidean vacuum state using the identity from eq. (B.8) $\left[e^{\lambda\hat{a}^\dagger\hat{b}^\dagger}, \hat{a}\right] = -\lambda\hat{b}^\dagger\, e^{\lambda\hat{a}^\dagger\hat{b}^\dagger}$ and the fact that the corresponding annihilation operators annihilate the vacuum state (see proof 15):

$$\begin{aligned}
\hat{a}_{\tilde{\omega}}^{\mathrm{I}} \left|\Omega_E\right\rangle =& \prod_{\omega=0}^{\infty} \sqrt{1-e^{-2\pi\omega\ell}}\, \hat{a}_{\tilde{\omega}}^{\mathrm{I}} e^{e^{-\pi\omega\ell}(\hat{a}_\omega^{\mathrm{I}})^\dagger(\hat{a}_\omega^{\mathrm{II}})^\dagger} \left|\Omega_{\mathrm{I}}\right\rangle \otimes \left|\Omega_{\mathrm{II}}\right\rangle \\
=& \prod_{\omega=0}^{\infty} \sqrt{1-e^{-2\pi\omega\ell}} \Big\{ e^{e^{-\pi\omega\ell}(\hat{a}_\omega^{\mathrm{I}})^\dagger(\hat{a}_\omega^{\mathrm{II}})^\dagger} \hat{a}_{\tilde{\omega}}^{\mathrm{I}} - \Big[e^{e^{-\pi\omega\ell}(\hat{a}_\omega^{\mathrm{I}})^\dagger(\hat{a}_\omega^{\mathrm{II}})^\dagger}, \hat{a}_{\tilde{\omega}}^{\mathrm{I}}\Big]\Big\} \left|\Omega_{\mathrm{I}}\right\rangle \otimes \left|\Omega_{\mathrm{II}}\right\rangle \\
=& \prod_{\omega=0}^{\infty} \sqrt{1-e^{-2\pi\omega\ell}} \Big\{ - \Big[-e^{-\pi\omega\ell}(\hat{a}_{\tilde{\omega}}^{\mathrm{II}})^\dagger e^{e^{-\pi\omega\ell}(\hat{a}_\omega^{\mathrm{I}})^\dagger(\hat{a}_\omega^{\mathrm{II}})^\dagger}\Big]\Big\} \left|\Omega_{\mathrm{I}}\right\rangle \otimes \left|\Omega_{\mathrm{II}}\right\rangle \\
=& e^{-\pi\tilde{\omega}\ell}(\hat{a}_{\tilde{\omega}}^{\mathrm{II}})^\dagger \left|\Omega_E\right\rangle \\
\hat{a}_{\tilde{\omega}}^{\mathrm{II}} \left|\Omega_E\right\rangle =& \prod_{\omega=0}^{\infty} \sqrt{1-e^{-2\pi\omega\ell}}\, \hat{a}_{\tilde{\omega}}^{\mathrm{II}} e^{e^{-\pi\omega\ell}(\hat{a}_\omega^{\mathrm{I}})^\dagger(\hat{a}_\omega^{\mathrm{II}})^\dagger} \left|\Omega_{\mathrm{I}}\right\rangle \otimes \left|\Omega_{\mathrm{II}}\right\rangle \\
=& \prod_{\omega=0}^{\infty} \sqrt{1-e^{-2\pi\omega\ell}} \Big\{ e^{e^{-\pi\omega\ell}(\hat{a}_\omega^{\mathrm{I}})^\dagger(\hat{a}_\omega^{\mathrm{II}})^\dagger} \hat{a}_{\tilde{\omega}}^{\mathrm{II}} - \Big[e^{e^{-\pi\omega\ell}(\hat{a}_\omega^{\mathrm{I}})^\dagger(\hat{a}_\omega^{\mathrm{II}})^\dagger}, \hat{a}_{\tilde{\omega}}^{\mathrm{II}}\Big]\Big\} \left|\Omega_{\mathrm{I}}\right\rangle \otimes \left|\Omega_{\mathrm{II}}\right\rangle \\
=& \prod_{\omega=0}^{\infty} \sqrt{1-e^{-2\pi\omega\ell}} \Big\{ - \Big[-e^{-\pi\omega\ell}(\hat{a}_{\tilde{\omega}}^{\mathrm{I}})^\dagger e^{e^{-\pi\omega\ell}(\hat{a}_\omega^{\mathrm{I}})^\dagger(\hat{a}_\omega^{\mathrm{II}})^\dagger}\Big]\Big\} \left|\Omega_{\mathrm{I}}\right\rangle \otimes \left|\Omega_{\mathrm{II}}\right\rangle \\
=& e^{-\pi\tilde{\omega}\ell}(\hat{a}_{\tilde{\omega}}^{\mathrm{I}})^\dagger \left|\Omega_E\right\rangle
\end{aligned}$$

Plugging this in it follows that

$$\begin{aligned}
& (\star) \left|\Omega_E\right\rangle \\
=& \frac{1}{1-e^{-2\pi\tilde{\omega}\ell}} \Bigg(\underbrace{(\hat{a}_{\tilde{\omega}}^{\mathrm{I}})^\dagger e^{-\pi\tilde{\omega}\ell}(\hat{a}_{\tilde{\omega}}^{\mathrm{II}})^\dagger}_{=(i)} - \underbrace{(\hat{a}_{\tilde{\omega}}^{\mathrm{I}})^\dagger e^{-\pi\tilde{\omega}\ell}(\hat{a}_{\tilde{\omega}}^{\mathrm{II}})^\dagger}_{=(i)} - \underbrace{e^{-\pi\tilde{\omega}\ell}\hat{a}_{\tilde{\omega}}^{\mathrm{II}} e^{-\pi\tilde{\omega}\ell}(\hat{a}_{\tilde{\omega}}^{\mathrm{II}})^\dagger}_{=(ii)} + \underbrace{e^{-2\pi\tilde{\omega}\ell}\hat{a}_{\tilde{\omega}}^{\mathrm{II}}(\hat{a}_{\tilde{\omega}}^{\mathrm{II}})^\dagger}_{=(ii)} \\
& \underbrace{-(\hat{a}_{\tilde{\omega}}^{\mathrm{II}})^\dagger e^{-\pi\tilde{\omega}\ell}(\hat{a}_{\tilde{\omega}}^{\mathrm{I}})^\dagger}_{=(iii)} + \underbrace{(\hat{a}_{\tilde{\omega}}^{\mathrm{II}})^\dagger e^{-\pi\tilde{\omega}}(\hat{a}_{\tilde{\omega}}^{\mathrm{I}})^\dagger}_{=(iii)} + \underbrace{e^{-\pi\tilde{\omega}\ell}\hat{a}_{\tilde{\omega}}^{\mathrm{I}} e^{-\pi\tilde{\omega}\ell}(\hat{a}_{\tilde{\omega}}^{\mathrm{I}})^\dagger}_{=(iv)} - \underbrace{e^{-2\pi\tilde{\omega}\ell}\hat{a}_{\tilde{\omega}}^{\mathrm{I}}(\hat{a}_{\tilde{\omega}}^{\mathrm{I}})^\dagger}_{=(iv)} \Bigg) \left|\Omega_E\right\rangle = 0
\end{aligned}$$

It directly follows that

$$\mathcal{H}_E \left|\Omega_E\right\rangle = 0$$

□

B.10. Wightman function in static coordinates

We consider the Wightman function of two local observers following Killing trajectories in static coordinates. We identify $x = x_m$ and $x' = x_n$, introduce the quantization with static coordinates, and expand the denominator of eq. (3.37) in the components:

$$\begin{aligned}
&-(x_m^0 - x_n^0 - \mathrm{i}\varepsilon)^2 + |\vec{x}_m - \vec{x}_n|^2 \\
=&-(x_m^0 - x_n^0 - \mathrm{i}\varepsilon)^2 + (x_m^1 - x_n^1)^2 + (x_m^2 - x_n^2)^2 \\
=&-\left(\sqrt{\ell^2 - r_m^2}\sinh\left(\frac{t_m}{\ell}\right) - \sqrt{\ell^2 - r_n^2}\sinh\left(\frac{t_n}{\ell}\right) - \mathrm{i}\varepsilon\right)^2 \\
&+\left(\sqrt{\ell^2 - r_m^2}\cosh\left(\frac{t_m}{\ell}\right) - \sqrt{\ell^2 - r_n^2}\cosh\left(\frac{t_n}{\ell}\right)\right)^2 + (r_m - r_n)^2
\end{aligned}$$

We evaluate this to the first order in ε. This means that we can multiply the first order in ε with arbitrary positive constants and can add arbitrary higher order ε terms. The hyperbolic functions are expanded as follows:

$$\begin{aligned}
\sinh(x) \pm \mathrm{i}\varepsilon + \mathcal{O}(\varepsilon^2) =& \sum_{n=0}^{\infty} \frac{x^{2n+1}}{(2n+1)!} \pm \mathrm{i}\varepsilon + \mathcal{O}(\varepsilon^2) = \sum_{n=0}^{\infty} \frac{(x + \mathrm{i}\varepsilon)^{2n+1}}{(2n+1)!} + \mathcal{O}(\varepsilon^2) \\
=& \sinh(x \pm \mathrm{i}\varepsilon) + \mathcal{O}(\varepsilon^2) \\
\cosh(x) + \mathcal{O}(\varepsilon^2) =& \sum_{n=0}^{\infty} \frac{x^{2n}}{(2n)!} + \mathcal{O}(\varepsilon^2) = \sum_{n=0}^{\infty} \frac{(x \pm \mathrm{i}\varepsilon)^{2n}}{(2n)!} + \mathcal{O}(\varepsilon^2) \\
=& \cosh(x + \mathrm{i}\varepsilon) + \mathcal{O}(\varepsilon^2)
\end{aligned}$$

It directly follows:

$$\begin{aligned}
&-(x_m^0 - x_n^0 - \mathrm{i}\varepsilon)^2 + |\vec{x}_m - \vec{x}_n|^2 \\
=&-\left(\sqrt{\ell^2 - r_m^2}\sinh\left(\frac{t_m}{\ell} - \frac{\mathrm{i}\varepsilon}{2}\right) - \sqrt{\ell^2 - r_n^2}\sinh\left(\frac{t_n}{\ell} + \frac{\mathrm{i}\varepsilon}{2}\right)\right)^2 \\
&+\left(\sqrt{\ell^2 - r_m^2}\cosh\left(\frac{t_m}{\ell} - \frac{\mathrm{i}\varepsilon}{2}\right) - \sqrt{\ell^2 - r_n^2}\cosh\left(\frac{t_n}{\ell} + \frac{\mathrm{i}\varepsilon}{2}\right)\right)^2 + (r_m - r_n)^2 \\
=&(\ell^2 - r_m^2) - 2\sqrt{\ell^2 - r_m^2}\sqrt{\ell^2 - r_n^2}\cosh\left(\frac{t_m}{\ell} - \frac{t_n}{\ell} - \mathrm{i}\varepsilon\right) + (\ell^2 - r_n^2) + r_m^2 - 2r_m r_n + r_n^2 \\
=&-2\sqrt{\ell^2 - r_m^2}\sqrt{\ell^2 - r_n^2}\cosh\left(\frac{t_m}{\ell} - \frac{t_n}{\ell} - \mathrm{i}\varepsilon\right) + 2\ell^2 - 2r_m r_n
\end{aligned}$$

we replace the coordinate time t with the proper time $\tau_i = \sqrt{1 - r_i^2/\ell^2}\, t_i$ and introduce the parameter $\kappa_i = \frac{1}{\sqrt{\ell^2 - r_i^2}}$ which simplifies the expression as follows (with $\tau_m = \tilde{\tau}$ and $\tau_n = \tau$):

$$-(x_m^0 - x_n^0 - \mathrm{i}\varepsilon)^2 + |\vec{x}_m - \vec{x}_n|^2 = 2\ell^2 - \frac{2\cosh(\kappa_m\tau - \kappa_n\tau - \mathrm{i}\varepsilon)}{\kappa_m\kappa_n} + r_m r_n$$

$$= - \frac{2\big(\cosh(\kappa_m\tilde{\tau} - \kappa_n\tau - \mathrm{i}\varepsilon) + \kappa_m r_m \kappa_n r_n - \kappa_m\kappa_n\ell^2\big)}{\kappa_m\kappa_n}$$
$$= - \frac{2}{\kappa_m\kappa_n}\Big(\cosh(\kappa_m\tilde{\tau} - \kappa_n\tau - \mathrm{i}\varepsilon) + \sqrt{\kappa_m^2\ell^2 - 1}\sqrt{\kappa_n^2\ell^2 - 1} - \kappa_m\kappa_n\ell^2\Big)$$

For the Wightman function, it follows

$$W(x_m, x_n) = - \frac{1}{4\pi^2}\frac{1}{(x^0 - (x')^0 - \mathrm{i}\varepsilon)^2 - |\vec{x} - \vec{x}'|^2}$$
$$= - \frac{\kappa_m\kappa_n}{8\pi^2}\frac{1}{\cosh(\kappa_m\tilde{\tau} - \kappa_n\tau - \mathrm{i}\varepsilon) + \sqrt{\kappa_m^2\ell^2 - 1}\sqrt{\kappa_n^2\ell^2 - 1} - \kappa_m\kappa_n\ell^2}$$

We use the hyperbolic identity

$$\sinh^2\Big(\frac{x}{2}\Big) = \frac{1}{2}(\cosh(x) - 1) \qquad \Leftrightarrow \qquad \cosh(x) = 1 + 2\sinh\Big(\frac{x}{2}\Big)$$

The Wightman function is

$$W_{m,n}(s) = - \frac{\kappa_m\kappa_n}{8\pi^2}\frac{1}{1 + 2\sinh^2\big(\frac{\kappa_m\tilde{\tau} - \kappa_n\tau}{2} - \mathrm{i}\varepsilon\big) + \sqrt{\kappa_m^2\ell^2 - 1}\sqrt{\kappa_n^2\ell^2 - 1} - \kappa_m\kappa_n\ell^2}$$
$$= - \frac{\kappa_m\kappa_n}{16\pi^2}\frac{1}{\sinh^2((\kappa_m\tilde{\tau} - \kappa_n\tau)/2 - \mathrm{i}\varepsilon) - b_{mn}} \tag{B.9}$$

with $\kappa_i = 1/\sqrt{\ell^2 - r_i^2}$ and

$$b_{mn} = - \frac{1}{2}\big(1 + \kappa_m r_m \kappa_n r_n - \kappa_m\kappa_n\ell^2\big) = \frac{1}{2}\Big(\kappa_m\kappa_n l^2 - \sqrt{\kappa_m^2\ell^2 - 1}\sqrt{\kappa_n^2\ell^2 - 1} - 1\Big). \tag{B.10}$$

As we know, that $r_i^2 \leq \ell^2$. We can directly see that b_{mn} is non-negative when introducing a rescaled variable $x_i = \frac{r_i}{\ell}$ whose absolute value is always smaller than one. For the parameter b_{mn} we obtain

$$b_{mn} = \frac{1}{2}\left(\frac{(1 - x_m x_n)}{\sqrt{1 - x_m^2}\sqrt{1 - x_n^2}} - 1\right)$$

Here we can see that b_{mn} vanishes for identical trajectories ($x_m = x_n$) and is positive otherwise.

B.11. Fourier expansion of Wightman function

Here, we derive the Fourier expansion of the Wightman function in terms of its variable

$$s = \kappa_m\tilde{\tau} - \kappa_n\tau$$

The variable s is a variable whose dimension is the product of time and acceleration. The Wightman function from eq. (B.9), which we now expand in terms of its Fourier modes, is

$$W_{m,n}(s) = \frac{a}{\sinh^2(s/2 - \mathrm{i}\varepsilon) - b_{mn}} \qquad \text{with} \quad a = -\frac{\kappa_m\kappa_n}{16\pi^2}$$

The Fourier transform of the Wightman function is defined in terms of the variable λ

$$\widetilde{\mathcal{W}}_{m,n}(\lambda) = \mathcal{F}[W_{m,n}(s)](\lambda) = \frac{1}{\sqrt{2\pi}}\int_{-\infty}^{\infty} W_{m,n}(s)e^{-\mathrm{i}\lambda s}\mathrm{d}s \tag{B.11}$$

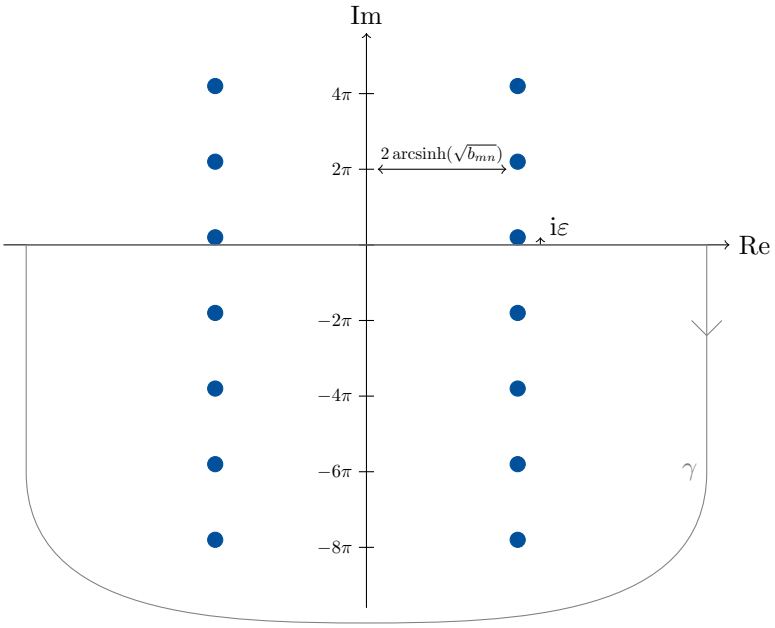

Figure 42.: Visualization of solving the integral from eq. (B.11) using Residue theorem where the blue dots are the poles of the function $W_{m,n}(s)$ and the gray line is the integration contour

The poles of the Wightman function lie at

$$s_n = \left\{ \pm 2 \operatorname{arcsinh}\left(\sqrt{b_{mn}}\right) + 2\mathrm{i}\pi n \right\} \quad \text{with } n \in \mathbb{Z}$$

The $\mathrm{i}\varepsilon$ in the argument of the sinh hereby shifts the pole off the real axis, which is the curve we evaluate the integral on as depicted in 42. We use the Residue theorem to evaluate the integral:

$$\oint_\gamma W_{m,n}(s) e^{-\mathrm{i}\lambda s} \mathrm{d}s = 2\pi\mathrm{i} \sum_{n=1}^{N} I(\gamma, s_n) \mathrm{Res}(W_{m,n}(s) e^{-\mathrm{i}\lambda s}, s_n)$$

where t_n are the poles, the winding number $I(\gamma, t_n)$ is one if the pole is in the interior of γ and 0 if the pole is outside. Its sign depends on the orientation of the curve: for clockwise integration curves, we get a minus sign. The integration contour γ is chosen along the real axis and closed via a half circle in the negative imaginary plane around all poles with negative n.

$$\mathrm{Res}_n^1 = \mathrm{Res}\left(W_{m,n}(s) e^{-\mathrm{i}\lambda s}, 2 \operatorname{arcsinh}\left(\sqrt{b_{mn}}\right) + 2\mathrm{i}\pi n\right) = \frac{a e^{2\lambda\left(\pi n - \mathrm{i} \operatorname{arcsinh}\left(\sqrt{b_{mn}}\right)\right)}}{\sqrt{b_{mn}(b_{mn}+1)}}$$

$$\mathrm{Res}_n^2 = \mathrm{Res}\left(W_{m,n}(s) e^{-\mathrm{i}\lambda s}, -2 \operatorname{arcsinh}\left(\sqrt{b_{mn}}\right) + 2\mathrm{i}\pi n\right) = -\frac{a e^{2\lambda\left(\pi n + \mathrm{i} \operatorname{arcsinh}\left(\sqrt{b_{mn}}\right)\right)}}{\sqrt{b_{mn}(b_{mn}+1)}}$$

As a solution to the integral B.11, we get

$$\oint_\gamma W_{m,n}(s) e^{-\mathrm{i}\lambda s} \mathrm{d}s = -2\pi\mathrm{i} \sum_{n=1}^{\infty} \left(\mathrm{Res}_{-n}^1 + \mathrm{Res}_{-n}^2\right) = -\frac{4\pi a \sin\left(2\lambda \operatorname{arcsinh}\left(\sqrt{b_{mn}}\right)\right)}{\sqrt{b_{mn}(b_{mn}+1)}(e^{2\pi\lambda}-1)}$$

$$\widetilde{\mathcal{W}}_{m,n}(\lambda) = \frac{1}{\sqrt{2\pi}} \oint_\gamma W_{m,n}(s) e^{-\mathrm{i}\lambda s} \mathrm{d}s = -\frac{1}{\sqrt{2\pi}} \frac{4\pi a \sin\left(2\lambda \operatorname{arcsinh}\left(\sqrt{b_{mn}}\right)\right)}{\sqrt{b_{mn}(b_{mn}+1)}(e^{2\pi\lambda}-1)}$$

With the inverse Fourier transform, we can express the Wightman function in terms of its Fourier modes:

$$W_{m,n}(s) = \frac{1}{\sqrt{2\pi}} \int_{-\infty}^{\infty} \widetilde{\mathcal{W}}_{m,n}\,(\lambda) e^{\mathrm{i}\lambda s} \mathrm{d}\lambda = -\int_{-\infty}^{\infty} \frac{2a \sin\bigl(2\lambda \operatorname{arcsinh}\bigl(\sqrt{b_{mn}}\bigr)\bigr)}{\sqrt{b_{mn}(b_{mn}+1)}(e^{2\pi\lambda}-1)} e^{\mathrm{i}\lambda s} \mathrm{d}\lambda \tag{B.12}$$

Appendix C

Symmetries

C.1. Matrix representation for the action of isometries on the future boundary of de Sitter spacetime

In this appendix, we explicitly calculate the coordinate representation of the homomorphism

$$h : \mathrm{SL}(2,\mathbb{R}) \to \mathrm{SO}(1,2)$$

introduced in eq. (5.1).
We introduced an auxiliary vector space $\mathcal{V}$ with the following basis elements:

$$e_1 = \mathrm{i}\sigma_y = \begin{pmatrix} 0 & 1 \\ -1 & 0 \end{pmatrix}, \quad e_2 = \sigma_x = \begin{pmatrix} 0 & 1 \\ 1 & 0 \end{pmatrix}, \quad e_3 = \sigma_z = \begin{pmatrix} 1 & 0 \\ 0 & -1 \end{pmatrix}.$$

With respect to this basis, the bilinear form

$$\langle x, y\rangle = \frac{1}{2}\,\mathrm{tr}(xy) \quad \text{with } x, y \in \mathcal{V}.$$

the matrix elements $\langle e_j, e_k\rangle$ are equivalent to the Minkowski metric with matrix representation:

$$\begin{pmatrix} \langle e_1, e_1\rangle & \langle e_1, e_2\rangle & \langle e_1, e_3\rangle \\ \langle e_2, e_1\rangle & \langle e_2, e_2\rangle & \langle e_2, e_3\rangle \\ \langle e_3, e_1\rangle & \langle e_3, e_2\rangle & \langle e_3, e_3\rangle \end{pmatrix} = \begin{pmatrix} -1 & 0 & 0 \\ 0 & 1 & 0 \\ 0 & 0 & 1 \end{pmatrix},$$

This allows us to identify Minkowski spacetime $\mathbb{R}^{1,2}$ with the vector space $\mathcal{V}$ via the matrix representation $\eta_{jk} = \langle e_j, e_k\rangle$.

We now explicitly calculate the matrix elements of the transformation $h \in \mathrm{SO}(1,2)$ corresponding to a given element $g \in \mathrm{SL}(2,\mathbb{R})$ with matrix representation

$$g = \begin{pmatrix} a & b \\ c & d \end{pmatrix}.$$

Any $x \in \mathcal{V}$ can be expressed as a linear combination of the basis elements e_1, e_2, and e_3. In order to express the function h with respect to this basis, we exploit the homomorphism:

$$e_j \mapsto g e_j g^{-1} \equiv h_{1j}\, e_1 + h_{2j}\, e_2 + h_{3j}\, e_3$$

This leads to the following matrix representation:

$$h(g) = \begin{pmatrix} \frac{1}{2}\big(a^2+b^2+c^2+d^2\big) & \frac{1}{2}\big(a^2-b^2+c^2-d^2\big) & -ab-cd \\ \frac{1}{2}\big(a^2+b^2-c^2-d^2\big) & \frac{1}{2}\big(a^2-b^2-c^2+d^2\big) & cd-ab \\ -ac-bd & bd-ac & bc+ad \end{pmatrix}. \tag{C.1}$$

Proof 18: Matrix representation of homeomorphism $h(g)$

$$
\begin{aligned}
e_1 \mapsto g e_1 g^{-1} &= \begin{pmatrix} -ac-bd & a^2+b^2 \\ -c^2-d^2 & ac+bd \end{pmatrix} \\
&= \frac{1}{2}\big(a^2+b^2+c^2+d^2\big)e_1 + \frac{1}{2}\big(a^2+b^2-c^2-d^2\big)e_2 + (-ac-bd)e_3 \\
&\equiv h_{11}e_1 + h_{21}e_2 + h_{31}e_3 \\
e_2 \mapsto g e_3 g^{-1} &= \begin{pmatrix} bd-ac & (a-b)(a+b) \\ d^2-c^2 & ac-bd \end{pmatrix} \\
&= \frac{1}{2}\big(a^2-b^2+c^2-d^2\big)e_1 + \frac{1}{2}\big(a^2-b^2-c^2+d^2\big)e_2 + (bd-ac)e_3 \\
&\equiv h_{12}e_1 + h_{22}e_2 + h_{32}e_3 \\
e_3 \mapsto g e_2 g^{-1} &= \begin{pmatrix} 2ad-1 & -2ab \\ 2cd & 1-2ad \end{pmatrix} \\
&= (-ab-cd)e_1 + (-ab+cd)e_2 + (ad+bc)e_3 \\
&\equiv h_{13}e_1 + h_{32}e_2 + h_{33}e_3
\end{aligned}
$$

which is exactly the result from the matrix representation in eq. (C.1). □

C.2. Action of homomorphism applied to null geodesics

The action of the homomorphism $h : \mathrm{SL}(2,\mathbb{R}) \to \mathrm{SO}(1,2)$ on the null geodesics has the following form:

$$
x(s) = \begin{pmatrix} s \\ u+vs \\ v-us \end{pmatrix} \quad \to \quad x'(s') = h(g)x(s) = \begin{pmatrix} s' \\ u'+v's' \\ v'-u's' \end{pmatrix} = \begin{pmatrix} x'_0 \\ x'_1 \\ x'_2 \end{pmatrix}
$$

This can be expanded in matrix form using the matrix form of the homeomorphism from eq. (C.1):

$$
x' = \begin{pmatrix} \frac{1}{2}\big((sv+u)\big(a^2-b^2+c^2-d^2\big) + s\big(a^2+b^2+c^2+d^2\big)\big) + (su-v)(ab+cd) \\ \frac{1}{2}\big((sv+u)\big(a^2-b^2-c^2+d^2\big) + s\big(a^2+b^2-c^2-d^2\big)\big) + (v-su)(cd-ab) \\ (v-su)(ad+bc) + (sv+u)(bd-ac) - s(ac+bd) \end{pmatrix}.
$$

We are interested in the symmetry action of the temporal boundaries, from which we infer the transformation rules of the tessellation and, therefore, our holographic network. By considering the limit $s' \to \infty$ we obtain the action of $h(g)$ on the temporal future boundary $\mathcal{I}^+$:

$$
\frac{x'(s)}{s'} = \begin{pmatrix} 1 \\ \frac{u'}{s'} + v' \\ \frac{v'}{s'} - u' \end{pmatrix} \underset{s'\to\infty}{\longrightarrow} \begin{pmatrix} 1 \\ v' \\ -u' \end{pmatrix}.
$$

With this expression for the symmetry action on the future boundary of de Sitter spacetime, the parameters u' and v' can easily be calculated using the relation derived in appendix A.6.1. The new parameters u' and v' satisfy the condition $u'^2 + v'^2 = 1$.

$$
u' = \frac{x'_1 - x'_0 x'_2}{1+(x'_0)^2} = \frac{-(-acu+adv+bcv+bdu)\big(u\big(a^2-b^2+c^2-d^2\big) - 2v(ab+cd)\big)}{2\Big(\frac{1}{4}\big(u(a^2-b^2+c^2-d^2) - 2v(ab+cd)\big)^2 + 1\Big)}
$$

$$+\frac{u\big(a^2-b^2-c^2+d^2\big)+v(2cd-2ab)}{2\Big(\frac{1}{4}(u(a^2-b^2+c^2-d^2)-2v(ab+cd))^2+1\Big)}$$

$$v'=\frac{x_2'+x_0'x_1'}{1+(x_0')^2}=\frac{\frac{1}{4}\big(u\big(a^2-b^2-c^2+d^2\big)-2abv+2cdv\big)\big(u\big(a^2-b^2+c^2-d^2\big)-2v(ab+cd)\big)}{\frac{1}{4}(u(a^2-b^2+c^2-d^2)-2v(ab+cd))^2+1}$$

$$+\frac{u(bd-ac)+v(2ad-1)}{\frac{1}{4}(u(a^2-b^2+c^2-d^2)-2v(ab+cd))^2+1}.$$

Appendix D

Holographic network

D.1. Distance time-slices

The size of de Sitter spacetime at the time τ is easiest derived in global coordinates

$$\vec{x}_G = \begin{pmatrix} \ell \sinh(\tau/\ell) \\ \ell \cos\theta \cosh(\tau/\ell) \\ \ell \sin\theta \cosh(\tau/\ell) \end{pmatrix}$$

where $\ell \cosh(\tau/\ell)$ is the radius of de Sitter spacetime at fixed time τ. The size of $1+1$ dimensional de Sitter spacetime at time τ accordingly is

$$d_{\mathrm{dS}}(\tau) = 2\pi\ell \cosh(\tau/\ell),$$

The time-slices in global and conformal coordinates are related as $\cosh\tau_n = \frac{1}{\cos T_n}$.
The ratio of the size of de Sitter spacetime at the consecutive time slices τ_n and τ_{n+1} is given by

$$\frac{d_{\mathrm{dS}}(\tau_{n+1})}{d_{\mathrm{dS}}(\tau_n)} = \frac{\cos\left(\frac{\pi}{2}(1-2^{-n})\right)}{\cos\left(\frac{\pi}{2}(1-2^{-(n+1)})\right)} \overset{n\to\infty}{\longrightarrow} 2.$$

D.2. Tensor network for smaller curvatures is partial isometry

Here we show, that the tensor network for larger de Sitter radii and with that for de Sitter spacetimes with smaller curvatures also is a partial isometry.

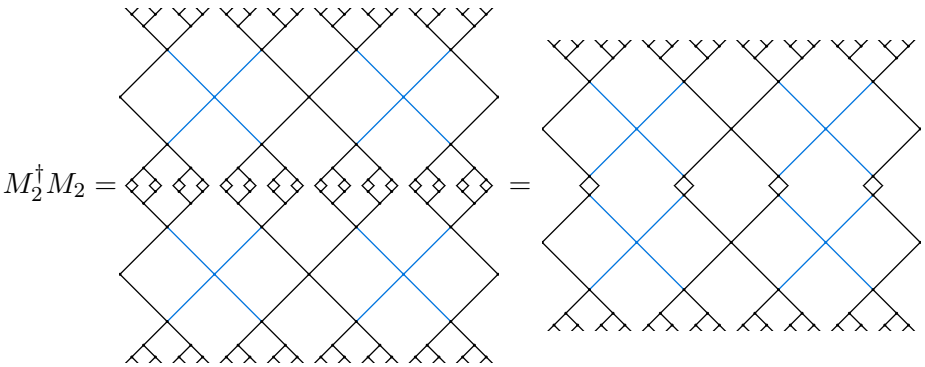

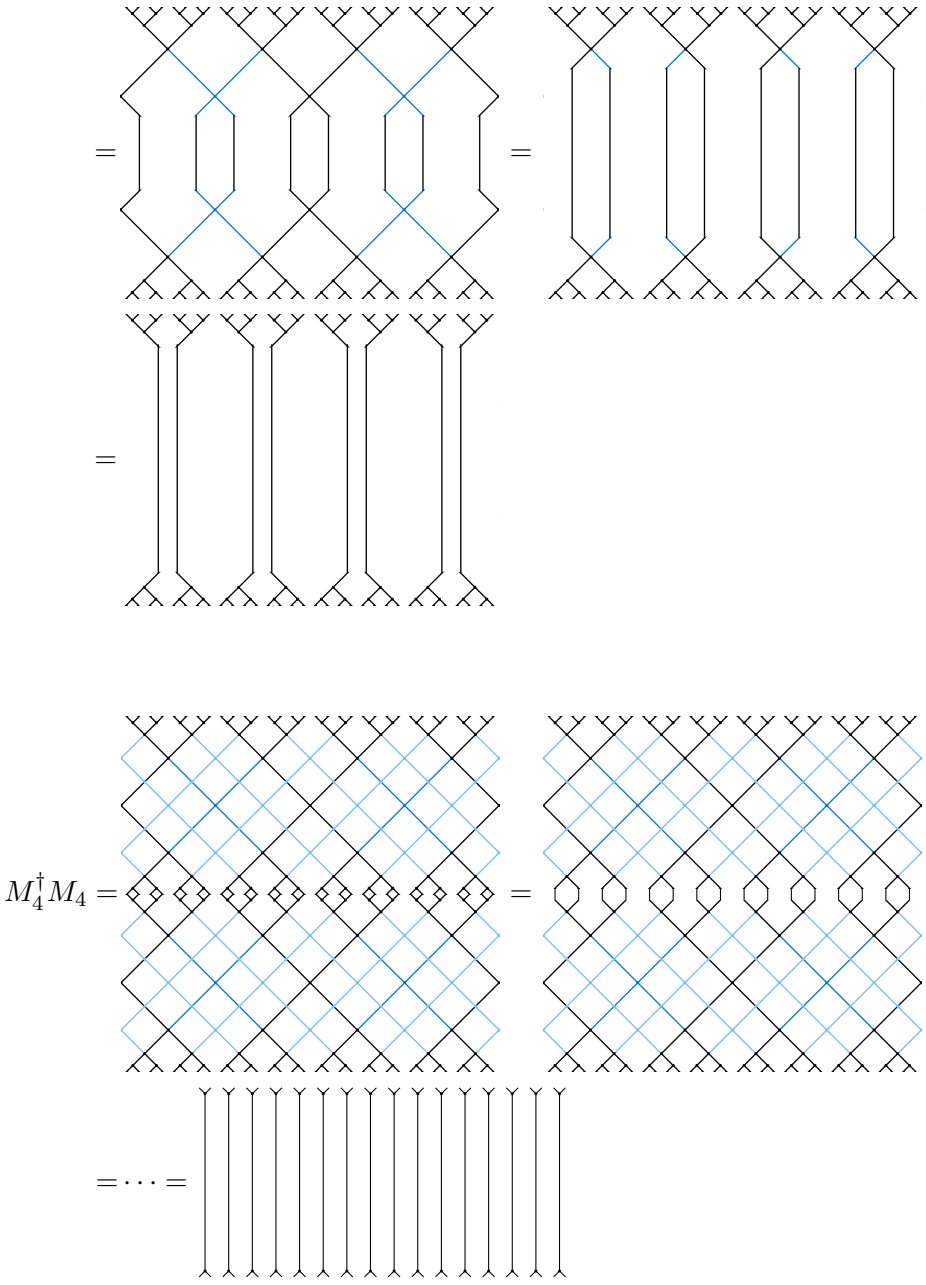

D.3. Transformed tensor network is partial isometry (unitary representation)

$$
\begin{aligned}
P_f \equiv (M^f)^\dagger M^f =& \Big(U(f)MU(S)^\dagger U(f)^\dagger U(S)^\dagger\Big)^\dagger U(f)MU^\dagger(S)U^\dagger(f)U(S)^\dagger \\
=& U(S)U(f)U(S)M^\dagger U(f)^\dagger U(f)MU^\dagger(S)U^\dagger(f)U(S)^\dagger \\
=& U(S)U(f)U(S)M^\dagger MU^\dagger(S)U^\dagger(f)U(S)^\dagger \\
P_f^2 =& U(S)U(f)U(S)M^\dagger MU^\dagger(S)U^\dagger(f)U(S)^\dagger U(S)U(f)U(S)M^\dagger MU^\dagger(S)U^\dagger(f)U(S)^\dagger \\
=& U(S)U(f)U(S)M^\dagger MM^\dagger MU^\dagger(S)U^\dagger(f)U(S)^\dagger \\
=& U(S)U(f)U(S)M^\dagger MU^\dagger(S)U^\dagger(f)U(S)^\dagger \\
=& P_f
\end{aligned}
$$

D.4. Invariance of vacuum state

In order to show that the vacuum state is invariant under the family of tensor networks M^f, we apply the vacuum state to the tensor network and perform the first simplifications in more detail. Here, the tensors corresponding to the tensor network are (first) depicted in gray:

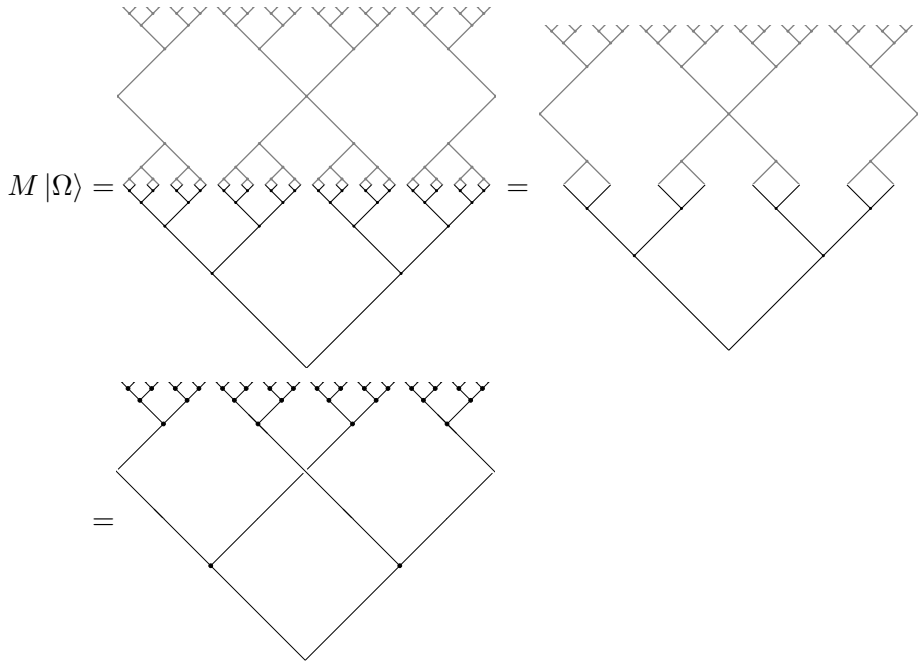

In the last step, we have introduced the braiding condition. This is simplified further in the main part (section 6.5.3). This also describes the action of M^S since this tensor network has the same shape as M.

The same thing can is done for C which is the second generator of $\mathrm{PSL}(2,\mathbb{Z})$:

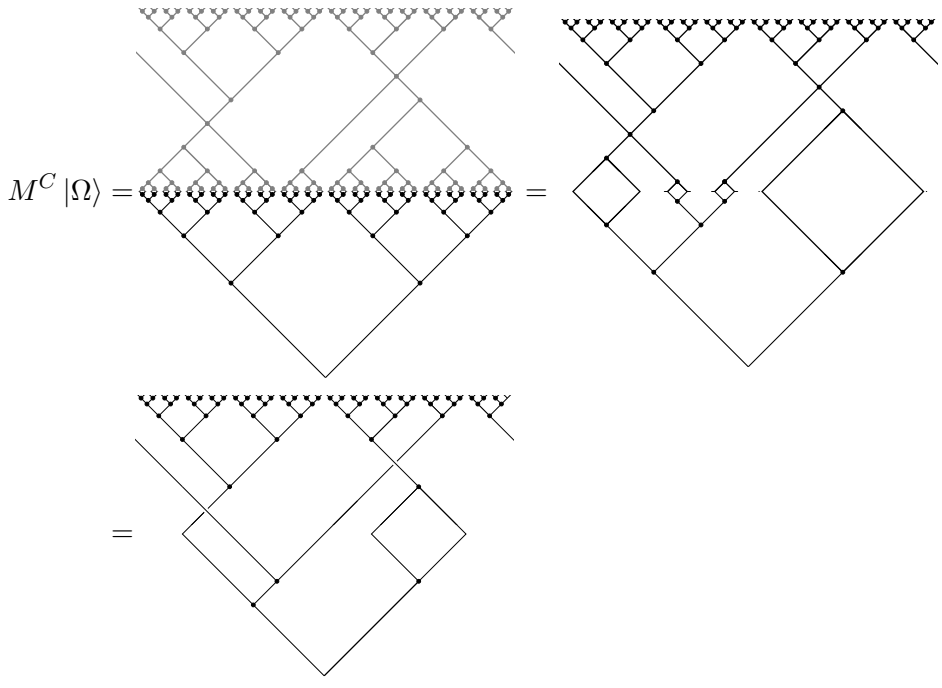

Here, we have introduced both the braiding and pivotality conditions in the last step.

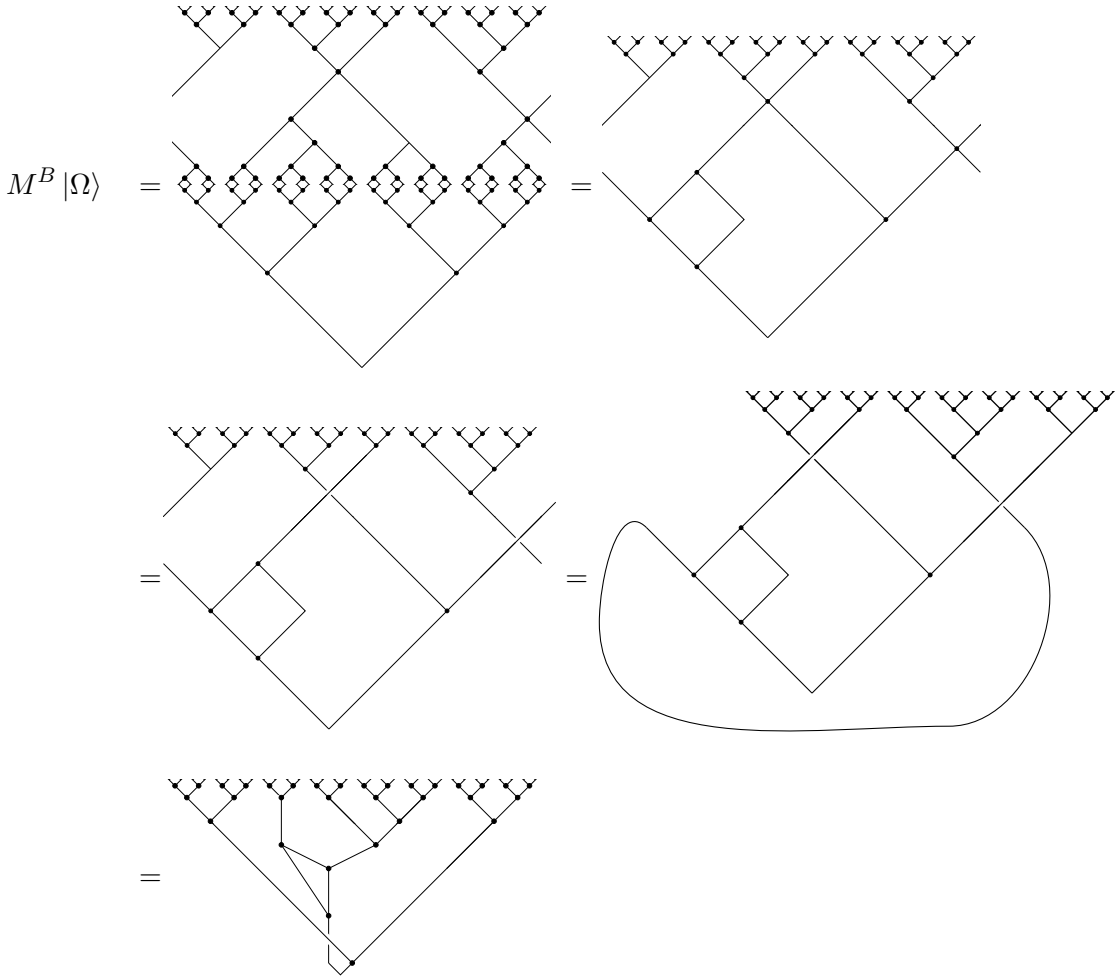

D.5. Modify physical state in contracting spacetime

The spacetime dynamics of a contracting universe can be described with an isometry $V^\dagger$ where the dimension of $\mathcal{H}_{\text{in}} = \mathfrak{h}^{\otimes m}$ is larger than the dimension of $\mathcal{H}_{\text{out}} = \mathfrak{h}^{\otimes n}$ with $m > n$. A contracting part of the tensor network is characterized by the following adjoint isometry:

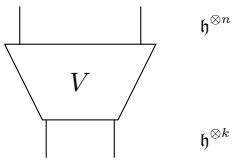

$$V^\dagger : \mathcal{H}_{\text{in}} \to \mathcal{H}_{\text{out}} = \mathfrak{h}^{\otimes m} \to \mathfrak{h}^{\otimes n} \quad \text{with } n < m.$$

This isometry satisfies the identity $V^\dagger V = \mathbb{1}_n$. A new state $|\psi'\rangle \in \mathcal{H}_{\text{in}}$ at a finite timeslice of a contracting spacetime again has to fulfil the condition from eq. 7.2: This is directly solved by the following state $|\psi'\rangle$:

$$|\psi'\rangle = V\mathcal{W}V^\dagger\,|\psi\rangle$$

It is straightforward to see, that this state is normalized:

$$\langle\psi'|\psi'\rangle = \Big(\langle\psi|\,V\mathcal{W}^\dagger V^\dagger\Big)\Big(V\mathcal{W}V^\dagger\,|\psi\rangle\Big) = \langle\psi|\,VV^\dagger\,|\psi\rangle = \langle V^\dagger\psi|V^\dagger\psi\rangle = 1$$

D.6. Haar integral identity

First, we introduce some basic identities. The swap operation can be expressed with respect to an orthonormal basis λ^α as follows:

$$\text{swap} = \sum_\alpha (\lambda^\alpha \otimes \mathbb{1})(\mathbb{1} \otimes \lambda^\alpha) = \sum_\alpha \lambda^\alpha \otimes \lambda^\alpha = \sum_\alpha$$

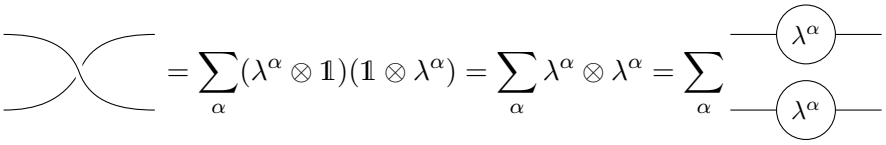

(D.1)

By connecting the two outputs we can directly derive another identity:

$$\sum_\alpha \quad = \sum_\alpha \quad = \quad = d\mathbb{1}$$

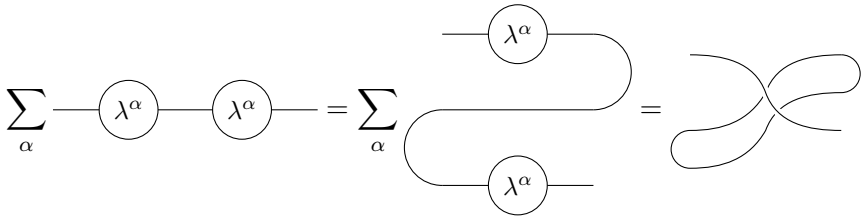

(D.2)

With this we can derive the identity of the Haar integral S_2:

$$S_2 = \int \mathrm{d}U\, U^\dagger \otimes U = \frac{1}{d}\text{swap} \tag{D.3}$$

Proof 19: Identity for Haar integral S_2 from eq. (D.3)
We consider the Haar integral S_2 and make an infinitesimal substitution:

$$\begin{aligned}
S_2 =& \int dU\, U^\dagger \otimes U \mapsto \int dU\, (U^\dagger e^{-i\epsilon X}) \otimes (e^{i\epsilon X} U) \\
=& \int dU\, (U^\dagger(\mathbb{1} - i\varepsilon X) \otimes (\mathbb{1} + i\varepsilon X)U) + \mathcal{O}(\varepsilon^2) \\
=& \int dU \left[U^\dagger \otimes U - i\varepsilon U^\dagger X \otimes U + i\varepsilon U^\dagger \otimes XU\right] + \mathcal{O}(\varepsilon^2) \\
=& S_2 - i\varepsilon S_2(X \otimes \mathbb{1}) + i\varepsilon(\mathbb{1} \otimes X)S_2 + \mathcal{O}(\varepsilon^2) \\
\Rightarrow 0 =& (\mathbb{1} \otimes X)S_2 - S_2(X \otimes \mathbb{1})
\end{aligned}$$

We choose the hermitian operator X to be a Hilbert-Schmidt orthonomal operator basis λ^α and right-multiply with $(\lambda^\alpha \otimes \mathbb{1})$. Summing over α yields

$$\sum_\alpha \quad = \sum_\alpha S_2(\lambda^\alpha \lambda^\alpha \otimes \mathbb{1}) = \sum_\alpha (\mathbb{1} \otimes \lambda^\alpha) S_2 (\lambda^\alpha \otimes \mathbb{1})$$

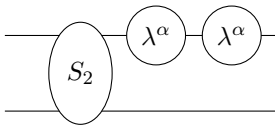

$$= \sum_\alpha$$

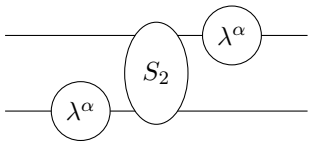

We now use the identities of the swap operation (D.1) and the swap operation with connected outputs (D.2):

d

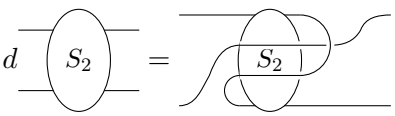

The integral representation of S_2 directly gives

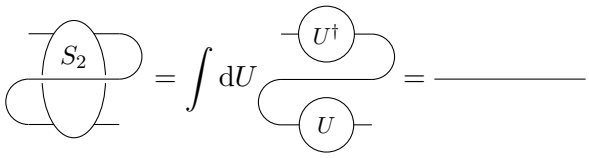

Plugging all this together we get

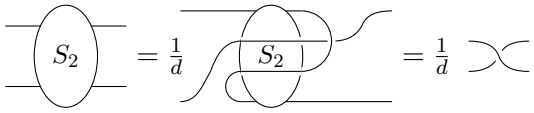

□

The Haar integral we are really interested in is of the form

$$S_4 = \int dU \Big(U^\dagger \otimes U^\dagger \otimes U \otimes U \Big) = \int \mathrm{d}U$$

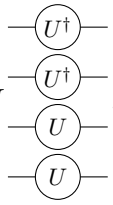

.

We will derive the following identity for the operator S_4.

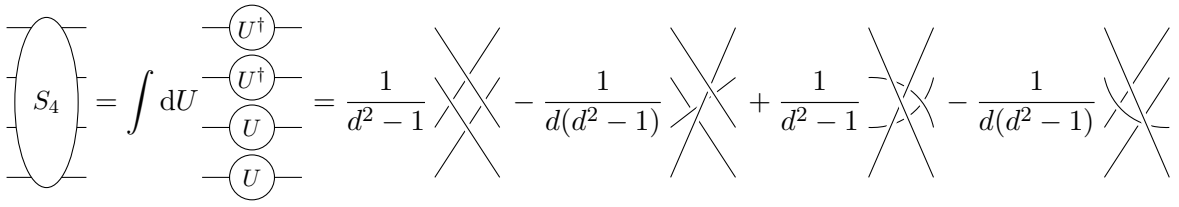

(D.4)

Proof 20: Indentity for Haar integral S_4 from eq. (D.4)
To derive this identity we make an infinitesimal change of variables $U \mapsto e^{i\varepsilon X}U$. We consider X to be a hermitian operator and evaluate the expression to first order in ε:

$$\begin{aligned}
S_4 &= \int dU \Big(U^\dagger \otimes U^\dagger \otimes U \otimes U \Big) \mapsto \int dU \Big(\big(e^{i\varepsilon X}U\big)^\dagger \otimes \big(e^{i\varepsilon X}U\big)^\dagger \otimes e^{i\varepsilon X}U \otimes e^{i\varepsilon X}U \Big) \\
&= \int dU \Big(U^\dagger e^{-i\varepsilon X} \otimes U^\dagger e^{-i\varepsilon X} \otimes e^{i\varepsilon X}U \otimes e^{i\varepsilon X}U \Big) \\
&= \int dU \Big(U^\dagger(\mathbb{1} - i\varepsilon X) \otimes U^\dagger(\mathbb{1} - i\varepsilon X) \otimes (\mathbb{1} + i\varepsilon X)U \otimes (\mathbb{1} + i\varepsilon X)U \Big) + \mathcal{O}(\varepsilon^2) \\
&= \int dU \Big[\Big(U^\dagger \otimes U^\dagger \otimes U \otimes U \Big) - i\varepsilon \Big(U^\dagger X \otimes U^\dagger \otimes U \otimes U \Big) - i\varepsilon \Big(U^\dagger \otimes U^\dagger X \otimes U \otimes U \Big) \\
&\quad + i\varepsilon \Big(U^\dagger \otimes U^\dagger \otimes XU \otimes U \Big) + i\varepsilon \Big(U^\dagger \otimes U^\dagger \otimes U \otimes XU \Big) \Big] + \mathcal{O}(\varepsilon^2) \\
&= S_4 - i\varepsilon S_4(X \otimes \mathbb{1} \otimes \mathbb{1} \otimes \mathbb{1}) - i\varepsilon S_4(\mathbb{1} \otimes X \otimes \mathbb{1} \otimes \mathbb{1}) + i\varepsilon(\mathbb{1} \otimes \mathbb{1} \otimes X \otimes \mathbb{1})S_4 \\
&\quad + i\varepsilon(\mathbb{1} \otimes \mathbb{1} \otimes \mathbb{1} \otimes X)S_4 + \mathcal{O}(\varepsilon^2)
\end{aligned}$$

It directly follows:

$$S_4(X \otimes \mathbb{1} \otimes \mathbb{1} \otimes \mathbb{1}) + S_4(\mathbb{1} \otimes X \otimes \mathbb{1} \otimes \mathbb{1}) = (\mathbb{1} \otimes \mathbb{1} \otimes X \otimes \mathbb{1})S_4 + (\mathbb{1} \otimes \mathbb{1} \otimes \mathbb{1} \otimes X)S_4 \quad \text{(D.5)}$$

which holds for all hermitian operators X. We choose $X = \lambda^\alpha$ to be the Hilbert-Schmidt orthonomal operator basis with $\mathrm{tr}(\lambda^\alpha \lambda^\beta) = \delta^{\alpha\beta}$ and right-multiply (D.5) with $(\lambda^\alpha \otimes \mathbb{1} \otimes \mathbb{1} \otimes \mathbb{1})$. In tensor network notation we then get

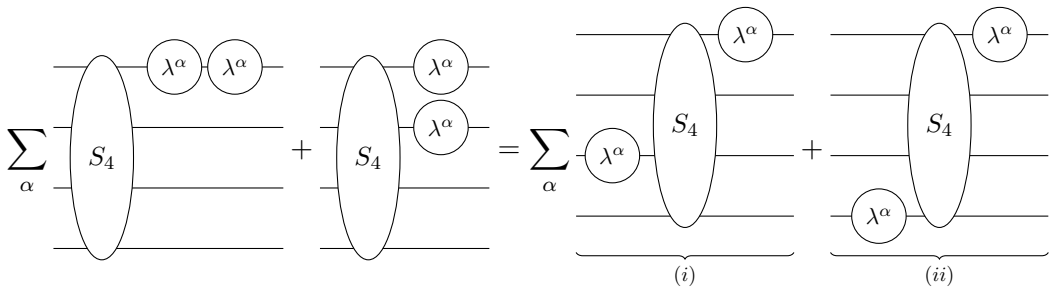

(D.6)

To simplify this further we use the identity for the Haar integral S_2 eq. (D.3):

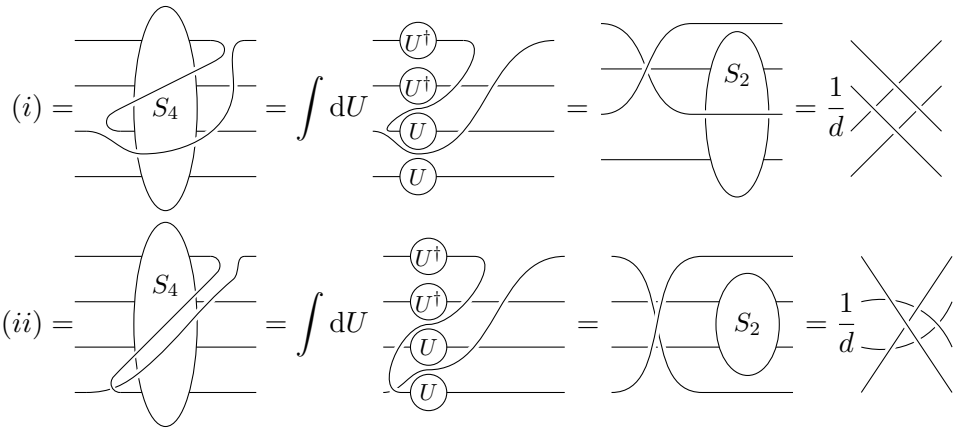

The LHS of (D.6) can be factorized as

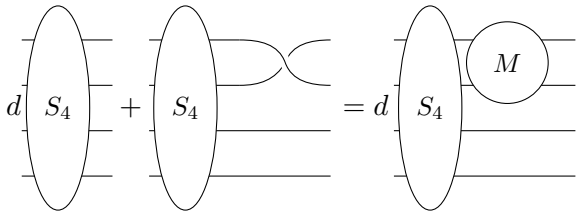

where

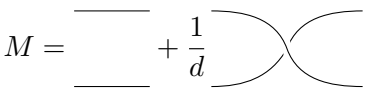

The inverse of M is

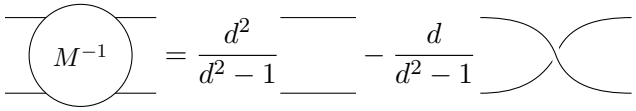

This results is a simplified version of eq. (D.6):

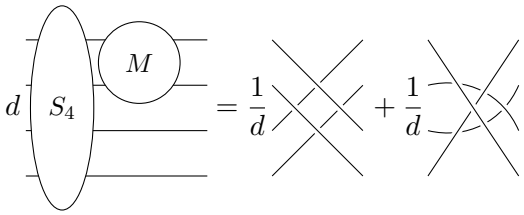

(D.7)

We can derive the identity (D.4) for S_4 by right-multiplying both sides of eq. (D.7) with $M^{-1}\otimes\mathbb{1}\otimes\mathbb{1}$:

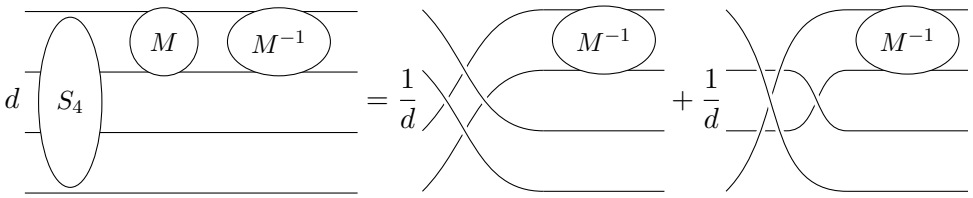

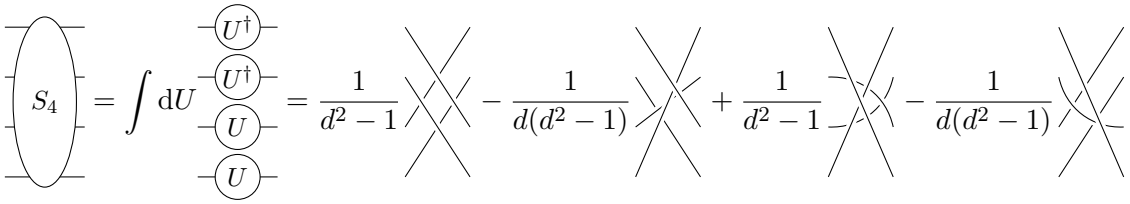

□

To apply the identity from D.4 and calculate the Haar integral in (7.6) we need to reorder the expression and adapt it do the different order of U and $U^\dagger$:

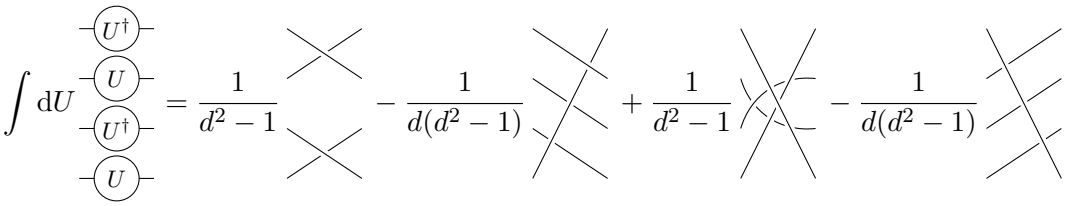

D.7. Calculation Haar Integral

We introduce a color code for the lines to keep track of the dimensions:

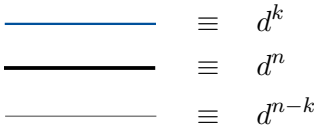

We want to calculate the Haar integral using the identity derived in (7.7) where the dimension of the entire system is d^n:

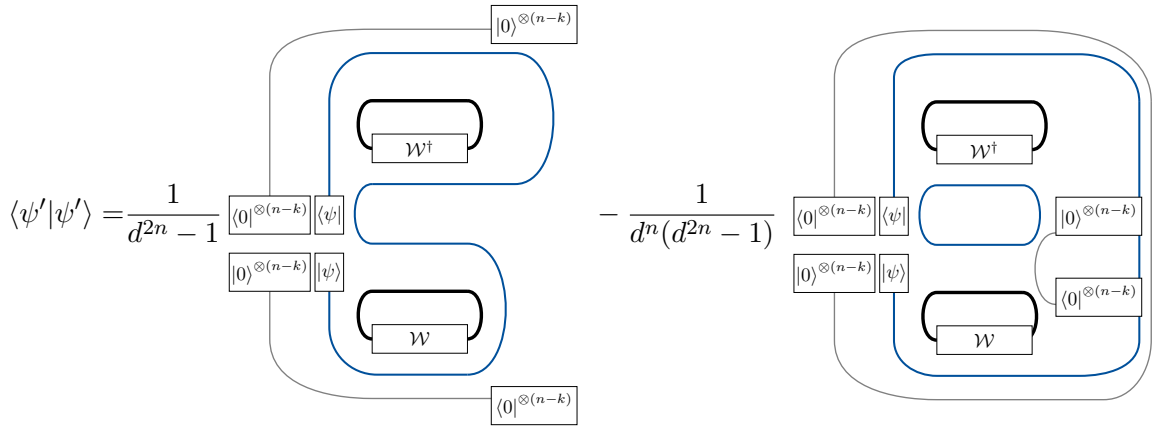

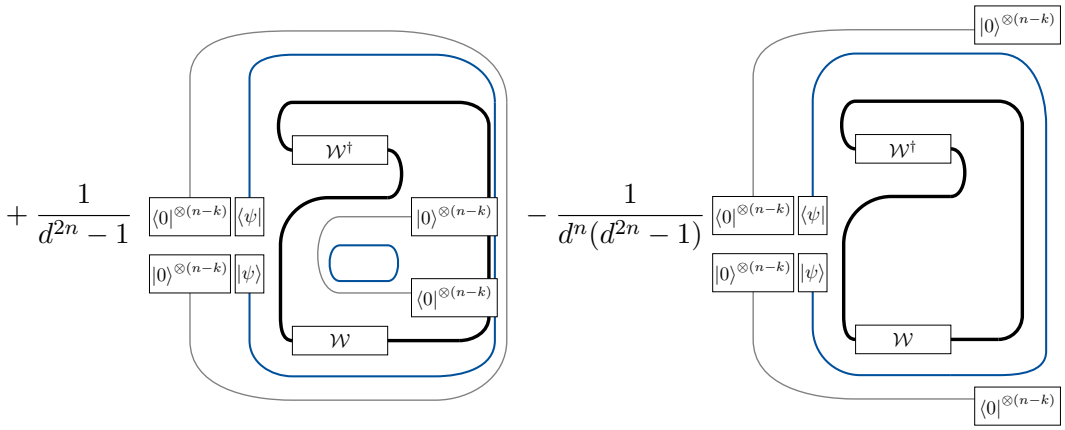

the tensor network expressions translate back as follows:

$$d^k =$$

$$d^n = \operatorname{tr}(W^\dagger W) d^{n-1} =$$

$\mathcal{W}^\dagger$
$\mathcal{W}$

$$1 = \langle 0|0\rangle^{\otimes(n-k)} =$$

$|0\rangle^{\otimes(n-k)}$ $\langle 0|^{\otimes(n-k)}$

$$1 = \langle 0|0\rangle^{\otimes k} =$$

$|\psi\rangle$ $\langle\psi|$

$$d^{n-1}\operatorname{tr}(W) =$$

$\mathcal{W}$

This gives us the following result:

$$\begin{aligned}
\langle\Omega'|\Omega'\rangle =& \frac{1}{d^{2n}-1}\langle\Omega|\Omega\rangle\langle 0|0\rangle^{\otimes(n-1)}\langle 0|0\rangle^{\otimes(n-1)} d^{n-1}\operatorname{tr}(W) d^{n-1}\operatorname{tr}(W^\dagger) \\
&- \frac{1}{d^n(d^{2n}-1)}\langle\Omega|\Omega\rangle\langle 0|0\rangle^{\otimes(n-1)}\langle 0|0\rangle^{\otimes(n-1)} d^k d^{n-1}\operatorname{tr}(W) d^{n-1}\operatorname{tr}(W^\dagger) \\
&+ \frac{1}{d^{2n}-1}\langle\Omega|\Omega\rangle\langle 0|0\rangle^{\otimes(n-1)}\langle 0|0\rangle^{\otimes(n-1)} d^k d^{n-1}\operatorname{tr}(W^\dagger W) \\
&- \frac{1}{d^n(d^{2n}-1)}\langle\Omega|\Omega\rangle\langle 0|0\rangle^{\otimes(n-1)}\langle 0|0\rangle^{\otimes(n-1)} d^{n-1}\operatorname{tr}(W^\dagger W) \\
=& \frac{d^{2n-2}}{d^{2n}-1}\operatorname{tr}(W)\operatorname{tr}(W^\dagger) - \frac{d^k d^{2n-2}}{d^n(d^{2n}-1)}\operatorname{tr}(W)\operatorname{tr}(W^\dagger) + \frac{d^k d^n}{d^{2n}-1} - \frac{d^n}{d^n(d^{2n}-1)} \\
=& \operatorname{tr}(W)\operatorname{tr}(W^\dagger)\frac{d^{2n-2}}{d^{2n}-1}\left(1-\frac{d^k}{d^n}\right) + \frac{d^n}{d^{2n}-1}\left(d^k - \frac{1}{d^n}\right) \\
=& |\operatorname{tr}(W)|^2\frac{d^{-2}}{1-d^{-2n}}\left(1-d^k d^{-n}\right) + \frac{d^{-n}}{1-d^{-2n}}\left(d^k - d^{-n}\right) \\
\langle\Omega'|\Omega'\rangle =& \frac{|\operatorname{tr}(W)|^2\left(1-d^k d^{-n}\right)}{d^2(1-d^{-2n})} + \frac{d^{-n}\left(d^k - d^{-n}\right)}{1-d^{-2n}}
\end{aligned}$$

Modification: consider a local operator acting on j sites:

$$\langle\Omega'|\Omega'\rangle = \operatorname{tr}(W)\operatorname{tr}(W^\dagger)\frac{d^{2(n-j)}}{d^{2n}-1}\left(1-\frac{d^k}{d^n}\right) + \frac{d^n}{d^{2n}-1}\left(d^k - \frac{1}{d^n}\right)$$

$$=|\operatorname{tr}(W)|^2 \frac{d^{-2j}}{1-d^{-2n}}\left(1-d^k d^{-n}\right)+\frac{d^{-n}}{1-d^{-2n}}\left(d^k-d^{-n}\right)$$

$$\lim_{n\to\infty}\langle\Omega'|\Omega'\rangle = |\operatorname{tr}(W)|^2 d^{-2j}$$

With the dimension of the operator W being d^j we can use the bound $|\operatorname{tr}(W)|^2 \leq (d^j)^2 = d^{2j}$:

$$\lim_{n\to\infty}\langle\Omega'|\Omega'\rangle \leq d^{2j}d^{-2j} = 1$$

D.8. Tracenorm of unitary operator

We want to show the bound from eq. (7.9):

$$|\operatorname{tr} W|^2 \leq d^2$$

We consider the unitary operator W, which acts on a subsystem $\mathfrak{h}$ of dimension d.

For any unitary operator W with eigenvalue λ the following holds:

$$W|\phi\rangle = \lambda|\phi\rangle \qquad \Rightarrow \qquad \langle\phi| W^\dagger = \langle\phi|\lambda^*$$

We can consider the norm of eigenstate $|\phi\rangle$:

$$\langle\phi|\phi\rangle = \langle\phi|\mathbb{1}|\phi\rangle = \langle\phi|W^\dagger W|\phi\rangle = \langle\phi|\lambda^*\lambda|\phi\rangle = |\lambda|^2\langle\phi|\phi\rangle$$

It directly follows (assuming $\lambda \neq 0$), that $|\lambda|^2 = 1$. Since the eigenvalues of a unitary matrix have norm 1 they can be written as

$$\lambda = e^{i\theta}$$

Bound

The trace of a (square) matrix equals the sum of the eigenvalues (counted with the respective multiplicities).

$$\begin{aligned}
\operatorname{tr} W &= \sum_{j=1}^{d} e^{i\theta_j} \\
|\operatorname{tr} W|^2 &= \left(\sum_{j=1}^{d} e^{i\theta_j}\right)\left(\sum_{k=1}^{d} e^{-i\theta_k}\right) = \sum_{j=1}^{d}\sum_{k=1}^{d} e^{i(\theta_j-\theta_k)} \\
&= \sum_{j=k=1}^{d} e^0 + \sum_{j=1}^{d}\sum_{k=j+1}^{d}\left(e^{i(\theta_j-\theta_k)} + e^{i(\theta_k-\theta_j)}\right) \\
&\qquad e^{i(a-b)} + e^{i(b-a)} = 2\cos(a-b) \\
&= d + 2\sum_{j=1}^{d}\sum_{k=j+1}^{d}\cos(\theta_j-\theta_k)
\end{aligned}$$

Since the range of $\cos(x)$ is the interval $[-1,1]$ this directly implies a bound for the trace:

$$|\operatorname{tr} W|^2 \leq d^2 \tag{D.8}$$

Condition for equality

We want to know, what needs to hold for (D.8) to be an equality. We know, that W is a unitary operator and therefore the rows and columns of W are orthonormal vectors. Since the columns are orthonormal vectors it directly follows, that

$$|[W]_{jk}| \leq 1$$

$$|\operatorname{tr} W| = d = \left| \sum_{j=1}^{d} [W]_{jj} \right| \leq \sum_{j=1}^{d} |[W]_{jj}| \leq \sum_{j=1}^{d} 1 = d$$

This can only be true if the above terms are equal and therefore the diagonal elements of the unitary operator W are equal to 1:

$$|[W]_{jj}| = 1$$

Since the vectors in the columns are normalized and the diagonal entries equal to 1 the off-diagonal elements have to be equal to 0.

Accordingly W has to be the identity if $|\operatorname{tr} W| = d$.

$$|\operatorname{tr}(W)|^2 = d^2 \Leftrightarrow W = \mathbb{1}$$

D.9. Local operator on a subsystem is maximally mixed

We can also look at the properties of a local density matrix of a subsystem j and how this system can be influenced by applying a operator $\mathcal{W}$ at the future boundary. We will show, that (for nontrivial $\mathcal{W}$) the local operator ρ_j is maximally mixed.

For all valid physical states (which for now is the vacuum state $|\Omega\rangle$ and for random isometries V the following holds:

$$\left|\left| \rho_j - \frac{\mathbb{1}}{d} \right|\right|_2^2 \leq \varepsilon \tag{D.9}$$

where $\rho_j = \operatorname{tr}_{\hat{j}}\left(V |\Omega\rangle \langle\Omega| V^\dagger\right)$.

In words: Any local operator which we could model using the described approach would be very close to the identity. No other local operations would be possible.

Note: We consider N to be the size of the system including n (output) tensor legs each having dimension d. The dimension of our local subsystem (which is attached to one tensor leg) has dimension d.

$$\begin{aligned} \left|\left| \rho_j - \frac{\mathbb{1}}{d} \right|\right|_2^2 &= \operatorname{tr}\left(\left(\rho_j - \frac{\mathbb{1}}{d} \right)^2 \right) = \operatorname{tr}\left(\left(\rho_j - \frac{\mathbb{1}}{d} \right) \left(\rho_j - \frac{\mathbb{1}}{d} \right) \right) \\ &= \operatorname{tr}\left(\rho_j^2 - \frac{2}{d}\rho_j + \frac{1}{d^2}\mathbb{1} \right) \end{aligned}$$

$$
\begin{aligned}
&= \operatorname{tr}\left(\rho_j^2\right) - \frac{2}{d}\operatorname{tr}(\rho_j) + \frac{1}{d^2}\operatorname{tr}(\mathbb{1}) \\
&= \operatorname{tr}\left(\rho_j^2\right) - \frac{2}{d} + \frac{1}{d^2}d \\
&= \operatorname{tr}\left(\rho_j^2\right) - \frac{1}{d}
\end{aligned}
$$

Sanity check: If we consider the state on subsystem j to be a pure state we know that

$$\operatorname{tr}\left(\rho_j^2\right) - \frac{1}{d} = \frac{1}{d} - \frac{1}{d} = 0 \leq \varepsilon$$

We now consider a more general reduced density operator on a single subsystem:

$$\operatorname{tr}(\rho_j^2) = \operatorname{tr}\left(\operatorname{tr}_{\hat{j}}\left(V\left|\Omega\right\rangle\left\langle\Omega\right|V^\dagger\right)^2\right)$$

We describe the random isometries using random unitaries with an attached ancilla system.
We consider a random unitary U and the initial state $|\Omega\rangle$.
For any arbitrary state $|\Omega\rangle$ there exists a unitary operator T such that

$$T\left|0\right\rangle^{\otimes n} = \left|\Omega\right\rangle\left|0\right\rangle^{\otimes(n-k)}$$

If we apply a random unitary U to this we get:

$$UT\left|0\right\rangle^{\otimes n} = U\left|\Omega\right\rangle\left|0\right\rangle^{\otimes(n-k)}$$

We can now translate $\operatorname{tr}(\rho_j^2)$ to tensor network notation where the trace operation is represented by joining up corresponding external tensor legs:

$\operatorname{tr}(\rho_j^2) =$

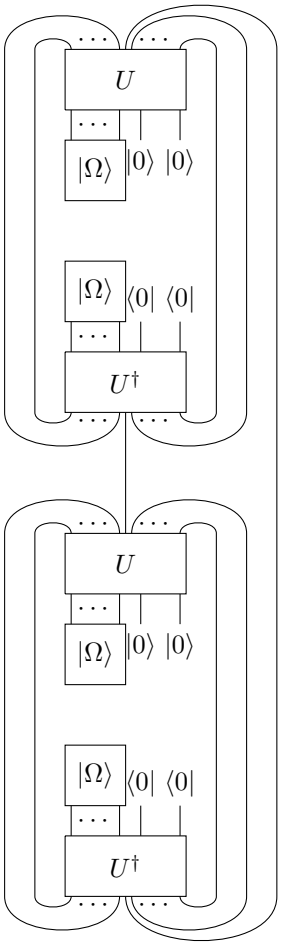

In order to evaluate this expression with a random unitary operator U we use the Haar measure introduced in (7.5). The Haar measure ist left- (respectively, right-) invariant, which is why the unitary T which describes the initial conditions is absorbed in the integral.

In order to apply the identity from (D.4) and calculate the Haar integral it is helpful to rearrange this expression (exchange operators 1 and 4) to be able to distinguish between incoming and outgoing legs more easily (left: input legs/past, right: output legs/future):

To make the figure less cluttered we introduce the following color code:

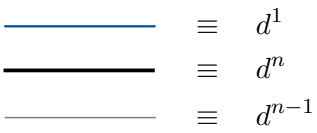

We use that the random isometry acting on the vacuum state can be encoded in a random unitary acting on a larger vacuum state with ancilla quibits and a fixed unitary operator. This fixed unitary operator can be neglected due to the right-invariance of the Haar measure.

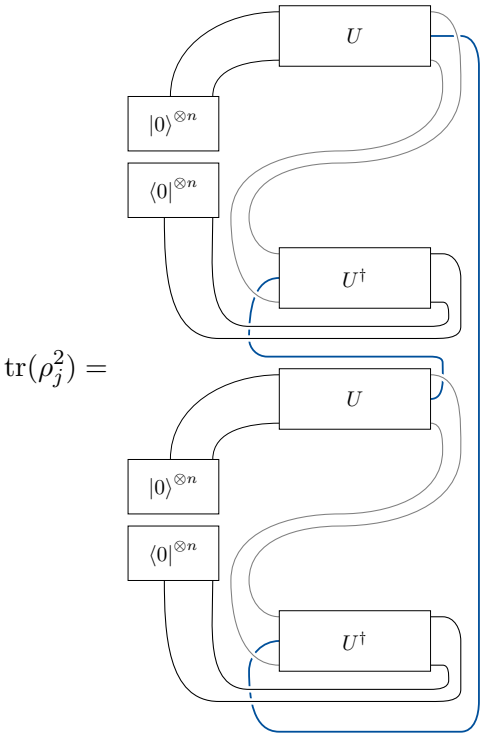

Because the order of the unitaries with and without daggers differs between this case and eq. (D.4) we need to take this reordering into account. The identity we need to apply now reads

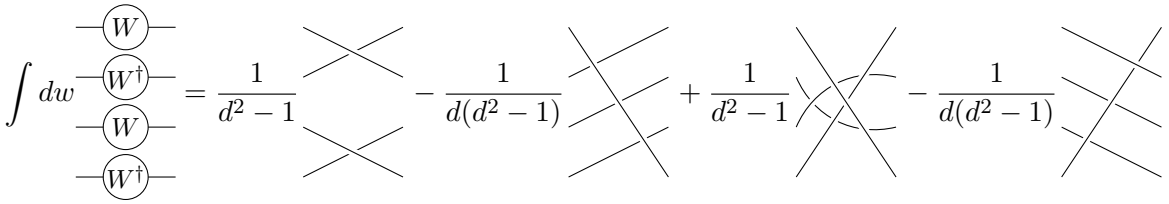

(D.10)

Therfore, we get four terms that we consider seperately.

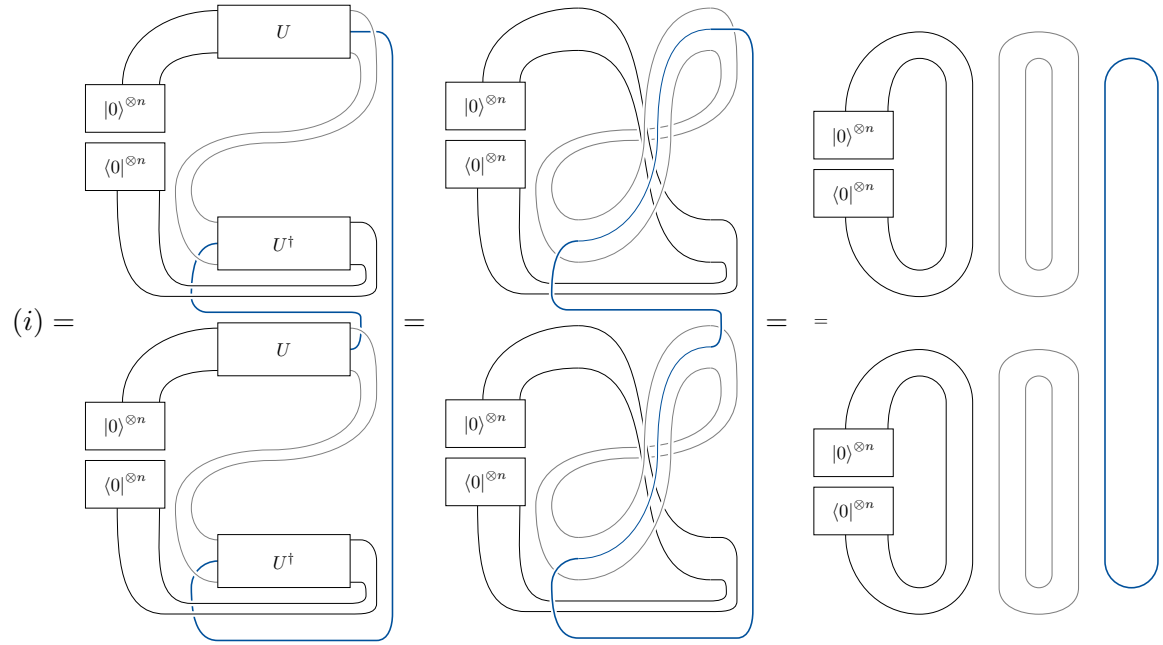
(i) =
U
$|0\rangle^{\otimes n}$
$\langle 0|^{\otimes n}$
$U^\dagger$
=
=
=

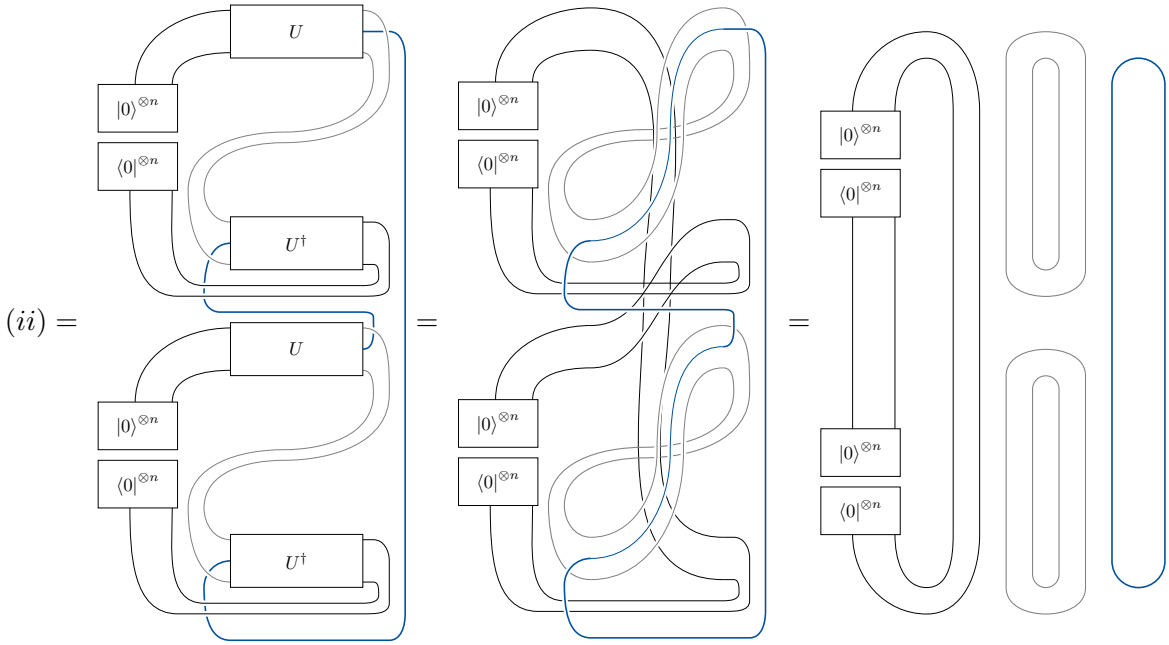
(ii) =
U
$|0\rangle^{\otimes n}$
$\langle 0|^{\otimes n}$
$U^\dagger$
=
=

$(iii) =$

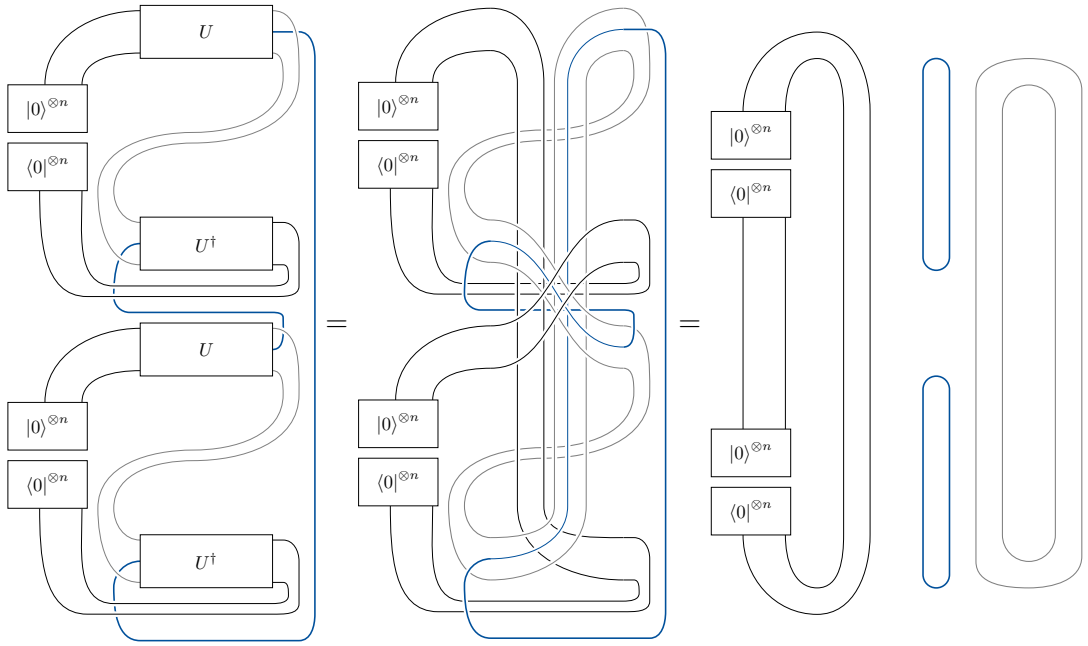

$(iv) =$

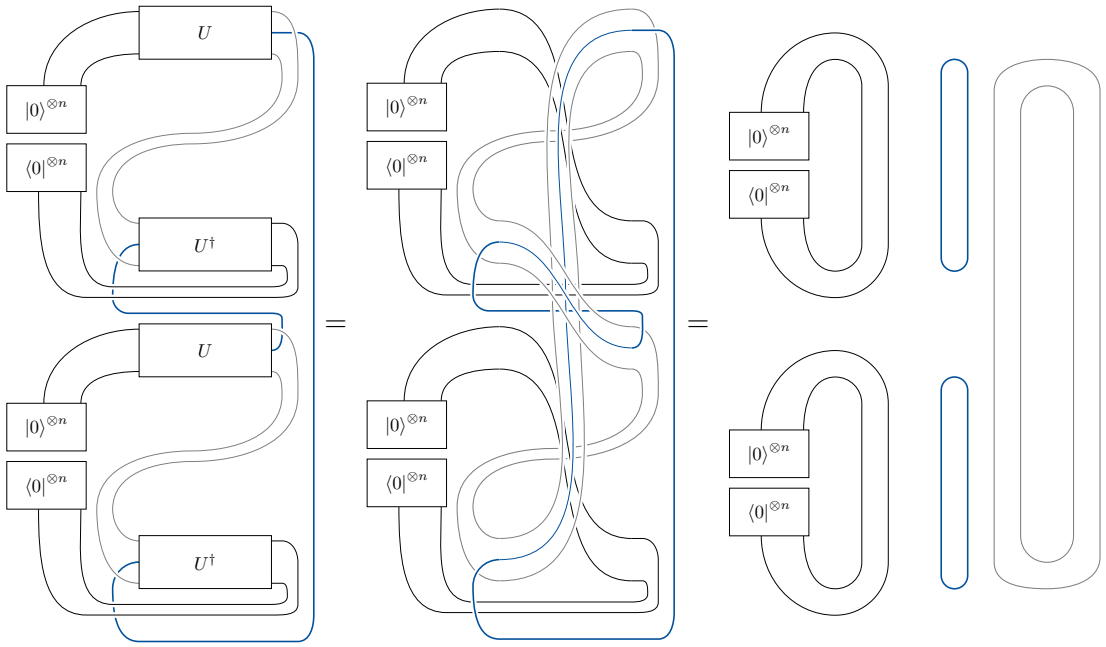

We can now need to summarize and interpret these results and plug them into eq. (D.10). Because we consider the entire system and not just a subsystem, the dimension of the system is $N = d^n$:

$$\mathrm{tr}(\rho_j^2) = \frac{(i)}{N^2-1} - \frac{(ii)}{N(N^2-1)} + \frac{(iii)}{N^2-1} - \frac{(iv)}{N(N^2-1)}$$

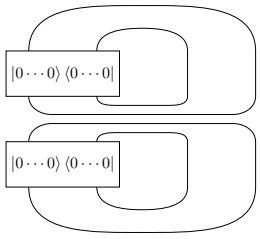

$$= \mathrm{tr}(|0\cdots0\rangle\langle0\cdots0|)\,\mathrm{tr}(|0\cdots0\rangle\langle0\cdots0|) = \langle0\cdots0|0\cdots0\rangle\langle0\cdots0|0\cdots0\rangle = 1$$

$(\star)$

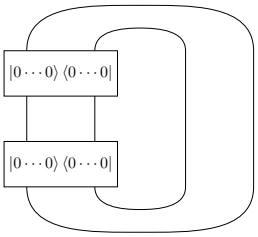

$$= \mathrm{tr}(|0\cdots0\rangle\langle0\cdots0|\,|0\cdots0\rangle\langle0\cdots0|) = \langle0\cdots0|0\cdots0\rangle\langle0\cdots0|0\cdots0\rangle = 1 \tag{$\star\star$}$$

$$\mathrm{tr}(\rho_j^2) = \frac{(\star)}{N^2-1}$$  $$- \frac{(\star\star)}{N(N^2-1)}$$  $$+ \frac{(\star\star)}{N^2-1}$$  $$- \frac{(\star)}{N(N^2-1)}$$ 

$$= \frac{1}{d^{2n}-1}\left((\star\star) - \frac{(\star)}{d^n}\right) + \frac{1}{d^{2n}-1}\left((\star) - \frac{(\star\star)}{d^n}\right)$$

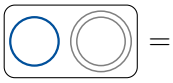 $= d^n$  $= d^{n-1}$  $= d$

$$= \frac{1}{d^{2n}-1}\left(d^{n+1} - \frac{d^{n+1}}{d^n} + d^{2n-1} - \frac{d^{2n-1}}{d^n}\right)$$

$$= \frac{d^{n+1} - d + d^{2n-1} - d^{n-1}}{d^{2n}-1}$$

$$= \frac{(d^n-1)(d+d^{n-1})}{(d^n-1)(d^n+1)}$$

$$= \frac{d+d^{n-1}}{d^n+1} = \frac{1}{d}\left(\frac{d^2+d^n}{d^n+1}\right) = \frac{1}{d}\left(\frac{1+d^{2-n}}{1+d^{-n}}\right) = \frac{1}{d}\left(\frac{1+d^2d^{-n}}{1+d^{-n}}\right) \overset{n>>1}{\longrightarrow} \frac{1}{d}$$

For large n we can taylor expand around d^{-n}:

$$\frac{1+d^2d^{-n}}{1+d^{-n}} = 1 + (d^2-1)d^{-n} + (1-d^2)d^{-2n} + (d^2-1)d^{-3n} + \cdots$$

Now, we need to remember the bound (D.9) we wanted to prove:

$$\left|\left|\rho_j - \frac{\mathbb{1}}{d}\right|\right|_2^2 \leq \varepsilon$$
$$\Leftrightarrow \qquad \mathrm{tr}\big(\rho_j^2\big) - \frac{1}{d} \leq \varepsilon$$

This is true in leading order which means, that the density matrix ρ_j needs to be very close to the identity (we cannot generate arbitrary local states).

Most straightforward generalization: consider a subsystem of size m (m tensor legs, $m < n$):

$$\mathrm{tr}(\rho_m^2) = \frac{1}{d^{2n}-1}\left((\star\star) - \frac{(\star)}{d^n}\right) + \frac{1}{d^{2n}-1}\left((\star) - \frac{(\star\star)}{d^n}\right)$$

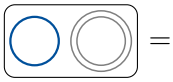 $= d^n$  $= d^{n-m}$  $= d^m$

$$
\begin{aligned}
=&\frac{1}{d^{2n}-1}\left(d^{n+m}-\frac{d^{n+m}}{d^n}+d^{2n-m}-\frac{d^{2n-m}}{d^n}\right)\\
=&\frac{d^{n+m}-d^m+d^{2n-m}-d^{n-m}}{d^{2n}-1}\\
=&\frac{1}{d^m}\frac{d^{2m}+d^n}{1+d^n}\\
=&\frac{1}{d^m}\frac{d^{2m}d^{-n}+1}{d^{-n}+1}
\end{aligned}
$$

$$
\begin{aligned}
\frac{d^{2m}d^{-n}+1}{d^{-n}+1} =&1+(d^{2m}-1)d^{-n}+(1-d^{2m})d^{-2n}+(d^{2m}-1)d^{-3n}+\cdots\\
=&1+d^{2m-n}-d^{-n}+d^{-2n}-d^{2m-2n}+d^{2m-3n}-d^{-3n}+\cdots
\end{aligned}
$$

Consider the case $m=n$:

$$
\operatorname{tr}(\rho_{m=n}^2)=\frac{1}{d^m}\frac{d^{2m}d^{-n}+1}{d^{-n}+1}\overset{m=n}{=}1
$$

This would correspond applying a global operator which then does not need to be maximally mixed.
Here it is not taken into account how big the expansion rate is that is given by the isometry (relation of k input and n output legs). This is "swallowed" in the encoding using the ancilla qubits which is performed with a fixed unitary operator swallowed by the Haar measure (right invariance of Haar measure).

D.10. Operator pushing with maximally entangled state

For all matrices M and N and the maximally entangled state

$$
|\psi_{AB}\rangle=\frac{1}{\sqrt{d}}\sum_{j=1}^{d}|j\rangle|j\rangle
$$

The following property holds

$$
\begin{aligned}
(M\otimes N)|\psi_{AB}\rangle=&(M\otimes N)\left(\frac{1}{\sqrt{d}}\sum_{j=1}^{d}|j\rangle\otimes|j\rangle\right)\\
=&\left(\frac{1}{\sqrt{d}}(MN^{-1}N\otimes N)\sum_{j=1}^{d}|j\rangle\otimes|j\rangle\right)\\
=&\left(\frac{1}{\sqrt{d}}(MN^{-1}\otimes\mathbb{1})\sum_{j=1}^{d}(N|j\rangle)\otimes(N|j\rangle)\right)\\
=&\left(\frac{1}{\sqrt{d}}(MN^{-1}\otimes\mathbb{1})\sum_{k=1}^{d}|k\rangle\otimes|k\rangle\right)\\
=&(MN^{-1}\otimes\mathbb{1})|\psi_{AB}\rangle
\end{aligned}
$$

In tensor network language this translates to

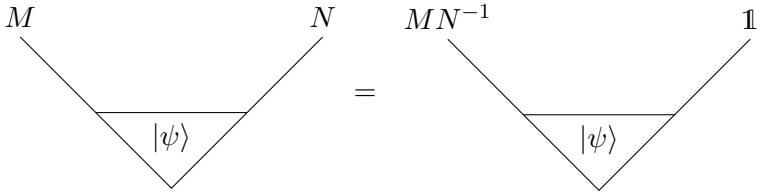

Appendix E

Unruh effect cloning

E.1. Express the initial state of de Sitter spacetime with static patch modes

Here, we calculate the expression of the initial state of the universe eq. (B.8) (multi-rail state) in terms of static patch modes. For this, we use the identity derived in eq. (B.8)

$$
\begin{aligned}
|\psi\rangle =& \sum_{j=1}^{d} c_j (\hat{a}_{\omega_j})^\dagger |\Omega\rangle \\
=& \sum_{j=1}^{d} c_j \frac{1}{\sqrt{1-e^{-2\pi\omega_i}}} \left[(\hat{a}^{\mathrm{I}}_{\omega_j})^\dagger - e^{-\pi\omega_i} \hat{a}^{\mathrm{II}}_{\omega_j} \right] |\Omega\rangle \\
=& \sum_{j=1}^{d} c_j \frac{1}{\sqrt{1-e^{-2\pi\omega_i}}} \left[(\hat{a}^{\mathrm{I}}_{\omega_j})^\dagger - e^{-\pi\omega_i} \hat{a}^{\mathrm{II}}_{\omega_j} \right] \prod_{\omega=0}^{\infty} \sqrt{1-e^{-2\pi\omega}} e^{e^{-\pi\omega} (\hat{a}^{\mathrm{I}}_{\omega})^\dagger (\hat{a}^{\mathrm{II}}_{\omega})^\dagger} |\Omega_{\mathrm{I}}\rangle \otimes |\Omega_{\mathrm{II}}\rangle \\
=& \sum_{j=1}^{d} \frac{c_j (\hat{a}^{\mathrm{I}}_{\omega_j})^\dagger}{\sqrt{1-e^{-2\pi\omega_j}}} \prod_{\omega=0}^{\infty} \sqrt{1-e^{-2\pi\omega}} e^{e^{-\pi\omega} (\hat{a}^{\mathrm{I}}_{\omega})^\dagger (\hat{a}^{\mathrm{II}}_{\omega})^\dagger} |\Omega_{\mathrm{I}}\rangle \otimes |\Omega_{\mathrm{II}}\rangle \\
& - \sum_{j=1}^{d} \frac{c_j e^{-\pi\omega_j}}{\sqrt{1-e^{-2\pi\omega_j}}} \prod_{\omega=0}^{\infty} \sqrt{1-e^{-2\pi\omega}} \left\{ e^{e^{-\pi\omega} (\hat{a}^{\mathrm{I}}_{\omega})^\dagger (\hat{a}^{\mathrm{II}}_{\omega})^\dagger} \hat{a}^{\mathrm{II}}_{\omega_j} + \left[\hat{a}^{\mathrm{II}}_{\omega_j}, e^{e^{-\pi\omega} (\hat{a}^{\mathrm{I}}_{\omega})^\dagger (\hat{a}^{\mathrm{II}}_{\omega})^\dagger} \right] \right\} |\Omega_{\mathrm{I}}\rangle \otimes |\Omega_{\mathrm{II}}\rangle \\
=& \sum_{j=1}^{d} \frac{c_j (\hat{a}^{\mathrm{I}}_{\omega_j})^\dagger}{\sqrt{1-e^{-2\pi\omega_j}}} \prod_{\omega=0}^{\infty} \sqrt{1-e^{-2\pi\omega}} e^{e^{-\pi\omega} (\hat{a}^{\mathrm{I}}_{\omega})^\dagger (\hat{a}^{\mathrm{II}}_{\omega})^\dagger} |\Omega_{\mathrm{I}}\rangle \otimes |\Omega_{\mathrm{II}}\rangle \\
& - \sum_{j=1}^{d} \frac{c_j e^{-\pi\omega_j}}{\sqrt{1-e^{-2\pi\omega_j}}} \prod_{\omega=0}^{\infty} \sqrt{1-e^{-2\pi\omega}} \left[(\hat{a}^{\mathrm{I}}_{\omega_j})^\dagger e^{-\pi\omega_j} e^{e^{-\pi\omega} (\hat{a}^{\mathrm{I}}_{\omega})^\dagger (\hat{a}^{\mathrm{II}}_{\omega})^\dagger} \right] |\Omega_{\mathrm{I}}\rangle \otimes |\Omega_{\mathrm{II}}\rangle \\
=& \sum_{j=1}^{d} \frac{c_j (\hat{a}^{\mathrm{I}}_{\omega_j})^\dagger \left(1-e^{-2\pi\omega_j}\right)}{\sqrt{1-e^{-2\pi\omega_j}}} |\Omega\rangle \\
=& \sum_{j=1}^{d} c_j (\hat{a}^{\mathrm{I}}_{\omega_j})^\dagger \sqrt{1-e^{-2\pi\omega_j}} |\Omega\rangle
\end{aligned}
$$

E.2. Two-mode transformation

Here we consider the Bogoliubov transformation of two modes which are associated with the creation/annihilation operators $\hat{a}^{(\dagger)} = (\hat{a}^{\mathrm{I}}_{\omega})^{(\dagger)}$ and $\hat{b}^{(\dagger)} = (\hat{a}^{\mathrm{II}}_{\omega})^{(\dagger)}$ which we refer to as U^{AB}. For

the transformation of two modes, the transformation U^{AB} can be expressed as

$$U^{AB}(\theta) = \exp\Big[\theta(\hat{a}^\dagger\hat{b}^\dagger - \hat{a}\hat{b})\Big].$$

Using the disentangling theorem [BR03, eq. (A5.17)]

$$e^{\mathrm{i}\,\theta(\hat{K}_+ + \hat{K}_-)} = e^{\mathrm{i}\,(\tanh\theta)\hat{K}_+} e^{-\ln(\cosh^2\theta)\hat{K}_3} e^{\mathrm{i}\,(\tanh\theta)\hat{K}_-}$$

where the operators satisfy the commutation relations $[\hat{K}_3, \hat{K}_\pm] = \pm\hat{K}_\pm$ and $[\hat{K}_+, \hat{K}_-] = -2\hat{K}_3$ we can rewrite U^{AB} in the following way:

$$U^{AB}(\theta) = \exp\Big[\theta(\hat{a}^\dagger\hat{b}^\dagger - \hat{a}\hat{b})\Big] = \frac{1}{\cosh\theta} e^{\tanh\theta\hat{a}^\dagger\hat{b}^\dagger} e^{-\ln(\cosh\theta)(\hat{a}^\dagger\hat{a}+\hat{b}^\dagger\hat{b})} e^{-\tanh\theta\,\hat{a}\hat{b}}$$

It needs to be noted that this expression greatly simplifies when applied to a vacuum state:

$$U^{AB}\,|\Omega\rangle_{AB} = \frac{1}{\cosh\theta} e^{\tanh\theta\hat{a}^\dagger\hat{b}^\dagger}\,|\Omega\rangle_{AB}$$

For many calculations, we use more general expressions to allow for easier generalization.

Proof 21: Expand unitary two mode transformation

First, we check that the commutation relations are fulfilled such that we can use the disentangling theorem from above:

$$\begin{aligned}
\mathrm{i}\hat{K}_+ =& \hat{a}^\dagger\hat{b}^\dagger && \Rightarrow && \hat{K}_+ = -\mathrm{i}\hat{a}^\dagger\hat{b}^\dagger \\
\mathrm{i}\hat{K}_- =& -\hat{a}\hat{b} && \Rightarrow && \hat{K}_- = \mathrm{i}\hat{a}\hat{b} \\
\hat{K}_3 =& \frac{1}{2}(\hat{a}^\dagger\hat{a} + \hat{b}\hat{b}^\dagger) = \frac{1}{2}(\hat{a}^\dagger\hat{a} + \hat{b}^\dagger\hat{b} + 1) \\
\Big[\hat{K}_+, \hat{K}_-\Big] =& -\Big[\mathrm{i}\hat{K}_+, \mathrm{i}\hat{K}_-\Big] = -\Big[\hat{a}^\dagger\hat{b}^\dagger, -\hat{a}\hat{b}\Big] = \Big[\hat{a}^\dagger\hat{b}^\dagger, \hat{a}\hat{b}\Big] \\
=& \hat{a}^\dagger\Big[\hat{b}^\dagger, \hat{a}\hat{b}\Big] + \Big[\hat{a}^\dagger, \hat{a}\hat{b}\Big]\hat{b}^\dagger = -(\hat{a}^\dagger\hat{a} + \hat{b}\hat{b}^\dagger) = -2\hat{K}_3 \\
\Big[\hat{K}_3, \hat{K}_+\Big] =& -\frac{\mathrm{i}}{2}\Big[\hat{a}^\dagger\hat{a} + \hat{b}\hat{b}^\dagger, \hat{a}^\dagger\hat{b}^\dagger\Big] = -\frac{\mathrm{i}}{2}\Big(\Big[\hat{a}^\dagger\hat{a}, \hat{a}^\dagger\hat{b}^\dagger\Big] + \Big[\hat{b}\hat{b}^\dagger, \hat{a}^\dagger\hat{b}^\dagger\Big]\Big) \\
=& -\frac{\mathrm{i}}{2}\Big(\hat{a}^\dagger\Big[\hat{a}, \hat{a}^\dagger\Big]\hat{b}^\dagger + \Big[\hat{b}, \hat{b}^\dagger\Big]\hat{a}^\dagger\hat{b}^\dagger\Big) = -\mathrm{i}\hat{a}^\dagger\hat{b}^\dagger = \hat{K}_+ \\
\Big[\hat{K}_3, \hat{K}_-\Big] =& \frac{\mathrm{i}}{2}\Big[\hat{a}^\dagger\hat{a} + \hat{b}\hat{b}^\dagger, \hat{a}\hat{b}\Big] = \frac{\mathrm{i}}{2}\Big(\Big[\hat{a}^\dagger\hat{a}, \hat{a}\hat{b}\Big] + \Big[\hat{b}\hat{b}^\dagger, \hat{a}\hat{b}\Big]\Big) \\
=& \frac{\mathrm{i}}{2}\Big(\hat{a}\Big[\hat{a}^\dagger, \hat{a}\Big]\hat{b} + \hat{b}\hat{a}\Big[\hat{b}^\dagger, \hat{b}\Big]\Big) = -\mathrm{i}\hat{a}\hat{b} = -\hat{K}_-
\end{aligned}$$

Plugging this into the disentangling theorem, we get:

$$\begin{aligned}
& U^{AB}(\theta) \\
=& e^{\mathrm{i}(\tanh\theta)(-\mathrm{i}\hat{a}^\dagger\hat{b}^\dagger)} e^{-\ln(\cosh^2\theta)\frac{1}{2}(\hat{a}^\dagger\hat{a}+\hat{b}\hat{b}^\dagger)} e^{\mathrm{i}(\tanh\theta)\mathrm{i}\hat{a}\hat{b}} \\
=& e^{\tanh\theta\hat{a}^\dagger\hat{b}^\dagger} \underbrace{e^{-\ln(\cosh^2\theta)\frac{1}{2}(\hat{a}^\dagger\hat{a}+\hat{b}^\dagger\hat{b}+1)}}_{(\star)} e^{-\tanh\theta\,\hat{a}\hat{b}} \\
& (\star) = \exp\Big[-(\ln(\cosh\theta) + \ln(\cosh\theta))\frac{1}{2}(\hat{a}^\dagger\hat{a} + \hat{b}^\dagger\hat{b} + 1)\Big] \\
& \quad = \exp\Big[-\ln(\cosh\theta)(\hat{a}^\dagger\hat{a} + \hat{b}^\dagger\hat{b} + 1)\Big] \\
& \quad = \exp\Big[-\ln(\cosh\theta)(\hat{a}^\dagger\hat{a} + \hat{b}^\dagger\hat{b}) - \ln(\cosh\theta)\Big]
\end{aligned}$$

$$
\begin{aligned}
&= \exp\Big[-\ln(\cosh\theta)(\hat{a}^\dagger\hat{a} + \hat{b}^\dagger\hat{b})\Big] \exp[-\ln(\cosh\theta)] \\
=&\frac{1}{\cosh\theta} e^{\tanh\theta \hat{a}^\dagger\hat{b}^\dagger} e^{-\ln(\cosh\theta)(\hat{a}^\dagger\hat{a}+\hat{b}^\dagger\hat{b})} e^{-\tanh\theta\,\hat{a}\hat{b}}
\end{aligned}
$$

□

When applying this transformation to the tensor product of the (single mode) vacuum states corresponding to $\hat{a}$ and $\hat{b}$, we get the following transformed vacuum state:

$$
\begin{aligned}
|\psi_{AB}\rangle =& U^{AB}(\theta)\,|\Omega_a\rangle \otimes |\Omega_b\rangle \\
=& \frac{1}{\cosh\theta} \exp\Big[\tanh\theta \hat{a}^\dagger\hat{b}^\dagger\Big] \\
& \cdot \exp\Big[-\ln(\cosh\theta)(\hat{a}^\dagger\hat{a} + \hat{b}^\dagger\hat{b})\Big] \\
& \cdot \exp\Big[-\tanh\theta\,\hat{a}\hat{b}\Big]\,|\Omega_a\rangle \otimes |\Omega_b\rangle \\
=& \frac{1}{\cosh\theta} \exp\Big[\tanh\theta \hat{a}^\dagger\hat{b}^\dagger\Big]\,|\Omega_a\rangle \otimes |\Omega_b\rangle
\end{aligned}
$$

We can relate this expression directly to the transformation between the static patch vacuum states and the Euclidean vacuum from eq. (3.34) by making a coefficient comparison:

$$
\begin{aligned}
|\Omega_E\rangle =& \bigotimes_{\omega=0}^{\infty} U_\omega(|\Omega_{\mathrm{I}}\rangle \otimes |\Omega_{\mathrm{II}}\rangle) \\
=& \bigotimes_{\omega=0}^{\infty} \frac{1}{\cosh\theta} e^{\tanh\theta(\hat{a}^{\mathrm{I}}_\omega)^\dagger(\hat{a}^{\mathrm{II}}_\omega)^\dagger}(|\Omega_{\mathrm{I}}\rangle \otimes |\Omega_{\mathrm{II}}\rangle)
\end{aligned}
$$

$$
\frac{1}{\cosh(\theta)} = \sqrt{1 - e^{-2\pi\omega}} \quad \Rightarrow \quad \tanh(\theta) = e^{-\pi\omega}
$$

It directly follows

$$
U_\omega = \sqrt{1 - e^{-2\pi\omega}} e^{e^{-\pi\omega}(\hat{a}^{\mathrm{I}}_\omega)^\dagger(\hat{a}^{\mathrm{II}}_\omega)^\dagger} e^{\frac{1}{2}\ln(1-e^{-2\pi\omega})((\hat{a}^{\mathrm{I}}_\omega)^\dagger\hat{a}^{\mathrm{I}}_\omega + (\hat{a}^{\mathrm{II}}_\omega)^\dagger\hat{a}^{\mathrm{II}}_\omega)} e^{-e^{-\pi\omega}\,\hat{a}^{\mathrm{I}}_\omega\hat{a}^{\mathrm{II}}_\omega}
$$

This is similar to the regular setting of the Unruh effect, where every two-mode entangled Rindler state is assigned a state from Minkowski spacetime.

E.3. Transformation of the multi-rail state using the two-mode transformation

We consider the multi-rail state introduced as an input state in eq. (8.3). We look at the commutation relation between the unitary two-mode transformation U and the Euclidean creation operator $(\hat{a}^{E1}_\omega)^\dagger$ to derive alternative expressions.

$$
\begin{aligned}
|\psi\rangle =& \sum_{i=1}^{d} c_i(\hat{a}^E_i)^\dagger\,|\Omega_E\rangle \\
=& \sum_{i=1}^{d} c_i(\hat{a}^E_i)^\dagger U\,|\Omega_{\mathrm{I}}\rangle\,|\Omega_{\mathrm{II}}\rangle \\
=& \sum_{i=1}^{d} c_i U(\hat{a}^E_i)^\dagger\,|\Omega_{\mathrm{I}}\rangle\,|\Omega_{\mathrm{II}}\rangle - \sum_{i=1}^{d}\Big[U, (\hat{a}^E_i)^\dagger\Big]\,|\Omega_{\mathrm{I}}\rangle
\end{aligned}
$$

$$
\begin{aligned}
&\overset{(E.1)}{=} \sum_{i=1}^{d} c_i U \left(\frac{1}{\sqrt{1-e^{-2\pi\omega_i}}} (\hat{a}_i^{\mathrm{I}})^\dagger \right) |\Omega_{\mathrm{I}}\rangle |\Omega_{\mathrm{II}}\rangle - \sum_{i=1}^{d} \frac{U}{\sqrt{1-e^{-2\pi\omega_i}}} \left[1 - \sqrt{1-e^{-2\pi\omega_i}} \right] (\hat{a}_i^{\mathrm{I}})^\dagger |\Omega_{\mathrm{I}}\rangle |\Omega_{\mathrm{II}}\rangle \\
&= \sum_{i=1}^{d} c_i \frac{U}{\sqrt{1-e^{-2\pi\omega_i}}} \left(1 - \left[1 - \sqrt{1-e^{-2\pi\omega_i}} \right] \right) (\hat{a}_i^{\mathrm{I}})^\dagger |\Omega_{\mathrm{I}}\rangle |\Omega_{\mathrm{II}}\rangle \\
&= \sum_{i=1}^{d} c_i U (\hat{a}_i^{\mathrm{I}})^\dagger |\Omega_{\mathrm{I}}\rangle |\Omega_{\mathrm{II}}\rangle \\
&= \sum_{i=1}^{d} c_i \left((\hat{a}_i^{\mathrm{I}})^\dagger U + \left[U, (\hat{a}_i^{\mathrm{I}})^\dagger \right] \right) |\Omega_{\mathrm{I}}\rangle |\Omega_{\mathrm{II}}\rangle \\
&\overset{(E.2)}{=} \sum_{i=1}^{d} c_i \left((\hat{a}_i^{\mathrm{I}})^\dagger U + \left(\sqrt{1-e^{-2\pi\omega_i}} - 1 \right) (\hat{a}_i^{\mathrm{I}})^\dagger U \right) |\Omega_{\mathrm{I}}\rangle |\Omega_{\mathrm{II}}\rangle \\
&= \sum_{i=1}^{d} c_i \left(\sqrt{1-e^{-2\pi\omega_i}} \right) (\hat{a}_i^{\mathrm{I}})^\dagger U |\Omega_{\mathrm{I}}\rangle |\Omega_{\mathrm{II}}\rangle \\
&= \sum_{i=1}^{d} c_i \sqrt{1-e^{-2\pi\omega_i}} (\hat{a}_i^{\mathrm{I}})^\dagger |\Omega_E\rangle
\end{aligned}
$$

where we have used, that the operator U is a product of two mode transformations U_ω which commutes with all creation and annihilation operators $\hat{a}_{\tilde{\omega}}, (\hat{a}_{\tilde{\omega}})^\dagger$ with $\tilde{\omega} \neq \omega$. For a less cluttered notation we use $\hat{a}_{\omega_i} = \hat{a}_i$. It follows:

$$
[U, \hat{a}_i] = \left[\prod_{\omega_k} U_{\omega_k}, \hat{a}_i \right] = \prod_{\omega_k \neq \omega_i} U_{\omega_k} [U_{\omega_i}, \hat{a}_i]
$$

In order to calculate the commutators involving the two-mode transformation U_ω, we need the identities for commutators of exponential operators derived in appendix B.8.
The unitary operator U_ω describing the two-mode transformation can be expanded as

$$
U_{\omega_j} = \sqrt{1-e^{-2\pi\omega_j}} \underbrace{e^{e^{-\pi\omega_j} (\hat{a}_{\omega_j}^{\mathrm{I}})^\dagger (\hat{a}_{\omega_j}^{\mathrm{II}})^\dagger}}_{=U_j^{(3)}} \cdot \underbrace{e^{\frac{1}{2}\ln(1-e^{-2\pi\omega_j}) \left((\hat{a}_{\omega_j}^{\mathrm{I}})^\dagger \hat{a}_{\omega_j}^{\mathrm{I}} + (\hat{a}_{\omega_j}^{\mathrm{II}})^\dagger \hat{a}_{\omega_j}^{\mathrm{II}} \right)}}_{=U_j^{(2)}} \cdot \underbrace{e^{-e^{-\pi\omega_j}\, \hat{a}_{\omega_j}^{\mathrm{I}} \hat{a}_{\omega_j}^{\mathrm{II}}}}_{=U_j^{(1)}}.
$$

which we write down as

$$
\begin{aligned}
U_j^{(1)} &= \exp\left[\lambda_1 \hat{a}_{\omega_j}^{\mathrm{I}} \hat{a}_{\omega_j}^{\mathrm{II}} \right] && \lambda_1 = -e^{-\pi\omega_j} \\
U_j^{(2)} &= \exp\left[\lambda_2 (\hat{a}_{\omega_j}^{\mathrm{I}})^\dagger \hat{a}_{\omega_j}^{\mathrm{I}} \right] \exp\left[\lambda_2 (\hat{a}_{\omega_j}^{\mathrm{II}})^\dagger \hat{a}_{\omega_j}^{\mathrm{II}} \right] && \lambda_2 = \frac{1}{2}\ln(1-e^{-2\pi\omega_j}) \\
U_j^{(3)} &= \exp\left[\lambda_3 (\hat{a}_{\omega_j}^{\mathrm{I}})^\dagger (\hat{a}_{\omega_j}^{\mathrm{II}})^\dagger \right] && \lambda_3 = e^{-\pi\omega_j}
\end{aligned}
$$

Proof 22: Commutator two mode transformation and Euclidean creation operator

We can use these ingredients to calculate the commutator of the unitary operator and a Euclidean creation operator to be

$$
\left[U, (\hat{a}_\omega^E)^\dagger \right] = \frac{U}{\sqrt{1-e^{-2\pi\omega}}} \left\{ \left[1 - \sqrt{1-e^{-2\pi\omega}} \right] (\hat{a}_\omega^{\mathrm{I}})^\dagger + \left[-e^{-\pi\omega} \right] \hat{a}_\omega^{\mathrm{II}} \right\} \tag{E.1}
$$

There are two sets of Euclidean operators which are identical up to switching the static patches I and II. We will consider the creation operator we denoted as $(\hat{\omega}^{E1})^\dagger$, which can be expressed in static patch creation and annihilation operators as follows:

$$(\hat{a}^{E1}_\omega)^\dagger = \frac{1}{\sqrt{1-e^{-2\pi\omega}}}\Big((\hat{a}^{\mathrm{I}}_\omega)^\dagger - e^{-\pi\omega}\hat{a}^{\mathrm{II}}_\omega\Big)$$

We consider the commutator for mode ω (all commutators involving different modes vanish). First we look at the $U^{(2)}$ operator separately:

$$\begin{aligned}\Big[U^{(2)}, (\hat{a}^{\mathrm{I}}_\omega)^\dagger\Big] &= \Big[\exp\Big[\lambda_2(\hat{a}^{\mathrm{I}}_{\omega_j})^\dagger\hat{a}^{\mathrm{I}}_{\omega_j}\Big], (\hat{a}^{\mathrm{I}}_\omega)^\dagger\Big]\exp\Big[\lambda_2(\hat{a}^{\mathrm{II}}_{\omega_j})^\dagger\hat{a}^{\mathrm{II}}_{\omega_j}\Big] = (1-e^{-\lambda_2})U^{(2)}(\hat{a}^{\mathrm{I}}_\omega)^\dagger \\ \Big[U^{(2)}, \hat{a}^{\mathrm{II}}_\omega\Big] &= \exp\Big[\lambda_2(\hat{a}^{\mathrm{I}}_{\omega_j})^\dagger\hat{a}^{\mathrm{I}}_{\omega_j}\Big]\Big[\exp\Big[\lambda_2(\hat{a}^{\mathrm{II}}_{\omega_j})^\dagger\hat{a}^{\mathrm{II}}_{\omega_j}\Big], \hat{a}^{\mathrm{II}}_\omega\Big] = (1-e^{\lambda_2})U^{(2)}\hat{a}^{\mathrm{II}}_\omega\end{aligned}$$

The commutator to be derived can be calculated as follows:

$$\begin{aligned}\Big[U, (\hat{a}^{E}_\omega)^\dagger\Big] =& \Big[\sqrt{1-e^{-2\pi\omega}}U^{(3)}U^{(2)}U^{(1)}, \frac{1}{\sqrt{1-e^{-2\pi\omega}}}\Big((\hat{a}^{\mathrm{I}}_\omega)^\dagger - e^{-\pi\omega}\hat{a}^{\mathrm{II}}_\omega\Big)\Big] \\ =& \Big[U^{(3)}U^{(2)}U^{(1)}, (\hat{a}^{\mathrm{I}}_\omega)^\dagger\Big] - e^{-\pi\omega}\Big[U^{(3)}U^{(2)}U^{(1)}, \hat{a}^{\mathrm{II}}_\omega\Big] \\ =& \Big[U^{(3)}, (\hat{a}^{\mathrm{I}}_\omega)^\dagger\Big]U^{(2)}U^{(1)} + U^{(3)}\Big[U^{(2)}, (\hat{a}^{\mathrm{I}}_\omega)^\dagger\Big]U^{(1)} + U^{(3)}U^{(2)}\Big[U^{(1)}, (\hat{a}^{\mathrm{I}}_\omega)^\dagger\Big] \\ & - e^{-\pi\omega}\Big(\Big[U^{(3)}, \hat{a}^{\mathrm{II}}_\omega\Big]U^{(2)}U^{(1)} + U^{(3)}\Big[U^{(2)}, \hat{a}^{\mathrm{II}}_\omega\Big]U^{(1)} + U^{(3)}U^{(2)}\Big[U^{(1)}, \hat{a}^{\mathrm{II}}_\omega\Big]\Big) \\ =& U^{(3)}\Big[(1-e^{-\lambda_2})U^{(2)}(\hat{a}^{\mathrm{I}}_\omega)^\dagger\Big]U^{(1)} + U^{(3)}U^{(2)}\Big[\lambda_1\hat{a}^{\mathrm{II}}_\omega U^{(1)}\Big] \\ & - e^{-\pi\omega}\Big(\Big[-U^{(3)}\lambda_3(\hat{a}^{\mathrm{I}}_\omega)^\dagger\Big]U^{(2)}U^{(1)} + U^{(3)}\Big[(1-e^{\lambda_2})U^{(2)}\hat{a}^{\mathrm{II}}_\omega\Big]U^{(1)}\Big) \\ =& U^{(3)}\Big\{(1-e^{-\lambda_2})U^{(2)}\Big(U^{(1)}(\hat{a}^{\mathrm{I}}_\omega)^\dagger - \Big[U^{(1)}, (\hat{a}^{\mathrm{I}}_\omega)^\dagger\Big]\Big) + U^{(2)}U^{(1)}\lambda_1\hat{a}^{\mathrm{II}}_\omega \\ & -e^{-\pi\omega}\Big(-\lambda_3\Big(U^{(2)}(\hat{a}^{\mathrm{I}}_\omega)^\dagger - \Big[U^{(2)}, (\hat{a}^{\mathrm{I}}_\omega)^\dagger\Big]\Big)U^{(1)} + (1-e^{\lambda_2})U^{(2)}U^{(1)}\hat{a}^{\mathrm{II}}_\omega\Big)\Big\} \\ =& U^{(3)}U^{(2)}\Big\{(1-e^{-\lambda_2})\Big(U^{(1)}(\hat{a}^{\mathrm{I}}_\omega)^\dagger - \Big[\lambda_1 U^{(1)}\hat{a}^{\mathrm{II}}_\omega\Big]\Big) + U^{(1)}\lambda_1\hat{a}^{\mathrm{II}}_\omega \\ & -e^{-\pi\omega}\Big(-\lambda_3\Big((\hat{a}^{\mathrm{I}}_\omega)^\dagger - \Big[(1-e^{-\lambda_2})(\hat{a}^{\mathrm{I}}_\omega)^\dagger\Big]\Big)U^{(1)} + (1-e^{\lambda_2})U^{(1)}\hat{a}^{\mathrm{II}}_\omega\Big)\Big\} \\ =& U^{(3)}U^{(2)}U^{(1)}\Big\{(1-e^{-\lambda_2})\Big((\hat{a}^{\mathrm{I}}_\omega)^\dagger - \lambda_1\hat{a}^{\mathrm{II}}_\omega\Big) + \lambda_1\hat{a}^{\mathrm{II}}_\omega \\ & -e^{-\pi\omega}\Big(-\lambda_3 e^{-\lambda_2}\Big[(\hat{a}^{\mathrm{I}}_\omega)^\dagger - \big(\lambda_1\hat{a}^{\mathrm{II}}_\omega\big)\Big] + (1-e^{\lambda_2})\hat{a}^{\mathrm{II}}_\omega\Big)\Big\} \\ =& U^{(3)}U^{(2)}U^{(1)}\Big\{(1-\frac{1}{\sqrt{1-e^{-2\pi\omega}}})\Big((\hat{a}^{\mathrm{I}}_\omega)^\dagger + e^{-\pi\omega}\hat{a}^{\mathrm{II}}_\omega\Big) - e^{-\pi\omega}\hat{a}^{\mathrm{II}}_\omega \\ & -e^{-\pi\omega}\Big(-e^{-\pi\omega}\frac{1}{\sqrt{1-e^{-2\pi\omega}}}\Big[(\hat{a}^{\mathrm{I}}_\omega)^\dagger + e^{-\pi\omega}\hat{a}^{\mathrm{II}}_\omega\Big] + (1-\sqrt{1-e^{-2\pi\omega}})\hat{a}^{\mathrm{II}}_\omega\Big)\Big\} \\ =& \frac{U}{\sqrt{1-e^{-2\pi\omega}}}\Big\{\Big[1-\sqrt{1-e^{-2\pi\omega}}\Big](\hat{a}^{\mathrm{I}}_\omega)^\dagger + \big[-e^{-\pi\omega}\big]\hat{a}^{\mathrm{II}}_\omega\Big\}\end{aligned}$$

□

Proof 23: Commutator two mode transformation and static patch creation operator acting on static patch vacuum states

We directly consider the commutator when acting on the static patch vacuum states, which evaluates to

$$\Big[U_{\omega_k}, (\hat{a}^{\mathrm{I}}_{\omega_k})^\dagger\Big]|\Omega_{\omega_k}\rangle_{\mathrm{I}}\otimes|\Omega_{\omega_k}\rangle_{\mathrm{II}} = \Big(\sqrt{1-e^{-2\pi\omega_k}}-1\Big)(\hat{a}^{\mathrm{I}}_{\omega_k})^\dagger U_{\omega_k}|\Omega_{\omega_k}\rangle_{\mathrm{I}}\otimes|\Omega_{\omega_k}\rangle_{\mathrm{II}} \tag{E.2}$$

This can be calculated as follows:

$$
\begin{aligned}
&\left[U_{\omega_k}, (\hat{a}^{\mathrm{I}}_{\omega_k})^\dagger\right] |\Omega_{\omega_k}\rangle_{\mathrm{I}} \otimes |\Omega_{\omega_k}\rangle_{\mathrm{II}} = \\
=&\sqrt{1-e^{-2\pi\omega_k}}\left[U_k^{(3)}U_k^{(2)}U_k^{(1)}, (\hat{a}^{\mathrm{I}}_{\omega_k})^\dagger\right] |\Omega_{\omega_k}\rangle_{\mathrm{I}} \otimes |\Omega_{\omega_k}\rangle_{\mathrm{II}} \\
=&\sqrt{1-e^{-2\pi\omega_k}}\Big(\left[U_k^{(3)}, (\hat{a}^{\mathrm{I}}_{\omega_k})^\dagger\right]U_k^{(2)}U_k^{(1)} + U_k^{(3)}\left[U_k^{(2)}, (\hat{a}^{\mathrm{I}}_{\omega_k})^\dagger\right]U_k^{(1)} \\
&+U_k^{(3)}U_k^{(2)}\left[U_k^{(1)}, (\hat{a}^{\mathrm{I}}_{\omega_k})^\dagger\right]\Big) |\Omega_{\omega_k}\rangle_{\mathrm{I}} \otimes |\Omega_{\omega_k}\rangle_{\mathrm{II}} \\
&\text{use (B.4) with } \lambda_1 = -e^{-\pi\omega_k} \text{ and (B.6)} \\
=&\sqrt{1-e^{-2\pi\omega_k}}\Big(U_k^{(3)}\left[U_k^{(2)}, (\hat{a}^{\mathrm{I}}_{\omega_k})^\dagger\right] + U_k^{(3)}U_k^{(2)}\left(e^{-\pi\omega_k}\hat{a}^{\mathrm{II}}_{\omega_k}U_k^{(1)}\right)\Big) |\Omega_{\omega_k}\rangle_{\mathrm{I}} \otimes |\Omega_{\omega_k}\rangle_{\mathrm{II}} \\
=&\sqrt{1-e^{-2\pi\omega_k}}\Big(U_k^{(3)}\left[U_k^{(2)}, (\hat{a}^{\mathrm{I}}_{\omega_k})^\dagger\right]\Big) |\Omega_{\omega_k}\rangle_{\mathrm{I}} \otimes |\Omega_{\omega_k}\rangle_{\mathrm{II}} \\
=&\sqrt{1-e^{-2\pi\omega_k}}\left(U_k^{(3)}\left[e^{\ln\sqrt{1-e^{-2\pi\omega_k}}(\hat{a}^{\mathrm{I}}_{\omega_k})^\dagger\hat{a}^{\mathrm{I}}_{\omega_k}}, (\hat{a}^{\mathrm{I}}_{\omega_k})^\dagger\right]e^{\ln\sqrt{1-e^{-2\pi\omega_k}}(\hat{a}^{\mathrm{II}}_{\omega_k})^\dagger\hat{a}^{\mathrm{II}}_{\omega_k}}\right) |\Omega_{\omega_k}\rangle_{\mathrm{I}} \otimes |\Omega_{\omega_k}\rangle_{\mathrm{II}} \\
&\text{use (B.5) with } \lambda_2 = \ln\sqrt{1-e^{-2\pi\omega_k}} \\
=&\sqrt{1-e^{-2\pi\omega_k}}\left(U_k^{(3)}\left(1-e^{-\ln\sqrt{1-e^{-2\pi\omega_k}}}\right)e^{\ln\sqrt{1-e^{-2\pi\omega_k}}(\hat{a}^{\mathrm{I}}_{\omega_k})^\dagger\hat{a}^{\mathrm{I}}_{\omega_k}}(\hat{a}^{\mathrm{I}}_{\omega_k})^\dagger e^{\ln\sqrt{1-e^{-2\pi\omega_k}}(\hat{a}^{\mathrm{II}}_{\omega_k})^\dagger\hat{a}^{\mathrm{II}}_{\omega_k}}\right) \\
&|\Omega_{\omega_k}\rangle_{\mathrm{I}} \otimes |\Omega_{\omega_k}\rangle_{\mathrm{II}} \\
=&\sqrt{1-e^{-2\pi\omega_k}}\left(U_k^{(3)}\left(1-e^{-\ln\sqrt{1-e^{-2\pi\omega_k}}}\right)e^{\ln\sqrt{1-e^{-2\pi\omega_k}}}(\hat{a}^{\mathrm{I}}_{\omega_k})^\dagger\right) |\Omega_{\omega_k}\rangle_{\mathrm{I}} \otimes |\Omega_{\omega_k}\rangle_{\mathrm{II}} \\
=&\sqrt{1-e^{-2\pi\omega_k}}\Big(U_k^{(3)}\Big(\sqrt{1-e^{-2\pi\omega_k}}-1\Big)(\hat{a}^{\mathrm{I}}_{\omega_k})^\dagger\Big) |\Omega_{\omega_k}\rangle_{\mathrm{I}} \otimes |\Omega_{\omega_k}\rangle_{\mathrm{II}} \\
=&\sqrt{1-e^{-2\pi\omega_k}}\Big(\sqrt{1-e^{-2\pi\omega_k}}-1\Big)(\hat{a}^{\mathrm{I}}_{\omega_k})^\dagger U_k^{(3)} |\Omega_{\omega_k}\rangle_{\mathrm{I}} \otimes |\Omega_{\omega_k}\rangle_{\mathrm{II}} \\
=&\Big(\sqrt{1-e^{-2\pi\omega_k}}-1\Big)(\hat{a}^{\mathrm{I}}_{\omega_k})^\dagger U_{\omega_k} |\Omega_{\omega_k}\rangle_{\mathrm{I}} \otimes |\Omega_{\omega_k}\rangle_{\mathrm{II}}
\end{aligned}
$$

We used that the exponential functions of the creation and annihilation operators act on the respective vacuum states as follows:

$$
\begin{aligned}
e^{\lambda_1\hat{a}\hat{b}} |\Omega_a\rangle |\Omega_b\rangle &= |\Omega_a\rangle |\Omega_b\rangle \\
e^{\lambda_2\hat{a}^\dagger\hat{a}} |\Omega_a\rangle = e^{\lambda_2\hat{n}} |\Omega_a\rangle &= \sum_{k=0}^{\infty}\frac{1}{k!}(\lambda_2\hat{n})^k |\Omega_a\rangle = \sum_{k=0}^{\infty}\frac{1}{k!}(\lambda_2\cdot 0)^k |\Omega_a\rangle = e^0 |\Omega_a\rangle = |\Omega_a\rangle \\
e^{\lambda_2\hat{a}^\dagger\hat{a}}\hat{a}^\dagger |\Omega_a\rangle = e^{\lambda_2\hat{a}^\dagger\hat{a}} |1_a\rangle &= e^{\lambda_2} |1_a\rangle = e^{\lambda_2}\hat{a}^\dagger |\Omega_a\rangle
\end{aligned}
$$

□

E.4. Transformation dual rail state with multinomial theorem

We now want to look at alternate forms of the transformed multi-rail state (8.4). We expand the exponential function, apply the multinomial theorem, and use multi-index notation:

$$
\begin{aligned}
|\psi_E\rangle &= \sum_{k=1}^{d} c_k\sqrt{1-e^{-2\pi\omega_k}}(\hat{a}^{\mathrm{I}}_{\omega_k})^\dagger\prod_{\omega}\sqrt{1-e^{-2\pi\omega}}\exp\left[e^{-\pi\omega}(\hat{a}^{\mathrm{I}}_{\omega})^\dagger(\hat{a}^{\mathrm{II}}_{\omega})^\dagger\right] |\Omega_{\mathrm{I}}\rangle \otimes |\Omega_{\mathrm{II}}\rangle \\
&= \sum_{k=1}^{d} c_k\sqrt{1-z_k^2}(\hat{a}^{\mathrm{I}}_{\omega_k})^\dagger\left(\prod_{\omega}\sqrt{1-z^2}\right)\sum_{n=0}^{\infty}\frac{1}{n!}\left(\sum_{\omega} z(\hat{a}^{\mathrm{I}}_{\omega})^\dagger(\hat{a}^{\mathrm{II}}_{\omega})^\dagger\right)^n |\Omega_{\mathrm{I}}\rangle \otimes |\Omega_{\mathrm{II}}\rangle
\end{aligned}
$$

$$= \sum_{k=1}^{d} c_k \sqrt{1-z_k^2} \sum_{n=0}^{\infty} \sum_{L_n} \left(\prod_{\omega} \sqrt{1-z^2} z^{l_j} \right) \underbrace{(\hat{a}^{\mathrm{I}}_{\omega_k})^\dagger \left| l_1 l_2 \dots l_d \right\rangle_{\mathrm{I}}}_{=\sqrt{l_k+1}\left|L^{(k)}\right\rangle_{\mathrm{I}}} \otimes \underbrace{\left| l_1 l_2 \dots l_d \right\rangle_{\mathrm{II}}}_{=\left|L\right\rangle_{\mathrm{II}}}$$

$$= \sum_{k=1}^{d} c_k \sqrt{1-z_k^2} \sum_{n=0}^{\infty} z^n \left(\prod_{\omega} \sqrt{1-z^2} \right) \sum_{L_n} \sqrt{l_k+1} \left| L^{(k)} \right\rangle_{\mathrm{I}} \left| L \right\rangle_{\mathrm{II}}$$

Here, we expanded the unitary transformation, expanded the exponential function using the Taylor series, and applied the multinomial theorem:

$$\frac{1}{k!} \left(\sum_{i=1}^{d} \hat{a}_i^\dagger \hat{b}_i^\dagger \right)^k = \sum_{l_1+l_2+\dots+l_d=k} \frac{1}{l_1! l_2! \dots l_d!} (\hat{a_1}^\dagger \hat{b}_1^\dagger)^{l_1} \cdots (\hat{a_d}^\dagger \hat{b}_d^\dagger)^{l_d}$$

E.5. Unruh cloning channel

We take the initial state from eq. (8.6):

$$\left|\psi\right\rangle = \sum_{k=1}^{d} c_k \sqrt{1-z_k^2} \sum_{n=0}^{\infty} \left(\prod_{j=1}^{d} z_j^n \sqrt{1-z_j^2} \right) \sum_{L_n} \sqrt{l_k+1} \left| L^{(k)} \right\rangle_{\mathrm{I}} \left| L \right\rangle_{\mathrm{II}}$$

With this expression of $\left|\psi\right\rangle$ we derive the Unruh channel from eq. (8.7)

$$\mathcal{E}(\psi) = \mathrm{tr}_{\mathrm{II}}(\left|\psi\right\rangle \left\langle\psi\right|) = \rho_{\mathrm{I}}$$

. In doing so, we split the channel into two parts: the diagonal part, where identical frequencies are excited, and the off-diagonal part, where different frequencies are excited. This distinction affects the index we call k, which is the mode excited in the multi-rail state.

$$\begin{aligned}
\mathcal{E}(\psi) &= \mathrm{tr}_{\mathrm{II}}(\left|\psi\right\rangle \left\langle\psi\right|) = \rho_{\mathrm{I}} \\
&= \mathrm{tr}_{\mathrm{II}} \left[\left\{ \sum_{k=1}^{d} c_k \sqrt{1-z_k^2} \sum_{n=0}^{\infty} \sum_{L_n} \left(\prod_{j=1}^{d} z_j^{l_j} \sqrt{1-z_j^2} \right) \sqrt{l_k+1} \left| L^{(k)} \right\rangle_{\mathrm{I}} \left| L \right\rangle_{\mathrm{II}} \right\} \right. \\
&\quad \left. \cdot \left\{ \sum_{\tilde{k}=1}^{d} c_{\tilde{k}}^* \sqrt{1-z_{\tilde{k}}^2} \sum_{n=0}^{\infty} \sum_{L_n} \left(\prod_{j=1}^{d} z_j^{l_j} \sqrt{1-z_j^2} \right) \sqrt{l_{\tilde{k}}+1} \left\langle L^{(\tilde{k})} \right|_{\mathrm{I}} \left\langle L \right|_{\mathrm{II}} \right\} \right] \\
&= \sum_{k,\tilde{k}=1}^{d} c_k c_{\tilde{k}}^* \sqrt{1-z_k^2} \sqrt{1-z_{\tilde{k}}^2} \prod_{j}^{d} (1-z_j^2) \sum_{L_n} \sum_{n=0}^{\infty} z_j^{2l_j} \sqrt{l_k+1} \sqrt{l_{\tilde{k}}+1} \left| L^{(k)} \right\rangle \left\langle L^{(\tilde{k})} \right|_{\mathrm{I}} \\
&= \sum_{k=1}^{d} |c_k|^2 (1-z_k^2) \prod_{j=1}^{d} (1-z_j^2) \sum_{L_n} \sum_{n=0}^{\infty} z_j^{2l_j} \sum_{L_n} (l_k+1) \left| L^{(k)} \right\rangle \left\langle L^{(k)} \right|_{\mathrm{I}} \\
&\quad + \sum_{\substack{k,\tilde{k}=1 \\ k \neq \tilde{k}}}^{d} c_k c_{\tilde{k}}^* \sqrt{1-z_k^2} \sqrt{1-z_{\tilde{k}}^2} \prod_{j=1}^{d} (1-z_j^2) \sum_{L_n} \sum_{n=0}^{\infty} z_j^{2l_j} \sqrt{l_k+1} \sqrt{l_{\tilde{k}}+1} \left| L^{(k)} \right\rangle \left\langle L^{(\tilde{k})} \right|_{\mathrm{I}}
\end{aligned}$$

Under the assumption that we do not have to consider different z, this simplifies in the following way:

$$\mathcal{E}(\psi) = \sum_{k=1}^{d} (1-z^2)^{d+1} \sum_{k=1}^{d} |c_k|^2 \sum_{n=0}^{\infty} z^{2n} \sum_{L_n} (l_k+1) \left| L^{(k)} \right\rangle_{\mathrm{I}} \left\langle L^{(k)} \right|_{\mathrm{I}}$$

$$
\begin{aligned}
&+ \sum k, \tilde{k} = 1^d \left(1 - z^2\right)^{d+1} \sum_{k=1}^{d} c_k c_{\tilde{k}}^* \sum_{n=0}^{\infty} z^{2n} \sum_{L_n} \sqrt{l_k + 1} \sqrt{l_{\tilde{k}} + 1} \, |L^{(k)}\rangle_{\mathrm{I}} \, \langle L^{(\tilde{k})}|_{\mathrm{I}} \\
=&(1 - z^2)^{d+1} \sum_{n=0}^{\infty} z^{2n} \rho_{\mathrm{I}}^{(n+1)}
\end{aligned}
$$

with

$$
\rho_{\mathrm{I}}^{(n+1)} = \sum_{L_n} \left[\sum_{k=1}^{d} |c_k|^2 (l_k + 1) \, |L^{(k)}\rangle \, \langle L^{(k)}|_{\mathrm{I}} + \sum_{\substack{k,\tilde{k}=1 \\ k \neq \tilde{k}}}^{d} c_k c_{\tilde{k}}^* \sqrt{l_k + 1} \sqrt{l_{\tilde{k}} + 1} \, |L^{(k)}\rangle \, \langle L^{(\tilde{k})}|_{\mathrm{I}} \right]
$$

E.6. Identify Unruh channel with cloning channel

First, we compare the coefficients of the block diagonal density matrices of the Unruh channel from eq. (8.8) and the cloning channel from eq. (4.3).

First, we consider the diagonal part:

$$
\begin{aligned}
\text{Unruh:} \quad & \sum_{k=1}^{d} (l_k + 1) = n + d \\
\text{Cloning:} \quad & \left(\sum_{i=1}^{n} \frac{2 + n}{2n + 2} \right) + \frac{1}{2} \mathbb{1} = n \left(\frac{2 + n}{2n + 2} + \frac{1}{2} \right) = n \left(1 + \frac{1}{2(1 + n)} \right) = n + \frac{1}{2/n + 2}
\end{aligned}
$$

Now, we consider the off-diagonal part for both channels:

$$
\begin{aligned}
\text{Unruh:} \quad & \sum_{\substack{k,\tilde{k}=1 \\ k \neq \tilde{k}}}^{d} \sqrt{l_k + 1} \sqrt{l_{\tilde{k}} + 1} = (\sqrt{n + d})^2 = n + d \\
\text{Cloning:} \quad & \left(\sum_{\substack{i,j=1 \\ i \neq j}}^{n} \frac{n - 2}{(n + 1)^2} \right) = n(n - 1) \frac{n - 2}{(n + 1)^2} = n \left(\frac{(1 - 1/n)(1 - 2/n)}{(1 + 1/n)^2} \right) = n \left(1 + \frac{1 - 5n}{(1 + n)^2} \right) \\
& = n + \frac{1/n - 5}{2 + n + 1/n}
\end{aligned}
$$

We can see that the leading orders of the coefficients match the dimensionality of the cloning channel as needed.

Appendix F

Unruh effect superposition

F.1. Calculation scalar product of states of the field

To obtain an explicit expression for the final state from eq. (9.5), we need to calculate the scalar product $\langle \omega_j, m | \omega_i, n \rangle_{\mathrm{F}}$. For this, we use the Wightman function from section 3.8. An alternative approach would be to use Bogoliubov transformations, which are not employed in this paper.

$$\begin{aligned}\langle \omega_j, m | \omega_i, n \rangle_{\mathrm{F}} &= \int_{-\infty}^{\infty} \mathrm{d}\tau \int_{-\infty}^{\infty} \mathrm{d}\tilde{\tau} \chi(\tau)\chi^*(\tilde{\tau}) \mathrm{e}^{\mathrm{i}(\omega_i \tau - \omega_j \tilde{\tau})} \underbrace{\langle 0| \hat{\phi}^\dagger(x_m)\hat{\phi}(x_n) |0\rangle_{\mathrm{F}}}_{W(x_m,x_n)} \\ &= \int_{-\infty}^{\infty} \mathrm{d}\tau \int_{-\infty}^{\infty} \mathrm{d}\tilde{\tau} \frac{1}{(2\pi)^{1/4}} \mathrm{e}^{-\tau^2/(4T^2)} \frac{1}{(2\pi)^{1/4}} \mathrm{e}^{-\tilde{\tau}^2/(4T^2)} \mathrm{e}^{\mathrm{i}(\omega_i \tau - \omega_j \tilde{\tau})} W(x_m, x_n) \\ &= \int_{-\infty}^{\infty} \mathrm{d}\tau \int_{-\infty}^{\infty} \mathrm{d}\tilde{\tau} \frac{1}{\sqrt{2\pi}} \exp\big[-(\tau^2+\tilde{\tau}^2)/(4T^2) + \mathrm{i}(\tau\omega_i - \tilde{\tau}\omega_j)\big] W(x_m, x_n) \end{aligned} \tag{F.1}$$

The Wightman function $W(x_m, x_n)$ refers to trajectories in a de Sitter static patch in a spacetime with de Sitter radius ℓ at constant r_m and r_n, respectively. The Wightman function is calculated in appendix B.10. We plug this in and obtain the following expression for eq. (F.1):

$$\begin{aligned}\langle \omega_j, m | \omega_i, n \rangle_{\mathrm{F}} = \int_{-\infty}^{\infty} \mathrm{d}\tau \int_{-\infty}^{\infty} \mathrm{d}\tilde{\tau} \frac{1}{\sqrt{2\pi}} \exp\big[-(\tau^2+\tilde{\tau}^2)/(4T^2) + \mathrm{i}(\tau\omega_i - \tilde{\tau}\omega_j)\big] \\ \cdot \frac{-1}{16\pi^2} \frac{\kappa_m \kappa_n}{\sinh^2[(\kappa_m\tilde{\tau} - \kappa_n\tau)/2] + \frac{1}{2}(1 + \kappa_m r_m \kappa_n r_n - \kappa_m\kappa_n \ell^2) - \mathrm{i}\varepsilon\kappa_m\kappa_n/4}\end{aligned}$$

where $\kappa_{m,n} = 1/\sqrt{\ell^2 - r_{m,n}^2}$. To simplify the time dependence of the Wightman function, we use the expansion of the Wightman function in terms of the Fourier modes calculated in eq. (B.12):

$$\langle \omega_j, m | \omega_i, n \rangle_{\mathrm{F}} = -\int_{-\infty}^{\infty} \mathrm{d}\tau \int_{-\infty}^{\infty} \mathrm{d}\tilde{\tau} \chi(\tau)\chi^*(\tilde{\tau}) e^{\mathrm{i}(\tau\omega_i - \tilde{\tau}\omega_j)} \int_{-\infty}^{\infty} -\frac{\kappa_m\kappa_n}{16\pi^2} \frac{2\sin\big(2\lambda \operatorname{arcsinh}\big(\sqrt{b_{mn}}\big)\big)}{\sqrt{b_{mn}(b_{mn}+1)}(e^{2\pi\lambda}-1)} e^{\mathrm{i}\lambda s} \mathrm{d}\lambda$$

where the parameter b_{mn} defined in eq. (B.10) captures the dependence on the trajectories x_m and x_n and s is defined to be $s = (\kappa_m\tilde{\tau} - \kappa_n\tau)/2$.
This way, we can separate the time-independent part and solve the time integrals:

$$\langle \omega_j, m | \omega_i, n \rangle_{\mathrm{F}} = \int_{-\infty}^{\infty} \frac{\kappa_m\kappa_n}{16\pi^2} \frac{2\sin\big(2\lambda \operatorname{arcsinh}\big(\sqrt{b_{mn}}\big)\big)}{\sqrt{b_{mn}(b_{mn}+1)}(e^{2\pi\lambda}-1)} \int_{-\infty}^{\infty} \mathrm{d}\tau \int_{-\infty}^{\infty} \mathrm{d}\tilde{\tau} \chi(\tau)\chi(\tilde{\tau}) e^{\mathrm{i}(\tau\omega_i - \tilde{\tau}\omega_j)} e^{\mathrm{i}\lambda s} \mathrm{d}\lambda \tag{F.2}$$

Time integrals

Using the expression of the Wightman function from eq. (F.2) we can solve the time integrals

$$\begin{aligned}\int_{-\infty}^{\infty}\mathrm{d}\tau\int_{-\infty}^{\infty}\mathrm{d}\tilde{\tau}\chi(\tau)\chi(\tilde{\tau})e^{\mathrm{i}(\tau\omega_i-\tilde{\tau}\omega_j)}e^{\mathrm{i}\lambda s} &= \int_{-\infty}^{\infty}\mathrm{d}\tau\chi(\tau)e^{\mathrm{i}(\omega_i-\lambda\kappa_n)\tau}\int_{-\infty}^{\infty}\mathrm{d}\tilde{\tau}\chi(\tilde{\tau})e^{\mathrm{i}(-\omega_j+\lambda\kappa_m)\tilde{\tau}}\\ &= 2\pi\tilde{\chi}(\omega_i-\lambda\kappa_n)\tilde{\chi}(-\omega_j+\lambda\kappa_m)\end{aligned}$$

where $\tilde{\chi}(\Omega)$ is the Fourier transform of the switching function, which again is a Gaussian. The Fourier transform of the switching function takes the following form:

$$\tilde{\chi}(\Omega)=\sqrt[4]{\frac{2}{\pi}}Te^{-T^2\Omega^2}$$

With this, the time-dependent part overall simplifies to

$$\begin{aligned}\int_{-\infty}^{\infty}\mathrm{d}\tau\int_{-\infty}^{\infty}\mathrm{d}\tilde{\tau}\chi(\tau)\chi(\tilde{\tau})e^{\mathrm{i}(\tau\omega_i-\tilde{\tau}\omega_j)}e^{\mathrm{i}\lambda s} &= 2\sqrt{2\pi}T^2e^{-T^2(\omega_j-\kappa_m\lambda)^2}e^{-T^2(\omega_i-\kappa_n\lambda)^2}\\ &= 2\sqrt{2\pi}T^2e^{-T^2\kappa_m^2\left(\frac{\omega_j}{\kappa_m}-\lambda\right)^2}e^{-T^2\kappa_n^2\left(\frac{\omega_i}{\kappa_n}-\lambda\right)^2}\end{aligned}$$

We can simplify this further using the adiabaticity assumption from eq. (9.2) which requires a large interaction time T. As the switching function $\chi(\tau)$ is a Gaussian function with a large interaction time, we know that its Fourier transform $\tilde{\chi}(\Omega)$ is very sharp. Accordingly, the product of the two Fourier-transformed switching functions only contributes if their peaks (the respective means of the Gaussians) are close. The resulting condition is such that the peaks are close and the Gaussians do not vanish is

$$\frac{\omega_i}{\kappa_n}\approx\frac{\omega_j}{\kappa_m} \tag{F.3}$$

For this quotient, we introduce a quantity

$$q_{in}=\frac{\omega_i}{\kappa_n}.$$

With this quotient, the time integral and, therefore, the product of Fourier-transformed switching functions takes the following form:

$$\int_{-\infty}^{\infty}\mathrm{d}\tau\int_{-\infty}^{\infty}\mathrm{d}\tilde{\tau}\chi(\tau)\chi(\tilde{\tau})e^{\mathrm{i}(\tau\omega_i-\tilde{\tau}\omega_j)}e^{\mathrm{i}\lambda s}=2\sqrt{2\pi}T^2e^{-T^2\kappa_m^2(q_{jm}-\lambda)^2}e^{-T^2\kappa_n^2(q_{in}-\lambda)^2}$$

When plugging this back into the scalar product from eq. (F.2), we obtain

$$\langle\omega_j,m|\omega_i,n\rangle_{\mathrm{F}}=\int_{-\infty}^{\infty}\frac{\kappa_m\kappa_n}{16\pi^2}\frac{2\sin\left(2\lambda\,\mathrm{arcsinh}\left(\sqrt{b_{mn}}\right)\right)}{\sqrt{b_{mn}(b_{mn}+1)}(e^{2\pi\lambda}-1)}2\sqrt{2\pi}T^2e^{-T^2\kappa_m^2(q_{jm}-\lambda)^2}e^{-T^2\kappa_n^2(q_{in}-\lambda)^2}\mathrm{d}\lambda$$

which can be simplified using $q=q_{in}=q_{jm}$

$$\langle\omega_j,m|\omega_i,n\rangle_{\mathrm{F}}=\frac{\kappa_m\kappa_n}{16\pi^2}\frac{4\sqrt{2\pi}T^2}{\sqrt{b_{mn}(b_{mn}+1)}}\int_{-\infty}^{\infty}\frac{\sin\left(2\lambda\,\mathrm{arcsinh}\left(\sqrt{b_{mn}}\right)\right)}{e^{2\pi\lambda}-1}e^{-T^2(\kappa_m^2+\kappa_n^2)(q-\lambda)^2}\mathrm{d}\lambda \tag{F.4}$$

Solve Fourier integral

We approximate the λ-integral from eq. (F.4) by again using that the interaction time T is large, which was imposed by the condition introduced in (9.2) and then solve the integral using Laplace's method:

$$\int_a^b \mathrm{d}x f(x) e^{-ng(x)} \sim \sqrt{\frac{2\pi}{ng''(x_0)}} f(x_0) e^{-ng(x_0)} \qquad \text{for } n \to \infty$$

Here, the function $g(x)$ has to be differentiable twice (with a strict minimum such that $g'(x_0) = 0$) and $f(x_0) \neq 0$. We identify the different terms of the integrals as follows where our integration variable is λ:

$$\begin{aligned} n =& T^2 \\ f(\lambda) =& \frac{\sin\big(2\lambda \operatorname{arcsinh}\big(\sqrt{b_{mn}}\big)\big)}{e^{2\pi\lambda} - 1} \\ g(\lambda) =& (\kappa_m^2 + \kappa_n^2)(q - \lambda)^2, \qquad\qquad g''(\lambda) = 2(\kappa_n^2 + \kappa_m^2) \\ g'(\lambda_0) =& -2(\kappa_m^2 + \kappa_n^2)(q - \lambda_0) = 0 \quad \Rightarrow \quad \lambda_0 = q_{in} \end{aligned}$$

For large T, the following holds:

$$\langle \omega_j, m | \omega_i, n \rangle_{\mathrm{F}} = \frac{\kappa_m \kappa_n}{16\pi^2} \frac{4\sqrt{2}\pi T}{\sqrt{b_{mn}(b_{mn}+1)}} \frac{1}{\sqrt{\kappa_n^2 + \kappa_m^2}} \frac{\sin\big(2q \operatorname{arcsinh}\big(\sqrt{b_{mn}}\big)\big)}{e^{2\pi q} - 1} \tag{F.5}$$

F.2. Diagonal terms of scalar product

For obtaining the diagonal terms of the scalar product, we consider two identical trajectories $r = r_m = r_n$ and express b_{mn} in terms of the dimensionless variable x, which is the rescaled radial variable:

$$b_{mn} = \lim_{x_m \to x_n} \frac{1}{2} \left(\frac{(1 - x_m x_n)}{\sqrt{1 - x_m^2}\sqrt{1 - x_n^2}} - 1 \right) = 0$$

We consider the result from eq. (F.5) and consider the limiting case of identical trajectories:

$$\begin{aligned} \langle \omega_i, m | \omega_i, m \rangle =& \frac{\kappa_m \kappa_n}{16\pi^2} \frac{4\sqrt{2}\pi T}{e^{2\pi q} - 1} \frac{1}{\sqrt{\kappa_m^2 + \kappa_m^2}} \lim_{b \to 0} \frac{\sin\big(2q \operatorname{arcsinh}\big(\sqrt{b_{mn}}\big)\big)}{\sqrt{b_{mn}(b_{mn}+1)}} \\ =& \frac{\kappa_m \kappa_n}{16\pi^2} \frac{4\sqrt{2}\pi T}{e^{2\pi q} - 1} \frac{1}{\sqrt{2}\kappa_m} 2q \end{aligned} \tag{F.6}$$

Note, that we introduced the parameter $q \approx q_{im} = \frac{\omega_i}{\kappa_m}$. We can plug this back in to obtain

$$\langle \omega_i, m | \omega_i, m \rangle = \frac{\kappa_m \kappa_n}{16\pi^2} \frac{4\pi T}{e^{\frac{2\pi\omega_i}{\kappa_m}} - 1} \frac{1}{\kappa_m} 2 \frac{\omega_i}{\kappa_m}$$

This is the thermal spectrum with the de Sitter temperature $T_{\mathrm{dS}} = \frac{\kappa}{2\pi}$ from eq. (8.2):

$$\langle \omega_i, m | \omega_i, m \rangle = \frac{T}{2\pi} \frac{\omega_i}{\left(e^{\omega_i / T_{\mathrm{dS}}} - 1\right)} = \frac{T}{2\pi} \frac{\omega_i}{(e^{2\pi q} - 1)} \tag{F.7}$$

F.3. Normalized inner product

Here, we calculate the inner product of normalized states

$$\Lambda^{ij}_{nm} = \frac{\langle \omega_j, m | \omega_i, n \rangle_{\mathrm{F}}}{\sqrt{\langle \omega_i, n | \omega_i, n \rangle_{\mathrm{F}} \langle \omega_j, m | \omega_j, m \rangle_{\mathrm{F}}}}$$

with this we can expand the off-diagonal terms ($i \neq j$ and $n \neq m$) of the scalar product as follows:

$$\begin{aligned}
\langle \omega_j, m | \omega_i, n \rangle_{\mathrm{F}} =& \Lambda^{ij}_{nm} \sqrt{\langle \omega_i, n | \omega_i, n \rangle_{\mathrm{F}} \langle \omega_j, m | \omega_j, m \rangle_{\mathrm{F}}} \\
=& \Lambda^{ij}_{nm} \frac{T}{2\pi} \sqrt{\frac{\omega_i \omega_j}{(e^{2\pi q} - 1)(e^{2\pi q} - 1)}} \\
=& \Lambda^{ij}_{nm} \frac{T}{2\pi} \frac{\sqrt{\omega_i \omega_j}}{e^{2\pi q} - 1}
\end{aligned}$$

With this, we can see that the information of the off-diagonal terms is encoded in the normalized inner product. For further calculations, we need to plug in the explicit expression of the parameters from eq. (B.10) and the results of the scalar product from eq. (F.5) and its diagonal terms from eq. (F.7). We also use, that $q_{in} = \frac{\omega_i}{\kappa_n}$.

$$\begin{aligned}
\Lambda^{mn}_{ij} =& \frac{\kappa_m \kappa_n}{2\pi^2} \frac{\sqrt{2}\pi^2 \sin\left(2q \operatorname{arcsinh}\left(\sqrt{b_{mn}}\right)\right)}{\sqrt{b_{mn}(b_{mn}+1)} \sqrt{\kappa_n^2 + \kappa_m^2} \sqrt{\omega_i \omega_j}} \\
=& \frac{\sqrt{\kappa_m \kappa_n} \sin\left(2q \operatorname{arcsinh}\left(\sqrt{b_{mn}}\right)\right)}{\sqrt{2} q \sqrt{\kappa_n^2 + \kappa_m^2} \sqrt{b_{mn}(b_{mn}+1)}}
\end{aligned}$$

As a sanity check, we look at the normalized inner product for identical trajectories, which is obtained by taking the limit $b_{nn} \to 0$:

$$\Lambda^{nn}_{ii} = \frac{\sqrt{\kappa_n \kappa_n} \sin\left(2q \operatorname{arcsinh}\left(\sqrt{b_{nn}}\right)\right)}{\sqrt{2} q \sqrt{\kappa_n^2 + \kappa_n^2} \sqrt{b_{nn}(b_{nn}+1)}} = \frac{\sqrt{\kappa_n \kappa_n}}{\sqrt{2} q \sqrt{2\kappa_n^2}} 2q = 1$$

Bibliography

[ABF20] Pablo Arrighi, Cédric Bény, and Terry Farrelly. A quantum cellular automaton for one-dimensional QED. *Quantum Information Processing*, 19(3), jan 2020. doi:10.1007/s11128-019-2555-4. ↪ [88]

[ACT+11] G. Acquaviva, R. Di Criscienzo, M. Tolotti, L. Vanzo, and S. Zerbini. Unruh-DeWitt Detectors in Spherically Symmetric Dynamical Space-Times. *Int. J. Theor. Phys.*, 51(5):1555–1571, dec 2011, arXiv:1111.6389. doi:10.1007/s10773-011-1033-2. ↪ [4]

[ADH15] Ahmed Almheiri, Xi Dong, and Daniel Harlow. Bulk locality and quantum error correction in AdS/CFT. *J. High Energy Phys.*, 2015(4), 2015, arXiv:1411.7041. doi:10.1007/jhep04(2015)163. ↪ [2, 49, 50]

[AFR23] Shahnewaz Ahmed, Mir Mehedi Faruk, and Muktadir Rahman. Accelerated paths and Unruh effect II: finite time detector response in (Anti) de Sitter spacetime and Huygen's Principle. *arXiv*, 2023, arXiv:2301.08717. ↪ [4]

[AHM21] Stephon Alexander, Gabriel Herczeg, and João Magueijo. A generalized Hartle-Hawking wave function. *Class. Quantum Gravity*, 38(9):095011, apr 2021. doi:10.1088/1361-6382/abf2f6. ↪ [35]

[AHS16] Dionysios Anninos, Thomas Hartman, and Andrew Strominger. Higher spin realization of the dS/CFT correspondence. *Class. Quantum Gravity*, 34(1):015009, 2016, arXiv:1108.5735. doi:10.1088/1361-6382/34/1/015009. ↪ [3]

[Aic07a] F. Aicardi. Symmetries of quadratic forms classes and of quadratic surds continued fractions. Part II: Classification of the periods' palindromes. *Bull Braz Math Soc, New Series*, 2007, arXiv:0708.2082. doi:10.1007/s00574-010-0005-0. ↪ [75]

[Aic07b] Francesca Aicardi. Symmetries of quadratic forms classes and of quadratic surds continued fractions. Part I: A Poincaré model for the de Sitter world. *Bull Braz Math Soc, New Series*, August 2007, arXiv:0708.1571. doi:10.1007/s00574-009-0014-z. ↪ [75]

[All85] Bruce Allen. Vacuum states in de Sitter space. *Phys. Rev. D*, 32(12):3136–3149, dec 1985. doi:10.1103/physrevd.32.3136. ↪ [23, 34, 36]

[And07] James W. Anderson. *Hyperbolic geometry*. Springer undergraduate mathematics series. Springer, London, 2. ed., corr. print. edition, 2007. ↪ [47]

[AP03] Pablo Arrighi and Christophe Patricot. A note on the correspondence between qubit quantum operations and special relativity. *Journal of Physics A: Mathematical and General*, 36(20):L287–L296, may 2003. doi:10.1088/0305-4470/36/20/101. ↪ [88]

[AS64] Milton Abramowitz and Irene A. Stegun. *Handbook of mathematical functions with formulas, graphs, and mathematical tables*, volume 55. US Government printing office, 1964. ↪ [37, 150, 153, 154]

[Ban01] T. Banks. Cosmological Breaking of Supersymmetry? . *Int. J. Mod. Phys. A*, 16(05):910–921, 2001, arXiv:hep-th/0007146. doi:10.1142/s0217751x01003998. ↪ [2, 86]

[BB99] Hans-Juergen Borchers and Detlev Buchholz. Global Properties of Vacuum States in de Sitter Space. *Annales de l'I.H.P. Physique théorique*, 70:23–40, 1999, arXiv:gr-qc/9803036. URL `http://www.numdam.org/item/AIHPA_1999__70_1_23_0/`. ↪ [113]

[BC17] Jacob C. Bridgeman and Christopher T. Chubb. Hand-waving and interpretive dance: an introductory course on tensor networks. *Journal of Physics A: Mathematical and Theoretical*, 50(22):223001, may 2017. doi:10.1088/1751-8121/aa6dc3. ↪ [43]

[BCC+15] Ning Bao, ChunJun Cao, Sean M. Carroll, Aidan Chatwin-Davies, Nicholas Hunter-Jones, Jason Pollack, and Grant N. Remmen. Consistency conditions for an AdS multiscale entanglement renormalization ansatz correspondence. *Phys. Rev. D*, 91(12):125036, 2015, arXiv:1504.06632. doi:10.1103/physrevd.91.125036. ↪ [2]

[BCCCD17] Ning Bao, ChunJun Cao, Sean M. Carroll, and Aidan Chatwin-Davies. de Sitter space as a tensor network: Cosmic no-hair, complementarity, and complexity. *Phys. Rev. D*, 96(12):123536, 2017, arXiv:1709.03513. doi:10.1103/physrevd.96.123536. ↪ [3]

[BCCM17] Ning Bao, ChunJun Cao, Sean M. Carroll, and Liam McAllister. Quantum circuit cosmology: The expansion of the universe since the first qubit. February 2017, 1702.06959. ↪ [90]

[BCI+01] Samuel L. Braunstein, Nicolas J. Cerf, Sofyan Iblisdir, Peter van Loock, and Serge Massar. Optimal Cloning of Coherent States with a Linear Amplifier and Beam Splitters. *Phys. Rev. Lett.*, 86(21):4938–4941, May 2001. doi:10.1103/physrevlett.86.4938. ↪ [53]

[BCRAvB20] Luis C. Barbado, Esteban Castro-Ruiz, Luca Apadula, and Časlav Brukner. Unruh effect for detectors in superposition of accelerations. *Phys. Rev. D*, 102(4):045002, 2020, arXiv:2003.12603. doi:10.1103/PhysRevD.102.045002. ↪ [5, 6, 119, 120, 126, 129]

[BCT21] Jan Boruch, Pawel Caputa, and Tadashi Takayanagi. Path integral optimization from Hartle-Hawking wave function. *Phys. Rev. D*, 103(4):046017, feb 2021. doi:10.1103/physrevd.103.046017. ↪ [35]

[BD82] N. D. Birrell and P. C. W. Davies. *Quantum Fields in Curved Space*. Cambridge University Press, 1982. doi:10.1017/cbo9780511622632. ↪ [4, 11, 12, 24, 25, 27, 38, 41, 113, 119]

[BDBD+15] A. Bibeau-Delisle, A. Bisio, G. M. D'Ariano, P. Perinotti, and A. Tosini. Doubly special relativity from quantum cellular automata. *Europhysics Letters*, 109(5):50003, mar 2015. doi:10.1209/0295-5075/109/50003. ↪ [88]

[BdBM02] Vijay Balasubramanian, Jan de Boer, and Djordje Minic. Mass, entropy, and holography in asymptotically de Sitter spaces. *Phys. Rev. D*, 65(12):123508, 2002, arXiv:hep-th/0110108. doi:10.1103/physrevd.65.123508. ↪ [3]

[BDD+19] Souvik Banerjee, Ulf Danielsson, Giuseppe Dibitetto, Suvendu Giri, and Marjorie Schillo. De Sitter cosmology on an expanding bubble. *J. High Energy Phys.*, 2019(10), oct 2019, arXiv:1907.04268. doi:10.1007/jhep10(2019)164. ↪ [4]

[BDE+98] Dagmar Bruß, David P. DiVincenzo, Artur Ekert, Christopher A. Fuchs, Chiara Macchiavello, and John A. Smolin. Optimal universal and state-dependent quantum cloning. *Phys. Rev. A*, 57(4):2368–2378, April 1998. doi:10.1103/physreva.57.2368. ↪ [52]

[BDP17] Alessandro Bisio, Giacomo Mauro D'Ariano, and Paolo Perinotti. Quantum Walks, Weyl Equation and the Lorentz Group. *Foundations of Physics*, 47(8):1065–1076, apr 2017. doi:10.1007/s10701-017-0086-3. ↪ [88]

[Bek72] J. D. Bekenstein. Black holes and the second law. *Lettere Al Nuovo Cimento Series 2*, 4(15):737–740, August 1972. doi:10.1007/bf02757029. ↪ [108]

[Bel04] J. Belk. *Thompson's group F*. PhD thesis, Cornell University, 2004. URL `https://www.imo.universite-paris-saclay.fr/~emmanuel.breuillard/Belk.pdf`. ↪ [2, 61, 63]

[Bén13] Cédric Bény. Causal structure of the entanglement renormalization ansatz. *New J. Phys.*, 15(2):023020, 2013, arXiv:1110.4872. doi:10.1088/1367-2630/15/2/023020. ↪ [3, 88, 90]

[BGHL16] Arpan Bhattacharyya, Zhe-Shen Gao, Ling-Yan Hung, and Si-Nong Liu. Exploring the tensor networks/AdS correspondence. *J. High Energy Phys.*, 2016(8), 2016, arXiv:1606.00621. doi:10.1007/jhep08(2016)086. ↪ [2]

[BH96] V. Bužek and M. Hillery. Quantum copying: Beyond the no-cloning theorem. *Phys. Rev. A*, 54(3):1844–1852, sep 1996. doi:10.1103/physreva.54.1844. ↪ [52, 53]

[BH98] Vladimír Bužek and Mark Hillery. Universal Optimal Cloning of Arbitrary Quantum States: From Qubits to Quantum Registers. *Phys. Rev. Lett.*, 81(22):5003–5006, nov 1998. doi:10.1103/physrevlett.81.5003. ↪ [52, 53]

[BH99] Raphael Bousso and Stephen Hawking. Lorentzian condition in quantum gravity. *Phys. Rev. D*, 59(10):103501, mar 1999. doi:10.1103/physrevd.59.103501. ↪ [35]

[BHM01] Vijay Balasubramanian, Petr Horava, and Djordje Minic. Deconstructing de Sitter. *J. High Energy Phys.*, 2001(05):043–043, 2001, arXiv:hep-th/0103171. doi:10.1088/1126-6708/2001/05/043. ↪ [2, 108]

[BHP09] Kamil Brádler, Patrick Hayden, and Prakash Panangaden. Private information via the Unruh effect. *J. High Energy Phys.*, 2009(08):074–074, 2009, arXiv:0807.4536. doi:10.1088/1126-6708/2009/08/074. ↪ [4, 113, 116]

[BHP12] Kamil Brádler, Patrick Hayden, and Prakash Panangaden. Quantum Communication in Rindler Spacetime. *Commun. Math. Phys.*, 312(2):361–398, 2012, arXiv:1007.0997. doi:10.1007/s00220-012-1476-1. ↪ [4, 113, 116, 118]

[BHTW10] Kamil Brádler, Patrick Hayden, Dave Touchette, and Mark M. Wilde. Trade-off capacities of the quantum Hadamard channels. *Phys. Rev. A*, 81(6):062312, 2010, arXiv:1001.1732. doi:10.1103/physreva.81.062312. ↪ [4, 113, 116, 118]

[BKSS22] Shovon Biswas, Jani Kastikainen, Sanjit Shashi, and James Sully. Holographic BCFT Spectra from Brane Mergers. *J. High Energy Phys.*, 2022(11), nov 2022, arXiv:2209.11227. doi:10.1007/jhep11(2022)158. ↪ [73]

[BMM+17] Sougato Bose, Anupam Mazumdar, Gavin W. Morley, Hendrik Ulbricht, Marko Toroš, Mauro Paternostro, Andrew A. Geraci, Peter F. Barker, M. S. Kim, and Gerard Milburn. Spin Entanglement Witness for Quantum Gravity. *Physical Review Letters*, 119(24):240401, December 2017. doi:10.1103/physrevlett.119.240401. ↪ [5]

[BMS01] Raphael Bousso, Alexander Maloney, and Andrew Strominger. Conformal Vacua and Entropy in de Sitter Space. *Phys. Rev. D*, 2001, arXiv:hep-th/0112218. doi:10.1103/PhysRevD.65.104039. ↪ [15, 35, 36, 38, 39, 41, 153]

[Bou99a] Raphael Bousso. A covariant entropy conjecture. *J. High Energy Phys.*, 1999(07):004–004, 1999, arXiv:hep-th/9905177. doi:10.1088/1126-6708/1999/07/004. ↪ [2, 86]

[Bou99b] Raphael Bousso. Holography in general space-times. *J. High Energy Phys.*, 1999(06):028–028, 1999, arXiv:hep-th/9906022. doi:10.1088/1126-6708/1999/06/028. ↪ [2, 86]

[Bou00] Raphael Bousso. Positive vacuum energy and the N-bound. *J. High Energy Phys.*, 2000(11):038–038, 2000, arXiv:hep-th/0010252. doi:10.1088/1126-6708/2000/11/038. ↪ [2, 86]

[Bou01] Raphael Bousso. Bekenstein bounds in de Sitter and flat space. *J. High Energy Phys.*, 2001(04):035–035, April 2001. doi:10.1088/1126-6708/2001/04/035. ↪ [108]

[Bou02a] Raphael Bousso. Adventures in de Sitter space. *arXiv*, 2002, arXiv:hep-th/0205177. ↪ [89, 154]

[Bou02b] Raphael Bousso. The holographic principle. *Reviews of Modern Physics*, 74(3):825–874, aug 2002. doi:10.1103/revmodphys.74.825. ↪ [1, 73]

[BR03] Stephen M. Barnett and Paul M. Radmore. *Methods in Theoretical Quantum Optics*, volume 15 of *Oxford Series on Optical and Imaging Science*. Oxford University Press, USA, 2003. URL `https://global.oup.com/academic/product/methods-in-theoretical-quantum-optics-9780198563617?cc=de&lang=en&`. ↪ [188]

[BRS+16] Adam R. Brown, Daniel A. Roberts, Leonard Susskind, Brian Swingle, and Ying Zhao. Complexity, action, and black holes. *Phys. Rev. D*, 93(8):086006, apr 2016. doi:10.1103/physrevd.93.086006. ↪ [1]

[BS14] Robert Bieri and Ralph Strebel. On Groups of PL-homeomorphisms of the Real Line. *arXiv*, November 2014, arXiv:1411.2868. ↪ [64]

[Car01] Moshe Carmeli. Value of the cosmological constant: Theory versus experiment. In *AIP Conference Proceedings*. AIP, 2001, arXiv:astro-ph/0102033. doi:10.1063/1.1419571. ↪ [2]

[CCJ70] Curtis G. Callan, Sidney Coleman, and Roman Jackiw. A new improved energy-momentum tensor. *Ann. Phys.*, 59(1):42–73, jul 1970. doi:10.1016/0003-4916(70)90394-5. ↪ [24]

[CCO+11] R. Casadio, S. Chiodini, A. Orlandi, G. Acquaviva, R. Di Criscienzo, and L. Vanzo. On the Unruh effect in de Sitter space. *Mod. Phys. Lett. A*, 26(28):2149–2158, sep 2011, arXiv:1011.3336. doi:10.1142/s0217732311036516. ↪ [4, 113]

[CD18] Aidan Chatwin-Davies. *Gravity Informed*. PhD thesis, California Institute of Technology, 2018. doi:10.7907/ZD4W-4C63. ↪ [73]

[CDP08] Giulio Chiribella, Giacomo Mauro D'Ariano, and Paolo Perinotti. Optimal Cloning of Unitary Transformation. *Phys. Rev. Lett.*, 101(18):180504, October 2008. doi:10.1103/physrevlett.101.180504. ↪ [53]

[CDPC05] G. Chiribella, G. M. D'Ariano, P. Perinotti, and N. J. Cerf. Extremal quantum cloning machines. *Phys. Rev. A*, 72(4):042336, October 2005. doi:10.1103/physreva.72.042336. ↪ [53]

[CFP96] James W. Cannon, William J. Floyd, and Walter R. Parry. Introductory notes on Richard Thompson's groups. *Enseignement Mathématique*, 42:215–256, 1996. URL `https://www.e-periodica.ch/digbib/view?pid=ens-001:1996:42::85#416`. ↪ [2, 61, 62, 63]

[CG17] Chong-Sun Chu and Dimitrios Giataganas. Thermal bath in de Sitter space from holography. *Phys. Rev. D*, 96(2):026023, jul 2017, arXiv:1608.07431. doi:10.1103/physrevd.96.026023. ↪ [5]

[CHM08] Luís C. B. Crispino, Atsushi Higuchi, and George E. A. Matsas. The Unruh effect and its applications. *Rev. Mod. Phys.*, 80(3):787–838, jul 2008, arXiv:0710.5373. doi:10.1103/revmodphys.80.787. ↪ [27, 145]

[CHQY19] Jordan Cotler, Xizhi Han, Xiao-Liang Qi, and Zhao Yang. Quantum causal influence. *J. High Energy Phys.*, 2019(7), jul 2019. doi:10.1007/jhep07(2019)042. ↪ [88, 90, 108]

[Chr] Malin Christersson. Non-Euclidean Geometry: Interactive Hyperbolic Tiling in the Poincaré disc. `https://www.malinc.se/noneuclidean/en/poincaretiling.php`. Accessed: 06.12.2023. ↪ [49]

[CJ23] Jordan Cotler and Kristan Jensen. Isometric evolution in de Sitter quantum gravity. *arXiv*, 2023, arXiv:2302.06603. ↪ [3]

[CJM20] Jordan Cotler, Kristan Jensen, and Alexander Maloney. Low-dimensional de Sitter quantum gravity. *J. High Energy Phys.*, 2020(6), 2020, arXiv:1905.03780. doi:10.1007/jhep06(2020)048. ↪ [3, 12, 133, 134]

[CLMS15] Bartłomiej Czech, Lampros Lamprou, Samuel McCandlish, and James Sully. Integral geometry and holography. *J. High Energy Phys.*, 2015(10), 2015, arXiv:1505.05515. doi:10.1007/jhep10(2015)175. ↪ [3]

[CLMS16] Bartlomiej Czech, Lampros Lamprou, Samuel McCandlish, and James Sully. Tensor networks from kinematic space. *J. High Energy Phys.*, 2016(7), 2016, arXiv:1512.01548. doi:10.1007/jhep07(2016)100. ↪ [3, 88]

[CLPW23] Venkatesa Chandrasekaran, Roberto Longo, Geoff Penington, and Edward Witten. An algebra of observables for de Sitter space. *J. High Energy Phys.*, 2023(2), feb 2023. doi:10.1007/jhep02(2023)082. ↪ [107, 108]

[CR19] Marios Christodoulou and Carlo Rovelli. On the possibility of laboratory evidence for quantum superposition of geometries. *Physics Letters B*, 792:64–68, May 2019. doi:10.1016/j.physletb.2019.03.015. ↪ [5]

[CS22] Jordan Cotler and Andrew Strominger. The Universe as a Quantum Encoder. *arXiv*, 2022, arXiv:2201.11658. ↪ [3, 80]

[CS23] Jordan Cotler and Andrew Strominger. Cosmic ER=EPR in dS/CFT. *arXiv*, 2023, arXiv:2302.00632. ↪ [3]

[CT68] N. A. Chernikov and E. A. Tagirov. Quantum theory of scalar fieldin de Sitter space-time. *Ann. Inst. Henri Poincaré,*, IX(2):109 – 141, 1968. URL `http://www.numdam.org/item/AIHPA_1968__9_2_109_0.pdf`. ↪ [24, 38]

[CY14] Giulio Chiribella and Yuxiang Yang. Optimal asymptotic cloning machines. *New Journal of Physics*, 16(6):063005, June 2014. doi:10.1088/1367-2630/16/6/063005. ↪ [53]

[dBHMN16] Jan de Boer, Michal P. Heller, Robert C. Myers, and Yasha Neiman. Holographic de Sitter Geometry from Entanglement in Conformal Field Theory. *Phys. Rev. Lett.*, 116(6):061602, feb 2016. doi:10.1103/physrevlett.116.061602. ↪ [88]

[Deb19] Fabrice Debbasch. Action principles for quantum automata and Lorentz invariance of discrete time quantum walks. *Ann. Phys.*, 405:340–364, jun 2019. doi:10.1016/j.aop.2019.03.005. ↪ [88]

[DeW80] Bryce S. DeWitt. *General Relativity : An Einstein Centenary Survey*, chapter Quantum Gravity: The New Synthesis, pages 680–745. 1980. URL `https://inspirehep.net/literature/159073`. ↪ [5, 119]

[DFU76] P. C. W. Davies, S. A. Fulling, and W. G. Unruh. Energy-momentum tensor near an evaporating black hole. *Phys. Rev. D*, 13(10):2720–2723, 1976. doi:10.1103/physrevd.13.2720. ↪ [4, 26]

[Die14] Joe Diestel. *The joys of Haar measure*. Number volume 150 in Graduate Studies in Mathematics. American Mathematical Society, Providence, Rhode Island, 2014. Includes bibliographical references (pages 309-315) and index. - Electronic reproduction; Providence, Rhode Island; American Mathematical Society; 2014. - Description based on print version record. ↪ [104]

[DKSW07] Giacomo Mauro D'Ariano, Dennis Kretschmann, Dirk Schlingemann, and Reinhard F. Werner. Reexamination of quantum bit commitment: The possible and the impossible. *Phys. Rev. A*, 76(3):032328, September 2007. doi:10.1103/physreva.76.032328. ↪ [53]

[DL97] S. Deser and Orit Levin. Accelerated detectors and temperature in (anti-) de Sitter spaces. *Class. Quantum Gravity*, 14(9):L163–L168, sep 1997, arXiv:gr-qc/9706018. doi:10.1088/0264-9381/14/9/003. ↪ [4, 113]

[DL98] S. Deser and Orit Levin. Equivalence of Hawking and Unruh temperatures and entropies through flat space embeddings. *Class. Quantum Gravity*, 15(12):L85–L87, dec 1998. doi:10.1088/0264-9381/15/12/002. ↪ [115]

[DL99] S. Deser and Orit Levin. Mapping Hawking into Unruh thermal properties. *Phys. Rev. D*, 59(6):064004, feb 1999, arXiv:hep-th/9809159. doi:10.1103/physrevd.59.064004. ↪ [4, 113, 115]

[DMMW17] William Donnelly, Donald Marolf, Ben Michel, and Jason Wien. Living on the edge: a toy model for holographic reconstruction of algebras with centers. *J. High Energy Phys.*, 2017(4), apr 2017. doi:10.1007/jhep04(2017)093. ↪ [2]

[dS17a] Willem de Sitter. On the curvature of space. In *Proc. Kon. Ned. Akad. Wet*, volume 20, pages 229–243, 1917. URL `https://dwc.knaw.nl/DL/publications/PU00012216.pdf`. ↪ [1, 9]

[dS17b] Willem de Sitter. On the relativity of inertia. Remarks concerning Einstein's latest hypothesis. *Proc. Kon. Ned. Acad. Wet*, 1917. URL `https://dwc.knaw.nl/DL/publications/PU00012455.pdf`. ↪ [1, 9]

[Dui00] Johannes J. Duistermaat. *Lie Groups*. Springer, Berlin, 2000. doi:10.1007/978-3-642-56936-4. ↪ [105]

[DZ01] Sumit R. Das and Andrei Zelnikov. Unruh radiation, holography, and boundary cosmology. *Phys. Rev. D*, 64(10):104001, sep 2001, arXiv:hep-th/0104198. doi:10.1103/physrevd.64.104001. ↪ [4]

[EL03] Martin B. Einhorn and Finn Larsen. Interacting quantum field theory in de Sitter vacua. *Phys. Rev. D*, 67(2):024001, jan 2003, arXiv:hep-th/0209159. doi:10.1103/physrevd.67.024001. ↪ [41]

[EMV16] Julius Engelsöy, Thomas G. Mertens, and Herman Verlinde. An investigation of AdS2 backreaction and holography. *J. High Energy Phys.*, 2016(7), 2016. doi:10.1007/jhep07(2016)139. ↪ [12]

[EWŻ16] M. Enríquez, I Wintrowicz, and K. Życzkowski. Maximally Entangled Multipartite States: A Brief Survey. *Journal of Physics: Conference Series*, 698:012003, mar 2016. doi:10.1088/1742-6596/698/1/012003. ↪ [2, 107]

[FAZM23] Joshua Foo, Cemile Senem Arabaci, Magdalena Zych, and Robert B. Mann. Quantum superpositions of Minkowski spacetime. *Physical Review D*, 107(4):045014, February 2023, 2208.12083. doi:10.1103/physrevd.107.045014. ↪ [5, 119]

[FHKN75] Rodolfo Figari, Raphael Höegh-Krohn, and Chiara R. Nappi. Interacting relativistic boson fields in the De Sitter universe with two space-time dimensions. *Commun. Math. Phys.*, 44(3):265–278, October 1975. doi:10.1007/bf01609830. ↪ [113]

[FMZ20] Joshua Foo, Robert B. Mann, and Magdalena Zych. Schrödinger's cat for de Sitter spacetime. *Class. Quantum Gravity*, 38(11):115010, 2020, arXiv:2012.10025. doi:10.1088/1361-6382/abf1c4. ↪ [5, 119, 126, 128, 129]

[FMZ23] Joshua Foo, Robert B. Mann, and Magdalena Zych. Relativity and decoherence of spacetime superpositions. *arXiv*, February 2023, 2302.03259. ↪ [5, 119]

[FNA+20] Philippe Faist, Sepehr Nezami, Victor V. Albert, Grant Salton, Fernando Pastawski, Patrick Hayden, and John Preskill. Continuous Symmetries and Approximate Quantum Error Correction. *Phys. Rev. X*, 10(4):041018, October 2020. doi:10.1103/physrevx.10.041018. ↪ [51]

[Fos10] Ariadna Fossas. PSL(2,Z) as a non distorted subgroup of Thompson's group T. *Indiana University Mathematics Journal*, June 2010, arXiv:1006.0508. ↪ [63]

[FOZ20] Joshua Foo, Sho Onoe, and Magdalena Zych. Unruh-deWitt detectors in quantum superpositions of trajectories. *Phys. Rev. D 102, 085013 (2020)*, 102(8):085013, October 2020, 2003.12774. doi:10.1103/physrevd.102.085013. ↪ [5, 119]

[FPST94] Thomas M. Fiola, John Preskill, Andrew Strominger, and Sandip P. Trivedi. Black hole thermodynamics and information loss in two dimensions. *Phys.Rev.D*, 50:3987–4014, 1994, arXiv:hep-th/9403137. doi:10.1103/PhysRevD.50.3987. ↪ [40]

[Ful73] Stephen A. Fulling. Nonuniqueness of Canonical Field Quantization in Riemannian Space-Time. *Phys. Rev. D*, 7(10):2850–2862, 1973. doi:10.1103/physrevd.7.2850. ↪ [4, 23, 26]

[FWJ+14] Heng Fan, Yi-Nan Wang, Li Jing, Jie-Dong Yue, Han-Duo Shi, Yong-Liang Zhang, and Liang-Zhu Mu. Quantum cloning machines and the applications. *Physics Reports*, 544(3):241–322, nov 2014. doi:10.1016/j.physrep.2014.06.004. ↪ [53]

[FZ23] Joshua Foo and Magdalena Zych. Superpositions of thermalisation states in relativistic quantum field theory. *arXiv*, July 2023, 2307.02593. ↪ [5, 119]

[GAL+15] Dardo Goyeneche, Daniel Alsina, José I. Latorre, Arnau Riera, and Karol Życzkowski. Absolutely maximally entangled states, combinatorial designs, and multiunitary matrices. *Phys. Rev. A*, 92(3):032316, sep 2015, 1506.08857. doi:10.1103/physreva.92.032316. ↪ [2]

[Gar15] P. Garrett. Sporadic isogenies to orthogonal groups. available online from University of Minnesota, 2015. URL `http://www-users.math.umn.edu/~garrett/m/v/sporadic_isogenies.pdf`. ↪ [58]

[GGK+22] A. Ghodsi, J. K. Ghosh, E. Kiritsis, F. Nitti, and V. Nourry. Holographic QFTs on AdS_d, wormholes and holographic interfaces. *J. High Energy Phys.*, 2023(1), jan 2022, arXiv:2209.12094. doi:10.1007/jhep01(2023)121. ↪ [73]

[GH77a] G. W. Gibbons and S. W. Hawking. Action integrals and partition functions in quantum gravity. *Phys. Rev. D*, 15:2752–2756, 1977. doi:10.1103/PhysRevD.15.2752. ↪ [12, 113]

[GH77b] G. W. Gibbons and S. W. Hawking. Cosmological event horizons, thermodynamics, and particle creation. *Phys. Rev. D*, 15(10):2738–2751, May 1977. doi:10.1103/physrevd.15.2738. ↪ [4, 108, 114]

[GH93] Gary W. Gibbons and Stephen W. Hawking. *Euclidean quantum gravity*. World Scientific, Singapore, 1993. ↪ [35]

[GKP98] S. S. Gubser, I. R. Klebanov, and A. M. Polyakov. Gauge theory correlators from non-critical string theory. *Phys. Lett. B*, 428(1-2):105–114, 1998, arXiv:hep-th/9802109. doi:10.1016/s0370-2693(98)00377-3. ↪ [1]

[GKP+17] Steven S. Gubser, Johannes Knaute, Sarthak Parikh, Andreas Samberg, and Przemek Witaszczyk. p-Adic AdS/CFT. *Commun. Math. Phys.*, 352(3):1019–1059, jan 2017. doi:10.1007/s00220-016-2813-6. ↪ [4]

[GM97] N. Gisin and S. Massar. Optimal Quantum Cloning Machines. *Phys. Rev. Lett.*, 79(11):2153–2156, sep 1997. doi:10.1103/physrevlett.79.2153. ↪ [52, 53]

[GP04] Björn Garbrecht and Tomislav Prokopec. Unruh response functions for scalar fields in de Sitter space. *Class. Quantum Gravity*, 21(21):4993–5004, oct 2004, arXiv:gr-qc/0404058. doi:10.1088/0264-9381/21/21/016. ↪ [4, 113]

[GS16] Lisa Glaser and Sumati Surya. The Hartle-Hawking wave function in 2D causal set quantum gravity. *Class. Quantum Gravity*, 33(6):065003, feb 2016. doi:10.1088/0264-9381/33/6/065003. ↪ [35]

[Gub17] Steven S. Gubser. A p-adic version of AdS/CFT. *arXiv*, April 2017, arXiv:1705.00373. ↪ [4]

[GZ22] Evan P. G. Gale and Magdalena Zych. Relativistic Unruh-DeWitt detectors with quantized center of mass. *Phys. Rev. D 107, 056023 (2023)*, 107(5):056023, March 2022, 2211.10562. doi:10.1103/physrevd.107.056023. ↪ [119]

[Har16] D. Harlow. Jerusalem lectures on black holes and quantum information. *Reviews of Modern Physics*, 88(1):015002, feb 2016. doi:10.1103/revmodphys.88.015002. ↪ [1]

[Hau13] Markus Hauru. Multiscale Entanglement Renormalisation Ansatz. Master's thesis, University of Helsinki, 2013. URL `https://mhauru.org/MSc_thesis.pdf`. ↪ [90]

[Haw75] S. W. Hawking. Particle creation by black holes. *Commun. Math. Phys.*, 43(3):199–220, August 1975. doi:10.1007/bf02345020. ↪ [108]

[HE75] S. W. Hawking and G. F. R. Ellis. *The Large Scale Structure Of Spacetime*. Cambridge University Press, 1975. doi:10.1017/CBO9780511524646. ↪ [9, 12, 25, 74]

[HH83] J. B. Hartle and S. W. Hawking. Wave function of the Universe. *Phys. Rev. D*, 28(12):2960–2975, 1983. doi:10.1103/physrevd.28.2960. ↪ [35]

[HHH14] James B. Hartle, S. W. Hawking, and Thomas Hertog. Quantum probabilities for inflation from holography. *Journal of Cosmology and Astroparticle Physics*, 2014(01):015–015, jan 2014. doi:10.1088/1475-7516/2014/01/015. ↪ [35]

[HHH19] J. J. Halliwell, J. B. Hartle, and T. Hertog. What is the no-boundary wave function of the Universe? *Phys. Rev. D*, 99(4):043526, feb 2019. doi:10.1103/physrevd.99.043526. ↪ [35]

[Hig87] A. Higuchi. Quantisation of scalar and vector fields inside the cosmological event horizon and its application to the Hawking effect. *Class. Quantum Gravity*, 4(3):721–740, 1987. doi:10.1088/0264-9381/4/3/029. ↪ [4]

[HMS01] Stephen Hawking, Juan Maldacena, and Andrew Strominger. DeSitter entropy, quantum entanglement and ADS/CFT. *J. High Energy Phys.*, 2001(05):001–001, 2001, arXiv:hep-th/0002145. doi:10.1088/1126-6708/2001/05/001. ↪ [2]

[HNQ+16] Patrick Hayden, Sepehr Nezami, Xiao-Liang Qi, Nathaniel Thomas, Michael Walter, and Zhao Yang. Holographic duality from random tensor networks. *J. High Energy Phys.*, 2016(11), 2016, arXiv:1601.01694. doi:10.1007/jhep11(2016)009. ↪ [1, 2]

[Hol95] Sören Holst. Gott time machines in the Anti-de Sitter space. *Gen.Rel.Grav. 28 (1996) 387-403*, 28(4):387–403, April 1995, arXiv:gr-qc/9501010. doi:10.1007/bf02105083. ↪ [47]

[Hoo93] G. 't Hooft. Dimensional Reduction in Quantum Gravity. *arXiv*, October 1993, arXiv:gr-qc/9310026. ↪ [73]

[HS11] Daniel Harlow and Douglas Stanford. Operator Dictionaries and Wave Functions in AdS/CFT and dS/CFT. *arXiv*, April 2011, arXiv:1104.2621. ↪ [2]

[HSSS12] Daniel Harlow, Stephen H. Shenker, Douglas Stanford, and Leonard Susskind. Tree-like structure of eternal inflation: A solvable model. *Phys. Rev. D*, 85(6):063516, mar 2012. doi:10.1103/physrevd.85.063516. ↪ [4]

[HY18] Atsushi Higuchi and Kazuhiro Yamamoto. Vacuum state in de Sitter space-time with static charts. *Phys. Rev. D*, 98(6):065014, 2018, arXiv:1808.02147. doi:10.1103/physrevd.98.065014. ↪ [38, 40, 115, 116]

[Jac85] Roman Jackiw. Lower dimensional gravity. *Nucl. Phys. B*, 252:343–356, 1985. doi:10.1016/0550-3213(85)90448-1. ↪ [3, 11, 134]

[Jac92] R. Jackiw. Gauge theories for gravity on a line. *Theor. Math. Phys.*, 92(3):979–987, 1992, arXiv:hep-th/9206093. doi:10.1007/bf01017075. ↪ [3, 11]

[Jac98] Ted Jacobson. Comment on accelerated detectors and temperature in (anti-) de Sitter spaces. *Class. Quantum Gravity*, 15(1):251–253, jan 1998, arXiv:gr-qc/9709048. doi:10.1088/0264-9381/15/1/020. ↪ [4]

[Jäg08] Sebastian Jäger. Conserved quantities in asymptotically de Sitter spacetimes. Diplomarbeit, Georg-August-Universität zu Göttingen, 2008. ↪ [70, 71]

[Jen05] David Jennings. The brane universe as an Unruh observer. *arXiv*, 2005, arXiv:hep-th/0508215. ↪ [4, 113]

[Jen10] David Jennings. On the response of a particle detector in anti-de Sitter spacetime. *Class. Quantum Gravity*, 27(20):205005, sep 2010. doi:10.1088/0264-9381/27/20/205005. ↪ [113]

[Jen16] Kristan Jensen. Chaos in AdS_2 Holography. *Phys. Rev. Lett.*, 117(11):111601, 2016. doi:10.1103/physrevlett.117.111601. ↪ [12]

[Jon14] Vaughan F. R. Jones. Some unitary representations of Thompson's groups F and T. *J. Comb. Algebra*, 2014, arXiv:1412.7740. doi:10.4171/JCA/1-1-1. ↪ [2, 3, 65]

[Jon17] Vaughan F. R. Jones. A No-Go Theorem for the Continuum Limit of a Periodic Quantum Spin Chain. *Commun. Math. Phys.*, 357(1):295–317, jul 2017. doi:10.1007/s00220-017-2945-3. ↪ [2, 3]

[JTJ15] Lijuan Jia, Zehua Tian, and Jiliang Jing. Entropic uncertainty relation in de Sitter space. *Ann. Phys.*, 353:37–47, feb 2015, arXiv:1501.00623. doi:10.1016/j.aop.2014.10.019. ↪ [4]

[KB17] Raj Sinai Kunkolienkar and Kinjal Banerjee. Towards a dS/MERA correspondence. *Int. J. Mod. Phys. D*, 26(13):1750143, 2017, arXiv:1611.08581. doi:10.1142/s0218271817501437. ↪ [3, 88, 90]

[KdlHCRB22] Viktoria Kabel, Anne-Catherine de la Hamette, Esteban Castro-Ruiz, and Časlav Brukner. Quantum conformal symmetries for spacetimes in superposition. *arXiv*, June 2022, arXiv:2207.00021. ↪ [5, 126]

[Kim16] Sang Pyo Kim. Schwinger effect, Hawking radiation and Unruh effect. *Int. J. Mod. Phys. D*, 25(13):1645005, nov 2016, arXiv:1602.05336. doi:10.1142/s021827181645005x. ↪ [4]

[KKVV22] Joshua Kames-King, Evita M. H. Verheijden, and Erik P. Verlinde. No Page curves for the de Sitter horizon. *J. High Energy Phys.*, 2022(3), mar 2022, arXiv:2108.09318. doi:10.1007/jhep03(2022)040. ↪ [4]

[KPY22] Subeom Kang, Wan-il Park, and Dong-han Yeom. Novel phenomena of the Hartle-Hawking wave function. *arXiv*, August 2022, arXiv:2208.12380. ↪ [35]

[Laf89] R. Laflamme. Geometry and thermofields. *Nuclear Physics B*, 324(1):233–252, 1989. doi:10.1016/0550-3213(89)90191-0. ↪ [113]

[Lap78] A. S. Lapedes. Bogoliubov transformations, propagators, and the Hawking effect. *J. Math. Phys.*, 19(11):2289–2293, nov 1978. doi:10.1063/1.523607. ↪ [4]

[LHGZ17] Youning Li, Muxin Han, Markus Grassl, and Bei Zeng. Invariant perfect tensors. *New Journal of Physics*, 19(6):063029, jun 2017. doi:10.1088/1367-2630/aa7235. ↪ [2]

[LLCJ21] Shengshuai Liu, Yanbo Lou, Yingxuan Chen, and Jietai Jing. All-Optical Optimal N-to-M Quantum Cloning of Coherent States. *Phys. Rev. Lett.*, 126(6):060503, February 2021. doi:10.1103/physrevlett.126.060503. ↪ [53]

[LP78] D. Lohiya and N. Panchapakesan. Massless scalar field in a de Sitter universe and its thermal flux. *Journal of Physics A: Mathematical and General*, 11(10):1963–1968, oct 1978. doi:10.1088/0305-4470/11/10/014. ↪ [153]

[Mal98] Juan Maldacena. The large N limit of superconformal field theories and supergravity. *Advances in Theoretical and Mathematical Physics*, 2(2):231–252, 1998, arXiv:hep-th/9711200. doi:10.4310/atmp.1998.v2.n2.a1. ↪ [1]

[Mal99] Juan Maldacena. The Large-N Limit of Superconformal Field Theories and Supergravity. *Int. J. Theor. Phys.*, 38(4):1113–1133, 1999, arXiv:hep-th/9711200. doi:10.1023/a:1026654312961. ↪ [1]

[Mal03] Juan Maldacena. Eternal black holes in anti-de Sitter. *J. High Energy Phys.*, 2003(04):021–021, 2003. doi:10.1088/1126-6708/2003/04/021. ↪ [2]

[Mar18] T. Markkanen. De Sitter stability and coarse graining. *Eur. Phys. J. C*, 78(97), feb 2018, arXiv:1703.06898. doi:10.1140/epjc/s10052-018-5575-9. ↪ [4]

[Max23] Nelson Max. Constructing and Visualizing Uniform Tilings. *Computers*, 12(10):208, October 2023. doi:10.3390/computers12100208. ↪ [47]

[May17] A. May. Tensor networks for dynamic spacetimes. *J. High Energy Phys.*, 2017(6), 2017, arXiv:1611.06220. doi:10.1007/jhep06(2017)118. ↪ [2]

[Mot85] E. Mottola. Particle creation in de Sitter space. *Phys. Rev. D*, 31(4):754–766, feb 1985. doi:10.1103/physrevd.31.754. ↪ [4, 23, 113]

[MS13] J. Maldacena and L. Susskind. Cool horizons for entangled black holes. *Fortschr. Phys.*, 61(9):781–811, 2013, arXiv:1306.0533. doi:10.1002/prop.201300020. ↪ [1]

[MSY16] Juan Maldacena, Douglas Stanford, and Zhenbin Yang. Conformal symmetry and its breaking in two-dimensional nearly anti-de Sitter space. *Prog. Theor. Exp. Phys.*, 2016(12):12C104, 2016, arXiv:1606.01857. doi:10.1093/ptep/ptw124. ↪ [12]

[MV17] C. Marletto and V. Vedral. Gravitationally Induced Entanglement between Two Massive Particles is Sufficient Evidence of Quantum Effects in Gravity. *Physical Review Letters*, 119(24):240402, December 2017. doi:10.1103/physrevlett.119.240402. ↪ [5]

[MV18a] Ashley Milsted and Guifre Vidal. Geometric interpretation of the multi-scale entanglement renormalization ansatz. *arXiv*, 2018, arXiv:1812.00529. ↪ [3, 90]

[MV18b] Ashley Milsted and Guifre Vidal. Tensor networks as path integral geometry. *arXiv*, July 2018, arXiv:1807.02501. ↪ [88, 90]

[MW07] Viatcheslav Mukhanov and Sergei Winitzki. *Introduction to Quantum Effects in Gravity*. Cambridge University Press, 2007. doi:10.1017/CBO9780511809149. ↪ [24]

[NB24] Laura Niermann and Luis Cortés Barbado. Particle detectors in superposition in de Sitter spacetime. *arXiv*, 2024, 2403.02087. ↪ [5, 119]

[NC00] Michael A. Nielsen and Isaac Chuang. *Quantum computation and quantum information*. Cambridge University Press, 2000. doi:10.1017/CBO9780511976667. ↪ [51]

[NO22] Laura Niermann and Tobias J. Osborne. Holographic networks for (1+1)-dimensional de Sitter space-time. *Phys. Rev. D*, 105(12):125009, 2022, arXiv:2102.09223. doi:10.1103/physrevd.105.125009. ↪ [3, 57, 73, 80]

[NO24] Laura Niermann and Tobias J. Osborne. The evolution of expanding spacetime realizes approximate quantum cloning. *arXiv*, 2024, 2405.04965. ↪ [4, 114]

[Nom82] Katsumi Nomizu. The Lorentz-Poincaré metric on the upper half-space and its extension. *Hokkaido Mathematical Journal*, 11(3), feb 1982. doi:10.14492/hokmj/1381757803. ↪ [57]

[NPT96] H. Narnhofer, I. Peter, and W. Thirring. How hot is de Sitter space? *International Journal of Modern Physics B*, 10(13n14):1507–1520, 1996. doi:10.1142/s0217979296000611. ↪ [113]

[OS19] Tobias J. Osborne and Deniz E. Stiegemann. Quantum fields for unitary representations of Thompson's groups F and T. *arXiv*, 2019, arXiv:1903.00318. ↪ [65]

[OS20] Tobias J. Osborne and Deniz E. Stiegemann. Dynamics for holographic codes. *J. High Energy Phys.*, 2020(4), apr 2020. doi:10.1007/jhep04(2020)154. ↪ [49, 65, 94]

[Pad03] T. Padmanabhan. Cosmological constant—the weight of the vacuum. *Physics Reports*, 380(5-6):235–320, jul 2003. doi:10.1016/s0370-1573(03)00120-0. ↪ [113]

[Pad05] T. Padmanabhan. Gravity and the thermodynamics of horizons. *Physics Reports*, 406(2):49–125, jan 2005. doi:10.1016/j.physrep.2004.10.003. ↪ [113]

[PAG+99] S. Perlmutter, G. Aldering, G. Goldhaber, R. A. Knop, P. Nugent, P. G. Castro, S. Deustua, S. Fabbro, A. Goobar, D. E. Groom, I. M. Hook, A. G. Kim, M. Y. Kim, J. C. Lee, N. J. Nunes, R. Pain, C. R. Pennypacker, R. Quimby, C. Lidman, R. S. Ellis, M. Irwin, R. G. McMahon, P. Ruiz-Lapuente, N. Walton, B. Schaefer, B. J. Boyle, A. V. Filippenko, T. Matheson, A. S. Fruchter, N. Panagia, H. J. M. Newberg, W. J. Couch, and The Supernova Cosmology Project. Measurements of Ω and Λ from 42 High-Redshift Supernovae. *Astrophys. J.*, 517(2):565, 1999, astro-ph/9812133. doi:10.1086/307221. ↪ [2]

[Par67] Leonard Emanuel Parker. *The Creation Of Particles in an Expanding Universe*. PhD thesis, Harvard University, 1967. URL `https://www.proquest.com/dissertations-theses/creation-particles-expanding-universe/docview/302228771/se-2?accountid=14486`. ↪ [4, 113]

[Par68] L. Parker. Particle Creation in Expanding Universes. *Phys. Rev. Lett.*, 21(8):562–564, aug 1968. doi:10.1103/physrevlett.21.562. ↪ [4, 113]

[Par69] Leonard Parker. Quantized Fields and Particle Creation in Expanding Universes. I. *Physical Review*, 183(5):1057–1068, jul 1969. doi:10.1103/physrev.183.1057. ↪ [4, 113]

[Par73] Leonard Parker. Conformal Energy-Momentum Tensor in Riemannian Space-Time. *Phys. Rev. D*, 7(4):976–983, feb 1973. doi:10.1103/physrevd.7.976. ↪ [24]

[PB23] Jerzy Paczos and Luis C. Barbado. Hawking radiation for detectors in superposition of locations outside a black hole. *arXiv*, August 2023, arXiv:2308.15149. ↪ [5, 6, 119, 120, 129]

[PBO20] Kyle Poland, Kerstin Beer, and Tobias J. Osborne. No Free Lunch for Quantum Machine Learning. *arXiv*, 2020, arXiv:2003.14103. ↪ [105]

[PKV+03] H. V. Peiris, E. Komatsu, L. Verde, D. N. Spergel, C. L. Bennett, M. Halpern, G. Hinshaw, N. Jarosik, A. Kogut, M. Limon, S. S. Meyer, L. Page, G. S. Tucker, E. Wollack, and E. L. Wright. First-Year Wilkinson Microwave Anisotropy Probe (WMAP)* Observations: Implications For Inflation. *Astrophys. J. Suppl. Ser.*, 148(1):213–231, 2003, arXiv:astro-ph/0302225. doi:10.1086/377228. ↪ [2]

[Poi04] Eric Poisson. *A Relativist's Toolkit: The Mathematics of Black-Hole Mechanics*. Cambridge University Press, 2004. doi:10.1017/cbo9780511606601. ↪ [135]

[Pol89a] D. Polarski. On the Hawking effect in de Sitter space. *Class. Quantum Gravity*, 6(5):717–722, 1989. doi:10.1088/0264-9381/6/5/013. ↪ [153]

[Pol89b] D. Polarski. The scalar wave equation on static de Sitter and anti-de Sitter spaces. *Class. Quantum Gravity*, 6(6):893–900, 1989. doi:10.1088/0264-9381/6/6/013. ↪ [153]

[PR17] Alex Peach and Simon F. Ross. Tensor network models of multiboundary wormholes. *Class. Quantum Gravity*, 34(10):105011, apr 2017. doi:10.1088/1361-6382/aa6b0f. ↪ [2]

[PT09] Leonard Parker and David Toms. *Quantum Field Theory in Curved Spacetime*. Cambridge University Press, 2009. doi:10.1017/cbo9780511813924. ↪ [23, 24, 31, 33, 34]

[PYHP15] Fernando Pastawski, Beni Yoshida, Daniel Harlow, and John Preskill. Holographic quantum error-correcting codes: toy models for the bulk/boundary correspondence. *J. High Energy Phys.*, 2015(6), 2015, arXiv:1503.06237. doi:10.1007/jhep06(2015)149. ↪ [2, 3, 4, 43, 47, 49, 51, 79, 80, 85, 101, 107]

[Qi13] Xiao-Liang Qi. Exact holographic mapping and emergent space-time geometry. *arXiv*, 2013, arXiv:1309.6282. ↪ [3, 50]

[Raa10] Mark Van Raamsdonk. Building up spacetime with quantum entanglement. *Gen. Relativ. Gravit.*, 42(10):2323–2329, 2010, arXiv:1005.3035. doi:10.1007/s10714-010-1034-0. ↪ [1]

[Raa16] Mark Van Raamsdonk. Lectures on Gravity and Entanglement. In *New Frontiers in Fields and Strings*. WORLD SCIENTIFIC, nov 2016. doi:10.1142/9789813149441_0005. ↪ [73]

[RFC+98] Adam G. Riess, Alexei V. Filippenko, Peter Challis, Alejandro Clocchiatti, Alan Diercks, Peter M. Garnavich, Ron L. Gilliland, Craig J. Hogan, Saurabh Jha, Robert P. Kirshner, B. Leibundgut, M. M. Phillips, David Reiss, Brian P. Schmidt, Robert A. Schommer, R. Chris Smith, J. Spyromilio, Christopher Stubbs, Nicholas B. Suntzeff, and John Tonry. Observational evidence from supernovae for an accelerating universe and a cosmological constant. *The Astronomical Journal*, 116(3):1009–1038, September 1998. doi:10.1086/300499. ↪ [2]

[RGRA18] Zahra Raissi, Christian Gogolin, Arnau Riera, and Antonio Acín. Optimal quantum error correcting codes from absolutely maximally entangled states. *Journal of Physics A: Mathematical and Theoretical*, 51(7):075301, jan 2018. doi:10.1088/1751-8121/aaa151. ↪ [2]

[Rip13] A. Chris Ripken. Coordinate systems in de Sitter spacetime. Master's thesis, Radboud University Nijmegen, 2013. ↪ [12]

[RS61] H. Reeh and S. Schlieder. Bemerkungen zur unitäräquivalenz von lorentz-invarianten Feldern. *Il Nuovo Cimento*, 22(5):1051–1068, December 1961. doi:10.1007/bf02787889. ↪ [107]

[RT06] Shinsei Ryu and Tadashi Takayanagi. Holographic Derivation of Entanglement Entropy from the Anti-de Sitter Space/Conformal Field Theory Correspondence. *Phys. Rev. Lett.*, 96(18):181602, 2006. doi:10.1103/physrevlett.96.181602. ↪ [1, 51]

[RT17] Mukund Rangamani and Tadashi Takayanagi. Holographic Entanglement Entropy. In *Holographic Entanglement Entropy*, pages 35–47. Springer International Publishing, 2017. doi:10.1007/978-3-319-52573-0_4. ↪ [1]

[Sal19] Nicholas S. Salzetta. *Holography beyond AdS/CFT*. PhD thesis, University of California, Berkeley, 2019. URL `https://www.proquest.com/dissertations-theses/holography-beyond-ads-cft/docview/2385777029/se-2?accountid=14486`. ↪ [73]

[SIGA05] Valerio Scarani, Sofyan Iblisdir, Nicolas Gisin, and Antonio Acín. Quantum cloning. *Reviews of Modern Physics*, 77(4):1225–1256, nov 2005. doi:10.1103/revmodphys.77.1225. ↪ [53]

[SSP+98] Brian P. Schmidt, Nicholas B. Suntzeff, M. M. Phillips, Robert A. Schommer, Alejandro Clocchiatti, Robert P. Kirshner, Peter Garnavich, Peter Challis, B. Leibundgut, J. Spyromilio, Adam G. Riess, Alexei V. Filippenko, Mario Hamuy, R. Chris Smith, Craig Hogan, Christopher Stubbs, Alan Diercks, David Reiss, Ron Gilliland, John Tonry, Jose Maza, A. Dressler, J. Walsh, and R. Ciardullo. The High-Z Supernova Search: Measuring Cosmic Deceleration and Global Curvature of the Universe Using Type Ia Supernovae. *Astrophys. J.*, 507(1):46–63, 1998, arXiv:astro-ph/9805200. doi:10.1086/306308. ↪ [2, 9]

[SSV03] M. Spradlin, A. Strominger, and A. Volovich. De Sitter Space. In *Unity from Duality: Gravity, Gauge Theory and Strings*, pages 423–453. Springer Berlin Heidelberg, 2003. doi:10.1007/3-540-36245-2_6. ↪ [12]

[Sti18] Deniz E. Stiegemann. Approximating Diffeomorphisms by Elements of Thompson's Groups F and T. *Morfismos 23, 2 (2019), pp. 1-10*, October 2018, arXiv:1810.11041. ↪ [64]

[Sti19] Deniz E. Stiegemann. Thompson field theory. *arXiv*, 2019, 1907.08442. ↪ [61, 63]

[Str01a] Andrew Strominger. The dS/CFT correspondence. *J. High Energy Phys.*, 2001(10):034–034, 2001, arXiv:hep-th/0106113. doi:10.1088/1126-6708/2001/10/034. ↪ [3]

[Str01b] Andrew Strominger. Inflation and the dS/CFT Correspondence. *J. High Energy Phys.*, 2001(11):049–049, 2001, arXiv:hep-th/0110087. doi:10.1088/1126-6708/2001/11/049. ↪ [3]

[SU69] Roman U. Sexl and Helmuth K. Urbantke. Production of Particles by Gravitational Fields. *Physical Review*, 179(5):1247–1250, March 1969. doi:10.1103/physrev.179.1247. ↪ [4, 113]

[SUFK21] A. F. Santos, S. C. Ulhoa, T. F. Furtado, and Faqir C. Khanna. On the temperature of gravitation in the de Sitter space-time. *Eur. Phys. J. C*, 81(393), may 2021, arXiv:2104.12633. doi:10.1140/epjc/s10052-021-09189-3. ↪ [4, 113]

[Sun02] Vardarajan Suneeta. Notes on Euclidean de Sitter space. *J. High Energy Phys.*, 2002(09):040–040, sep 2002. doi:10.1088/1126-6708/2002/09/040. ↪ [9]

[Sus95] Leonard Susskind. The world as a hologram. *J. Math. Phys.*, 36(11):6377–6396, nov 1995. doi:10.1063/1.531249. ↪ [1, 73]

[SW04] B. Schumacher and R. F. Werner. Reversible quantum cellular automata. *arXiv*, May 2004, arXiv:quant-ph/0405174. ↪ [88]

[Swi12a] Brian Swingle. Constructing holographic spacetimes using entanglement renormalization. *arXiv*, September 2012, arXiv:1209.3304. ↪ [2, 49]

[Swi12b] Brian Swingle. Entanglement renormalization and holography. *Phys. Rev. D*, 86(6):065007, 2012, arXiv:0905.1317. doi:10.1103/physrevd.86.065007. ↪ [3, 49, 90]

[Tei83] Claudio Teitelboim. Gravitation and hamiltonian structure in two spacetime dimensions. *Phys. Lett. B*, 126(1-2):41–45, 1983. doi:10.1016/0370-2693(83)90012-6. ↪ [3, 11]

[Tug69] I. I. Tugov. Conformal covariance and invariant formulationof scalar wave equations. *Ann. Inst. Henri Poincaré, Section A*, XI(2):207–220, 1969. URL `http://www.numdam.org/item/AIHPA_1969__11_2_207_0.pdf`. ↪ [24]

[Unr76] W. G. Unruh. Notes on black-hole evaporation. *Phys. Rev. D*, 14(4):870–892, 1976. doi:10.1103/physrevd.14.870. ↪ [26, 27, 30]

[VCM09] F. Verstraete, J. I. Cirac, and V. Murg. Matrix Product States, Projected Entangled Pair States, and variational renormalization group methods for quantum spin systems. *Advances in Physics*, 57(2):143–224, March 2009, arXiv:0907.2796. doi:10.1080/14789940801912366. ↪ [49]

[Vid07] G. Vidal. Entanglement renormalization. *Physical Review Letters*, 99(22):220405, November 2007. doi:10.1103/physrevlett.99.220405. ↪ [90]

[Vid08] G. Vidal. Class of Quantum Many-Body States That Can Be Efficiently Simulated. *Phys. Rev. Lett.*, 101(11):110501, September 2008. doi:10.1103/physrevlett.101.110501. ↪ [50, 90]

[VPB98] Pelegrí Viader, Jaume Paradís, and Lluís Bibiloni. A New Light on Minkowski's ?(x) Function. *Journal of Number Theory*, 73(2):212–227, dec 1998. doi:10.1006/jnth.1998.2294. ↪ [66]

[Wal84] Robert M. Wald. *General relativity*. University of Chicago Press, 1984. ↪ [9, 10, 11, 17, 18, 19, 20, 28, 70]

[Wal88] M. Mitchell Waldrop. The Quantum Wave Function of the Universe. *Science*, 242(4883):1248–1250, dec 1988. doi:10.1126/science.242.4883.1248. ↪ [35]

[Wal94] Robert M. Wald. *Quantum field theory in curved spacetime and black hole thermodynamics*. University of Chicago Press, 1994. URL https://press.uchicago.edu/ucp/books/book/chicago/Q/bo3684008.html. ↪ [23, 24, 27, 28, 116]

[Wee] Jeff Weeks. Kaleidotile. https://www.geometrygames.org/KaleidoTile/. Freely available software for creating spherical, Euclidean and hyperbolic tessellations. ↪ [49]

[Wer98] R. F. Werner. Optimal cloning of pure states. *Phys. Rev. A*, 58(3):1827–1832, sep 1998. doi:10.1103/physreva.58.1827. ↪ [53]

[Wit98] Edward Witten. Anti De Sitter Space And Holography. *Advances in Theoretical and Mathematical Physics*, 2(2):253–291, 1998, arXiv:hep-th/9802150. doi:10.4310/atmp.1998.v2.n2.a2. ↪ [1]

[Wit01] Edward Witten. Quantum Gravity In de Sitter Space. *arXiv*, 2001, arXiv:hep-th/0106109. ↪ [2, 18, 75, 85]

[Wit18] Edward Witten. APS Medal for Exceptional Achievement in Research: Invited article on entanglement properties of quantum field theory. *Reviews of Modern Physics*, 90(4):045003, October 2018. doi:10.1103/revmodphys.90.045003. ↪ [107]

[Wit23] Edward Witten. Algebras, Regions, and Observers. *arXiv*, 2023, arXiv:2303.02837. ↪ [14, 19, 129]

[Wol21] Ramona Wolf. *Quantum Key Distribution*. Springer eBook Collection. Springer International Publishing, Cham, 2021. ↪ [53]

[WSX+11] Yi-Nan Wang, Han-Duo Shi, Zhao-Xi Xiong, Li Jing, Xi-Jun Ren, Liang-Zhu Mu, and Heng Fan. Unified universal quantum cloning machine and fidelities. *Phys. Rev. A*, 84(3):034302, September 2011. doi:10.1103/physreva.84.034302. ↪ [53]

[WVCZ21] Carolyn E. Wood, Harshit Verma, Fabio Costa, and Magdalena Zych. Operational models of temperature superpositions. *arXiv*, December 2021, 2112.07860. ↪ [119]

[WZ82] W. K. Wootters and W. H. Zurek. A single quantum cannot be cloned. *Nature*, 299(5886):802–803, 1982. doi:10.1038/299802a0. ↪ [51, 52]

[Yan17] Zhao Yang. *Holographic duality and random tensor network*. PhD thesis, Stanford U., 2017. URL https://stacks.stanford.edu/file/druid:mc960bw8174/dissertation-augmented.pdf. ↪ [73]

[YBC+19] Zhi Yang, Arpan Bhattacharyya, Long Cheng, Ling-Yan Hung, and Sirui Ning. Emergent Lorentz symmetry and the Unruh effect in a Lorentzian fermionic tensor network. *Phys. Rev. D*, 99(8):086007, apr 2019. doi:10.1103/physrevd.99.086007. ↪ [88]

[YHQ16] Zhao Yang, Patrick Hayden, and Xiao-Liang Qi. Bidirectional holographic codes and sub-AdS locality. *J. High Energy Phys.*, 2016(1), 2016, arXiv:1510.03784. doi:10.1007/jhep01(2016)175. ↪ [2]

[Yu11] Hongwei Yu. Open Quantum System Approach to the Gibbons-Hawking Effect of de Sitter Space-Time. *Phys. Rev. Lett.*, 106(6):061101, feb 2011, arXiv:1101.5235. doi:10.1103/physrevlett.106.061101. ↪ [4]

[Zhu07] Dongping Zhuang. Irrational Stable Commutator Length in Finitely Presented Groups. *arXiv*, September 2007, arXiv:0710.0026. ↪ [64]

Index

Curriculum Vitae

Full name:	Laura Charlotte Niermann
Date of birth:	31.12.1994
Place of birth:	Bielefeld, Germany
Citizenship:	German

Academic career

2019 – 2024	**PhD student** at Leibniz Universität Hannover Institute for Theoretical Physics Quantum information group, Prof. Dr. Tobias J. Osborne *Research, teaching*
2017 – 2019	**Master of Science in Physics** at Leibniz Universität Hannover Thesis: Holographic Networks for de Sitter Spacetime
2017	semester abroad at University of Nebraska-Lincoln, Lincoln (USA)
2013 – 2017	**Bachelor of Science in Physics** at Leibniz Universität Hannover Thesis: Quantenmechanische Aspekte magnetischer Monopole
2013	**Abitur** at Ricarda Huch Schule Hannover

Supervised theses

Sophie Müller	*Master thesis:* "Tessellations for de Sitter spacetime" co-supervised with Prof. T. J. Osborne (09/2020)
Althea Cappelli	*Bachelor thesis:* "Quantenmechanische Beschreibung der Rückgewinnung von Information aus einem Schwarzen Loch" co-supervised with Prof. T. J. Osborne (12/2020)
Kläre Wienecke	*Bachelor thesis:* "Holographic Networks for Hartle-Hawking States" co-supervised with Prof. T. J. Osborne (02/2022)
Fin Müller	*Bachelor thesis:* "Investigation of the Unruh effect in de Sitter space" examiner Prof. T. J. Osborne (02/2023)

List of Publications

Publications whose material appears in this thesis:

1. Laura Niermann and Tobias J. Osborne.
   Holographic codes for (1+1)-dimensional de Sitter spacetime (2022).
   Physical Review D **105**, 125009, arXiv:2102.09223

2. Laura Niermann and Tobias J. Osborne
   The evolution of expanding spacetime realizes approximate quantum cloning (2024).
   arXiv:2405.04965

3. Laura Niermann and Luis Cortés Barbado
   Particle detectors in superposition in de Sitter spacetime (2024).
   arXiv:2403.02087

Further publications:

4. Kerstin Beer, Dmytro Bondarenko, Alexander Hahn, Maria Kalabakov, Nicole Knust, Laura Niermann, Tobias J. Osborne, Christin Schridde, Stefan Seckmeyer, Deniz E. Stiegemann, and Ramona Wolf.
   From categories to anyons: a travelogue (2018). arXiv:1811.06670